Synthesis of siderophore-based conjugates to detect and treat bacterial infections

Von der Naturwissenschaftlichen Fakultät der

Gottfried Wilhelm Leibniz Universität Hannover

Zur Erlangung des Grades

Doktor der Naturwissenschaften (Dr. rer. nat.)

genehmigte Dissertation

von

Kevin Ferreira, Diplôme d'Ingénieur (Frankreich)

Erscheinungsjahr 2018

Referentin/Referent: [Prof. Dr. rer. nat. Mark Brönstrup]

Korreferentin/Korreferent: [Prof. Dr. rer. nat. Oliver Plettenburg]

Tag der Promotion: [09.04.2018]

L’habit ne fait pas le moine, mais il y contribue…

Olavio and Florence Ferreira

Acknowledgements

The past three years have been an intense experience. I feel changed and grown. This adventure offers me great opportunities but before starting a new page, I want to thank all the people who contributed.

First of all, I would like to thank Prof. Dr. Mark Brönstrup who gave me the opportunity to evolve in his department. I appreciated his professionalism and his trust in me. I also want to thank Prof. Dr. Markus Kalesse and Prof. Dr. Susanne Häußler for serving as my thesis committee members and their scientific suggestions.

It was a pleasure to work with Prof. Dr. Peter Müller, Dr. Verena Fetz, Prof. Dr. Haiyu Hu, Dr. Bushra Rais, Isabell Schneider, Vanessa Stiller, Wiebke Koschinsky, Laura Santos, Stephan Thomas, Katharina Fischer, Lukas Pinkert, Bianka Karge and Ulrike Beutling. This thesis would have never reached such a high quality in such a short period of time without their help and their enthusiasm is greatly appreciated. I would like to give my special thanks to Antje Ritter, who was like my second mother in Germany.

This experience enabled me to have strong links with Giambattista Testolin, Dr. Verena Fetz, Dr. Hans Prochnow and Volker Berndt. Their professionalism but also their humanity helped me in the worst moments. Verena shaped by knowledge in biology and learning from her expertise was an extraodinary and efficient experience that I will never forget.

I would like to express my gratitude to Dr. Philipp Klahn, Dr. Charlotte Grandclaudon, Dr. Arun Naini and Dr. Suryanarayana Birudukota for the countless pieces of advice but also their enthusiasm in our work environment.

I will never forget the major role of my family in what I have become. Sindi has never left me alone, Olavio has always supported me and my parents have always offered me the best chances to do what I wanted. This thesis is also directed to Papi Conde, Idalina, Antonio and Palmira: I am grateful for your endless efforts. Finally, I would never be there without you, Shiwani, thank you for your patience and your daily support.

Yours sincerely,

Kevin Ferreira

A mes chers parents, Sindi et Olavio

Zusammenfassung

Trotz der Entwicklung neuartiger Antiinfektiva steigen Morbidität und Mortalität aufgrund von Infektionen, die durch multiresistente Bakterien verursacht werden, weiter an.[1] Dies betrifft insbesondere Infektionen, die durch Gram-negative Bakterien verursacht werden.

Die Herausforderung bei der Findung neuer Antibiotika besteht darin zu verstehen, wie eine ausreichende Translokation bioaktiver Moleküle durch die Zellwand Gram-negativer Bakterien gewährleistet werden kann. Zudem besteht ein Mangel an verlässlichen und empfindlichen Methoden, die die Erkennung von Bakterien zu einem frühen Zeitpunkt von Infektionen ermöglichen, an welchem die Behandlung mit Antibiotika noch effektiv ist.[2]

Eine Möglichkeit bakterielle Zellwände zu durchdringen besteht in der Nutzung von Konjugaten, um die Internalisierung des Wirkstoffs über spezifische bakterielle Transportsysteme zu erleichtern.[2] So ist beispielsweise Eisen ein aktiv transportierter Nährstoff, der für Bakterien essentiell ist. Stabile, aktiv internalisierte Eisen(III)-Siderophorkomplexe können durch die sogenannte „Trojanisches-Pferd-Strategie“ genutzt werden.

Eine Reihe von Siderophorkonjugaten wurde synthetisiert. Diese Konjugate nehmen aktiv Bakterien ins Visier, mindern deren Wachstum und ermöglichten die Visualisierung bakterieller Infektionen. Diese Dissertation beschreibt die Synthese und strukturelle Charakterisierung verschiedener Siderophore und Konjugate. Ferner wurden die Markierung von Siderophoren und ihre antibiotischen Eigenschaften evaluiert.

20 Substanzen wurden gegen *E. coli* und *P. aeruginosa* getestet. Um die intrazelluläre Akkumulation solcher Konjugate zu quantifizieren wurde eine neue Methode angewandt, die auf dem fluoreszenz-aktivierenden Protein (*Fluorogen Activating Protein,* FAP) basiert. Damit wurde die Bestimmung der subzellulären Lokalisation der Malachitgrün-gekoppelten niedermolekularen Verbindungen ermöglicht. Die Nutzung des Prinzips des aktiven Targetings in Verbindung mit der beschriebenen DOTAM/Metall-Plattform sollte geeignet für die Entwicklung neuartiger Wirkstoffkonjugate sein, die verschiedene zelluläre Wirkungsweisen und –orte gegen Gram-negative Bakterien aufweisen. Design und Synthese neuartiger Siderophorkonjugate, sowohl mit BODIPY-Verbindungen als auch mit Ampicillin, Ciprofloxacin oder Sorangicin, deren Internalisierungs-Eigenschaften in dieser Dissertation maßgeblich dargestellt werden, repräsentieren einen Meilenstein bei der Verbesserung der Theranostik gegen Bakterien der ESKAPE-Gruppe.

Schlagworte: Siderophor - Konjugate - Bakterien

Abstract

Infections caused by multidrug-resistant Gram-negative bacteria result in significant mortality and morbidity worldwide despite the development of new anti-infective drugs.[1] The need for novel antibiotics is currently not met by R&D efforts, in particular in the area of infections caused by Gram-negative bacteria. One of the scientific needs is to understand how to assure a sufficient translocation of bioactive molecules across the Gram-negative cell wall. Another limitation is the lack of reliable and sensitive methods that permit the detection of bacteria at early stages of infections where antibiotic treatments would still be effective.[2]

One possibility to improve bacterial penetration is to generate conjugates and facilitate compound delivery through specific bacterial transport systems.[2] For example, iron is an essential actively transported nutrient: ferric siderophore complexes are internalized via recognition from the outer membrane and actively transported inside of Gram-positive and Gram-negative bacteria. Such stable, internalized complexes can be exploited with a so-called Trojan horse strategy.

A series of agents comprising siderophores that actively target bacteria, inhibit bacterial growth and demonstrate efficacy to visualize bacterial infections were synthesized. This thesis shows the synthesis and structural characterization of various siderophores and conjugates, followed by an investigation of the siderophoric, labelling and antibiotic properties of the molecules.

Designed conjugates were characterized as Fe(III) chelating agents. Among a list of 20 tested molecules on *E. coli* and *P. aeruginosa*, the DOTAM/catechol scaffolds showed high siderophoric effects. To quantify the intracellular accumulation of such conjugates, a fluorogen activating protein-based approach (FAP) that allows the determination of the subcellular localization of malachite green dye-coupled small molecules was pursued. This system served to validate the efficiency of vehicles for bacterial penetration.[3] The use of active targeting principles attached to the described DOTAM/Metal platform is expected to be appropriate for the development of new drug conjugates that have different cellular targets and modes of action against Gram-negative bacteria. The design and synthesis of novel BODIPY but also ampicillin, ciprofloxacin and sorangicin siderophore conjugates with a crucial demonstration of internalization described in this thesis represents a milestone towards improved theranostics against bacteria of the ESKAPE panel.

Keywords: Siderophore - conjugate - bacteria

Scientific publications

- K. Ferreira, H. Y. Hu, V. Fetz, H. Prochnow, B. Rais, P. P. Muller, M. Bronstrup, *Multivalent Siderophore-DOTAM Conjugates as Theranostics for Imaging and Treatment of Bacterial Infections, Angewandte Chemie, International Edition in English* **2017**, *56*, 8272-8276/ *Multivalente Siderophor-DOTAM-Konjugate als Theranostika zur Visualisierung und Behandlung bakterieller Infektionen, Angewandte Chemie* **2017***, 129,* 8384-8389.

- Prof. M. Brönstrup, Prof. H. Hu, Dr. G. Sergeev, Dr. B. Rais, K. Ferreira, Dr. V. Fetz, 1,4,7,10-tetrazacyclododecane based agents to target bacteria and its use **WO2016026841**.

.

Table of Contents

Table of Figures

Table of Tables

Abbreviations

Abbreviation	Full name
AL	aqueous layer
Bn	benzyl
Boc	tert-butyloxycarbonyl
Cal.	calculated
Conc	concentrated/concentration
CR	crude material
Cxfy	column number x, fraction number y
DCM	dichloromethane
DIPEA	*N*-ethyl-*N*-isopropylpropan-2-amine
DMAP	4-(dimethylamino)-pyridine
DMF	*N,N*-dimethylformamide
DMP	Dess-Martin periodinane
DMSO	dimethyl sulfoxide
DNA	deoxyribonucleic acid
DOTA	1,4,7,10-tetraazacyclododecane-1,4,7,10-tetraacetic acid
e.g.	*exempli gratia*
EDTA	ethylenediaminetetraacetic acid
Eq.	equivalents
FACS	fluorescence activated cell sorting
FAP	fFluorogen-activating protein
g	gram
h	hour(s)
HPLC	high performance liquid chromatography
HV	high vacuum
Hz	hertz
IC	inhibitory concentration
i.e.	*id est*
IFN	interferon
J	coupling constant

L	litter
LB	lysogeny broth
LC-(LR/HR)MS	liquid chromatography-(low resolution/high resolution) mass spectrometry
M	molar
Me	methyl
MIC	minimum inhibitory concentration
Min	minute(s)
mol	mole(s)
NMP	*N*-methyl-2-pyrolidone
NMR	nuclear magnetic resonance
OL	organic layer
PE	petroleum ether
ppm	parts per million
RM	reaction mixture
RP	reversed phase
RT	room temperature
THF	tetrahydrofuran
TLC	thin layer chromatography
UV	ultraviolet

1. Introduction

1.1. Need for accurate diagnosis and treatment of bacterial infections

Pathogenic bacteria are prokaryotic microorganism that cause infections such as tuberculosis, cholera or leprosy that result in millions of deaths per year. Fortunately, antibiotics have been discovered and developed to fight against these pathogenic bacteria and efficiently treat bacterial infections starting with Alexander Fleming's discovery of penicillin in 1928. The golden age of antibiotics was reached with the discovery of streptomycin by Walksman in the 1940's. The applied discovery platform remains valid until today,[4] which was acknowledged by a Nobel Prize.[5] Over the last 80 years, several classes of antibiotics were developed to have an effect on specific vital bacterial targets located in the periplasm or cytoplasm (Figure 1).

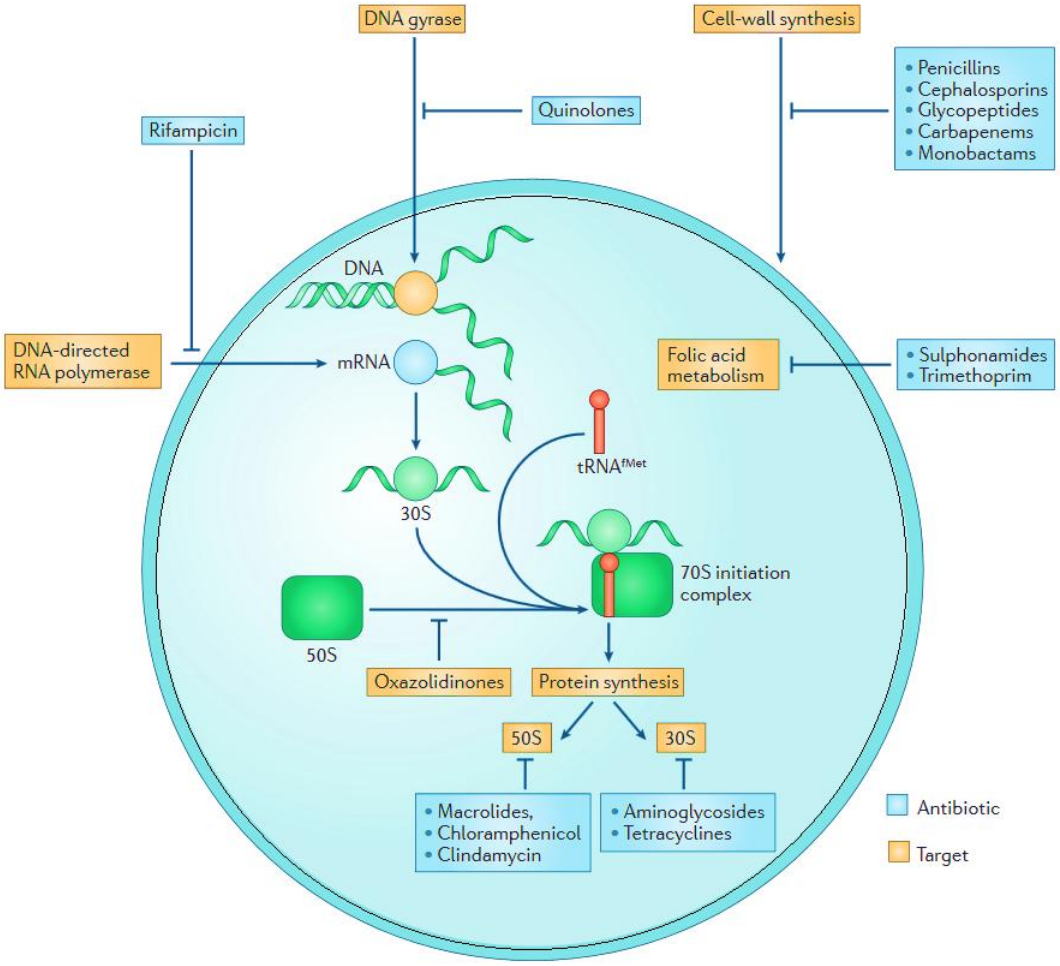

Figure 1 Different discovered antibiotics and their specific bacterial target (Figure taken from [4]).

In 1967, the Surgeon General of the USA claimed that “the time has come to close the book on infectious diseases”.[6] He unfortunately underestimated the the capacity of bacteria to develop resistance against antibiotics: all along this golden age, bacterial resistance was faster than antibiotic discoveries. Indeed, the first antibacterial resistance reported for most antibiotics was observed less than 10 years after their introduction to the market. Due to this effect but also due to poor market incentives, a big gap in antibiotic discovery occured from the 1970’s (Figure 2).

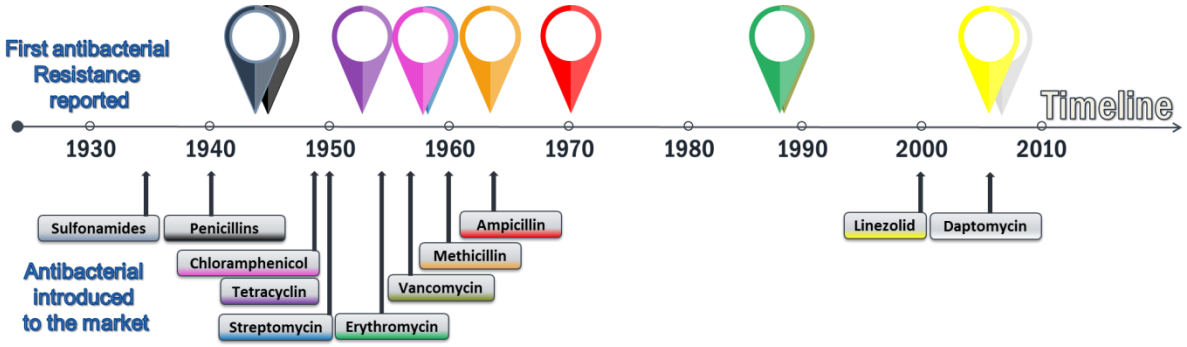

Figure 2 Historical timeline of antibacterial introduced to the marked and first antibacterial resistance reported from 1930 to 2010 (adapted from [7]).

Microbes have developed for millennia resistance mechanisms against antimicrobials.[8] However, there is now an urgent need for new antibacterial strategies due to the spread of pathogen populations. In 2017, it was estimated that 700 000 annual deaths were attributed to antimicrobial resistance, and this number is expected to increase to 10 million annual deaths by 2050.[9] Out of 400 000 cases of infection, about 25 000 people die every year due to antibiotic resistant bacteria in EU member states, Iceland and Norway.[10] Consequently, the number of extra hospital days is estimated to 2.5 million days. This urgent issue leads to an overall estimated cost of 1.5 billion euros in Europe and 35 billion euros in the USA[11] including extra in-hospital and outpatient costs and productivity losses due to the absence from work or due to patients who died from their infection.

Today, one of the main issues is the appearance and increasing number of multidrug-resistant (MDR) infections caused by “ESKAPE” organisms (*Enterococcus* spp., *Staphylococcus aureus*, *Klebsiella* spp. *Acinetobacter baumannii*, *Pseudomonas aeruginosa* and *Enterobacter* spp.).[12] In general, developing antibiotics against all of the members of the ESKAPE panel is a major goal.[12-13] In 2017, the World Health Organization (WHO) released the first antibiotic-resistant priority pathogen list including 20 bacterial species presenting the greatest threat to human health[14] and reported that bacterial resistance against commercially

available antibiotics represents a major threat to public. As an example, *A. baumannii* showed MDR and it is a growing threat in hospitals due to its opportunistic nosocomial characteristics. Colistin is nowadays in use again as a last option to treat the infection, although it showed toxicity problems and resistance is still observed.[15]

Also, an early diagnosis is important to avoid extensive interventions after the spread or the local manifestation of the infection. However, there is still an increasing need for diagnostic methods in order to detect infections located deep into the body. As a matter of fact, there is a lack of new innovative diagnostic tests to detect infections at unknown or inaccessible sites for sampling, especially for biomaterial-associated infections or endocarditis.[16] Moreover, an inadequate diagnosis can yield to the misuse of antimicrobial treatment and consequently to the development of antimicrobial resistance. Therefore, novel diagnostic methods are also necessary to improve treatment outcomes.

The scientific community has gained an understanding of the different mechanisms that bacteria use to develop resistance. Four different strategies are known to be used by bacteria to resist against antibiotics [17] (Figure 3):

-Target modification

-Production of detoxifying enzymes that inactivate the antibiotics by modifying or degrading them

-Membrane resistance to prevent internalization

- Increase in antibiotic efflux

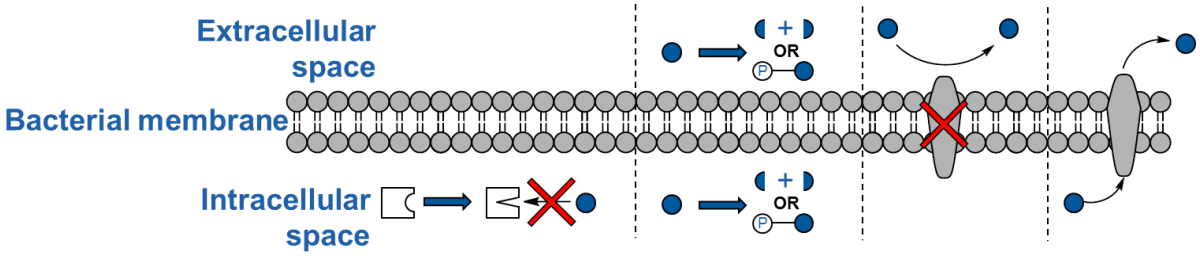

Figure 3 The different resistance mechanisms developed by bacteria against antibiotics (adapted from [7]).

Several diagnostic imaging techniques such as X-ray, computed tomography (CT) scans or magnetic resonance imaging (MRI) are currently used to produce pictures of organs and tissues *in vivo*. However, the positron emission tomography (PET) technique showed high interest due to the high sensitivity to detect radiotracers and the possibility to show organs and tissues. Nevertheless, PET agents in clinical use such as 2-[^{18}F]fluorodeoxyglucose (^{18}F-FDG) cannot distinguish bacterial infections and sterile inflammation. To compensate the need for

noninvasive diagnostic techniques via a PET imaging tracer, several specific bacterial labelling agents based on prothrombin,[18] maltodextrin,[2, 19] sorbitol,[20] vancomycin, or substrates for the micrococcal nuclease (MN) and for the ß-lactamases of M. tuberculosis were published, but the lack of potent candidates for infection diseases is still present. Recently new scaffolds such as 1,4,7,10-tetraazacyclodo-decane-1,4,7,10-tetraacetic amide (DOTAM) and 1,4,7-triazacyclononane-triacetic amide (NOTAM) have been selected due to their wide biocompatibility and imaging applications. This property can be applied to lanthanide-based magnetic resonance imaging, ^{68}Ga- or ^{64}Cu-based nuclear imaging and ^{90}Y-based radiotherapy.[21] The cited mycrocycles have several advantages such as high solubility, low toxicity and proven biocompatibility.[22]

The first function of the bacterial membrane is to act as an effective barrier to prevent passive leakage into or out of the cell. Other functions are to transport nutrients and secrete waste. These gateways are possible thanks to protein anchors, such as porins. The proteins located in the membrane are responsible for the regulation of the flow of nutrients and metabolic products, as well as for the generation and conservation of energy.[23] Gram-positive and Gram-negative bacteria are distinguished by different cell wall structures (Figure 4).

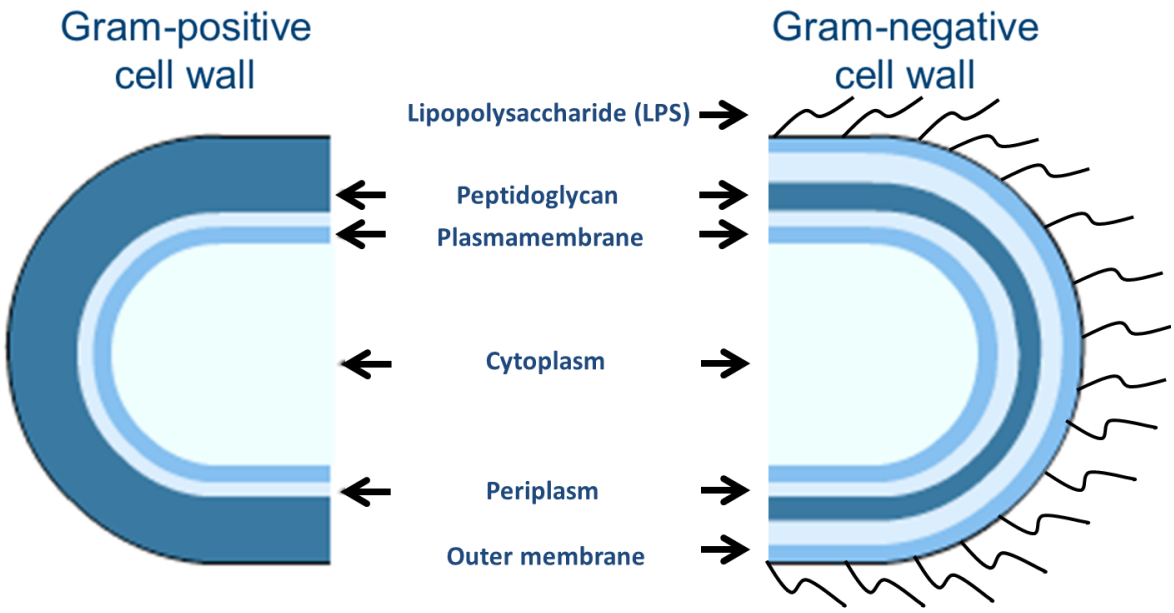

Figure 4 Comparison between Gram-positive and Gram-negative cell walls (adapted from [24]).

The Gram-positive bacterial cell wall contains a cytoplasmic plasma membrane mainly constituted of fatty acids that is covered by a thick peptidoglycan layer, also known as murein. The two layers are separated by a periplasmic space. In contrast, Gram-negative bacterial cell wall has a thinner peptidoglycan layer that is covered by an additional phospholipidic outer

membrane. This layer is decorated on its outer surface by lipopolysaccharides (LPS). Nevertheless, there are further differences such as the carbohydrate composition of the cell wall between particular bacterial strains, but also between bacterial species.[25] The outer membrane is a lipid bilayer, rich in lipopolysaccharides and porins, and impermeable for large and charged molecules.[23] The higher complexity of the Gram-negative cell wall is a substantial hurdle for the permeability of antibiotics.

All the mechanisms described above reduce the concentration of active molecules reaching their target and consequently decrease antimicrobial activity. After understanding the causes of such a decrease in the antibiotic efficiency, one must find novel strategies to improve their activities against the bacterial species of interest.

1.2. Trojan horse strategy

1.2.1. Fe(III) uptake into bacteria

One solution to improve the limited translocation of molecules into bacteria and increase the antibiotic accumulation at its target location is to use a so-called Trojan horse strategy against these specific bacteria. This strategy considers the use of actively transported nutrients that are essential for bacterial survival. By definition, these molecules have an efficient translocation. Therefore, by conjugation of poorly translocated agents with the studied nutrients, the conjugate can show better penetration properties compared to the parent agent alone.

According to Klechkowski and Hund's rules, Fe has the following electronic structure: $[Ar]3d^6 4s^2$. Therefore, Fe(III) offers high stability with the electronic structure $[Ar]3d^5 4s^0$. By following the same logic, Fe(II) is also a stable ion with its electronic structure $[Ar]3d^6$. However, under physiological conditions, Fe(II) tends to form hydroxyl radicals in the presence of H_2O_2 via Fenton chemistry, triggering severe cellular and tissue damage.[26] As a consequence, the main species encountered in the human body is Fe(III) to prevent oxidative damages to the host. Membrane-bound electron transport and redox enzymes of the intermediary metabolisms use this element due to the wide range of Fe^{2+}/Fe^{3+}redox potential from -0.3 V to +0.7 V. In addition, there are suggestions that small iron chelators called siderophores are related to oxidative stress alleviation.[27] Fe is needed for essential metabolic processes as a (co)factor: it is involved in the transport of oxygen, in the production of energy and plays major roles in respiration, in amino acid metabolism and in the biosynthesis of DNA and sterols. For example once bound to

S-containing proteins, the formed [Fe-S] protein complex can be used in the electron-transport and in the catalysis of necessary enzymatic reactions (Figure 5).[28]

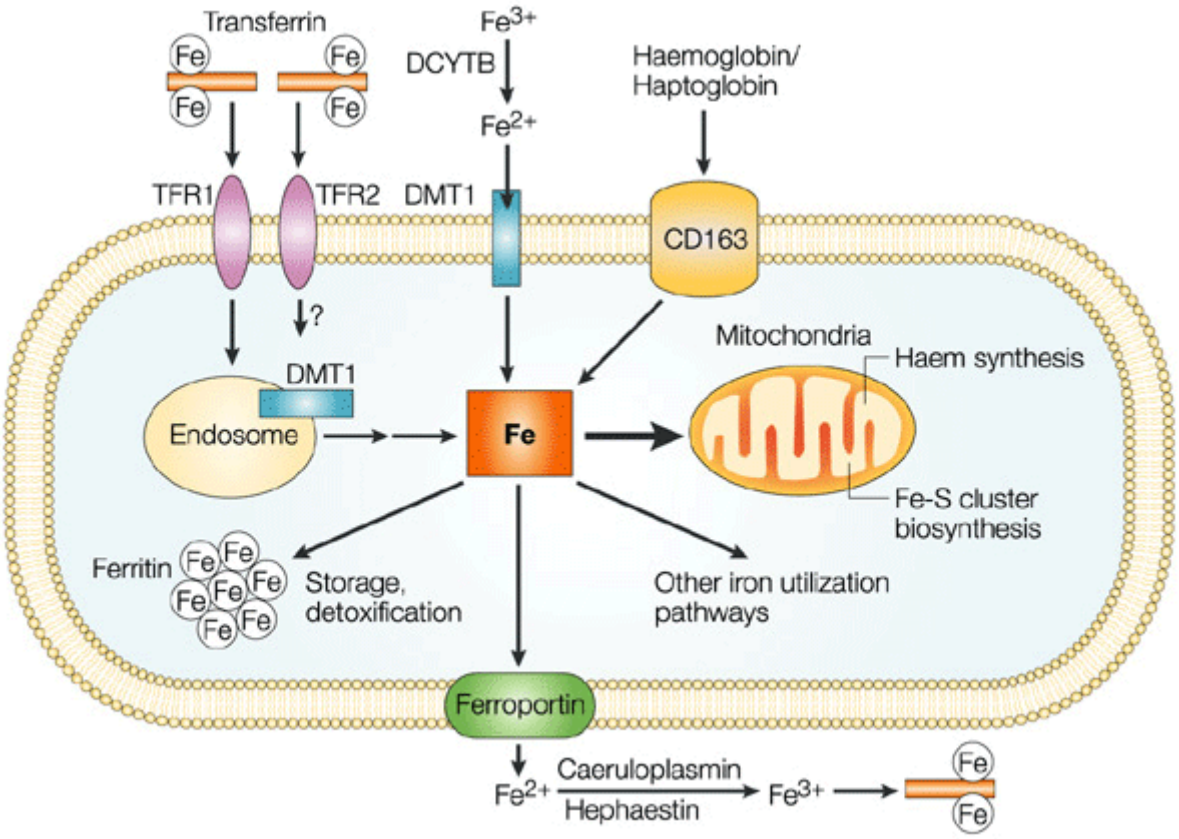

Figure 5 The use of Fe(III) in different metabolic processes (taken from [29]).

However, due to the poor solubility of iron hydroxide in the human body, Fe(III) is very often observed in a complex with ferritin-hemosiderin, hemoglobin or myoglobin.[30] It is also strongly bound to proteins such as transferrin, a serum protein whose iron association constant reaches around 10^{36}.[31] Moreover, host cells tightly regulate iron acquisition, because this metal is also essential for the host cells.[32] To scavenge iron from other proteins, bacteria uptake iron-complexing proteins via receptor mediated transport or use hemes as an iron source.[33] In addition, they biosynthesize siderophores: small molecules below 2 kDa whose affinity to iron is very high ($K_d<10^{-30}$) and that are used to capture free iron or even to steal iron from lower affinity chelators.

Iron acquisition is a big “tug of war” between bacteria and host cells. In order to avoid this Fe(III) piracy, the host cell in return is able to produce lipocalin-type proteins (lipocalin-2, siderocalin[34] and 24p3). For example, lipocalin 2 (Lcn2) is an antimicrobial protein that can sequester siderophore complexes such as Fe(III)-enterobactin, preventing Fe(III) translocation into the bacteria (Figure 6).[35] On the other hand, the role of siderocalin (Scn) is to scavenge

Fe(III) from the environment as an innate immunity factor, for example by hydrolysis of the triserine lactone forming the enterobactin core in mild acidic conditions.[35-36] It therefore has a growth factor role for different cell types.[37] However, pathogens are able to evade this resistance mechanism by producing stealth siderophores that do not interact with such proteins,[38] such as salmochelin or yersiniabactin.[39] Also to be able to regulate the host's inner Fe(III) concentration, ferroportin can export Fe(III) out of the cell and therefore minimize any excess of intracellular Fe(III) concentration.

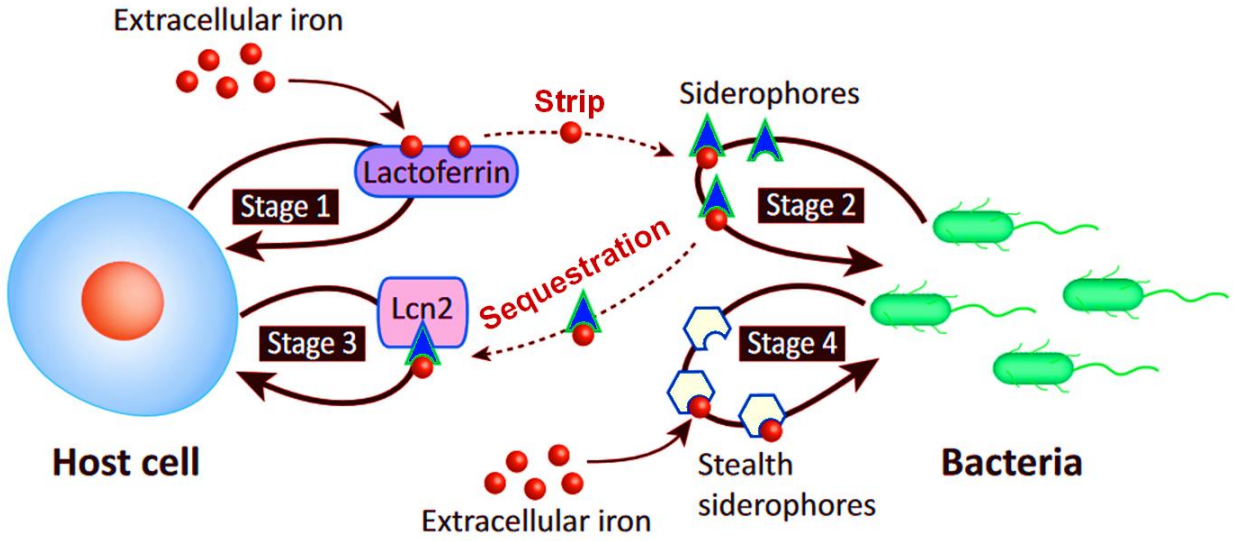

Figure 6 Different stages of iron "tug of war" between the host cell and bacteria (adapted from [40]).

1.2.2. Bacterial Fe uptake systems

The ratio of intracellular vs extracellular iron concentration in bacteria to the external media is very high in bacteria. Compared to other metals, this factor is one of the highest (Figure 7). For example, an *E. coli* cell, whose volume is about 0.6-0.7 μm^3,[41] has a need of 10^5 Fe(III) ions per generation in order to proliferate and maintain an internal concentration of 1 µM of Fe.[42] This concentration of iron is not maintained due to diffusion through porins, since the size of a siderophore is usually far above 600 Da, which renders the probability that these compounds can be taken up through passive diffusion low.[43] Instead, a highly regulated, active iron transport to the inner-bacterial space that relies on high affinity interactions is operative.

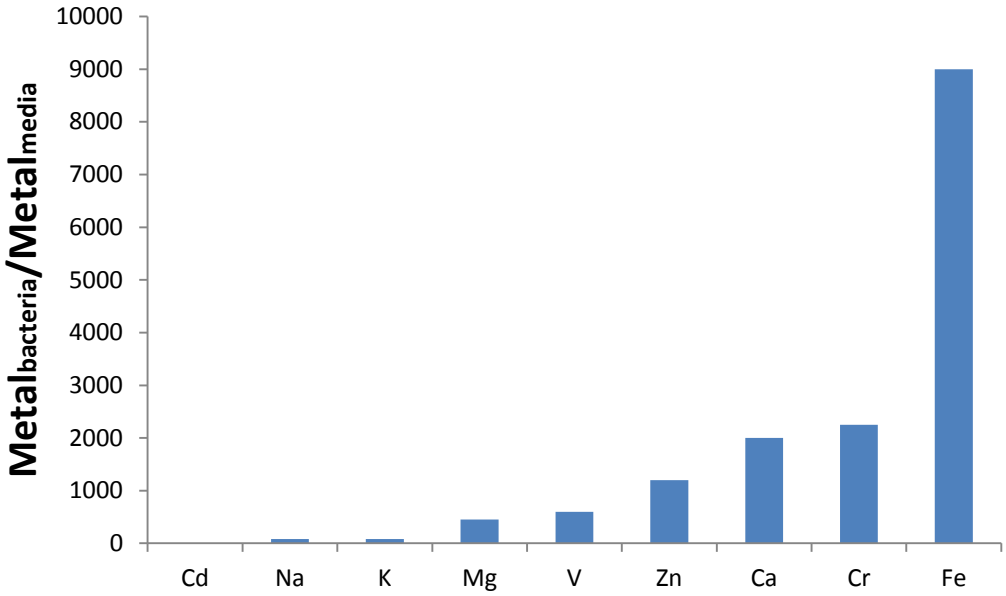

Figure 7 Concentration factors of metals in PAO1 cells grown in CAA medium (adapted from [44]).

The upregulation of specific outer membrane receptors (OMR) is necessary for optimal Fe(III)-siderophore complex uptake. Genes for siderophore transport systems are repressed when iron is sufficient in the media, whereas they are expressed under iron starvation conditions. *E. coli* siderophore uptake regulation is well understood. The transcriptional regulation of these proteins is mediated by the Fur protein that represses the transcription of several genes related to iron acquisition.[45] DxrR is another protein that can have a repressor role.[46] If intracellular iron concentration is too low, Fur loses affinity to DNA, thereby triggering gene transcription.

The recognition of the Fe(III) complex by the OMR occurs at its outer site for its translocation. For example, the Fe(III)-enterobactin complex in *E. coli* is specifically recognised by FepA at the OMR (Figure 8). An energy dependent mechanism promotes transport through the outer membrane.[47] TonB, a cytoplasmic membrane protein (CMP), firstly transduces a proton motive force from the cytoplasmic membrane to the outer membrane through different conformations. Despite the starvation conditions that the bacteria could face, this complex displays a highly efficient mechanism, so that the iron supply is guaranteed.[48] A necessary condition for such a transport is the direct contact between TonB C-terminal and OMR *N*-terminal domains.

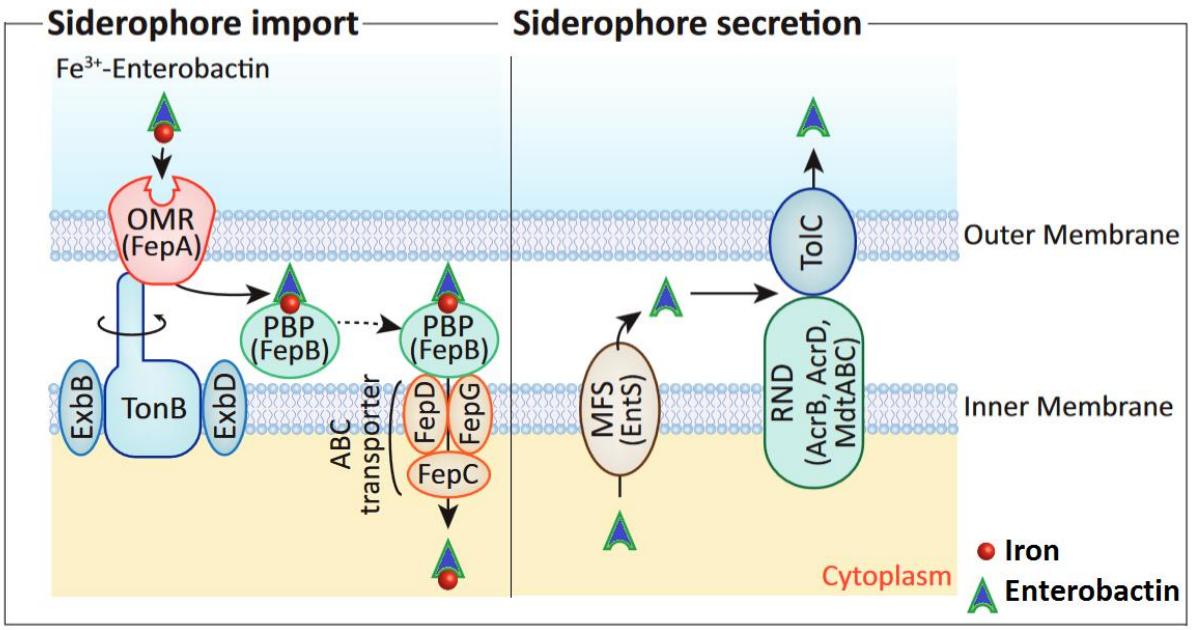

Figure 8 Scheme of Fe(III)-enterobactin import and secretion mechanism in *E. coli* (adapted from [40]).

After the translocation through the outer membrane, the periplasmic binding protein FepB (PBP) of *E. coli* enables the transport of iron-loaded enterobactin to an ABC transporter composed of FepC, FepD and FepG in the inner membrane. This ATP binding cassette transporter then promotes siderophore translocation from the periplasm to the cytoplasm.

Once in the cytoplasm, two mechanisms are possible for iron release:

- the first mechanism requires enzymes to decompose the ligand, and the formed by-product has a reduced affinity to Fe(III). As an example, the esterase Fes was demonstrated to enzymatically hydrolyze enterobactin and its iron complex, which is required for the iron release process.[49]

- the second and main mechanism is the reduction of Fe(III) to Fe(II) thanks to reductases, and consequently its kinetically and thermodynamically favored release/capture by intracellular small molecules or proteins.[45b, 50] Although aerobic environments tend to thermodynamically form Fe(III), Gram-negative bacteria have a strong reducing environment in the cytoplasm compared to the periplasmic space.[51]

After iron release, the apo-siderophore is degraded or secreted from the bacteria through efflux pumps for more cycles of Fe(III) translocation.[28, 48a, 48b, 50d] Apo-enterobactin is for example effluxed through the TolC membrane protein, but interestingly also via AcrB, AcrD and MtdABC efflux machineries, also known for the efflux of several drugs in *E. coli*.[52]

This type of transport mechanism is well suited to siderophores such as enterobactin in *E. coli*. However, the transport mechanism is not only siderophore-dependent but also species dependent. Enterobactin enters only into the periplasmic area of *P. aeruginosa* in comparison with *E. coli*.

Bacteria can import endogenous siderophores but also exogenous ones from other organisms called xenosiderophores by the use of specific uptake systems (Figure 9). In the case of *E. coli*, FhuA protein for example enables the uptake of xenosiderophores used by fungi such as *Ustilagosphaerogena* called Ferrichrome, but also coprogen or citrate.[53] The same phenomenon happens with *P. aeruginosa*, which is able to secrete the two endogenous siderophores: pyoverdine (pvd) and pyochelin (pch), but is also able to internalize xenosiderophores such as enterobactin by expressing specific receptors able to detect and translocate enterobactin complexes: pfeA [54] and pirA.[55] It has recently been shown that *Vibrio cholerae*, a major pathogen serving as a model for the *Vibrionaceae*, identifies the xenosiderophore enterobactin and transports the complex via a TonB system. The ferric reductase ViuB is not required for the reduction of some Fe(III)-siderophore complexes.[56] For some bacterial strains, the iron uptake mechanism by siderophore machineries has not yet been determined.

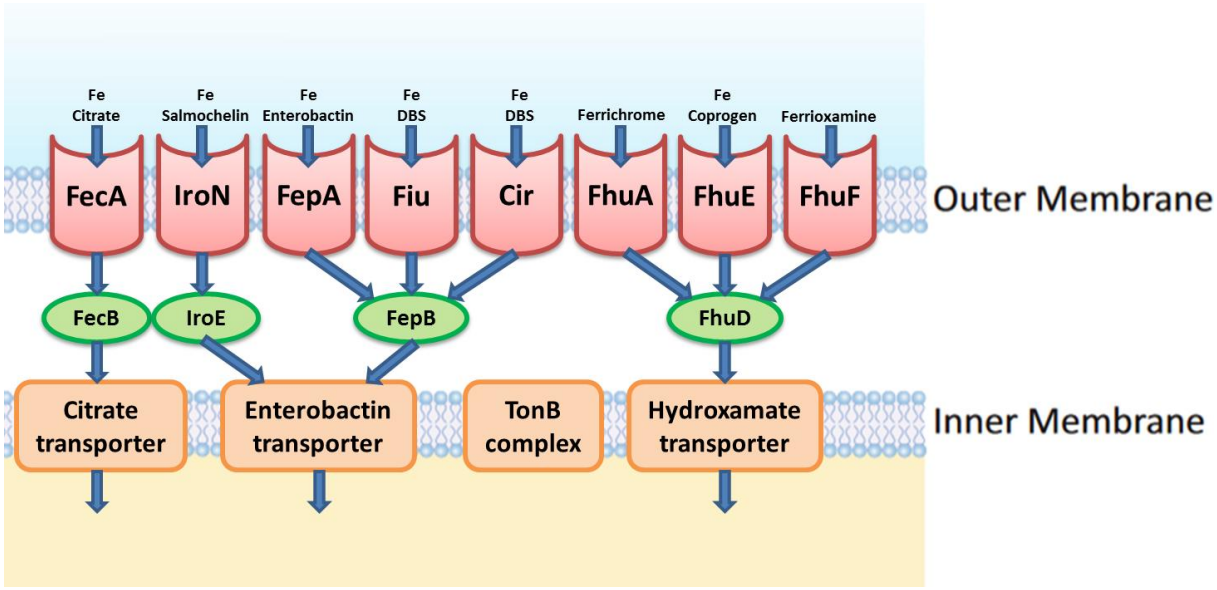

Figure 9: Scheme of different active transport of Fe(III)-siderophore complexes in *E. coli* (adapted from [50a]).

1.2.3. Description of siderophores

1.2.3.1. Siderophore structure and function

The discovery of siderophores dates back to 1912 with mycobactin.[57] The first natural catecholate was discovered in 1958. This 2,3-dihydroxybenzoic derivative was found and characterized from *Bacillus subtilis* under low iron conditions,[58] but the first tris-catechol siderophore was only identified in 1970.[59] Even today the arsenal of siderophores continues to grow and there are currently more than 500 siderophores that have been characterized from bacteria, fungi and plants.[43, 47a, 60] Each year the novel siderophores discovered result in a lot of interest among the scientific community.[61] As a matter of fact, the number of publications about siderophores on Pubmed increases constantly (Figure 10).

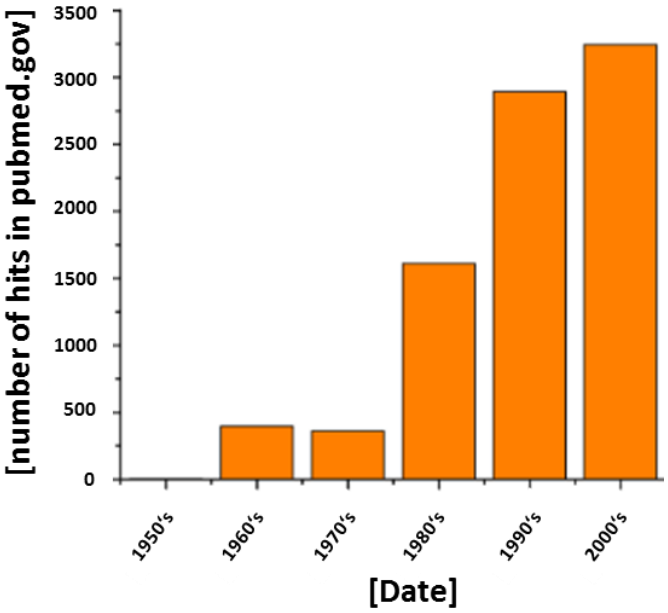

Figure 10 Illustration of the number of siderophore papers published in pubmed.gov over time (adapted from [62]).

Among all the known siderophores, several types of functional bidentate groups can interact with Fe(III). Because Fe(III) is a hard Lewis acid, it has affinity towards a hard electron-rich atom such as an oxygen. Moreover, there are few tripositive cations present in the growth environment compared to dipositive cations such as Ni(II), Cu(II), Mn(II) and Zn(II). Siderophores are more selective to the rare tripositive cations such as Fe(III). Among the hundreds of siderophores known in the literature, catecholates, hydroxamates (derived from the

acetylation of the non-proteogenic amino acid N^5-hydroxy-*L*-ornithine) and α-hydroxycarboxylates are the groups having the highest affinity and selectivity for Fe(III).[63]

The presence of hard electron-rich atoms on the ligands is required for the active translocation of siderophore complexes. Nevertheless, the rest of the molecule can vary, as long as the entire molecule is accepted by the Fe(III) transport system. Furthermore, the pK_A values of hydroxamate, catecholate and α-hydroxycarboxylate functions vary from 3.0 to 14.5 and therefore, their applications can be important depending on the environmental pH. For example, the highest Fe(III) affinity discovered at physiological pH is from catechol containing siderophores. However, at lower pH the protonation state of hydroxyl groups is less important for hydroxamates than catecholates (Table 1).

Table 1 Description of catecholate, hydroxamate, and α-hydroxycarboxylate functions and their pKa properties along with natural siderophore examples (adapted from [43]).

Name of Fe(III) binding moiety	**Catecholate**	**Hydroxamate**	**α-hydroxycarboxylate**
pK_A	9.2, 13.0	3.0, 14.5	9.0
Fe(III) complexation by the siderophore moiety	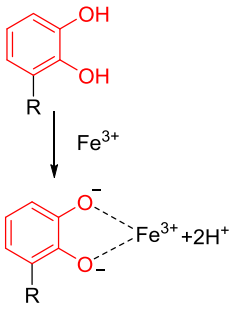	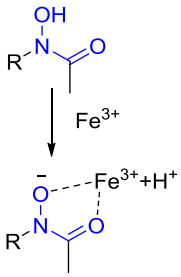	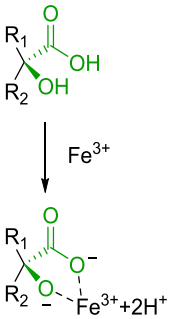
Example of natural siderophore	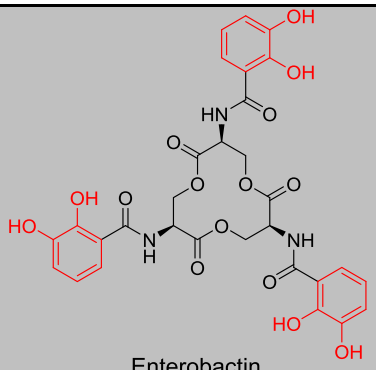 Enterobactin	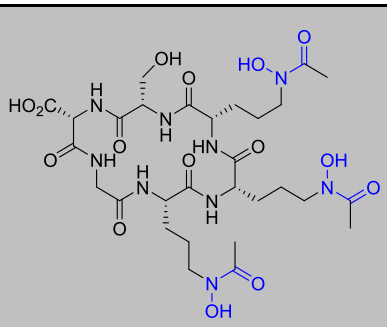 Ferrichrome	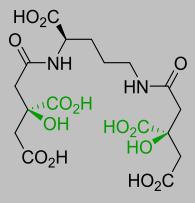 Staphyloferrin A

Catechol-type structures have in general very high affinities to Fe(III),[64] and that is the reason why they are excellent candidates for the Trojan horse strategy. The affinity of enterobactin to Fe(III) at pH = 7.4 is one of the highest ever reported in the literature (pFe = 35

at C_{Fe} = 1 µM and $C_{enterobactin}$ = 10 µM[65]). However, α-hydroxycarboxylate-typed siderophores are very often observed in acidic environment because of their relatively low pK_A. the Fe(III) affinity depends on the protonation stage of siderophores. Therefore, those presenting extremely high Fe(III)-affinities at a specific pH can have a much lower affinity compared to other Fe(III) chelators at a different pH..[66] Many natural siderophores contain several identical chelating entities that help to increase the affinity of the entire molecule to Fe(III) (Table 1). However, also mixed natural siderophores presenting more than one chemical chelating motif exist.[67]

Other chemical groups that bind Fe(III) in nature include α-amino acids, hydroxyphenyloxazolones, α-hydroxyimidazoles and salicylic acid derivatives (Figure 11).[43, 46] Bidentate ligands, involving nitrogen or sulfur as donor atoms also exist but exhibit a lower selectivity to chelate ferric iron compared to other metals.[43] Even recently, uncommon siderophores such as 7-hydroxytropolone from *Pseudomonas donghuensis* have been reported, where the ligand:Fe stoichiometry determined to be 2:1.[68]

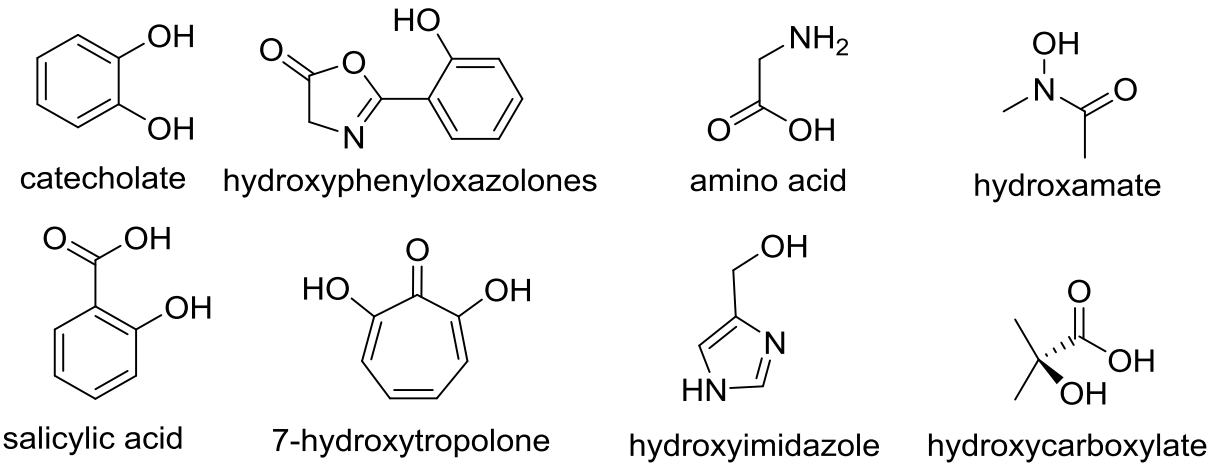

Figure 11 Structure of Fe(III) chelating functions.

Moreover, the same microbial species use different siderophores. For example, *K. pneumoniae* shows the possibility to combine the use of several siderophores such as enterobactin and salmochelin, a glycosylated enterobactin.[69] The glycosylation enables a higher hydrophilicity of the Fe(III) complex compared to enterobactin.[38] Thus, a (xeno)siderophore can be used by different bacteria, a bacterial species can produce several siderophores and use different (xeno)siderophores.

1.2.3.2. Bacterial siderophore biosynthesis

In order to work with specific siderophore-deficient strains and study the siderophoric effect of molecules, it is essential to understand the biosynthesis of siderophores of interest in Gram-negative bacteria. As one example, *E. coli* produces its main endogenous siderophore enterobactin from chorismate (Figure 12).

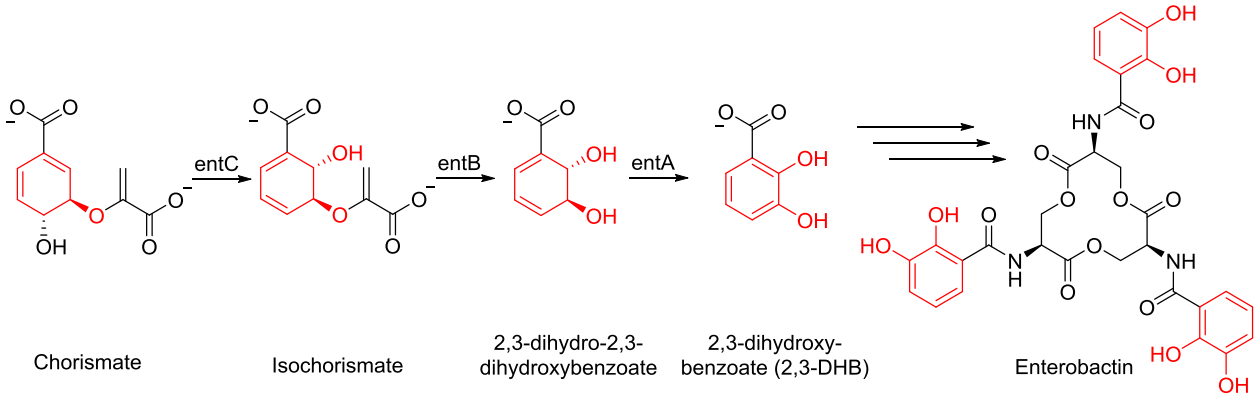

Figure 12 Biosynthetic scheme of enterobactin from chorismate.

First of all, chorismate is isomerized to isochorismate by entC and Mg^{2+} as a cofactor.[70] After the intervention of entB, triggering the elimination of the acrylate group, entA enables the oxidation of the ring to yield the aromatized 2,3-dihydroxybenzoate (2,3-DHB). After successive steps including the L-serine insertion with the help of enzymes entB, entD entE and entF, enterobactin is synthesized by *E. coli*.[71] Enzymes such as entA or entB were found to be essential for the biosynthesis of enterobactin in *E. coli*.

1.2.4. Improving antibiotic uptake by Trojan horse strategies

Iron siderophore complexes can enter bacteria cells due to a sophisticated iron uptake system that is substrate tolerant. By conjugating a labelling agent or an antibiotic to an Fe(III) complex, novel diagnosis, treatment or theranostic approaches can be available against bacterial infections (Figure 13).

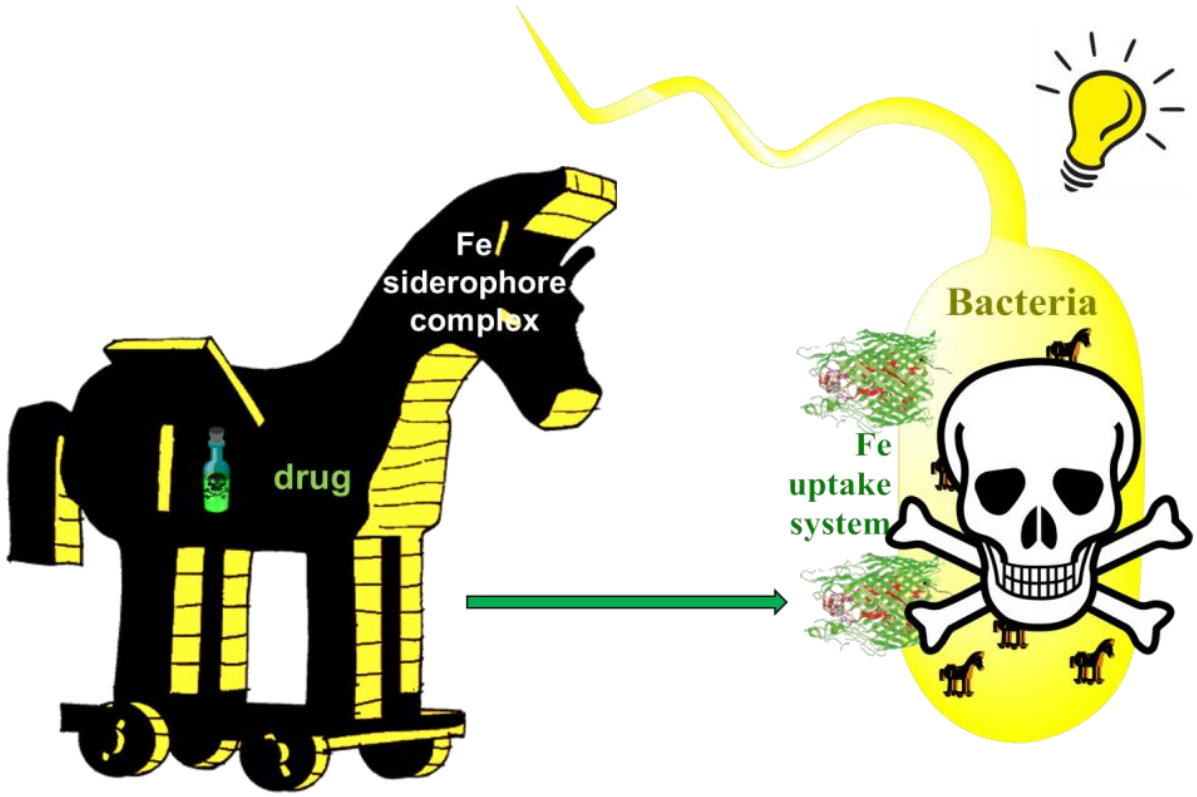

Figure 13 Trojan horse strategy against bacteria.

One important advantage of the Trojan horse strategy based on siderophore uptake systems is that bacterial iron translocation is essential for the growth of all bacteria but lactobacilli, which use cobalt and manganese instead.[72] Therefore, this strategy can dramatically decrease the bacterial permeability-related resistance mechanisms, which represents a significant issue especially concerning multidrug resistant pathogens.[73] The second main advantage is that biologically validated antibacterial scaffolds can be used, which reduces the risk of failure compared to the development of novel antibiotics. The previous extensive research on the antibiotic of interest permits efficient studies of the novel antibiotic conjugates.[74] Moreover, the commercial antibiotics of interest are clinically validated and have a known, manageable safety profile.

One of the potential threats for this strategy is the ability of the targeted bacteria to recognize the siderophore conjugate. If a bioconjugate can only enter the bacterial cell through few transporters, bacteria can prevent their translocation by transcriptional downregulation of the respective transporter. However, this resistance mechanism is unsuitable for conjugates that use many transport pathways.[75]

1.2.5. Trojan horse strategy inspired from natural sideromycins and examples in literature

1.2.5.1. Natural sideromycins

When actively transported, antibiotics are faster taken up by bacteria and at higher concentrations, resulting in more potent MIC values. In the best cases, active transport can enable an up to 1000 fold favorable ratio between the cytoplasmic and the external concentration.[42b] The Trojan horse strategy has also been observed in nature where microorganisms are able to produce toxin siderophore conjugates called natural sideromycins which under stress conditions fight against iron thievery to trigger the death of competing cells.[76]

One example of such molecules is salmycins (Figure 14). Salmycin B was isolated from *Streptomyces violaceus* DSM 8286 in 1995.[77] This group of compounds had MIC values lower than 10 nM against *Staphylococci* and *Streptococci*, including resistant strains.[48d] Some groups proposed a mechanism by which the antibiotic component was released by intramolecular cyclization.[78]

Another example of natural sideromycins is represented by the albomycins.[79] Albomycins contain a trihydroxamate-based siderophore portion and a thioribosyl-pyrimidine moiety. The thioribosyl-pyrimidine is a seryl-*t*-RNA synthetase inhibitor and it is cleaved by the action of a serine peptidase N. This drug release [80] results in potent inhibition of Gram-positive and Gram-negative bacteria *in vitro* and in mouse models.[81]

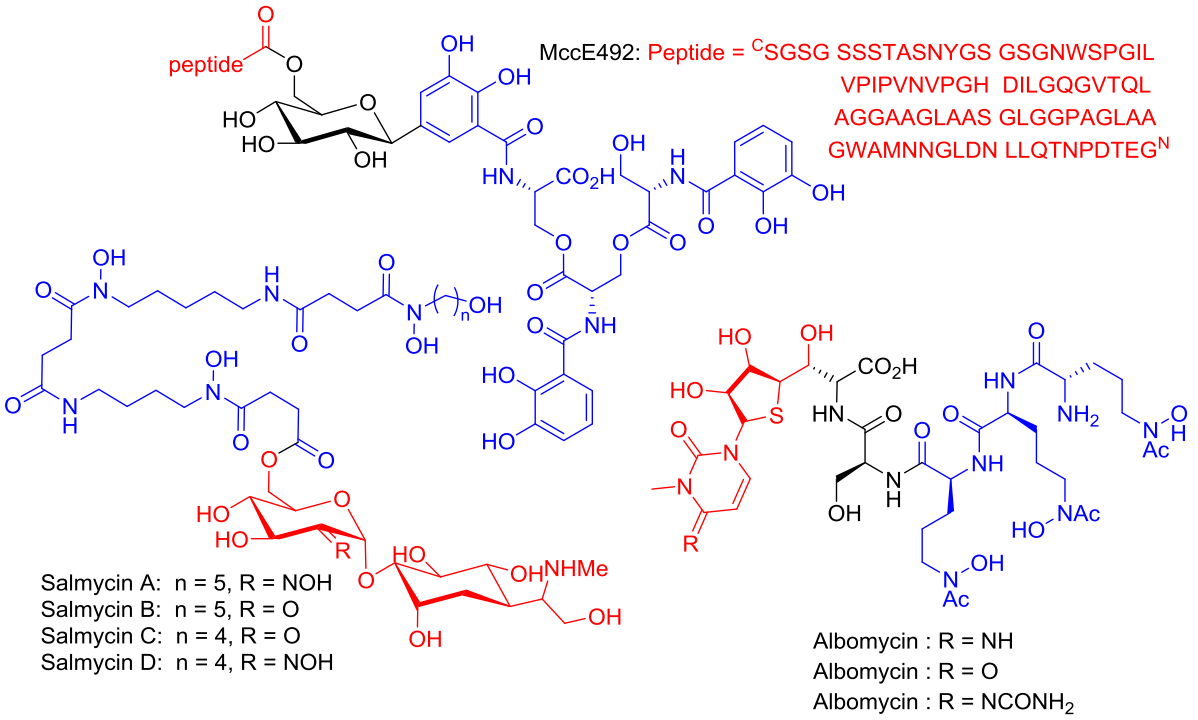

Figure 14 Chemical structures of three classes of natural sideromycins: salmycins, albomycins and microcins (adapted from [82]).

Some natural sideromycins are even able to carry large molecules such as antimicrobial peptides. For example, microcin mccE492 is a 22 kDa protein[83] showing the potential of siderophores to be tremendous drug carriers.[84]

1.2.5.2. Synthetic sideromycins in early-stage

Scientists were inspired by this natural strategy to design novel sideromimics in order to improve the *in vitro* and *in vivo* efficacy, to extend their activities from Gram-positive bacteria to Gram-negative bacteria and improve activity against drug resistant bacteria.

Research has mainly focused on Gram-negative strains, generally less sensitive to antibiotics, because they are protected by an outer membrane permeability barrier.[85]

Miller's research group conjugated ampicillin and amoxicillin to an acetylated tris-catechol construct, which enhances the MIC compared to the parent drug (Figure 15). He also enabled the activity of daptomycin conjugates against *A. baumanii* by conjugating lactivicin to filmsbactin, a mixed natural siderophore from *A. baumanii*.[86]

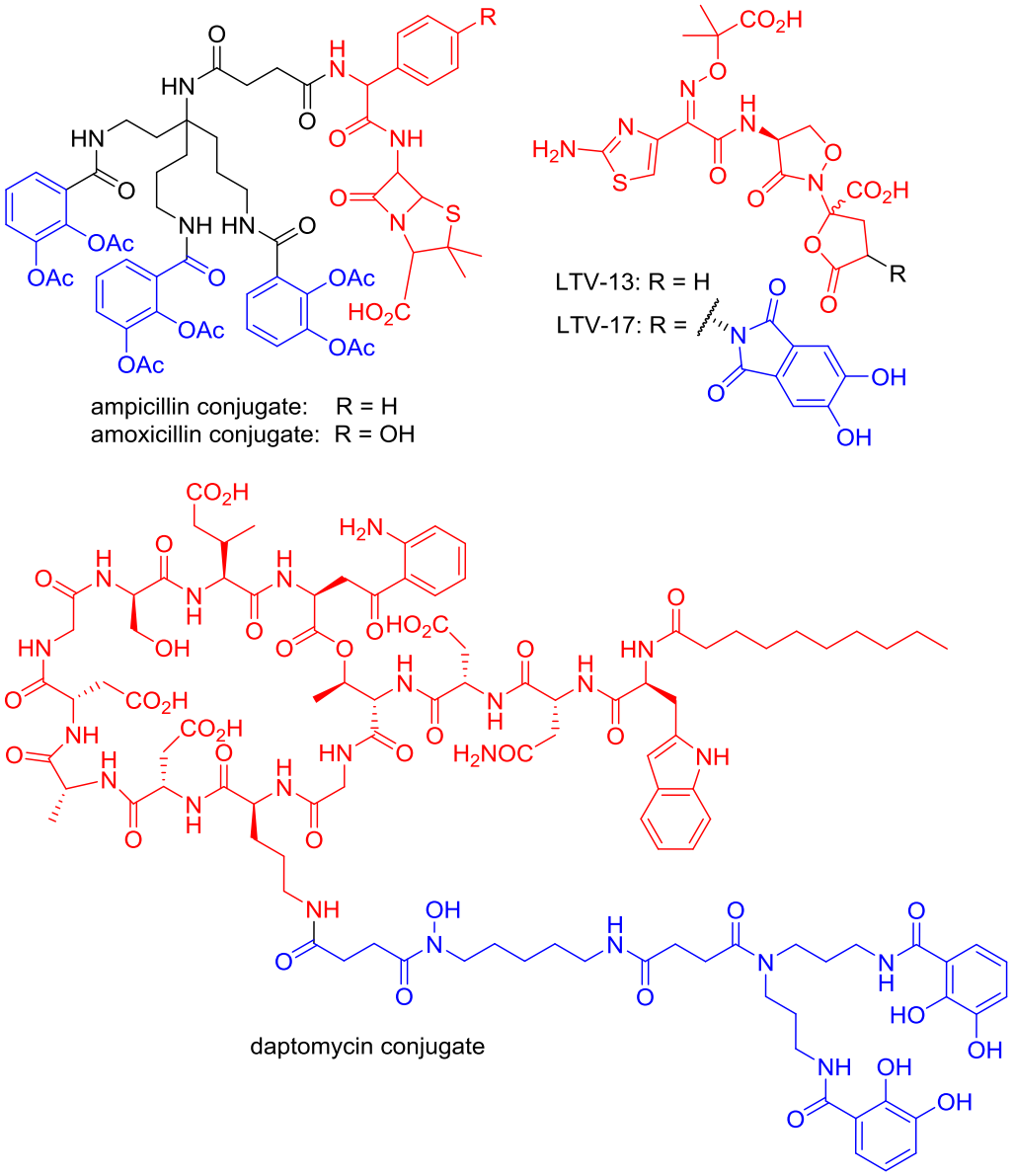

Figure 15 Chemical structures of two ß-lactam, daptomycin or lactivicin siderophore conjugates.

Other research groups also investigated the Trojan horse strategy on other antibiotics such as lactivicin conjugates: natural non β-lactam products that inhibit PBP[87] conjugated with different siderophores such as pyridones or catechols.[88] In particular, LTV-17 reached a 1000 fold improvement in the MIC against *stenotrophomonas maltophilia* K278a, compared to LTV-13 which does not contain any siderophore.[89]

1.2.5.3. Synthetic sideromycins in clinical trials

BAL30072 is a monosulfactam derived from tigemonam conjugated to dihydroxypyridone,[90] a bioisoster of catechol also known to bind Fe(III) and developed by Basilea (Figure 16).[91] BAL30072 passed a clinical phase 1 trial and showed greater activity than antibiotic comparators such as rifampicin.[91-92] The complex is thought to be actively transported into the bacteria.[93] In addition, the conjugate presented good activities against other Gram-negative bacteria in *in vitro* studies, against *A. baumannii in vivo*, and showed synergic effects with carbapenems.[91, 94]

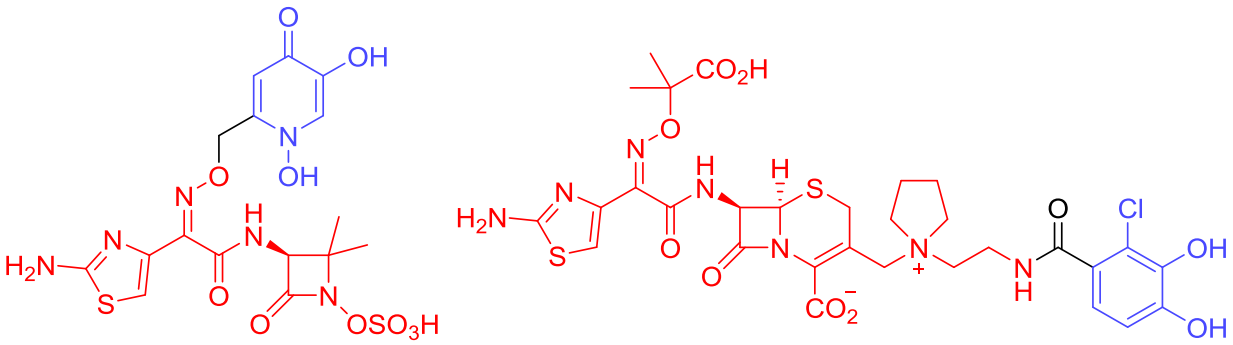

Figure 16 Chemical structures of BAL30072 and S-649266.

An improved ß-lactam version called S-649266[95] or cefiderocol, a catechol/cephalosporin conjugate from Shionogi pharmaceuticals, is currently in phase 3 clinical trials.[96] The chloro group on the catechol improves its stability.[97] This compound family is a promising siderophore conjugate application. For example, the molecule showed high activities especially against Gram-negative bacteria such as *P. aeruginosa, A. baumannii* and *K. pneumoniae*[95a, 98] and passed a clinical phase II study (Table 2). Moreover, the conjugate showed high stability to hydrolysis by carbapenemases with very low k_{cat}/K_M values with different molecular classes of ß-lactamases.[95b]

Table 2 Representation of the activity of cefiderocol compared to other ß-lactams against an extensive number of bacterial isolates (taken from [96]).

Organism (number of isolates)	MIC_{90} (µg/mL) S-649266	Cefepime	Piperacillin/Tazobactam	Meropenem
ESBL producers				
***E. coli* (50)**	0.25	>64	128	0.063
***K. pneumoniae* (50)**	0.5	>64	>256	0.125
***E. cloacae* (10)**	4	>64	128	0.5
***MBL producing P. aeruginosa* (33)**	4	>64	256	>32
Multidrug resistant				
***P. aeruginosa* (30)**	1	>64	>256	>32
A. baumannii (30)	4	>64	>256	>32
NDM-1 producers (50)	4	>32	-	>16
KPC producers (47)	0.5	>64	>256	>32

2. Aim of the thesis

Siderophores are essential Fe(III) chelators that are actively translocated into bacteria. On the other hand, the efficacy of intrinsically potent antibiotics is impaired by insufficient bacterial uptake. Therefore, siderophore conjugates are investigated as tools to improve antibiotic uptake. In this line, the aim of the doctoral thesis is divided into three distinct parts.

First of all, the Fe(III) affinity of designed, synthetic siderophores should be studied and compared to natural siderophores. For this purpose, Fe(III) chelating moieties should be coupled to a tetrapodal core called DOTAM, which can chelate an additional metal (Gd, Ga, Cu etc.) and an additional ligand.

Secondly, a wider series of artificial siderophores should be designed and synthesized. Their siderophoric effect should be assessed in order to optimize their chemical structures through iterative design-make-test cycles. The synthesis of fluorescently labelled conjugates was envisaged that permit the assessment of the bacterial labelling capacity of the synthetic siderophore conjugates as well as their internalization into bacterial cells.

Lastly, antibiotics should be conjugated to synthetic siderophores in order to assess the potential of siderophores to improve the antibacterial activity of antibiotics. In parallel, the toxicity properties of siderophores and siderophore conjugates should be evaluated.

3. Results and discussion

3.1. General synthetic siderophore (conjugate) design

This thesis is focused on improving the uptake of siderophore-based conjugates and the application of the optimized system to payloads of interest. Siderophore systems have been designed in a general manner and then modified to explore the effect of the core molecule, of the linker nature, the type of siderophore and the payload of interest (Figure 17).

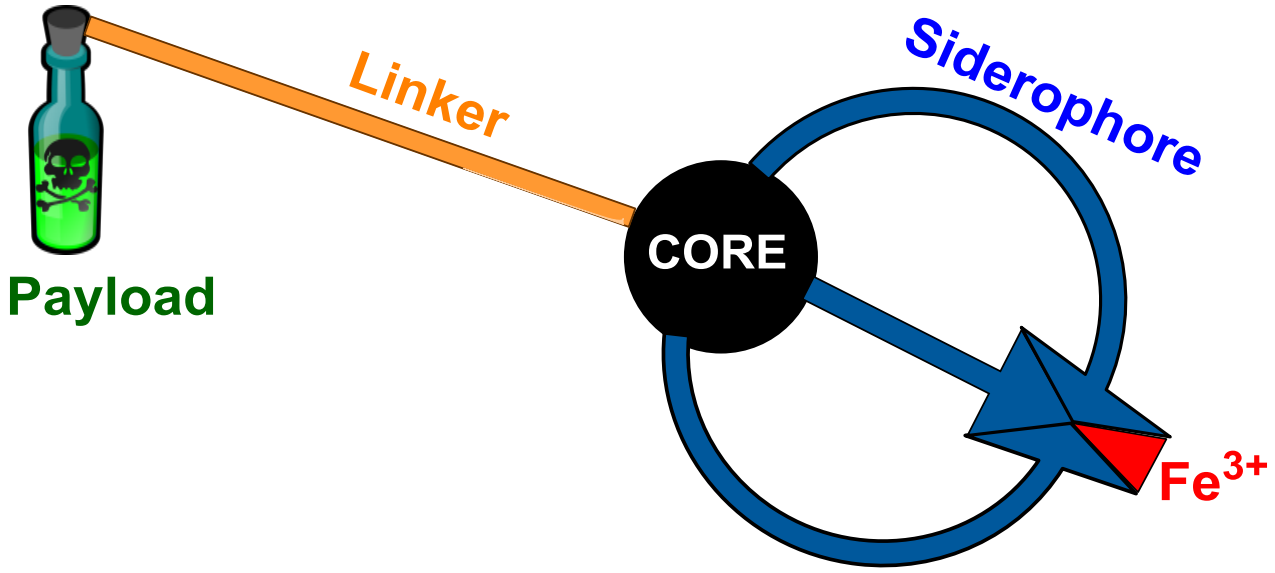

Figure 17 General structure of hexavalent siderophore conjugates.

Each synthetic conjugate is composed of a siderophore, a core unit, a linker and a labelling agent or a toxin moiety: each component is crucial to obtain a functional molecule. Non-mixed siderophore have the advantage of a straightforward chemical access. In addition, many natural siderophores such as enterobactin or ferrichrome are hexavalent siderophores. Therefore, the scope of this thesis is limited to the synthesis of non-mixed hexavalent siderophores. In order to increase the efficiency of the Trojan horse strategy, once the siderophore synthesis was established, the ability of the siderophore moieties to bind Fe(III) in competition with natural siderophores must be checked. As already mentioned, the natural tris-catecholate siderophore enterobactin shows a very high Fe(III) affinity under physiological conditions (pH = 7.4).[65] Therefore, the synthetic siderophore designs were based on enterobactin's chemical structure (Figure 18). Moreover, the amide functions observed in enterobactin between the catechols and the core scaffold were found to be beneficial.[71]

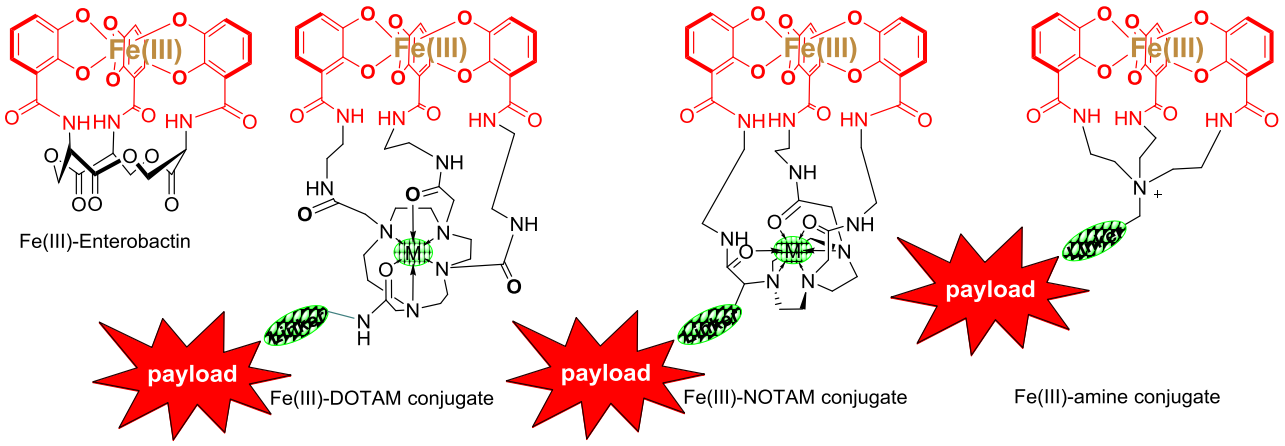

Figure 18 Proposed general 3D representation of designed synthetic siderophore complexes based on known complex crystal structures[99] compared to Fe(III)-enterobactin[100] complex.

A few research groups have previously used acylated catechols as pro-siderophores that are later activated by secreted bacterial esterases to promote selective internalization. This approach avoids pharmacological side methylation of the free hydroxyl version by catechol *O*-methyl transferases (COMT),[101] leading to the inactivation of the siderophoric Fe(III) chelator.[50d, 86, 97] Moreover, the use of acetyl groups also facilitates the chemical synthesis by using protecting groups which will not be deprotected.

The core unit is not essential for the Fe(III) complexation, but this part is crucial for the translocation of the entire Fe(III) complex and the modulation of Fe(III) affinity. This thesis focuses on tetrapodal-cored siderophores, where three arms are dedicated to the attachment of three siderophore moieties whereas a 4th arm is designed for the addition of variable linkers and payloads. The macrocyclic DOTAM, amine and NOTAM scaffolds were investigated and compared. A key advantage of DOTAM derivatives is the option to use the DOTAM as a positron emission tomographic (PET) imaging tracer that could be used in clinical studies, with Ga(III) for example. It is noteworthy to pinpoint the low concentration needed for such tracers in comparison with today's labelled glucose techniques, the low and short dosimetry, the short imaging protocols and the high diagnostic accuracy.[102] Cu(II) but also Ga(III) can be complexed for the enhancement of antibacterial and antibiofilm properties.[103] The DOTAM molecules also show a straightforward synthesis, high solubility, a low toxicity and are biocompatible.[22] The NOTAM core is a smaller tripodal core, but one of the arms can be derivatized like in NODAGA derivatives[104] in order to enable the conjugation of a payload. The NOTAM core also shows higher affinity to Ga(III).[105] The amino core has the advantage of being very small and compact. Furthermore, the idea of conjugating a payload on this amino center would trigger a very soluble, small, positively charged

quartenary amine. Previous studies have shown that the use of spacer groups such as a glycine could increase the siderophore activities.[106]

The payload of interest can be a labelling agent or an antimicrobial entity which are attached to the carrier part without spoiling any initial interaction with the target of interest. In other words, first of all, the structure-activity relationship (SAR) of the payload, but also the cellular accessibility of the target must be considered.[81] Second of all, the choice of the payload and consequently of the target determines if a cleavable or a non-cleavable linker is necessary for the final target interaction. The choice of the designed molecule will depend on the mode of action of the antibiotic and of the interactions with the specific protein.

3.2. Aim 1: Studies on Fe(III) complexation

3.2.1. Siderophore probes for Fe(III) complexation studies

Four siderophore mimics based on DOTAM scaffold were retrosynthetically designed from the commercially available cyclen molecule. The synthetic route was planned to be 3 to 5 steps long, depending on the chemical strategy and on the need to deprotect the catechol groups or to complex the DOTAM center (Figure 19).

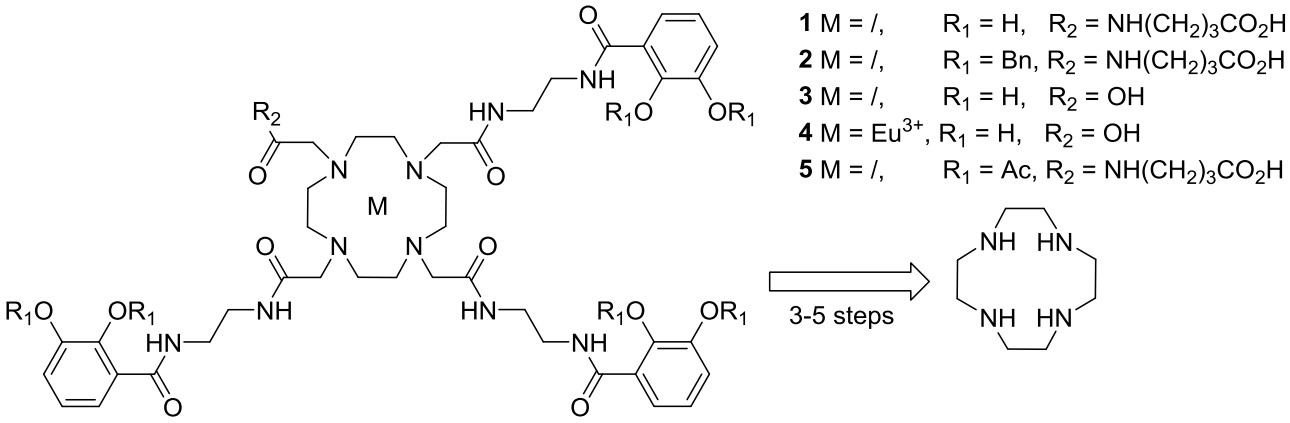

Figure 19 Design of siderophore probes for complexation studies.

Considering that an amine must be present for the coupling of the necessary carbonyl group of the DOTAM center, and that the catechol has a benzoic acid function, it was decided to add an ethylene diamine spacer between the DOTAM core and the catechols. This relatively short linker has the advantage of giving more flexibility for the Fe(III) complex formation between the three catechols. As an essential negative control, benzylated catechols were chosen. They were preferred in comparison with a methylated version, although both types of protecting groups are

stable under physiological conditions. Nevertheless, the benzylated catechols were preferred due to the relatively mild and easy-to-process cleavage by hydrogenation. The comparison between **1** and **3** will enable to observe the effect of the side chain R_2 on the Fe(III) complexation. On the other hand, comparing **3** and **4** will permit to observe the effect of the Eu(III)-DOTAM complexation on the Fe(III) complexation. The Eu(III) ion was chosen among other possible metals due to its widely known complexation to DOTAM cores and due to its further interesting Magnetic Resonance Imaging (MRI) contrasting agent properties.[107] Finally, **5** is the acetylated version of **1**. As acetylated versions of siderophores can be used as a prodrug or pro-carrier, [101] studies were performed to analyze the deacetylation process of **5** and the Fe(III) complexation of its deacetylated version.

For many target molecules, 2-bromo-carbonyls must be synthesized. The bromo derivatives will further be used for the selective alkylation of cyclen. Compound **32** was obtained following published methods[108] in three steps with a selective benzyl protection of 2,3-dihydroxybenzoic acid, followed by an amide coupling with *N*-Boc-ethylenediamine and a selective deprotection of the Boc group. The compound **34** was obtained by selective benzyl protection of γ-aminobutyric acid. The free amine functions of compounds **32** and **34** were reacted with bromo acetylbromide under similar conditions to perform an amide coupling in order to obtain the crude materials **33** and **35** with yields of 91 and 90 % respectively (Figure 20).

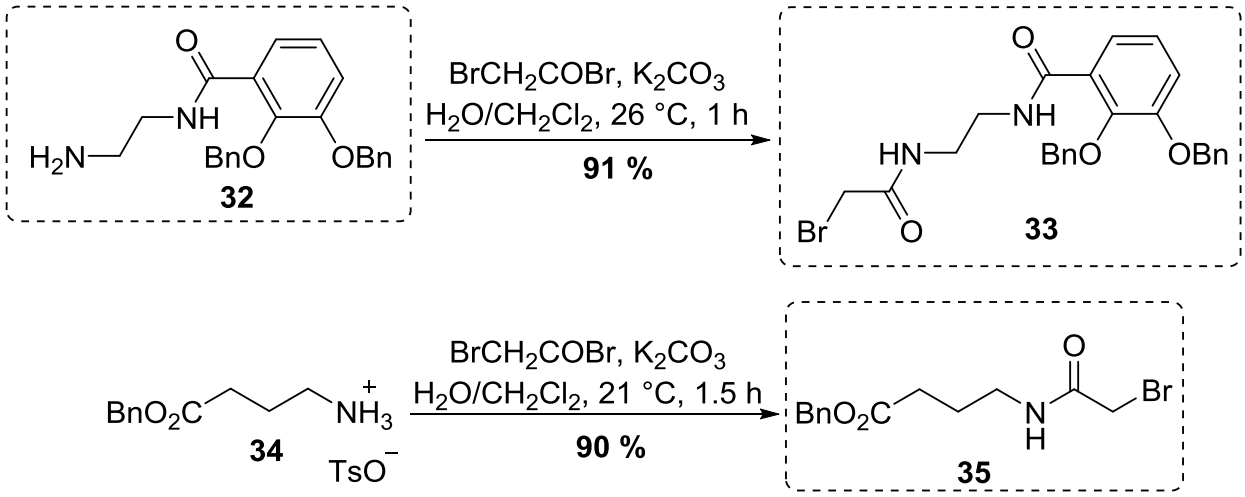

Figure 20 Synthesis of a catechol arm and a GABA linker.

Once the linkers were prepared, several strategies were persued to assemble the functionalized DOTAM cores. The first one consisted of decorating the DOTAM center first until the synthesis of the intermediate **38** (Figure 21). After optimizing conditions especially to 3.3 equivalents of diluted alkylating agent addition, the triple alkylation of the cyclen was obtained with a favorable distribution. A large excess was avoided to prevent the formation of the tetra-

substituted compound as a major product.[109] However, mono- bis- and tetra-alkylated species were observed by LCMS. The mono- and bis-alkylated products were separated during the aqueous workup. The tetraalkylated one is an unreactive molecule for the next alkylation and could be separated by RP column chromatography. The amide coupling of **32** to the HATU activated **37** led to the isolation of **38** with a yield of 91 %. To potentially accommodate a Eu(III) ion into the DOTAM core, $EuSO_3CF_3$ was added in MeOH in presence of **38**. The benzylated catechols were deprotected by hydrogenation, yielding compound **4**. A similar deprotection step was used to convert **38** to **3**. A second route involved is to directly use the advanced bromo-containing intermediates **33** and **35** and alkylate the cyclen via similar methods to reach the end of the synthesis of **1** and **2** within three steps. This strategy showed the highest yields and the fastest synthetic pathways.

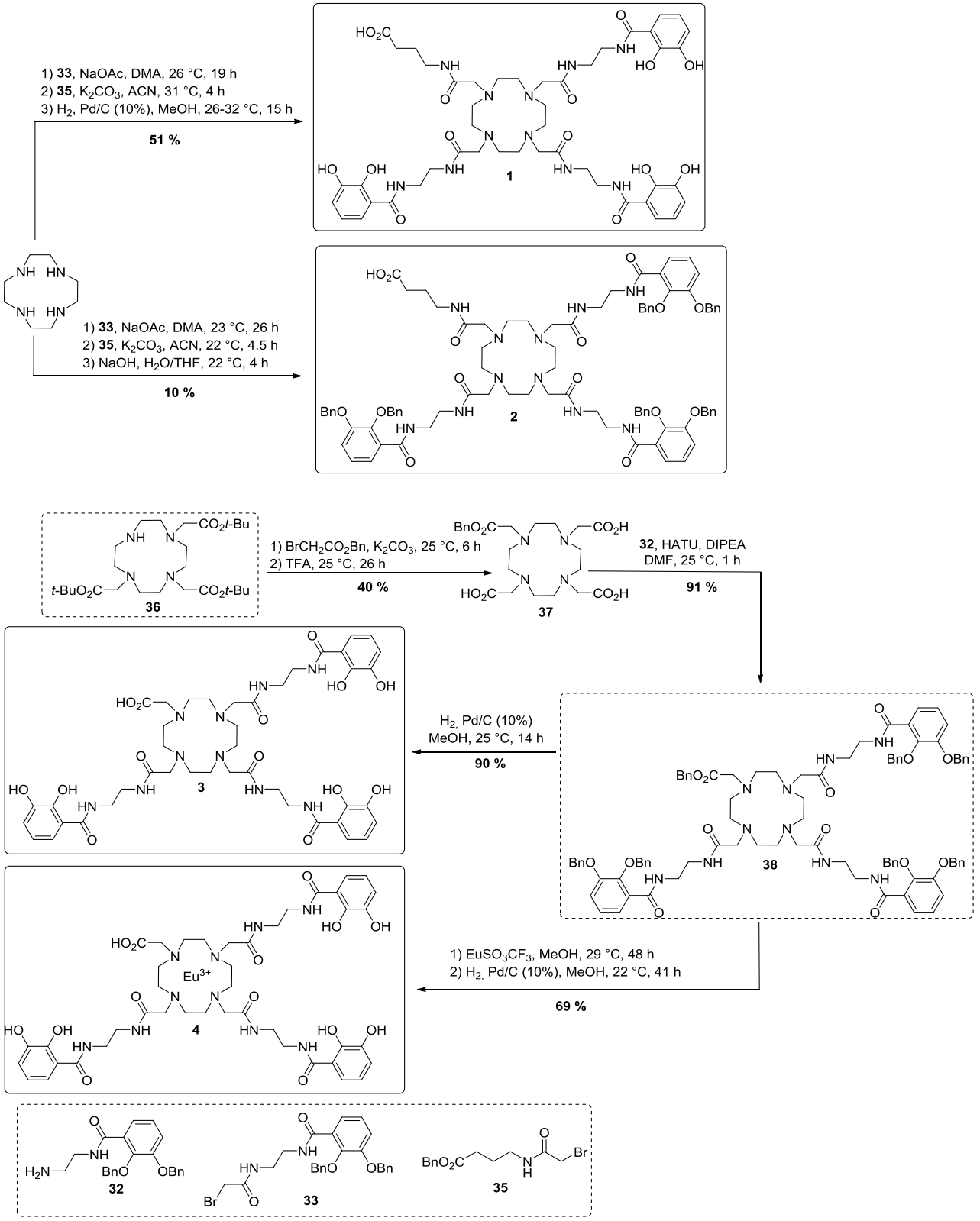

Figure 21 Synthesis of probes **1-4**.

The compound **5** was obtained in 5 steps starting from cyclen (Figure 22). After having reproduced literature-known conditions to form compounds **39**,[110] and **40**[111], a tris alkylation of the ethylene diamine derivate **39**, followed by a mono alkylation of the *O*-benzylated GABA linker **35**, and a direct mild TFA deprotection of the Boc protecting amine, enabled the isolation of the tris-amine **41**.

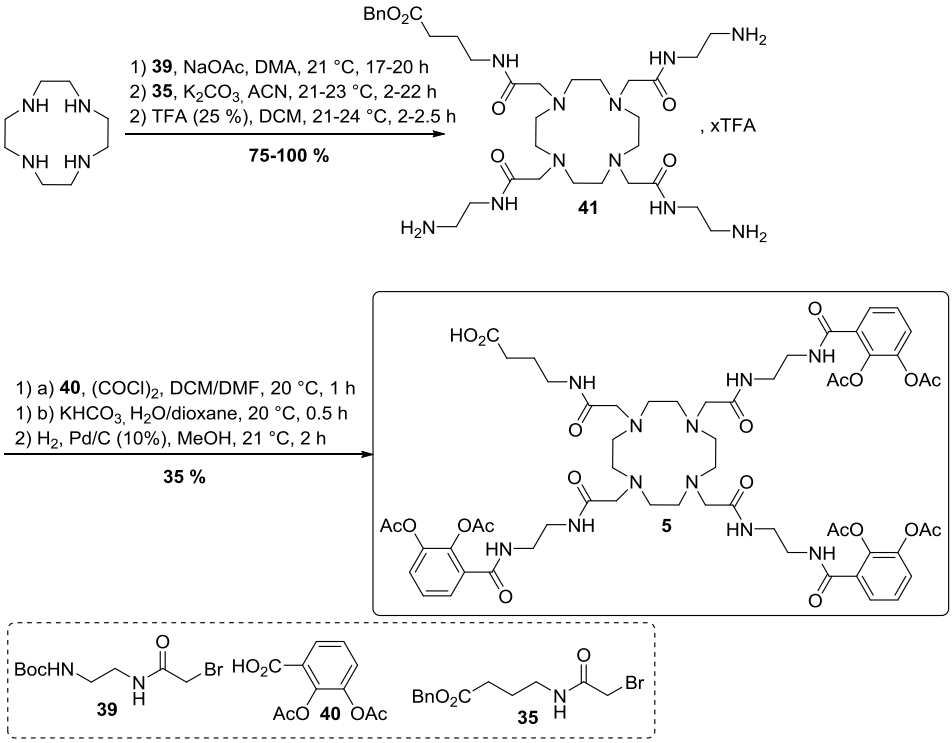

Figure 22 Synthesis of probe **5**.

An acyl chloride activation of the acetylated catechol **40**, and Schotten-Baumann conditions permitted the tris amide coupling of the siderophore moiety onto the DOTAM scaffold without significant deacetylation. This intermediate was directly hydrogenated to deprotect the carboxylic acid from its benzyl protecting group, in order to obtain **5** with an overall yield of 26 %.

3.2.2. The Fe(CAS) assay

The Fe(III) affinity of the synthetic probes **1-4** was checked by using the conventional colorimetric Fe(chrome azurol S) (Fe(CAS)) assay with a constant Fe(CAS) final concentration of 3 µM. CAS is a strong red dye, but when complexed with Fe(III), a strong blue colour is formed. Therefore, the complexation of a chelator of interest to Fe(III) can be observed by colorimetry as soon as its affinity towards Fe(III) is higher than for CAS. As a first step, the absorbance spectra of two representative samples were recorded to determine the optimal wavelength for the analysis of the CAS assay. The full spectrum of a freshly prepared Fe(CAS) solution was compared to the

spectra obtained with an excess of 3 eq of **3** and to those obtained with 3 eq of enterobactin as a positive control (Figure 23).

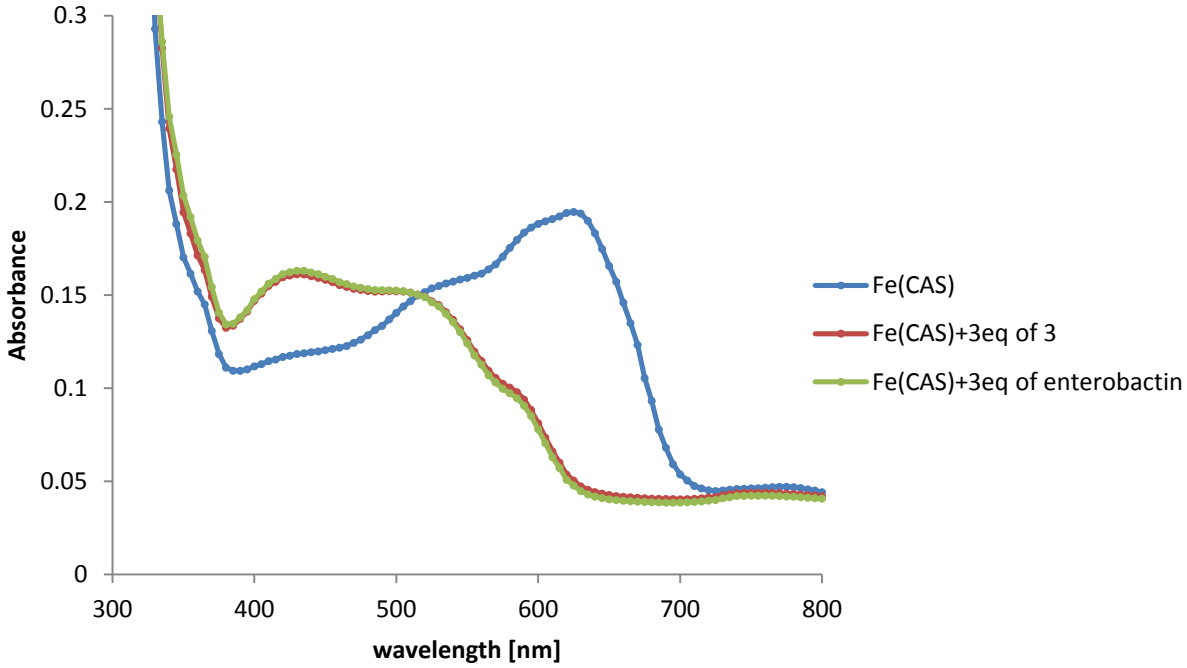

Figure 23 Absorbance spectra of Fe(CAS) under various conditions.

As earlier reported,[112] the absorbance at around 620 nm mainly depends on the concentration of Fe(CAS) in solution. A maximum of absorbance was observed at 620 nm, whereas when either enterobactin or the synthetic analogue **3** was added in excess, the absorbance decreased.

The Fe(CAS) method was established with a constant concentration of 3 µM of Fe(CAS) solution in a 96-well plate, and with an increasing concentration of probe **1-4** or enterobactin in a constant final volume of 200 µL (Figure 24).

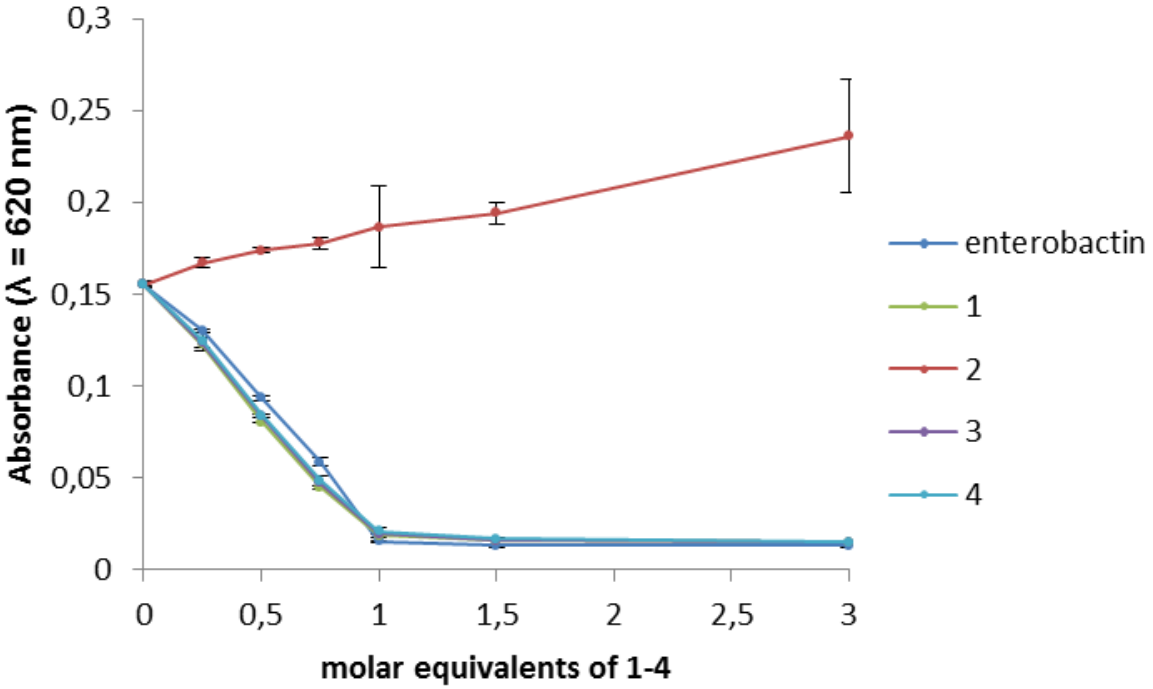

1 M = /, R_1 = H, R_2 = $NH(CH_2)_3CO_2H$
2 M = /, R_1 = Bn, R_2 = $NH(CH_2)_3CO_2H$
3 M = /, R_1 = H, R_2 = OH
4 M = Eu^{3+}, R_1 = H, R_2 = OH

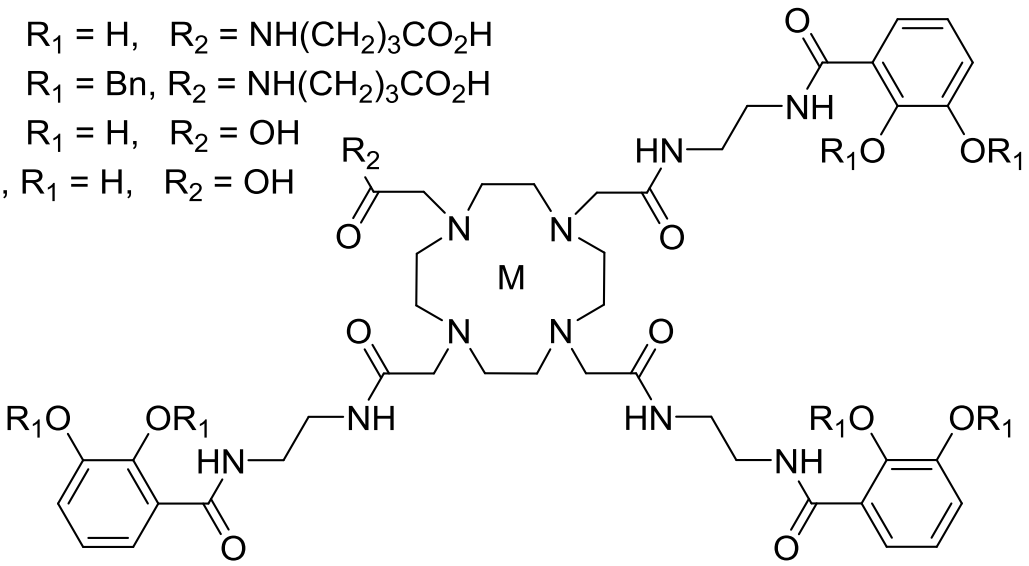

Figure 24 Iron binding assays using Fe(CAS) with **1-4** and enterobactin at λ = 620 nm.

Whereas **1** bound 1 equivalent of Fe(III), no binding was observed for **2**. This observation indicates that Fe(III) is complexed due to the free catechol moieties, but not due to the DOTAM core alone. This result also demonstrates that the ligand **1** forms a 1:1 complex with Fe(III) as it is extensively described for triscatechol-typed siderophores in the literature.[71] Moreover, enterobactin, **3** and **4** showed a similar pattern to **1**. Eu(III) does not seem to bind to catechols and its presence does not disturb the Fe(III) binding in the Fe(CAS) assay. It was therefore concluded that the core modification from the natural trislactone to the DOTAM scaffold, the extension of the

4th DOTAM arm to a GABA linker or the complexation of the DOTAM center to Eu^{3+} did not affect Fe(III) complexation in this experiment. This conclusion is in line with the literature studies on other artificial siderophores which have reported that modified cores of natural siderophores still led to Fe(III) complexation.[65]

3.2.3. MS-MS assay for deacetylation and complexation studies

In order to confirm the deacetylation and Fe(III) complexation of **5**, we first validated the Fe(III) complexation process of its deacetylated version **1** (Figure 25). To prove the existence of the Fe(III) complex, $FeCl_3$ was added to an equimolar **1** solution in ACN/H_2O (1/1) and stirred for 24 h at pH = 8.2. Afterwards, a high-resolution mass spectrometry (HRMS) measurement was performed to compare the observed isotope pattern to the theoretical isotope pattern.

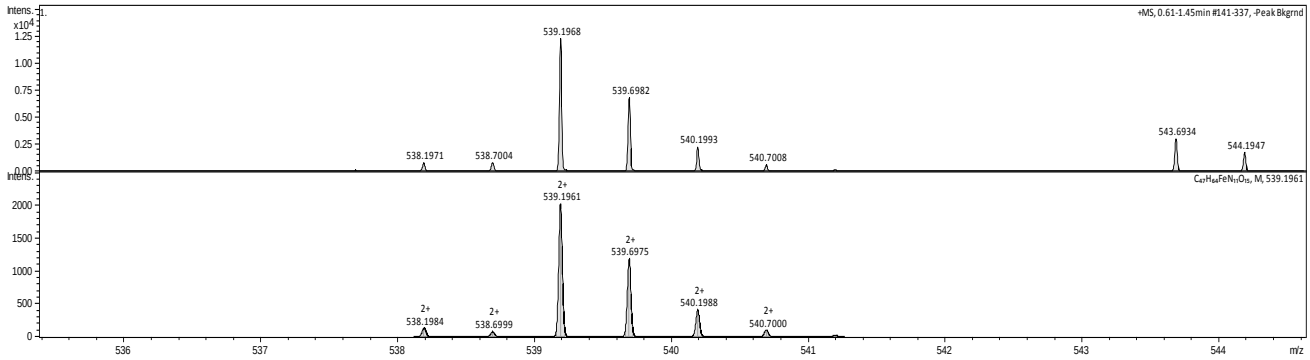

Figure 25 Isotope pattern of **1 + Fe(III)**, as measured (upper) and predicted (lower).

The detected isotope pattern was characteristic of an Fe(III) containing molecule and showed high similarities to the one predicted with an acceptable error of 1.3 ppm. Therefore, the Fe(III) formation could be observed by HRMS analysis.

The sample and the molecular weight information were then used to set up a multi reaction monitoring (MRM) method along with **1** and **5** (Table 3). For each entity, fragmented qualifier and quantifier ions could be observed. The strongest quantifier ion was used for quantification relative to a standard curve and the second strongest quantifier ion was used for explicit identification of the target molecule (qualifier). The correct ion mass supported the structure of the molecule. As an example, the precursor quantifier ion observed for **5** is its doubly charged version, and a detected fragment corresponded to its tris-deacetylated version. By extension, all the depicted ion masses observed for **1 + Fe(III)** could be assigned to Fe(III) containing proposed structures. This suggests that the observed quantifiers and qualifiers are characteristic of the Fe(III)-**1** complex.

Table 3 Ion transition of MRM analysis. Ion transitions used for identification of acetylated, deacetylated and Fe-complexed DOTAM siderphore by tandem mass spectrometry.

MOI	Precursor ion mass (Da*)	Proposed structure	Fragment ion mass (Da*)	Ion	Proposed structure
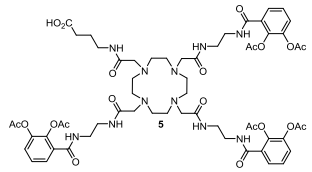	638.9*	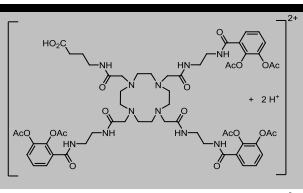	575.6*	Quantifier	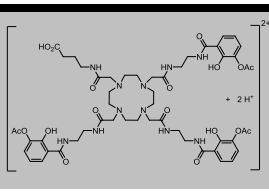
	638.9*	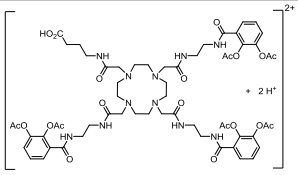	137.0	Qualifier	
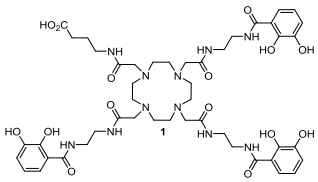	512.8*	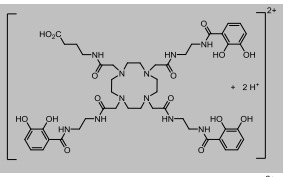	137.1	Quantifier	
	512.8*	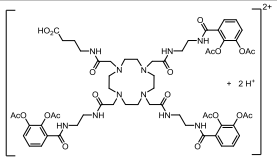	180.1	Qualifier	
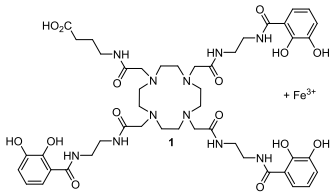	539.3*	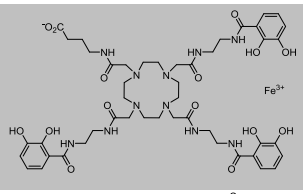	471.3*	Quantifier	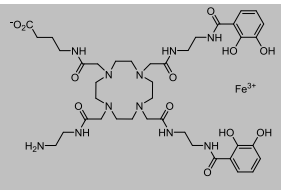
	539.3*	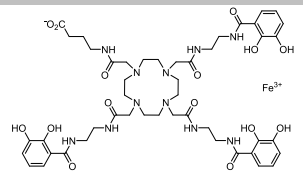	335.3*	Qualifier	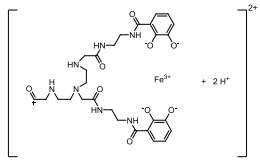

* All ions were doubly charged, as verified by full scan experiments

This study enabled kinetic experiments on the degradation or the formation of specific species, based on the quantifier ion, in the presence of living bacterial cells. After exposure of **5** in LB medium and *E. coli ΔentB*, **5**, **1** and **1 + Fe(III)** were quantified over 24 h (Figure 26).

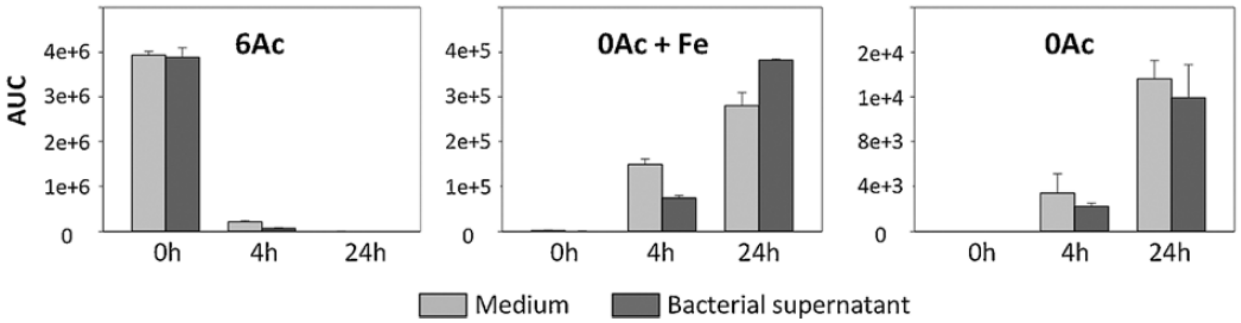

Figure 26 Relative quantification of deacetylation and iron complexation of **5**.[3] Compound **5** was incubated in LB media at a final concentration of 10 µM with (black bars) or without E. coli ΔentB (gray bars), extracted at the indicated time points, and quantified by LC-MS/MS. Area under the curve (AUC) values represent the abundance of the monitored quantifier ion for each molecule and are shown for **5** (with 6 acetyl groups: 6Ac, left), **1** in complex with Fe(III) (0 acetyl groups: 0Ac+Fe, middle), and **1** (0 acetyl groups: 0Ac, right). Ac=acetyl.

The intermediate compounds **5**-nAc and [Fe(**5**-nAc)] when n ϵ {1, 2, 3, 4, 5} could not be observed by LCMS in detectable amounts. However, the complete deacetylated product of **5** could be observed in increasing concentrations over time, proving the total deacetylation process of **5**. Moreover, the same characteristic was observed for the formation of Fe(III) complex. Therefore, the Fe(III) complexation of the deacetylated intermediate also occurs. However, for each experiment, bacterial supernatant and medium were separated and independently measured by MRM methods, and no significant differences could be observed. These results indicate a spontaneous deacetylation of the compounds in medium, even in the absence of bacterial enzymes.

3.3. Aim 2: Demonstration of siderophore uptake

3.3.1. Growth recovery assay

3.3.1.1. Siderophore probes for growth recovery assay studies

Our case studies are focused on two types of Gram-negative bacteria: *E. coli* and *P. aeruginosa*. Both bacterial strains are able to produce endogenous siderophores with catechol and hydroxamate functionalities and with different core designs. Therefore, this study will focus on synthetic catecholate and hydroxamate type siderophores (Figure 27). Also, three different cores were investigated: the DOTAM, the NOTAM and the amine core.

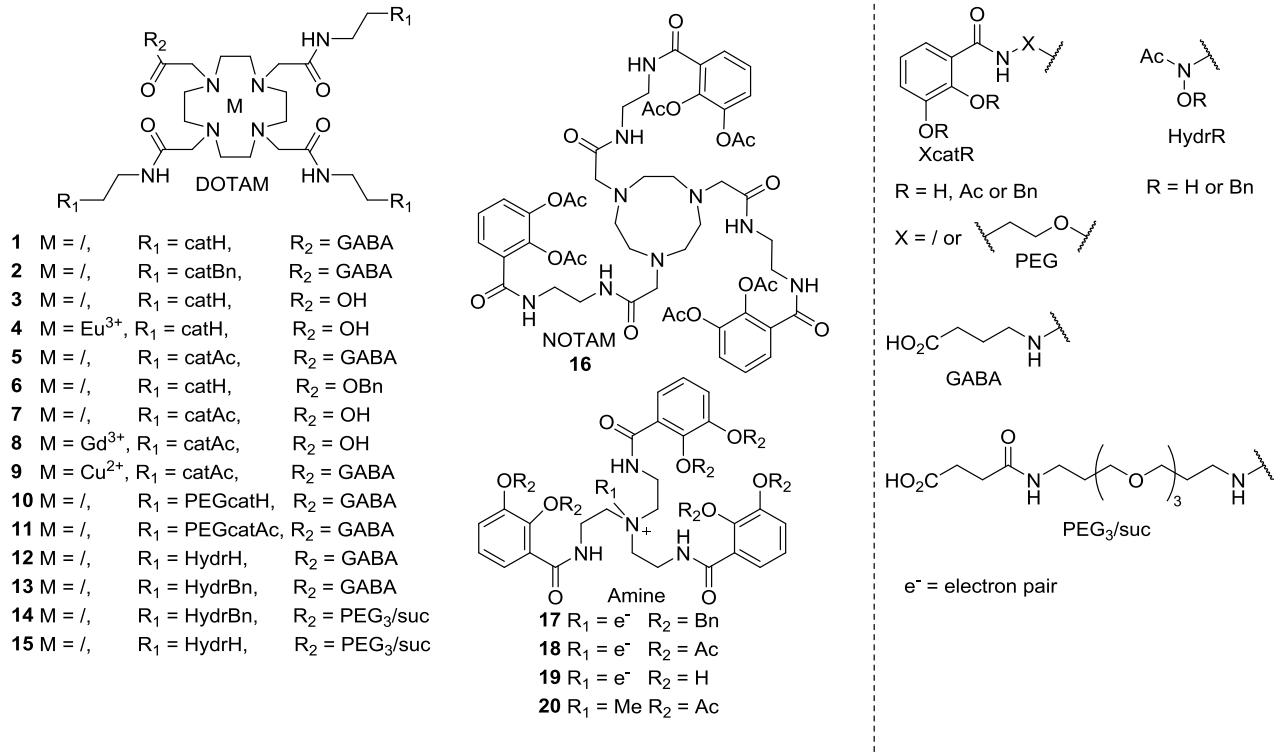

Figure 27 Design of siderophore probes **1-20** for growth recovery studies.

Several structure features were compared in growth recovery experiments. First of all, **3** and **6** were tested to determine the effect of the benzyl protecting groups versus the non-protected carboxylic acid at the 4th DOTAM arm. At the same time, **1** with **3** and **5** with **7** were assessed to establish the effect of the GABA linker on the same arm on the growth recovery. The studies on **12** and **15** will give a hint about additional extensions from a GABA to a PEG_3/suc linker. The PEG_3 was chosen because it is a long, flexible, water soluble, stable cheap linker and it was believed

that this would result in minimal disruption of binding interactions between the protein target and the conjugate.[113] Moreover, the comparisons between **1**/**2**/**5** or **3**/**7** or **17**/**18**/**19** will enable to discuss the effect of catechol groups on bacterial growth. In the same way, comparisons between **12** with **13** and **14** with **15** can lead to conclusions on the impact of protecting catechols or hydroxamates with stable covalently bound groups. Concerning the metal center of the DOTAM, **7**/**8** or **3**/**4** or **5**/**9** can be put in contrast to understand the effect of complexed Gd^{3+}, Eu^{3+} or Cu^{2+} by the DOTAM. Finally, a comparison of the compound sets **1**/**19** or **5**/**16**/**18**/**20** will show the influence of different cores on the development of bacteria.

As for the previous set of molecules, siderophoric intermediates had to be prepared for the synthesis of the various to-be-tested siderophores. Regarding the catechol-typed molecules, the siderophores must be elongated with an ethylenediamine spacer as previously discussed. In contrast to catechols, the hydroxamate linker already shows a free amine derived from the commercial *N*-Boc-ethanolamine and no ethylenediamine spacer is added (Figure 28).

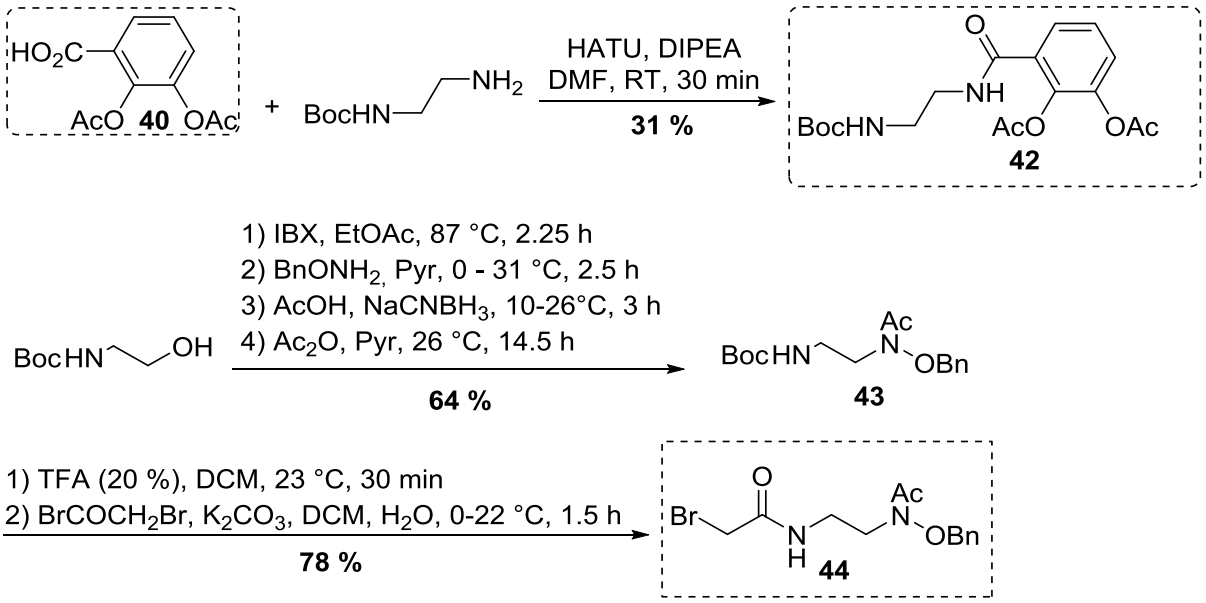

Figure 28 Synthesis of siderophoric arms for growth recovery probes.

The elongation of the acetyl-protected catechol was performed via an amide coupling with HATU activation in order to obtain **42** with a relatively low yield of 31 % due to spontaneous deacetylation of the catechol during the process. The preparation of the benzyl-protected hydroxamate **44** was obtained in 6 steps starting from the *N*-Boc-ethanolamine and optimized by the MSc student Isabell Schneider. First, its aldehyde form was obtained with IBX in reflux. Then an amination was undertaken with *O*-benzylhydroxylamine, followed by a reduction of the *O*-benzylated oxime with sodium cyanoborohydride. Finally the acetylation of the amine was performed to yield the N-Boc protected intermediate **43** with a good yield of 64 % over 4 steps. The

N-Boc deprotection in TFA and the amide coupling with bromoacetylbromide led to the bromo derivative **44**.

To synthesize the long, flexible and soluble linker **47**, the synthesis started with the monobenzylated succinic derivate **45** and the mono-Boc-protected PEG_3 diamine **46** (Figure 29). The activation of the free acid **45** with the ester pentafluorophenyl trifluoroacetate enabled the amide coupling with the diamine **46** to obtain **47** in high yields. The intermediate was directly deprotected with classical TFA conditions, and reacted with bromoacetylbromide to acquire the linker **48**. Following the same strategy, **49** was obtained from *N*-Boc-1,5-diamino-3-oxopentane.

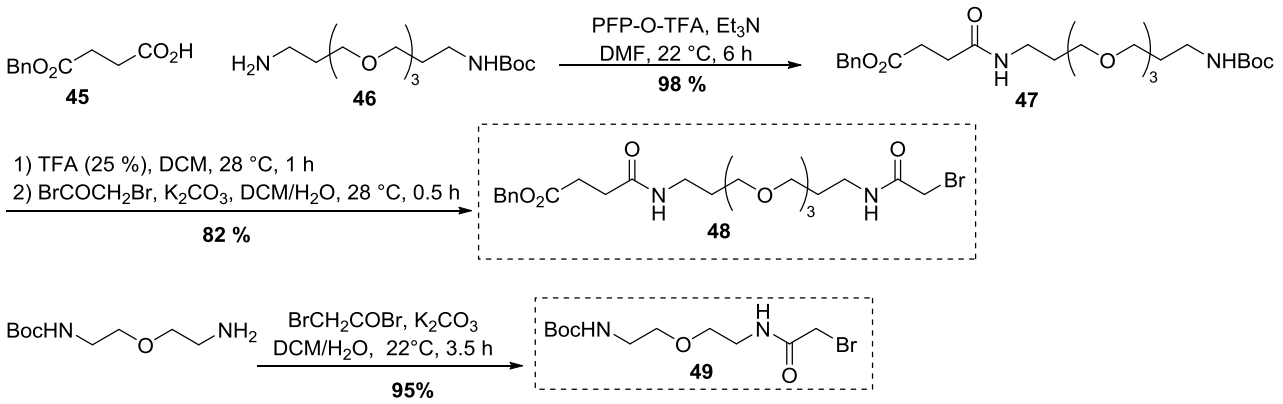

Figure 29 Synthesis of linker arms for growth recovery probes.

After all the necessary linker and siderophoric arms had been prepared, the siderophore probes were synthesized. A monoalkylation onto the secondary amine of the literature-known **36** with benzylbromoacetate and the deprotection of the *tert*-butyl esters enabled to isolate the free triscarboxylic acid **50** (Figure 30). The fresh preparation of the *N*-Boc deprotected version of **42** and its tris amide coupling onto **50** afforded the acetylated triscatecholated derivative. The reproductibility and yield of this transformation were low due to a fast deacetylation process worsening the efficiency of the amide coupling. A selective acetyl deprotection with DIPEA in MeOH was performed to yield the free triscatechol probe **6**.

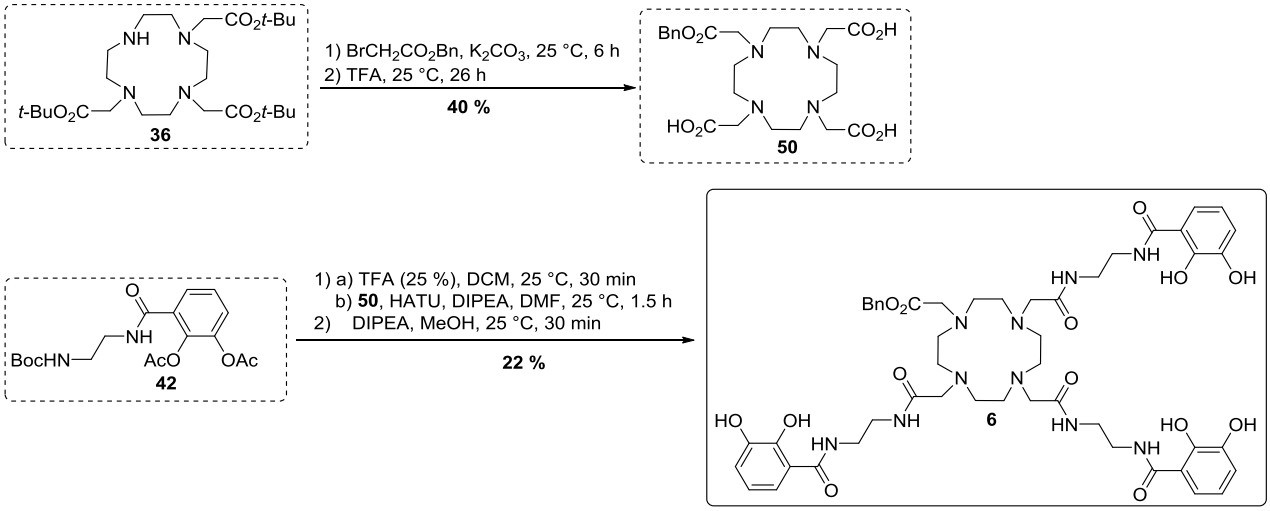

Figure 30 Synthesis of probe **6**.

In order to synthesize the acetylated probes **7** and **8**, the more robust Schotten-Baumann strategy was successfully investigated (Figure 31). The same strategy as for the synthesis of **5** was performed in order to obtain **7**. An overnight complexation was achieved by addition of $GdCl_3$ in MeOH. The acidic conditions applied for the isolation of the gadolinium complex promoted partial deacetylation of the catechols, explaining the low yield of 25 % of the desired product **8**.

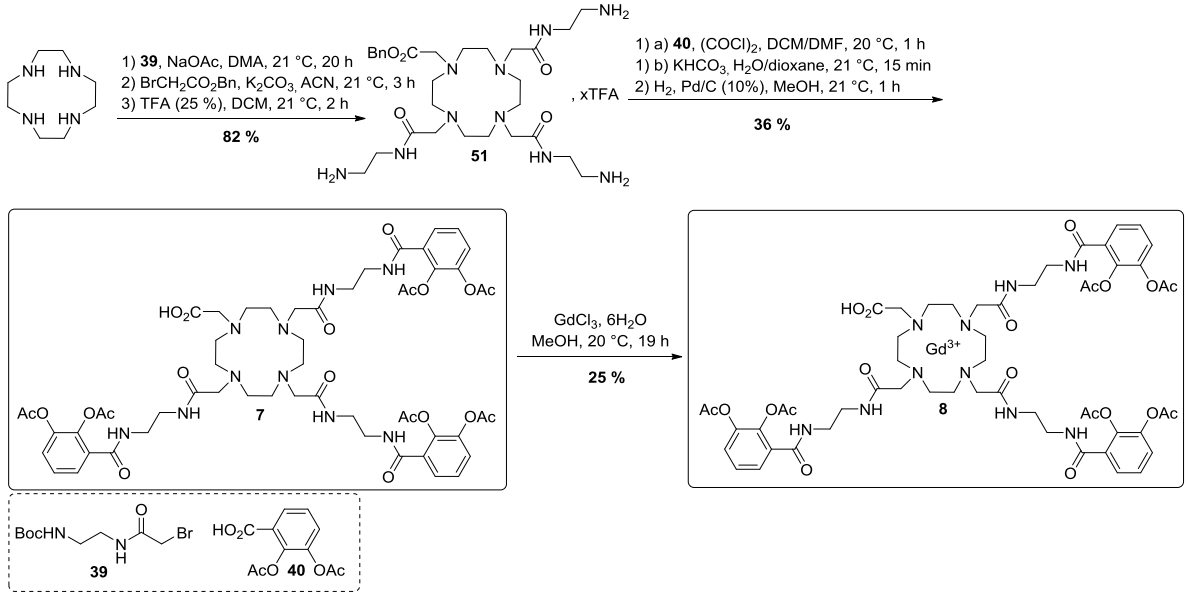

Figure 31 Synthesis of probes **7** and **8**.

The DOTAM center is also known to complex Cu(II). The compound **9** was obtained by a complexation of **6** with $CuSO_4$ in MeOH (Figure 32). The complexation of the Cu(II) into the DOTAM center was remarkably faster than the Gd(III) complexation of **7**. Although the reason for this is not known, several differences between both experiments were observed. First of all, the

metals and the ligands are not the same and this can affect the kinetics of complexation. Moreover, the Gd(III) complexation was performed with 30 % excess of the metal whereas 60 % excess was added for the Cu(II) experiment. Finally, the concentration of the ligand for the complexation of **6** was 20 mM, compared to 4 mM for **7**. Consequently, the higher concentration of ligand and of metal in MeOH can also increase the reaction rate. Although several factors such as the concentration of the reaction have been modified, the yields for the complexations are in the same range.

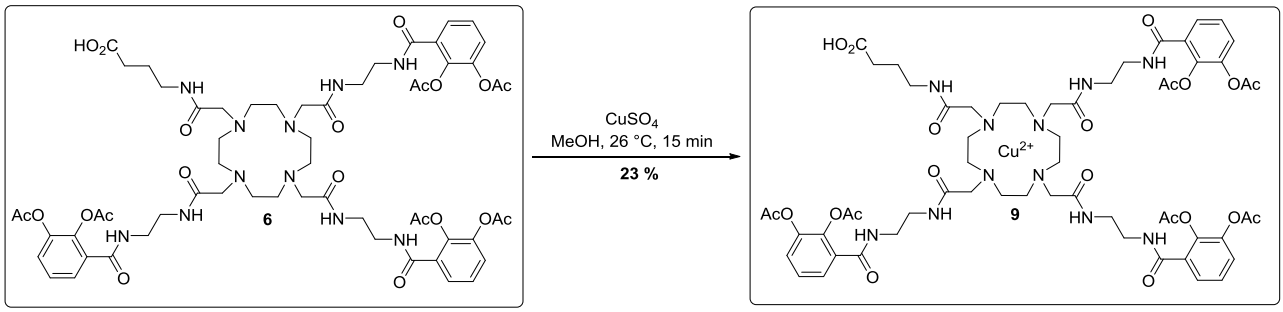

Figure 32 Synthesis of the probe **9**.

For the synthesis of PEG elongated siderophores **10** and **11**, the Schotten-Baumann strategy has been followed (Figure 33). Surprisingly, only 27 % of **52** could be isolated after 2 alkylating steps and the triple Boc deprotection step starting from cyclen. Nevertheless, this low yield could be explained by the unexpectedly long second alkylation and deprotection. The probe **10** was obtained by tris-coupling of the activated carboxylic acid form of **40** and selective hydrogenation of the benzylated carboxylic acid. The low yield is again explained by the deacetylation of the catechols. Moreover, the deacetylation was observed also during hydrogenation, pinpointing the possibility to deprotect the benzyl and the acetyl protecting groups by hydrogenation. Therefore, similar conditions with a longer hydrogenation time (20 h for **10** vs 1.5 h for **11**) permited the additional deprotection of the acetylated catechols, yielding **10**.

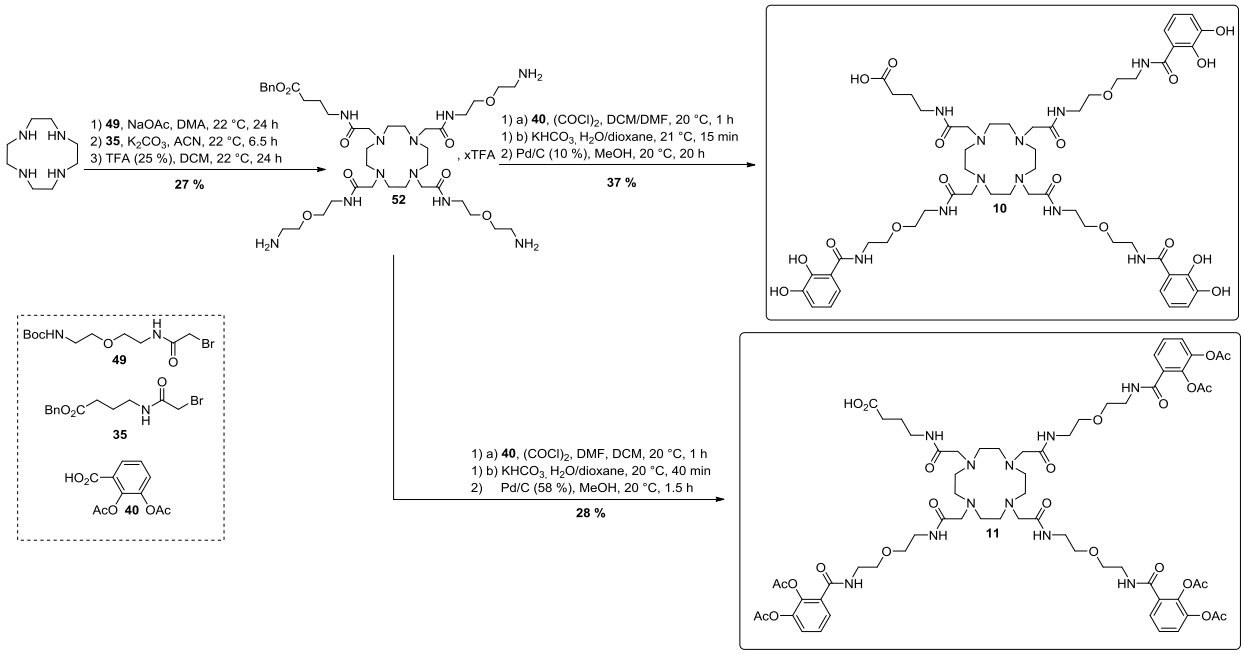

Figure 33 Synthesis of the PEG elongated probes **10** and **11**.

The synthesis of hydroxamate-linked DOTAM molecules **12-15**, carried out by the MSc student Isabell Schneider, was straightforward due to the design of the protecting groups, but also to the successful synthesis of the adapted linkers **44** and **48** without any degradation.

The synthesis of NOTAM derivatives was using the same Schotten-Baumann strategy as applied for DOTAM cores. In this synthetic route, no monoalkylation of a 4th arm was necessary after the trisalkylation of the siderophore spacer, because only three secondary amines are incorporated into the NOTAM core (Figure 34). Therefore, trisalkylation followed by *N*-Boc deprotection permitted the isolation of **53** in high yield. However, **16** was obtained with lower yields by a Schotten-Baumann amide coupling due to partial deacetylation of the product.

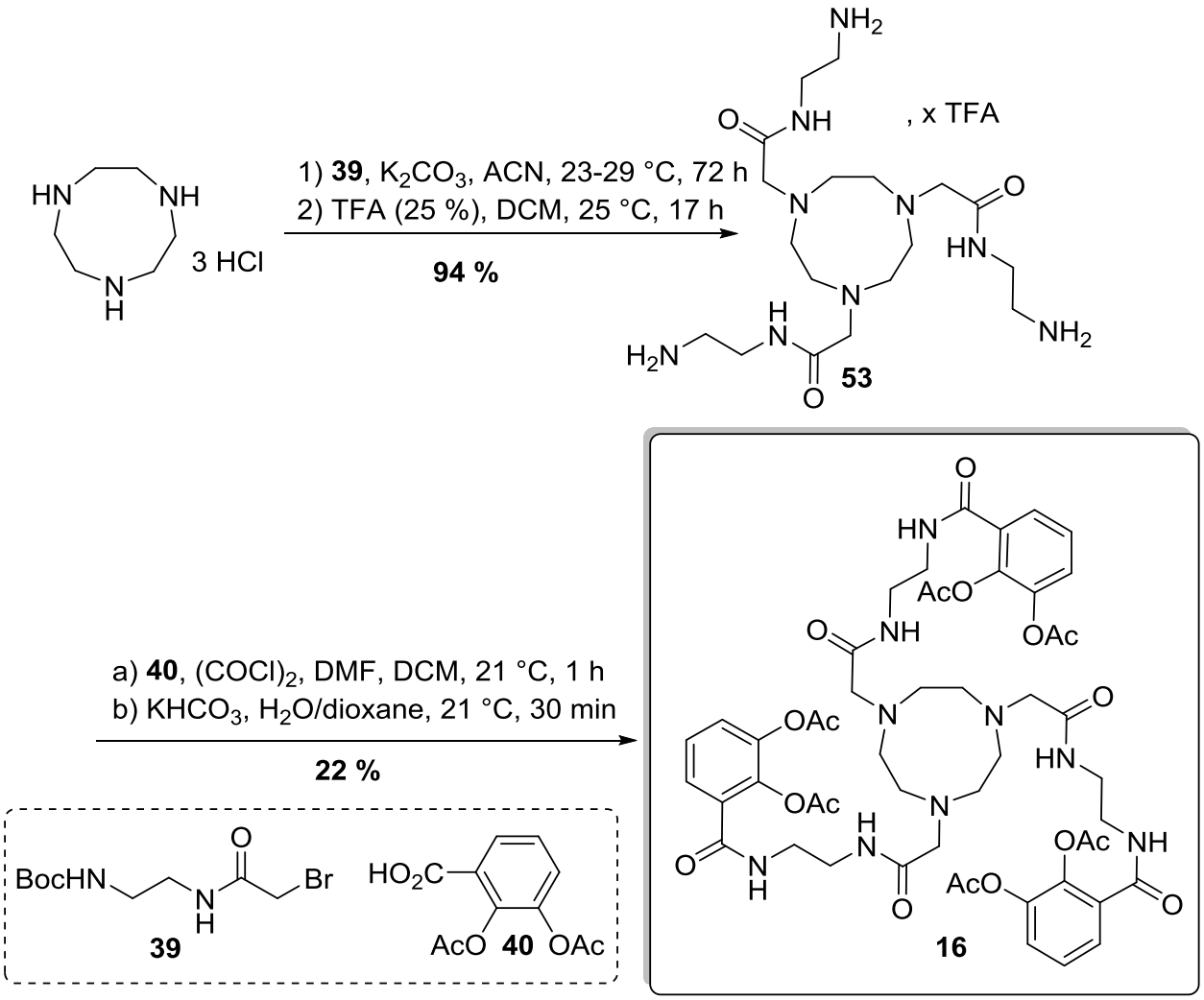

Figure 34 Synthesis of the NOTAM derivative **16**.

The amine-cored compounds **17**-**20** were prepared from tris(2-aminoethyl)amine. The HATU-activated acetylated or benzylated catechols were reacted under similar conditions with the tris amine to yield **17** and **18** with different yields irrespectively (Figure 35). The acetylated version showed lower yields due to partial deacetylation which was tolerated due to the very straightforward synthesis within one step. Although the intermediate **18** needed to be hydrogenated to form **19**, the overall yield for the synthesis of **19** was higher than the one of **18**. Both coupling reactions showed similar efficacy by LCMS. However, the difference in yield can be explained due to the very different polarity of both molecules, and consequently the use of different purification techniques for both compounds. The apolar **18** was purified by normal phase chromatography, whereas the more polar **19** was purified with a reversed phase preparative HPLC system. Therefore, the yield was decreased to 68 % mainly during the normal phase purification.

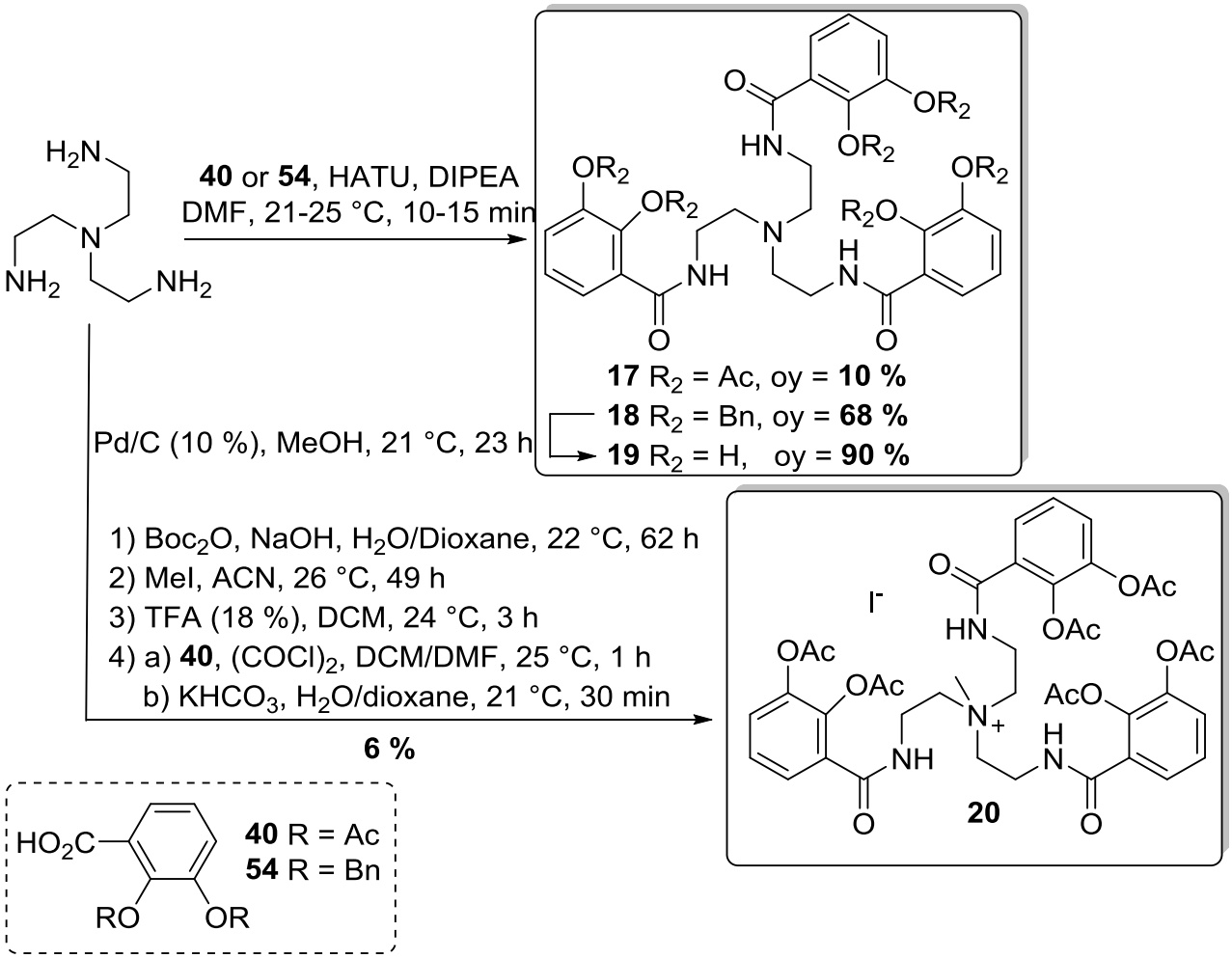

Figure 35 Synthesis of probes **17-20**.

On the other hand, the preparation of the quaternary amine **20** was challenging. The direct methylation of the tertiary amine **17** was not successful, probably due to the sterically hindered tertiary amine. Therefore, the less hindered, triply *N*-Boc protected tris(2-aminoethyl)amine was used. Although 13 equivalents of iodomethane were used, the reaction rate was slow. TFA was then added in order to deprotect the amines, which were directly reacted with the acetylated catechol **40** via a Schotten-Baumann reaction. Due to the difficult methylation and the partial deacetylation of the catechols, only 6 % of the expected cationic product **20** could be isolated. Despite the low overall yield, 2.5 mg were isolated, which was enough for growth recovery experiments.

3.3.1.2. Growth recovery experiments

In order to perform growth recovery experiments, siderophore-deficient bacterial strains were used. The main endogenous siderophore from *E. coli* is enterobactin. Consequently, *E. coli* strains lacking one of the enzymes essential for the enterobactin synthesis (i.e. entA or entB) are not able to biosynthesize enterobactin and thus do not grow under Fe-limited conditions. However *E. coli* ΔentA and ΔentB still possess the biological machinery to internalize and metabolize siderophores,[114] so when a siderophore is added to the growth medium, the bacteria will "recover" their growth, which is indicated by a rise in OD_{600}. The growth recovery assays are easy-to-perform and powerful biological experiments in order to enable the comparison of molecule effects on bacterial growth.[100]

Similar studies were performed with *P. aeruginosa*. Although *P. aeruginosa* uses several xenosiderophores, the primary siderophore synthesized by *P. aeruginosa* is the fluorescent pyoverdin. Pyochelin is another endogenous siderophore, but is only responsible for 5-10% of Fe(III) uptake.[115] Therefore, the strain *P. aeruginosa* Δpch/Δpvd, not being able to biosynthesize the siderophores pyochelin and pyoverdin, was used. They are very important mutant strains to assess the potential of the synthetic siderophores to deliver iron into the cell. The following tests were performed with a natural siderophore as a positive control (enterobactin, pyoverdin), and with the designed and synthesized artificial siderophores.

Before comparing the siderophores to one another, preliminary studies were performed in order to establish the biological assay. After 48 h of incubation, ΔentA and ΔpvdF/ΔpchA treated with solvent control (DMSO) showed no growth compared to the respective corresponding parental strains (wild type, Figure 36). In contrast to the siderophore-deficient strains, the parental strain can synthesize enterobactin/pyoverdin and pyochelin, and therefore is able to take up Fe(III) and grow.

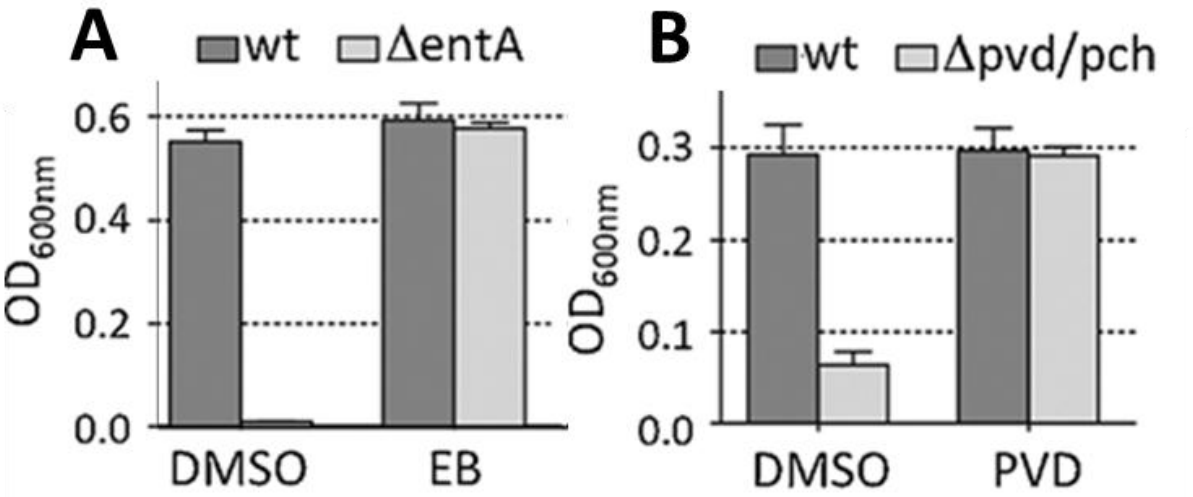

Figure 36 Growth recovery experiments with DMSO (solvent control) and exogenously added enterobactin (EB) or pyoverdin (PVD) a) The growth of *E. coli* BW25113 (wt) and the enterobactin deficient strain (ΔentA) was assessed 48 h after compound addition. b) The growth of the *P. aeruginosa* strain PAO1 (wt) and the pyoverdin/ pyochelin-deficient strain (ΔpvdF/ΔpchA) was assessed 24 h after compound addition. All values are OD_{600} measurements, n=2, ±SEM.

When enterobactin is added exogenously to the ΔentA strain, growth is always reaching similar values as the wild type blank control. Hence, the mutant strain can entirely recover its growth, when the missing siderophore is added to the medium. Similar results were obtained when pyoverdin was added exogenously to the ΔpvdF/ΔpchA strain. This observation proves that enterobactin for *E. coli* or pyoverdin for *P. aeruginosa* contribute to the growth of the respective bacteria.

Data obtained from several independent growth recovery assays were compared through a robust parameter $(OD_{probemutant}-OD_{DMSOmutant})/(OD_{DMSOwt}-OD_{DMSOmutant})$. This ratio represents the growth recovery observed by the addition of probe to the medium on the mutant strain relative to its wild type version, with the corresponding DMSO correction factor.

As indicated in Table 4, enterobactin recovers 99 % of growth, whereas only 80 % is observed for ferrichrome. This difference occurs because enterobactin is the endogenous siderophore for *E. coli* ΔentA., while ferrichrome is a natural siderophore mainly synthesized by fungi.[116] Nevertheless, the hydroxamate-type ferrichrome permitted good growth recovery of *E. coli* ΔentA, which supported its uptake. This result is also in accordance with published results, showing the capability of bacterial species such as *E. coli* to actively transport xenosiderophores such as hydroxamates.[43]

Compounds **3** and **6** are both siderophores containing three catechol moieties, but are differentiated regarding their 4th arm. **6** was designed with a benzyl protection group whereas **3** shows a free carboxylic acid position. Although both molecules showed substantial growth

recovery, the more polar molecule shows a 30 % improvement in bacterial growth recovery compared to the more apolar one. Moreover by comparing **1** with **3** and **5** with **7**, the elongation of this 4th arm with a GABA linker showed a recovery improvement from 8 to 13 %. Therefore, several GABA-linked derivatives were later on investigated. However, an additional extension from a GABA to a PEG_3/suc linker led to a drop of the growth recovery from 43 % to 0 %, as shown by a comparison of **12** and **15**.

When comparing **3**/**7** or **1**/**2**/**5** or **17**/**18**/**19**, several observations concerning the catechol groups were made. When acetylated groups are present a mild improvement from 8 to 15 % of growth recovery is achieved compared to free catechols. Although acetylated groups have so far not been observed in natural siderophores on their catechol positions, the insertion of these specific groups seems to slightly improve its bacterial growth. This observation can be justified by other studies explaining that methyl transferases could be at the origin of free catechol inactivation. If the methylation occurs, the converted catechols cannot bind anymore to Fe(III), which attenuates the bacterial growth. However, unexpected results were obtained when **10** and **11** are compared. This only case showed a slight better growth recovery for the free catechol compared to the acetylated one.

To prove that the catechols are responsible for the siderophore function, two benzylated siderophores were tested: **2** and **17**. **17** was compared to **18**, which has acetylated catechols. Although the latter synthetic siderophore showed growth recovery, the benzylated version did not. The main difference between these two amino-cored molecules is that acetylated catechols are pro-siderophores whose acetyl groups can be cleaved, whereas **17** presents completely stable protecting groups, and therefore cannot complex Fe(III). Moreover, the same trend was observed with DOTAM-cored molecule. A 63-78 % growth recovery reduction occured when **2** was used instead of **5** or **1**.

Similar conclusions can be drawn for hydroxamates. Several benzylated and free hydroxamates were tested and their results were compared. For example, **12** is a synthetic trishydroxamate siderophore, which showed 43 % of growth recovery. Although not catechols but hydroxamates are designed on that synthetic probe, growth recovery could be observed, which is in agreement with previous results obtained for hydroxamates. When its benzylated form **13** is tested, no growth is observed. This result also pinpoints the importance of free hydroxamates for bacterial growth. However, no conclusions could be drawn from the comparison of the benzylated hydroxamate **14** and the free hydroxamate **15**, because growth recovery was not observed for the free version. Distinct siderophore types can also be directly compared thanks to this assay. The difference between **1** and **12** is the presence of three catechols or hydroxamates attached to the

DOTAM core. Almost 40 % of increase in favor to the catechol-type molecule could be observed. Although such a drastic difference cannot be noticed between enterobactin and ferrichrome, and although their core structures are different, the catechol-type enterobactin showed favorable growth recovery.

Since DOTAM molecules can also complex a second metal ion at their center, several chelated versions were also tested and compared such as **7**/**8** or **3**/**4** or **5**/**9**. When Gd(III), Cu(II) or Eu(III) are chelated to DOTAM molecules, a drop in growth recovery between 31 and 70 % was measured. This effect can be due to many causes. First of all, some metals such as copper also have antibacterial activities. Therefore, the incorporation of metals can be a source of growth inhibition. Hence, although the Fe(CAS) assay showed favorable Fe(III) complexation even in presence of complexed DOTAM centers the central metal may impair the translocation efficiency. Therefore, the affinity of Fe(III) to the catechols in presence of complexed DOTAM and consequently the siderophoric properties can affected.

When DOTAM with acetylated catechols such as **5** or **7** are tested, more than 80 % of growth recovery is observed. However, when the DOTAM core is replaced by an amino core such as **18**, a significant drop to 43 % is measured. Moreover, the tertiary amine is only a tripodal core. In order to conjugate a payload via a 4th arm onto the core, the methylated version **20** was prepared. A maximal drop of activity was noticed. Two reasons explain this difference. First of all, the geometry and therefore the angle between the siderophore arms are not the same in **18** and **20**. As a consequence, its affinity to Fe(III) as well as Fe(III) complex recognition by the bacterial siderophore system may be different. Moreover, another main difference between **20** and **18** is that the quarternary amine contains a local positive charge on its core structure. Although this charge can enhance the water solubility of the molecule, the charge may be harmful for the Fe(III) complexation. Indeed, a similar drop in growth recovery was observed when metals were chelated into the DOTAM center. Surprisingly the tripodal NOTAM derivative **16** showed no growth recovery compared to its DOTAM version **5**. Compared to enterobactin, **5** also contains acetylated catechols. However, since acetylated catechols for most cases showed growth recovery improvement, this acetyl modification may not be the reason for such a decrease. The NOTAM derivative was chosen to be synthesized because of its higher affinity to Ga(III)[117], but also because it is a tripodal, 9-membered macrocycle like the natural product enterobactin. However, counter-intuitive results were obtained.

Table 4 List of the synthetic siderophore probes and their structural characteristics and their growth recovery results on *E. coli* ΔentA.

Name	Core	Linker	Siderophore	$\frac{OD_{probe\Delta entA} - OD_{DMSO\Delta entA}}{OD_{DMSOwt} - OD_{DMSO\Delta entA}}$ [%][1]
enterobactin	trilac	/	catH	99
ferrichrome	Pept1	/	HydrH	80
1	DOTAM	GABA	catH	82
2	DOTAM	GABA	catBn	19
3	DOTAM	OH	catH	74
4	EuDOTAM	OH	catH	4
5	DOTAM	GABA	catAc	97
6	DOTAM	OBn	catH	44
7	DOTAM	OH	catAc	84
8	GdDOTAM	OH	catAc	37
9	CuDOTAM	GABA	catAc	66
10	DOTAM	GABA	PEGcatH	97
11	DOTAM	GABA	PEGcatAc	88
12	DOTAM	GABA	HydrH	43
13	DOTAM	GABA	HydrBn	0
14	DOTAM	PEG_3/suc	HydrBn	0
15	DOTAM	PEG_3/suc	HydrH	0
16	NOTAM	/	catAc	0
17	Amine	e^-	catBn	0
18	Amine	e^-	catAc	23
19	Amine	e^-	catH	15
20	Amine	Me	catAc	1

[1] A minimum of 2 experimental replicates was performed; the experimental average standard deviation is 7 %,

The elongated siderophores **11** and **10** could be compared to the shorter version **5** and **1** respectively. Similar results were obtained. Therefore, a minor extension of the catechol arm does not significantly affect the growth recovery of *E. coli* ΔentA.

Taken together, the siderophores showing the highest growth recovery compared to the natural products are **1**, **5**, **7**, **10** and **11**. Remarkably, all of them present a DOTAM core. Also most

of them contain acetylated catechols and an ethylene or a PEG spacer between the core and the siderophore unit. Since the ethylene diamine linker was easily affordable and would enable the synthesis of a smaller final molecule, it was preferred for further studies.

Similar studies were performed on *P. aeruginosa* Δpch/pvd to compare their effect with the previously reported results on *E. coli* (Table 5).

First of all, the tested natural compounds but also **7** showed high growth revovery. Moreover, when **1** and **5** are compared, it is observed that adding acetyl groups to the catechols could not improve the growth recovery in *P. aeruginosa,* although the use of acetylated catechols showed promising results against *E. coli* and *P. aeruginosa*.[118] As previously discussed, the non-cleavable protection with benzyl groups on catechols or hydroxamates prevents growth recovery in *E. coli* mutant strains. Similar observations were made on *P. aeruginosa* strains. The benzylated version **2** showed no growth recovery, while its unprotected version **1** fully recovered growth. Concerning the hydroxamate version, the non-protected siderophore **12** and **15** showed 65 and 76 % growth recovery respectively, compared to their benzylated versions **13** and **14**, which showed growth between 0 and 5 %. Therefore, as for the *E. coli* recovery experiment, the stable protection of siderophores prevents any Fe(III) complexation, siderophore uptake and bacterial growth.

As for the *E. coli* experiment, when **7** is compared to **5**, the GABA elongation of the 4th DOTAM arm does not significantly affect the growth recovery of *P. aeruginosa* Δpch/pvd. Similar results are obtained with **14** and **12** when the same arm is elongated from a GABA to a PEG_3/suc linker in *E. coli* and *P. aeruginosa*.

Concerning the core structure, DOTAM and NOTAM molecules were tested. As for the *E. coli* growth recovery assay, **5** or **7** showed more than 65 % of growth recovery increase compared to **16**. However, the addition of a metal ion such as Gd(III) into the DOTAM core like **8** did not induce a drop in growth recovery for *P. aeruginosa* studies compared to **7** but maintained efficacy. This observation is different from the *E. coli* studies.

Table 5 List of the synthetic siderophore probes, and their growth recovery results on *P. aeruginosa* Δpch/pvd compared to *E. coli* ΔentA.

Name	Core	Linker	Siderophore	$\frac{OD_{probe\Delta entA} - OD_{DMSO\Delta entA}}{OD_{DMSOwt} - OD_{DMSO\Delta entA}}$ of *E. coli* [%][1]	$\frac{OD_{probe\Delta pch/pvd} - OD_{DMSO\Delta pch/pvd}}{OD_{DMSOwt} - OD_{DMSO\Delta pch/pvd}}$ of *P. aeruginosa* [%][1]
Ppyoverdin	Pept2	/	mixed	99	105
ferrichrome	Pept1	/	HydrH	80	110
1	DOTAM	GABA	catH	82	99
2	DOTAM	GABA	catBn	19	4
5	DOTAM	GABA	catAc	97	94
7	DOTAM	OH	catAc	84	103
8	GdDOTAM	OH	catAc	37	100
12	DOTAM	GABA	HydrH	43	65
13	DOTAM	GABA	HydrBn	0	0
14	DOTAM	PEG_3/suc	HydrBn	0	5
15	DOTAM	PEG_3/suc	HydrH	0	76
16	NOTAM	/	catAc	0	29

[1] A minimum of 2 experimental replicate was performed

The natural siderophores pyoverdin and ferrichrome showed high growth recovery. Nevertheless, the synthetic probes **1**, **5**, **7** and **8** showed equal potency. All these exogenous siderophores present a DOTAM core, which can be Gd(III) complexed, with or without a GABA extension on the 4th DOTAM arm, and free or acetylated catechols. However, none of the main endogenous siderophores from *P. aeruginosa*, pyochelin and pyoverdin have a tris-catecholated structure. Thus, a completely different structure, designed from enterobactin, can be taken up by *P. aeruginosa*.

On a global scale, similar effects were triggered on *E. coli* and *P. aeruginosa*. However, a few specific differences were also observed. While the NOTAM-cored **16** showed no growth on the *E. coli* mutant strain, 29 % of *P. aeruginosa* Δpch/pvd growth recovery was measured with the same probe. Therefore, the growth recovery can be species-dependent for specific core molecules such as the NOTAM. Also, the type of siderophore can also show different growth recovery results depending on the species of interest. As an example, although the hydroxamate **15** showed no growth with *E. coli*, a considerable growth of 76 % could be observed for *P. aeruginosa*. This improvement from *E. coli* to *P. aeruginosa* could be due to a more suited hydroxamate-type

siderophore transport system in *P. aeruginosa* Δpch/pvd strain, in comparison with the *E. coli* ΔentA strain.

3.3.2. Fluorescent microscopy of DOTAM-BODIPY conjugate

3.3.2.1. Synthesis of the BODIPY conjugate for fluorescence microscopy

In order to prove any *in vitro* labelling properties to bacteria, it was chosen to prepare an efficient labelling agent conjugated to siderophores. Since the previous studies showed excellent growth recovery with DOTAM/acetylated catechol molecules, it was chosen to work with this system. Concerning the choice of the dye, previous internal studies showed several advantages of using BODIPY-FL-N_3 (Figure 37). First of all, this labelling agent is not permeable to several bacteria of the ESKAPE panel. Therefore, the use of free BODIPY-FL-N_3 is an appropriate negative control for *in vitro* experiments. Moreover, this molecule is commercially available. Therefore, the availability of the molecule but also its known reactivity made this specific dye well-suited candidate for fluorescence microscopy.

Finally, the labelling agent contains an azide functionality which can selectively react with alkyne containing molecules via a click reaction. The formed 1,2,3 triazoles moiety is often found in pharmacophores of antifungal or antibacterial compounds.[119] In addition, this linker is stable, water soluble and biocompatible. The triazole moiety confers a better solubility to the molecule and in some cases additional favorable interactions with the molecular target, since two of the nitrogens can be hydrogen bond acceptors and the ring has a dipole which can align with the ones of other peptidic amides.[120]

The BODIPY conjugate was synthesized starting from cyclen with the successful Schotten-Baumann strategy (Figure 37). After synthesizing the literature-known linkers **39** and **55**, the successive alkylations followed by *N*-Boc deprotection yielded the free amino molecule **56**. One advantage of using a free alkyne as a linker for the 4th arm is to avoid any deprotection of the arm all along the carrier synthesis. Therefore, after the Schotten-Baumann reaction between **40** and **56**, the alkyne was purified to yield **57**.

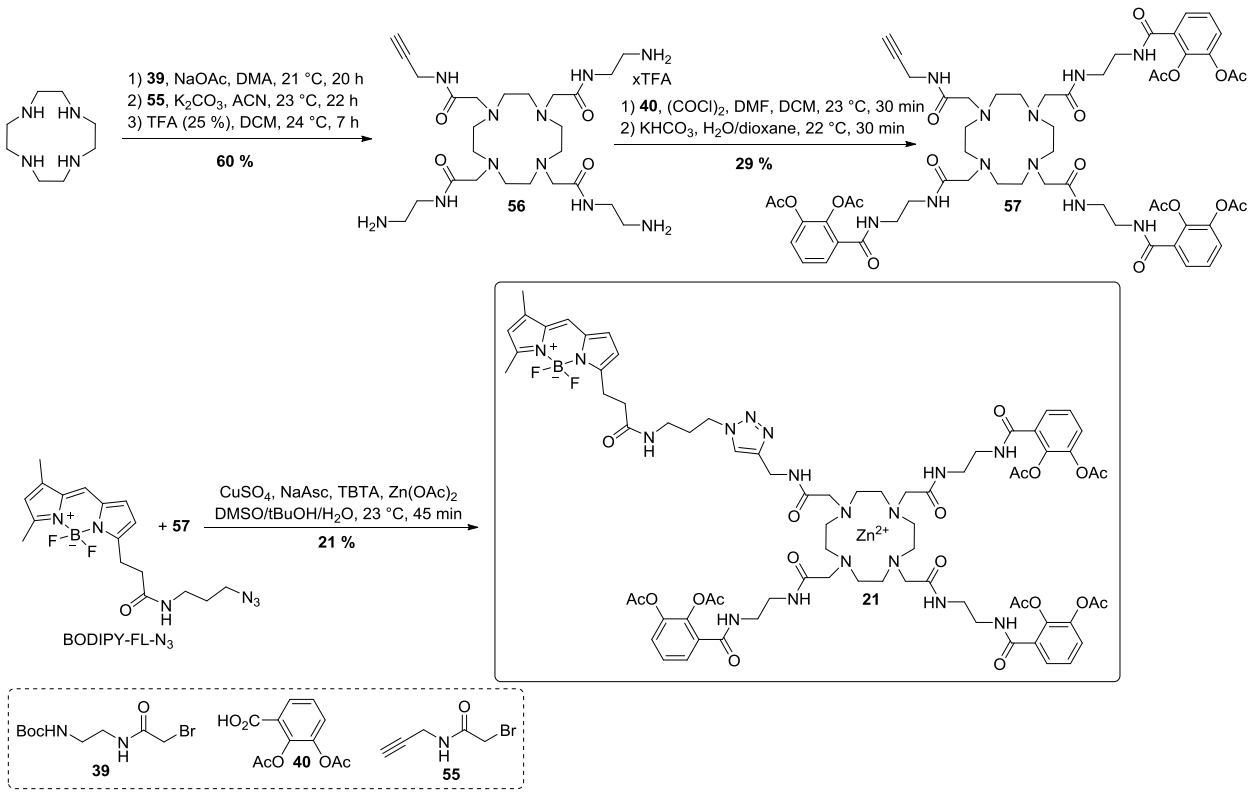

Figure 37 Synthesis of the BODIPY conjugate **21**.

The following click reaction was performed in presence of Cu(II) that was first reduced to Cu(I) in the presence of sodium ascorbate. However, partial copper complexation of the DOTAM center could be observed by LCMS. Moreover, Zn(II) was added into the DOTAM center since it has more affinity to the DOTAM than Cu(II). The DOTAM was fully complexed by the Zn(II) in order to avoid copper complexation. Fresh Cu(I) was prepared and added to the reaction mixture. In order to avoid Cu(II) complexation issues, a copper-free click reaction would have to be investigated. For this purpose, it would be necessary to synthesize another carrier containing cyclooctyne or other reactive elements that can be clicked to azides without a metal catalyst.[121] The BODIPY conjugate **21** was obtained with an overall yield of 4 % and was tested in fluorescence microscopy and flow cytometry experiments.

3.3.2.2. Accumulation of the BODIPY conjugate in bacteria

Two sets of assay were performed in order to prove any *in vitro* interaction between the synthetic BODIPY conjugate **21** and the different medically important bacterial pathogens of the ESKAPE panel, which comprises the Gram-negative species *A. baumannii, E. cloacae, E. coli, K. pneumoniae, and P. aeruginosa* as well as the Gram-positive species *E. faecium* and *S. aureus*.[12]

According to confocal microscopy images and flow-cytometry measurements, all bacteria of the ESKAPE panel were labelled by **21** (Figure 38).

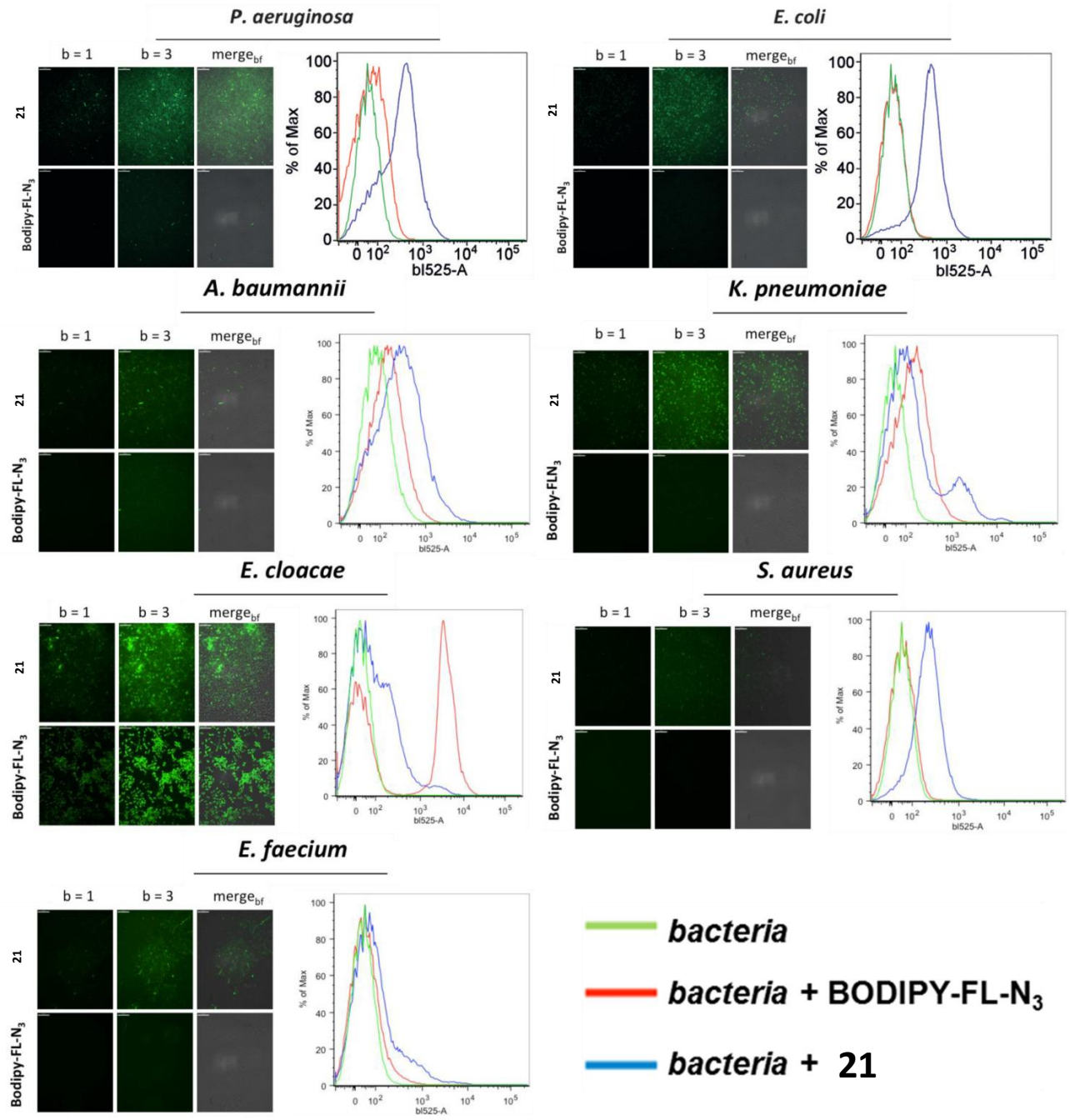

Figure 38 Labelling of ESKAPE pathogens by DOTAM-BODIPY conjugate **21** or BODIPY-FL-N_3 by confocal microscopy and flow cytometry. Confocal imaging and flow cytometric analysis of ESKAPE pathogens. Scale bars 11 µm, bl525-A BODIPY fluorescence intensity.

However, we observed varying labelling efficiencies within the respective bacterial populations. Some cells display a high fluorescence signal, whereas others showed lower signal intensities. In cases such as *S. aureus*, only a subpopulation was labelled. This might be

attributable to different growth phases of the bacteria and has to be addressed in further studies. For all bacteria except of *E. faecium*, we observed an increased fluorescence signal by confocal microscopy and flow cytometry upon incubation with **21** compared to BODIPY-FL-N_3. In repeated experiments we observed that incubation with BODIPY-FL-N_3 resulted in a strong and homogeneous labelling of *E. faecium*. *E. faecium* and *S. aureus* are the Gram positive members of the ESKAPE panel. As *S. aureus* does not display the intensive fluorescent signal upon incubation with free BODIPY as seen for *E. faecium*, this effect cannot be attributed to the general Gram-positive nature.

3.3.3. The fluorogen-activating protein system

The fluorogen-activating protein (FAP) assay is proves the internalization of molecules specifically in the periplasm or in the cytoplasm. It consists of a specific fluorogenic dye, which does not present any fluorescence when it is excited at a specific wavelength (Figure 39). However, once the small molecule is bound to a FAP, which is a protein derived from a single chain antibody, emission of fluorescence can be measured when it is excited at the same wavelength.

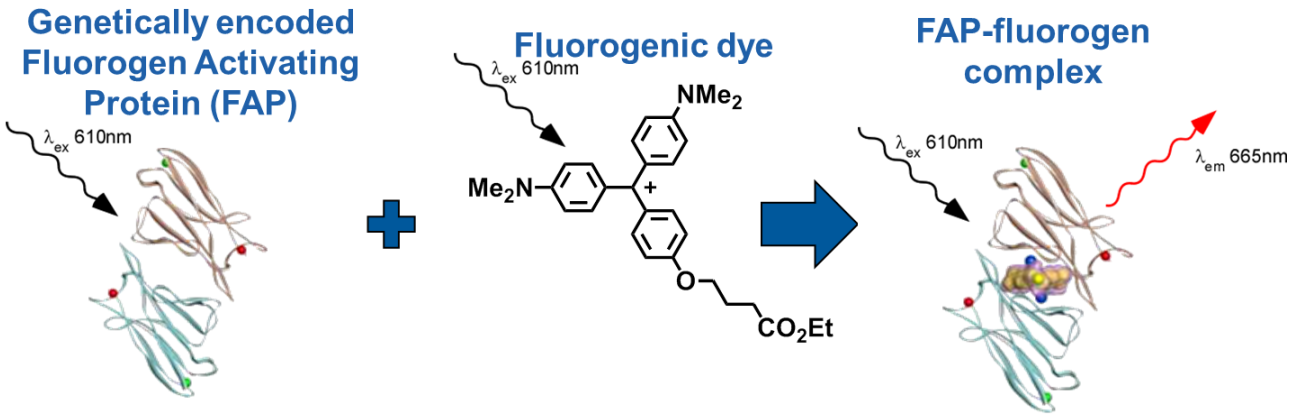

Figure 39 Concept of fluorogen activating protein system.

In the case study working with malachite green derivatives, recent experiments showed that once the malachite green and the FAP are complexed, emission of fluorescence can be measured at 665 nm when the complex is excited at 610 nm, unlike the apo-FAP protein and the fluorogenic dye separately.[122] Enhanced fluorescence is thought to occur because rapid rotation around a single bond within the chromophore is restrained upon binding to FAP. The FAP concept can be extremely useful to provide the necessary demonstration of conjugate internalization (Figure 40).

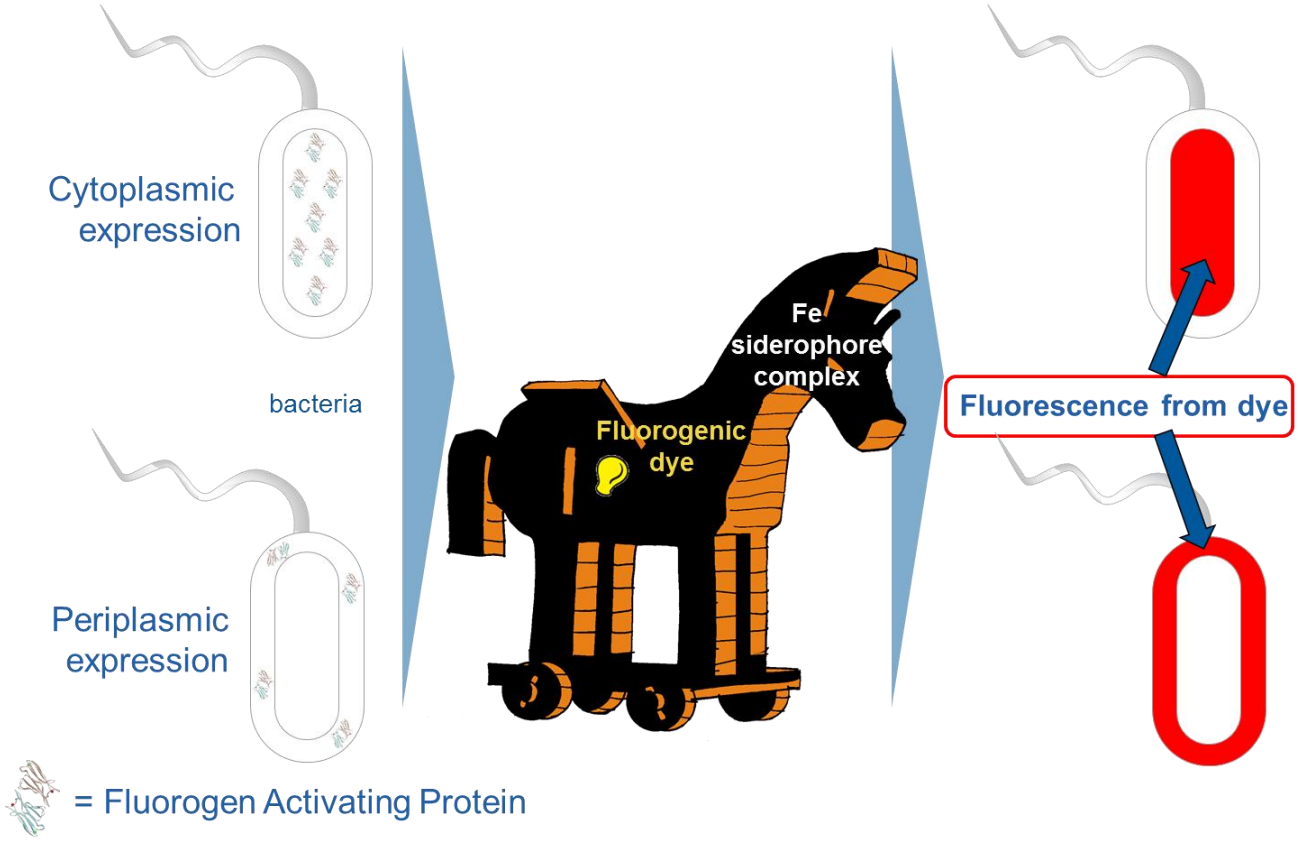

Figure 40 Conceptual scheme illustrating the FAP system applied on bacteria.

After the successful overexpression of the specific fluorogen activating protein of interest in the cytoplasm or in the periplasm of the bacteria, the modified bacteria are incubated with the fluorogenic dye conjugated to the siderophore. If compound internalization occurs, the conjugate encounters the overexpressed FAP and forms a complex. Moreover, the fact to have isolated cases where the FAP is expressed specifically in the cytoplasm or in the periplasm will enable the determination of the specific internal location of the conjugate. On the other hand, if no uptake of the conjugate is possible, the attached malachite green moiety cannot form a complex with the FAP and no fluorescence can be observed at 665 nm. While a recent adaptation of the FAP system was established for the imaging of prokaryotic cells,[123] this study represents the first adaptation to study translocation efficiencies of cargo-containing scaffolds in bacteria.

3.3.3.1. Synthesis of fluorogenic dye conjugates for fluorogen-activating protein assay

Two siderophore conjugates were synthesized to compare their potential to penetrate to the inner space of bacteria (Figure 41).

First of all, in order to perform the synthesis of such conjugates, malachite green intermediates that can be coupled via amides were prepared. Therefore, two malachite green precursors were synthesized having different functionalities: the carboxylic acid **58** and the amine **60**. The first intermediate **59** can be synthesized by oxidation of the literature known **58**.[122] The also literature-known ethylene diamine elongated version **60**[122] can be oxidized and then Boc-deprotected to yield the water soluble malachite green derivative **61**.

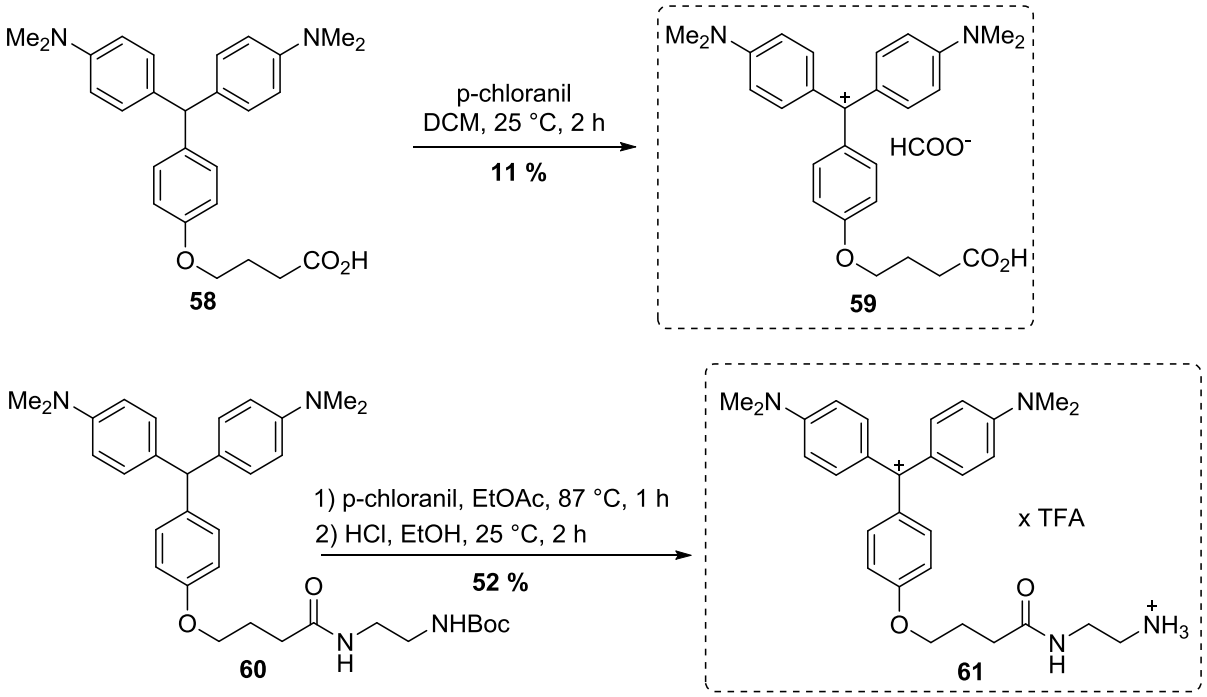

Figure 41 Synthesis of the malachite green precursors **59** and **61**.

The siderophore was linked to the malachite green via a PEG_3 diamine linker. The malachite green conjugate **23** was synthesized starting from the advanced cyclen **36** (Figure 42). After monoprotecting the PEG_3 diamine linker with a Cbz group and reacting the other amine with bromoacetylbromide, the alkylating linker was added to the intermediate **36** to yield the DOTA intermediate **63**. After the very sensitive deprotection of the catechol arm **42** and of the intermediate **63**, a triple amide coupling was performed to introduce the siderophoric function of the molecule **64**. The selective hydrogenation, followed by the amide coupling between the resulted amine and the carboxylic acid **59** enabled the isolation of the compound **23**. The successive preparative HPLC purifications in acidic conditions and the difficulty to prevent any deactylation process may explain that the yield of this final step was low (1 %).

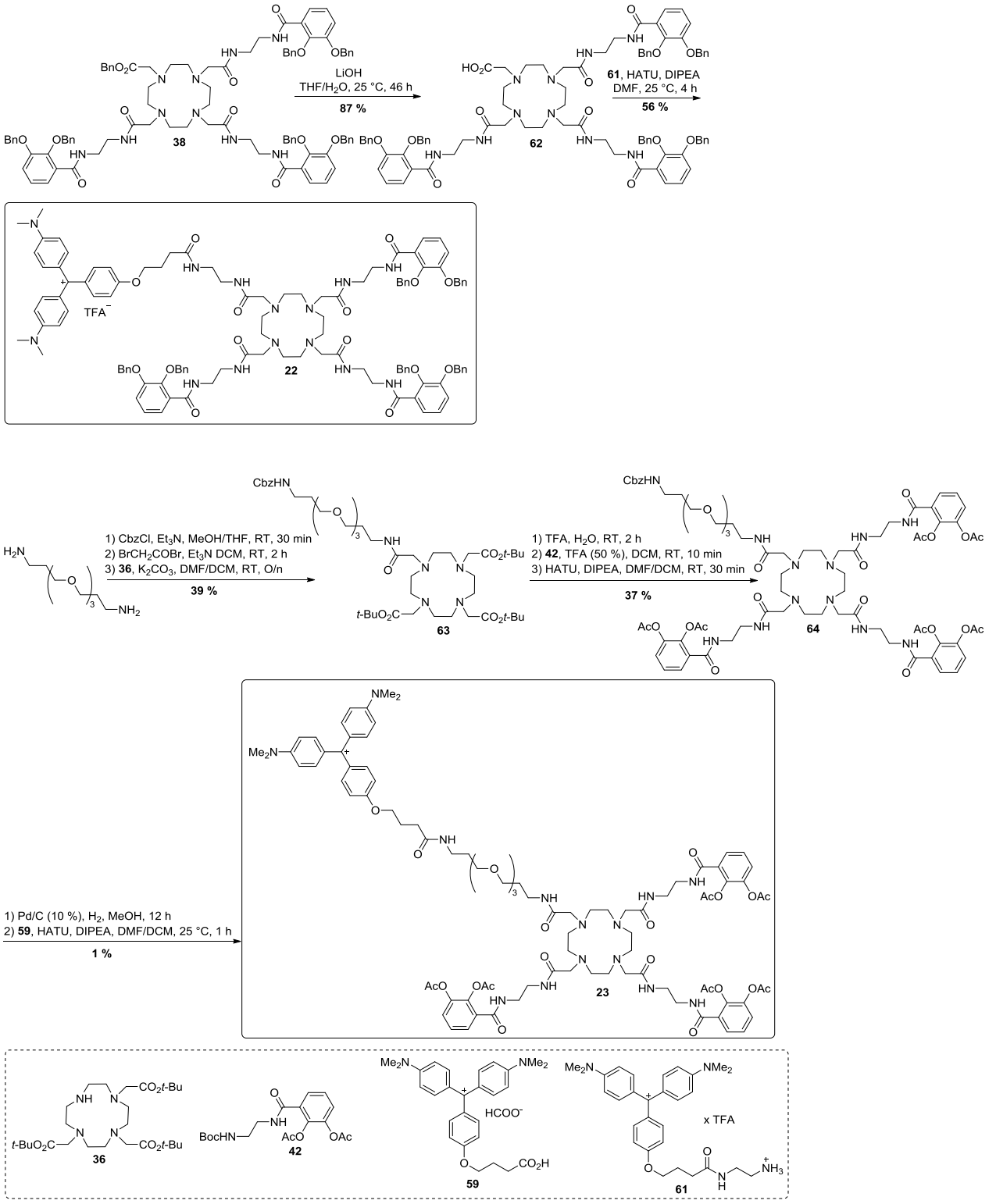

Figure 42 Synthesis of the fluorogenic dye conjugates **22** and **23**.

A negative control was designed in order to demonstrate the specific labelling properties of the compound **23**. The negative control must also contain malachite green, the DOTAM center but

also a stable protecting group on the catechols. Since successful results were already obtained by using benzyl protecting groups, the negative control **22** was designed. Similarly to the last step of the probe **23**, the intermediate **38** was selectively deprotected by hydrolysis of the benzylester in basic conditions to yield the carboxylic acid **62**. This protected siderophore was activated with HATU and added to the amine **61**. Higher yields of **22** were obtained due to the highly stable benzyl groups compared to the labile acetyl groups of **23**.

3.3.3.2. The fluorogen activating protein assay

Before testing the internalization of the conjugates, a proof of concept in solution was verified by using the commercially available malachite green ester. Three sets of samples were measured in a fluorescence plate reader: the first one contained only malachite green, the second one recombinantly expressed FAP6.2 and the third a mixture of both (MG + FAP6.2). After exciting each sample at 610 nm, the fluorescence emission spectrum for each sample was measured (Figure 43). No emission of fluorescence between 640 and 740 nm could be observed for the two first samples. However, the third one showed significant fluorescence emission with a maximum of 10^5 RFU at 665 nm. Therefore, one formation of a complex was proven which enhances the fluorescence of the MG.[122, 124] In order to use the FAP system to *in vitro* bacterial applications, the sequence of variant FAP6.2 (fused to a C-terminal His-tag) was cloned into the pET23b expression vector. The recombinant expression of the FAP6.2 in *E. coli* Origami_ B(DE3) was confirmed by Western Blot analysis. As pET23b-dependent expression is known to be activated by IPTG, an increase in the amount of recombinant FAP was detected by Western Blotting upon addition of IPTG during bacterial growth (Figure 43).

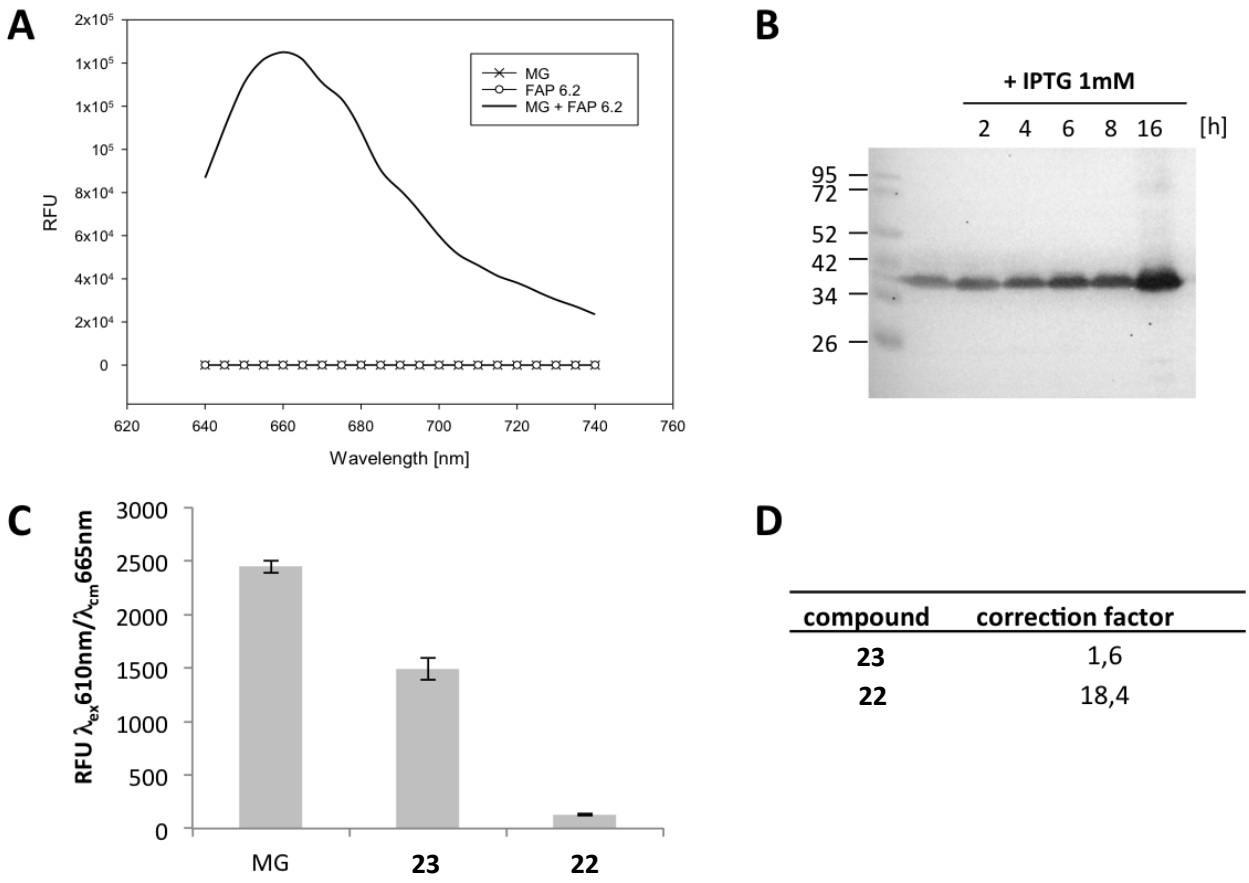

Figure 43 A. Fluorescence emission spectra of MG, FAP6.2 and MG + FAP6.2 with excitation at 610 nm. Only upon binding to FAP6.2 a fluorescence signal of MG can be detected. B. *E. coli FAP6.2* was induced by addition of 1 mM IPTG for different timespans and lysates were probed by α-His antibody on Western Blot. C. Recombinantly expressed FAP6.2 protein was incubated with MG-conjugates in a molar ratio of 4:1, and fluorescence was recorded with an excitation wavelength of 610 nm and an emission wavelength of 665 nm. D. The correction factor corresponds to the ratio of MG-fluorescence intensity divided by fluorescence intensity of the respective MG-conjugate.

In order to figure out if the DOTAM conjugates can go through the bacterial membrane, the MG conjugates **22** and **23** were tested. The incubation of the FAP6.2 with **22** or **23** induced emission of fluorescence at 665 nm. Therefore, although the MG has been derivatized and conjugated to the siderophore system, interaction still occured between the FAP and the dye conjugates. However, the fluorescence intensities vary compared to the free MG. This can be due to the lower quantum yield from the MG conjugate. Moreover, **22** showed more than 10 times lower fluorescent efficiency than **23**. This may be due to the choice of more hydrophobic catechol protecting groups, the conjugation of the MG via a shorter linker and electronic interactions between the aromatic groups and the MG.

Since both probes can interact with the protein target, the assay was performed with *E. coli_FAP6.2*, which was incubated with the benzylated MG conjugate **22**. The addition of the probe

did not trigger any fluorescence. Therefore, the benzylated conjugate **22** could not reach the location of the overexpressed FAP6.2. On the other hand, the incubation with the acetylated version **23** led to an increasing fluorescence over time, reaching maximum fluorescence intensity after ca. 10-12 h of incubation (Figure 44). Therefore, the acetylated version was taken up by the *E. coli_FAP6.2*, followed by the complexation of the conjugate.

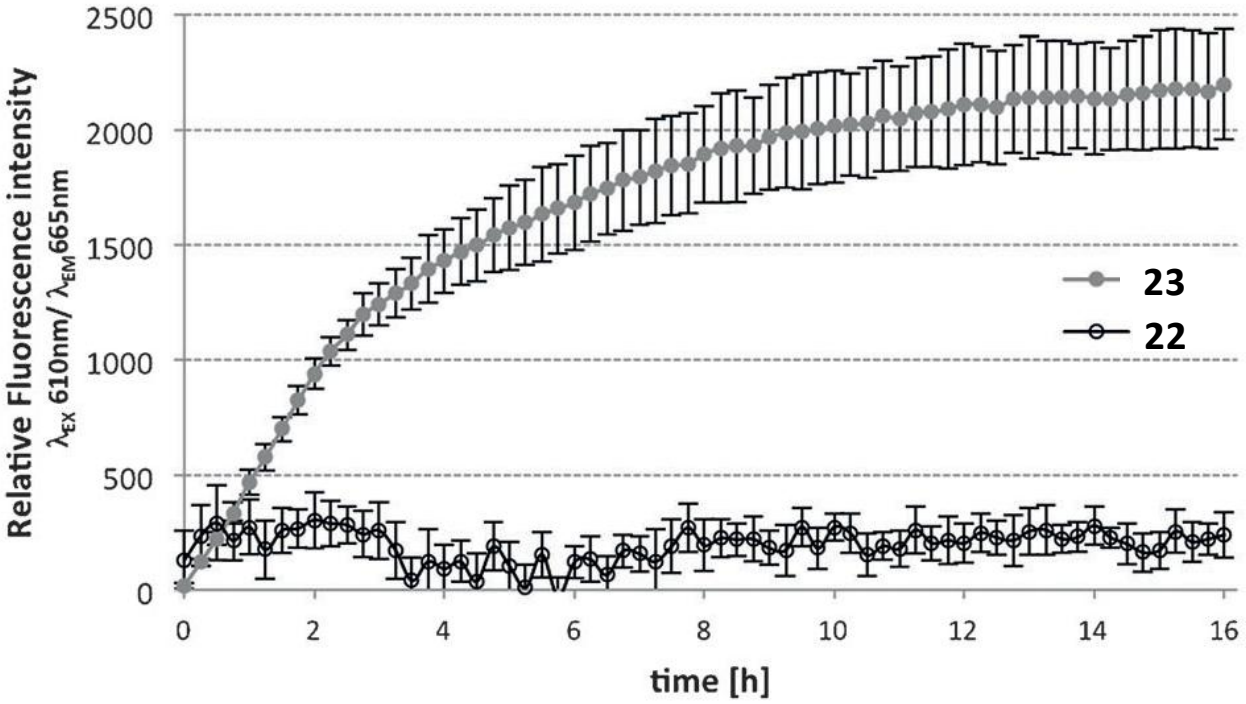

Figure 44 Kinetic studies on fluorescence emission of MG conjugates with *E. coli_FAP6.2*. The compounds **22** and **23** were added at a final concentration of 10 µM, the fluorescence was recorded at lEX=610 nm/lEM=665 nm for 16 h. **23** was translocated to the cytoplasm, whereas **22** was not.

After 16 h of incubation, the bacterial cells were further analyzed by flow cytometry and confocal microscopy. By comparison between brightfield and fluorescent images, co-localization between the bacteria and the fluorescence permits to conclude on the bacterial labelling properties of the fluorogenic dye conjugate **23**. To exclude any antibacterial effect of **23** during the uptake kinetic detection and confirm the assay in living bacteria, *E. coli FAP6.2* were then incubated with propidium iodide (PI), a dead cell-specific labelling agent, and imaged by confocal microscopy (Figure 45). No increasing amount of dead cells upon treatment with **23** was observed, proving that uptake into living bacteria occurred. Since the observed fluorescence is the consequence of binding of intracellular FAP to DOTAM-conjugated MG, these results provide evidence that **23** had indeed been taken up into the cytoplasm of *E. coli FAP6.2*.

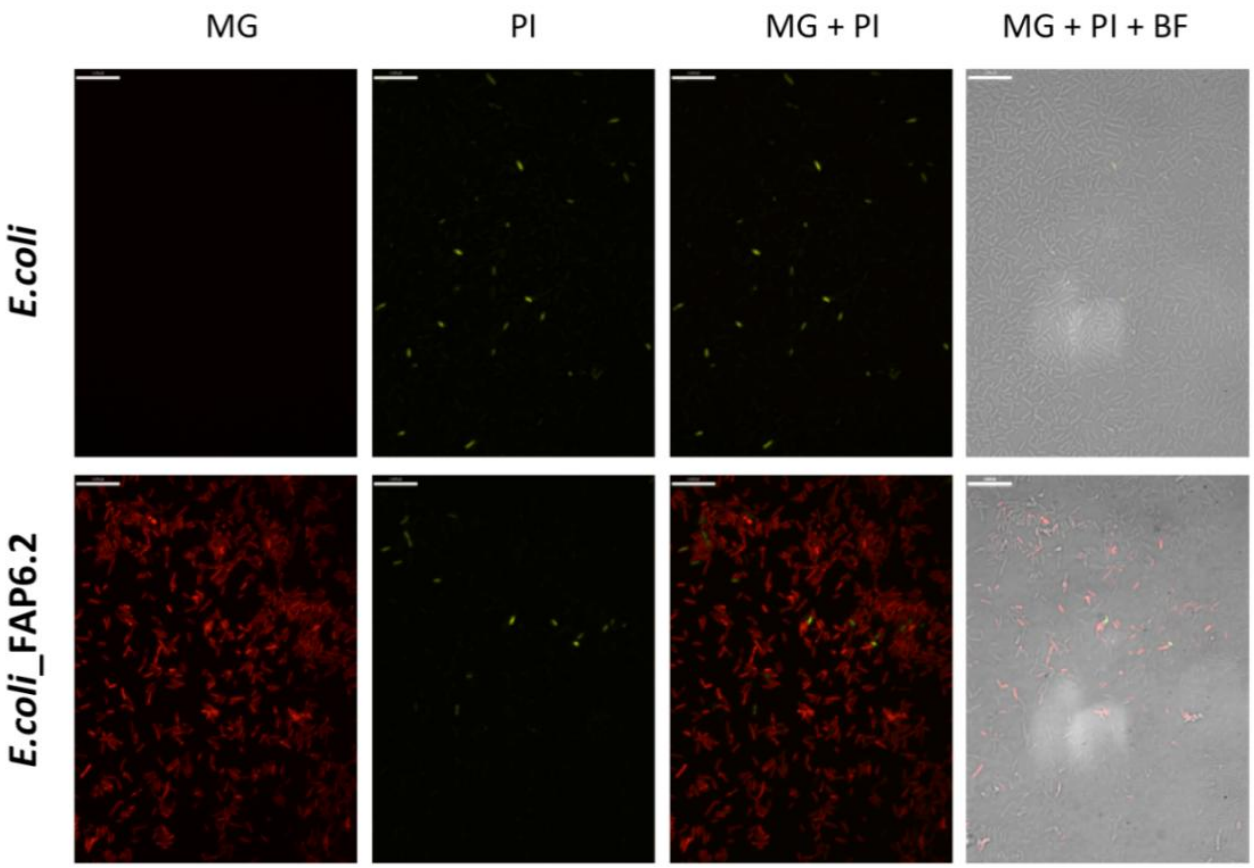

Figure 45 Co-incubation of **23** and propidium iodide. Confocal microscopy of *E. coli* parent strain or *E. coli_FAP6.2* upon incubation with **23** at a concentration of 10 µM for 16 h after an additional 20min incubation with 50 µg/mL propidium iodide (PI). BF brightfield. Scale bars 11 µm.

In order to compare both probes and verify that no bacterial labelling is possible with the probe **22** as well, fluorescence microscopy images were also provided. As mentioned in the kinetic studies, bacterial fluorescence labelling did not occur with **22** in comparison with **23** (Figure 46).

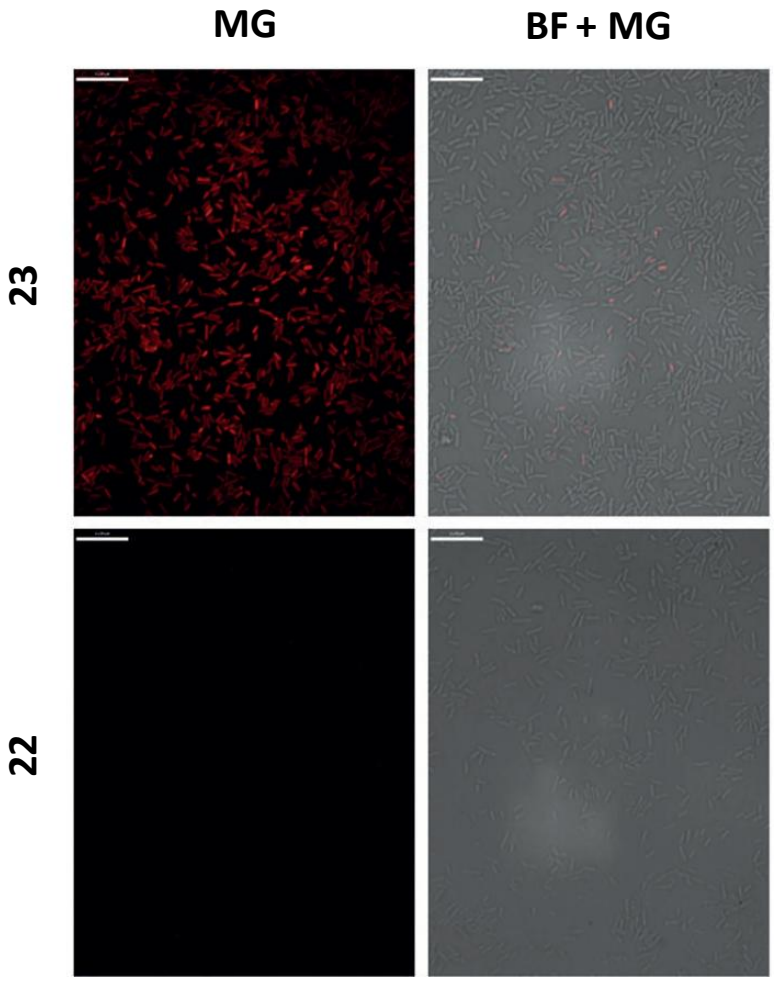

Figure 46 Confocal microscopy images of *E. coli_FAP6.2* upon incubation with 10 µM of **22** or **23** for 16 h. BF=bright field. Scale bars: 11 µm.

Finally quantification studies were performed by flow cytometry (Figure 47). While we observed no new populations by addition of **22** compared to the blank DMSO, a big new population displays a high fluorescent signal when **23** is added instead.

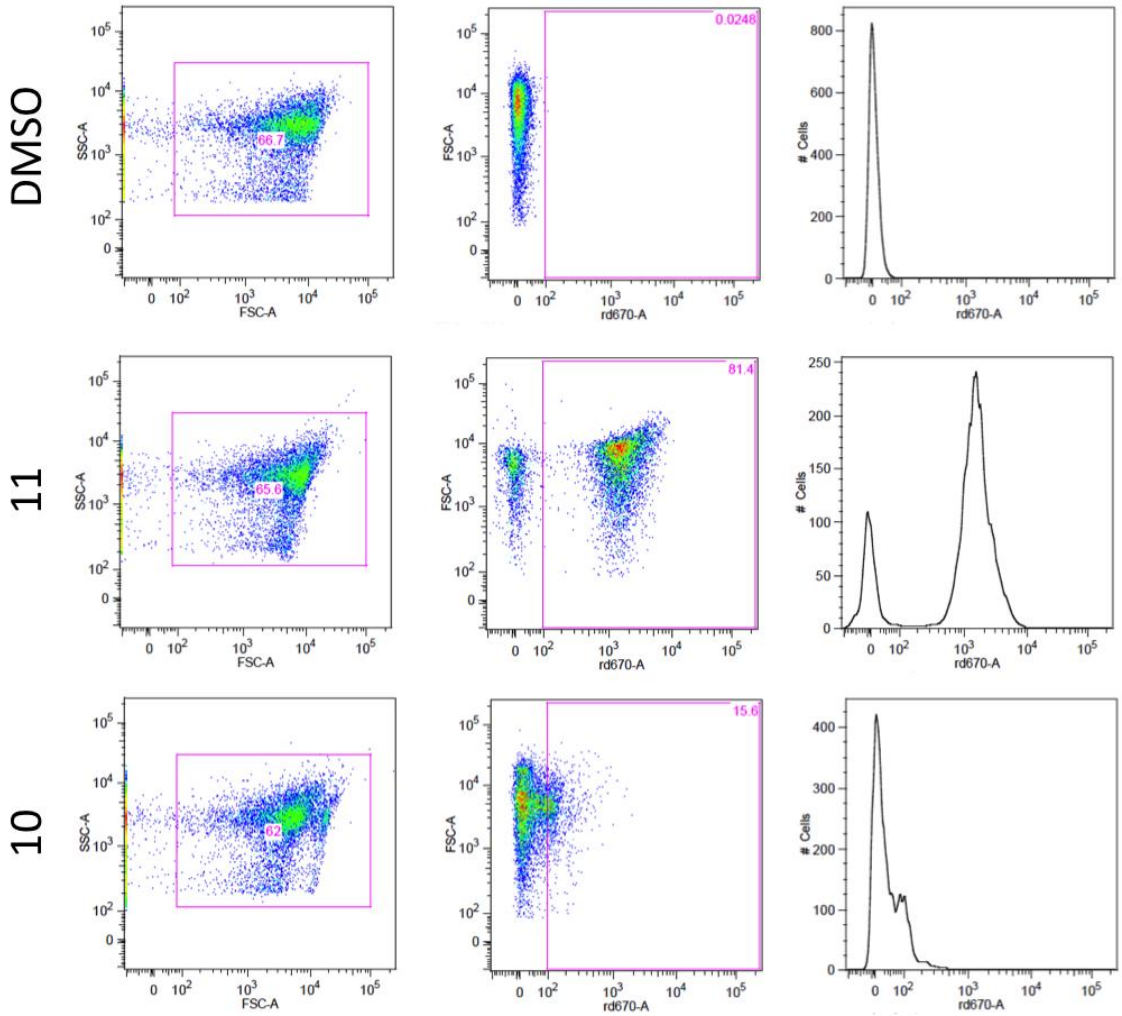

Figure 47 MG conjugate uptake quantified by flow cytometry. Flow cytometric analysis of *E. coli_FAP6.2* upon incubation with **22** or **23** at a concentration of 10 µM for 16 h. FSC forward scatter, SSC side scatter, rd670 MG fluorescence intensity.

However, less than 20 % of the whole population is still to be converted which might be due to different growth phases of the bacteria.

To sum up, the assay provided strong evidence for the bacterial translocation of a DOTAM-based fluorogen siderophore conjugate.

3.4. Aim 3: Studies on antibiotic siderophore conjugates activity

3.4.1. The ampicillin conjugates

After having successfully demonstrated the internalization of siderophores and siderophore conjugates, the conjugation of several antibiotics to the developed siderophore system was performed in order to improve the antimicrobial effect of the conjugates. If the first antibiotic conjugate shows at least similar activities compared to the parent drug, one can infer the acceptance of the conjugate as an iron carrier and its translocation.

For example, small ß-lactams such as ampicillin are relevant candidates for the sideromycin design. ß-lactams are very interesting drugs for such a research on Gram-negative bacteria[125] for several reasons. First of all, they do not need to go through two membranes, but only through the outer one.[126] Secondly, they are already clinically validated.[127] Thirdly, they are low molecular weight molecules, which is preferable for the Trojan horse strategy. Finally, although the main resistance mechanism of the bacteria against ß-lactams such as ampicillin is the degradation of the antibiotic, a decrease of ß-lactam permeability is also relevant. Porin channels in bacteria such as *P. aeruginosa* are narrower, which minimizes the ß-lactam translocation and increases bacterial resistance against this class of antibiotics.[128] The mode of action is based on the interaction with penicillin-binding proteins (PBP), which are more precisely transpeptidases necessary for the bacterial cell wall formation. Targeting this periplasmic protein family can be of great use if the conjugate is able to translocate into the periplasmic space. Besides, unlike many other antibiotics, the secondary amine of the ampicillin can be easily modified without spoiling its interaction with transpeptidases.[81] More precisely, the ampicillin is located at the edge of the PBP (Figure 48), and its amine is pointing towards the exit of the transpeptidase. Therefore, the design of a relatively short and non-cleavable short linker such as a γ-aminobutyric acid (GABA) linker between the amino function of the ampicillin and the core molecule is sufficient for the activity of the entire conjugate.[129] Also, as previously mentioned, ß-lactam conjugates already proved to be successful conjugates in the past.[50d] Finally, the chemistry of this antibiotic is well established in the literature, which makes it the perfect candidate for a first antibiotic siderophore conjugate.[73, 86, 100]

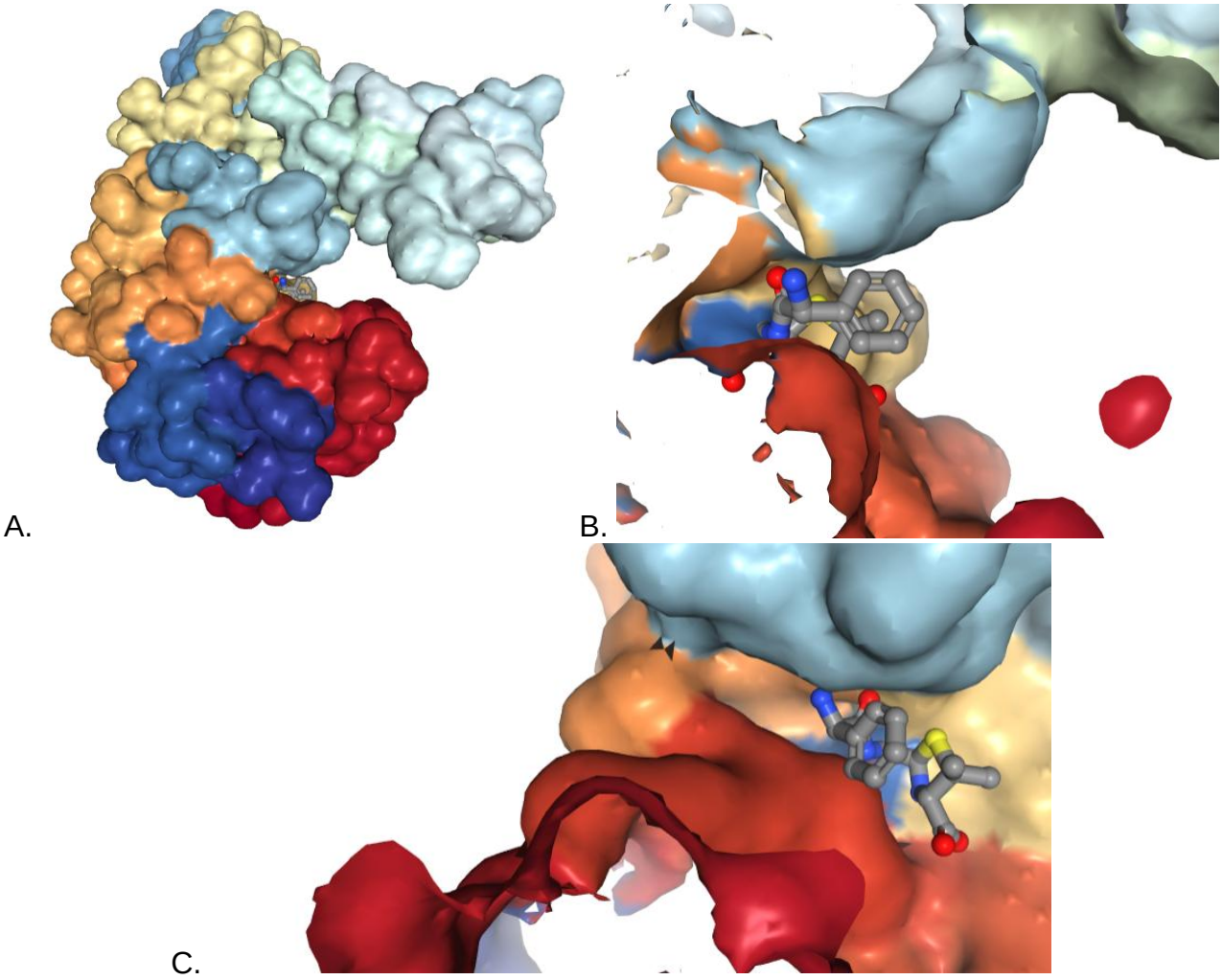

Figure 48 Co-crystal structure of penicillin binding protein 4 (dacB) from *E. coli,* complexed with ampicillin.[130] A. Global view B. zoom of global view C. Side zoom with ampicillin in balls and sticks and protein in rainbow surface representation.

3.4.1.1. Synthesis of ampicillin conjugates

Two probes were designed: the apo-DOTAM ampicillin conjugate **24** and the Cu(II) complexed DOTAM ampicillin conjugate **25** (Figure 49). Both compounds present acetylated catechols due to the positive translocation effect into the bacteria. The ampicillin and the DOTAM center are also designed to be covalently bound via a short non-cleavable linker. Also, **25** is the Cu(II) complexed version of **24**. This complexed probe was designed due to the known antimicrobial properties of copper. Therefore, by adding a Cu(II) ion, the new conjugate is hoped to have enhanced antibacterial function.

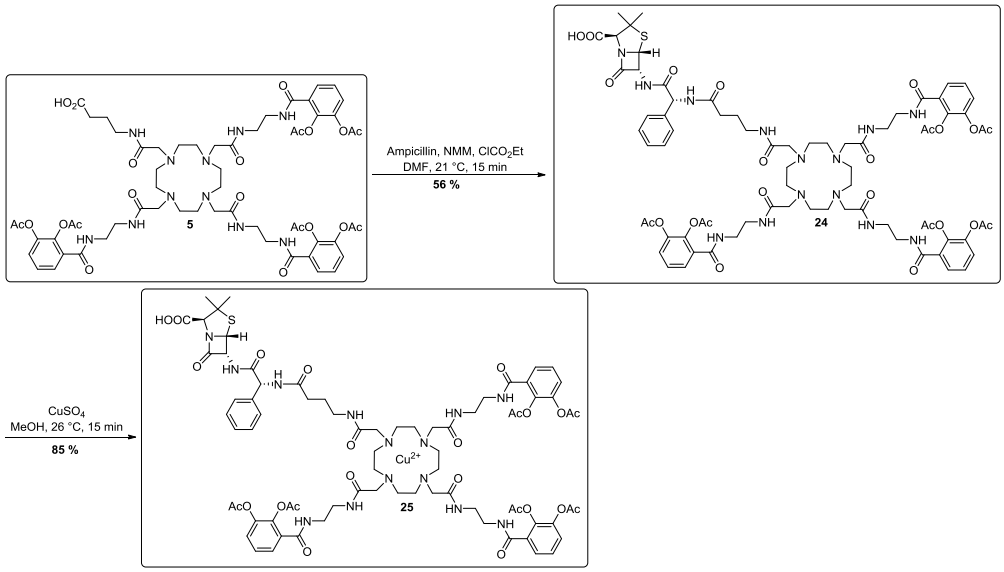

Figure 49 Synthesis of ampicillin conjugates **24** and **25**.

In order to obtain the ampicillin conjugate **24** with a decent overall yield of 15 %, **6** was activated via ethyl chloroformate. A fast reaction in presence of Cu(II) in MeOH enabled the isolation of **25** with limited deacetylation.

3.4.1.2. The inhibitory concentration (IC_{50}) assay on ampicillin conjugates

IC_{50} assays serve to quantify the antimicrobial effect of a given compound. Since the siderophore conjugates were proved to be able to penetrate into *E. coli*, the freshly prepared **24** and **25** were tested on specific *E. coli* strains of interest: the enterobactin-deficient strains *E. coli* ΔentA and *E. coli* ΔentB and the enterobactin receptor- deficient strain *E. coli* ΔfepA as well as their corresponding *E. coli* wt strain.

The probe **24** inhibited the growth of the *E. coli* wt, ΔentA and ΔentB and ΔfepA strains with IC_{50} values comparable to those of free ampicillin (Table 6). These results suggest the successful translocation of the ampicillin conjugate into the periplasmic space, where the targeted PBP is located. Consequently, through these results the conjugate at least proved to translocate through the bacterial outer membrane. In addition, the retention of activity against the enterobactin receptor-deficient strain (ΔfepA) compared with *E. coli* wt indicates the possibility of the siderophore conjugate to use different transporters than FepA to enter the bacterial cell. This suggests that bacterial uptake resistance mechanism cannot be driven by mutations or downregulation of FepA. Moreover, the 10-fold improvement of activity of **24** on the enterobactin-deficient strains compared to the wild type one emphasizes the competition effect to translocate

the ampicillin conjugate in presence of endogenous enterobactin. These results also imply the function of the DOTAM core as an iron carrier.

Table 6 Growth inhibitory activities (IC_{50}) of the ampicillin conjugates compared to ampicillin in µM.

Compounds	Core	Linker	Siderophore	Payload	*E. coli* wt	*E. coli* ΔentA	*E. coli* ΔentB	*E. coli* ΔfepA
				Ampicillin	4.3	2.1	6.2	3.8
24	DOTAM	GABA	catAc	Ampicillin	30.2	2.1	3.3	7.2
25	CuDOTAM	GABA	catAc	Ampicillin	>50	1.9	2.1	>50

The IC_{50} value of the *E. coli* ΔentA and *E. coli* ΔentB were slightly improved with the use of the Cu(II) version **25**, presumably due to the Cu(II) antimicrobial properties. However, **25** also led to a drop in activity against *E. coli* wt and ΔfepA. This effect could be explained by the competitive presence of endogenous enterobactin.

3.4.2. The ciprofloxacin conjugates

In the second step, synthetic sideromycins having cytoplasmic targets were chosen. Ciprofloxacin inhibits the cytoplasmic bacterial type IIA topoisomerase “DNA gyrase”. Until now the Torjan horse strategy applied to ciprofloxacin rarely improved its activity against Gram-negative bacteria,[73, 81, 103b, 131] or only showed improved selectivity towards *S. aureus*.[73] Moreover, the co-crystal structure of ciprofloxacin with gyrase and DNA in *S. aureus* shows some hindrance at the piperazine side chain of ciprofloxacin. However, ciprofloxacin is a well-suited candidate for the establishment of a Trojan horse concept and the study of cleavable linkers: the piperazine moiety is directed towards the exit of the DNA gyrase inhibition pocket. Moreover, ciprofloxacin is small, cheap and its reactivity and its mode of action are well-established. (Figure 50).

Indeed, due to the limited free space of the pocket at the target location, one conjugate containing a long, soluble and flexible linker and another one containing a cleavable linker were synthesized. In order to explore the different possibilities of the siderophore system, hydroxamates and catecholates were chosen to be linked to the DOTAM center.

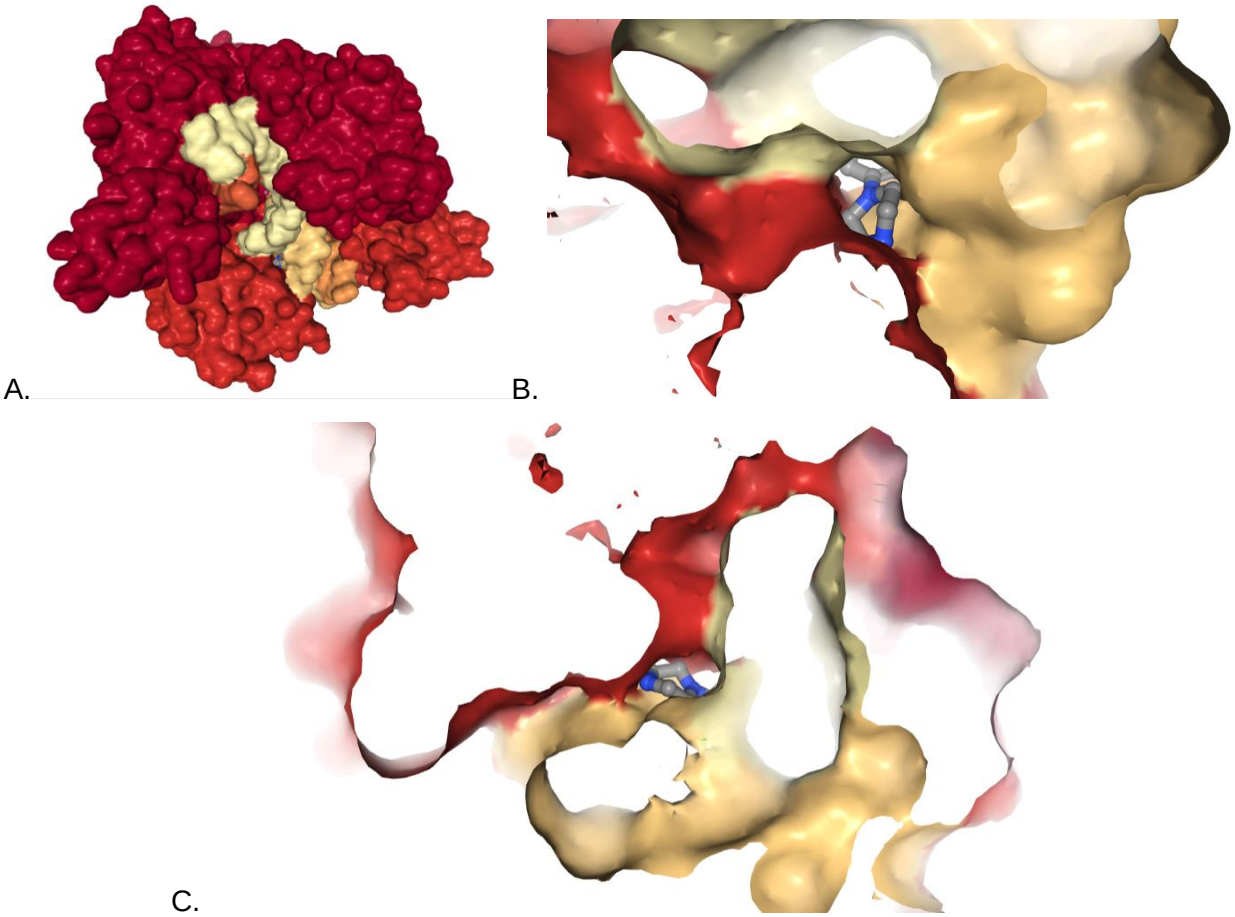

Figure 50 Co-crystal structure of the twinned 3.35 Å structure of *S aureus* gyrase complex with ciprofloxacin and DNA.[132] A. Global view B. zoom of global view C. Side zoom with ampicillin in balls and sticks and protein in chain surface representation.

Several investigations showed the possibility to derivatize the secondary amine by *N*-acylation without significantly harming the activity of the antibiotic.[133] Thus, a cleavable linker attached to ciprofloxacin was chosen in order to minimize steric hindrance by the linker and the carrier. A disulfide linker was selected due to differences of reducing conditions between the cytoplasm and the extracellular environment (Figure 51). The higher concentration of intracellular antioxidants such as glutathione (0.5-10 mM vs 2-10 µM) or of reducing enzymes such as glutathione reductases induces a selective intracellular disulfide bond cleavage and release of the payload.[134]

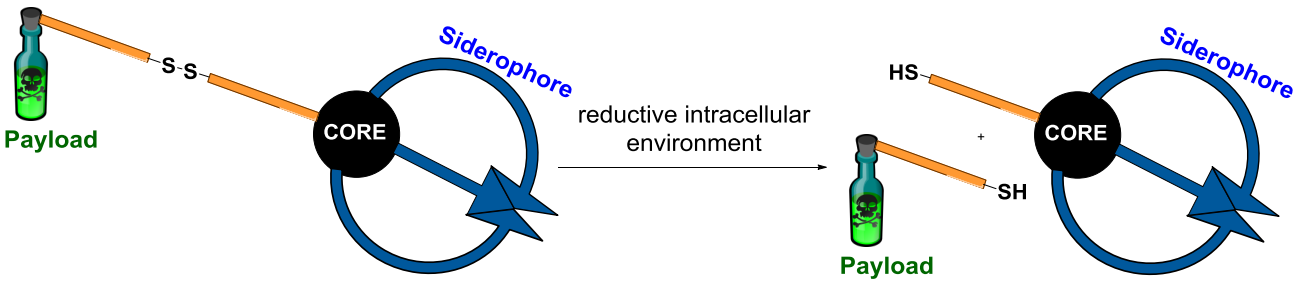

Figure 51 General cleavage mechanism for disulfide containing conjugates.

3.4.2.1. Synthesis of ciprofloxacin conjugates

Two ciprofloxacin conjugates were designed (Figure 52). The first one is a non-cleavable conjugate between ciprofloxacin and a hydroxamate-type siderophore, whereas the second one is a cleavable conjugate between ciprofloxacin and a catechol-type siderophore. The PEG_3 linker was selected for the design of the non-cleavable conjugate in order to limit negative interactions between the conjugate and the target protein. The synthesis of the conjugate **26** was performed by the MSc student Isabell Schneider.

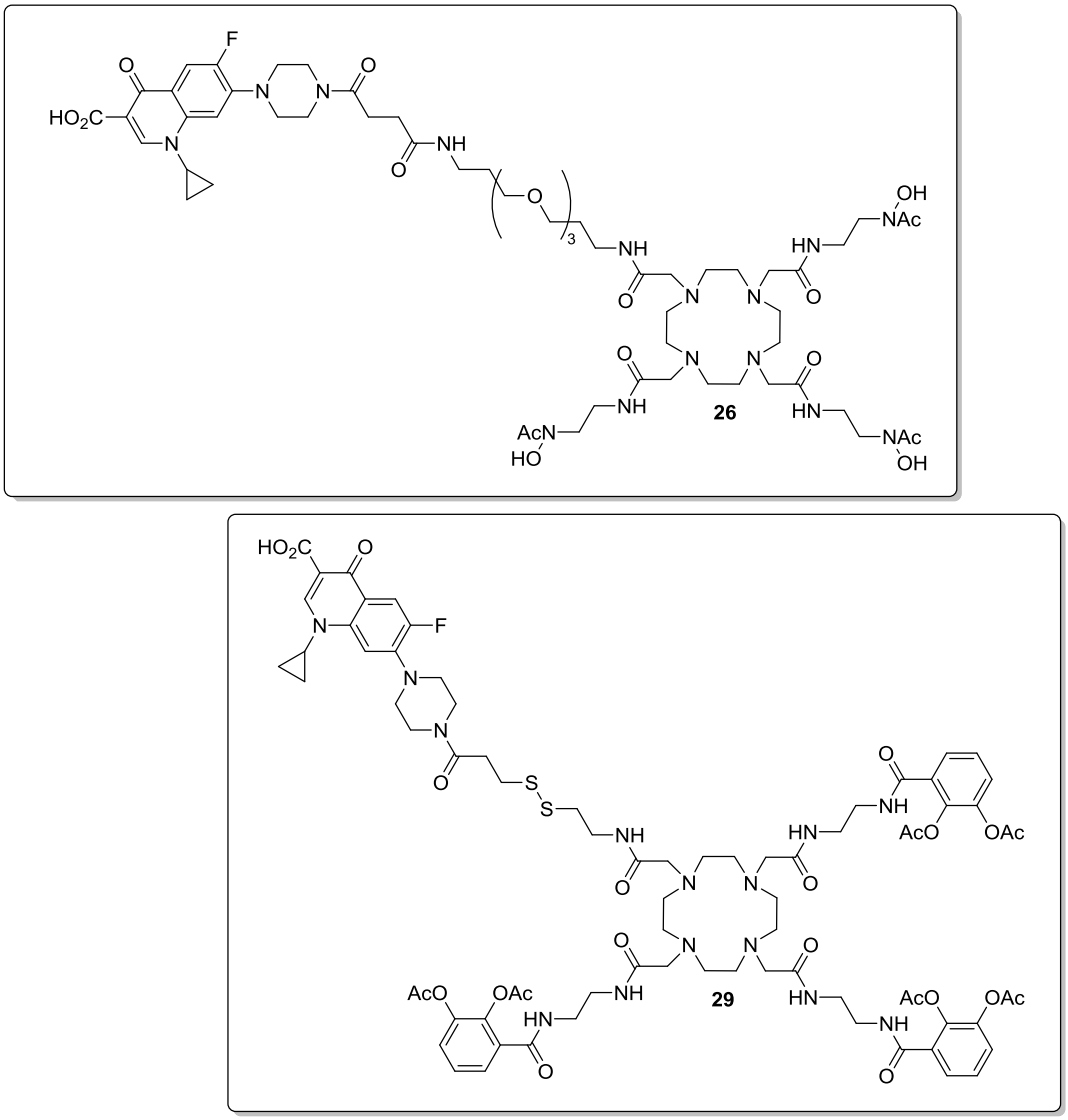

Figure 52 Design of the ciprofloxacin conjugates.

For the synthesis of the cleavable ciprofloxacin conjugate **29**, two strategies are available to access the final disulfide-containing probe (Figure 53). The first one consists of preparing an electron-poor thiol by adding a thiopyridyl group to a thiol group. This strategy implies the synthesis of a carrier with an electron-rich thiol. The second path follows the opposite strategy with an electron-rich thio-containing ciprofloxacin and an electron poor thio-containing siderophore.

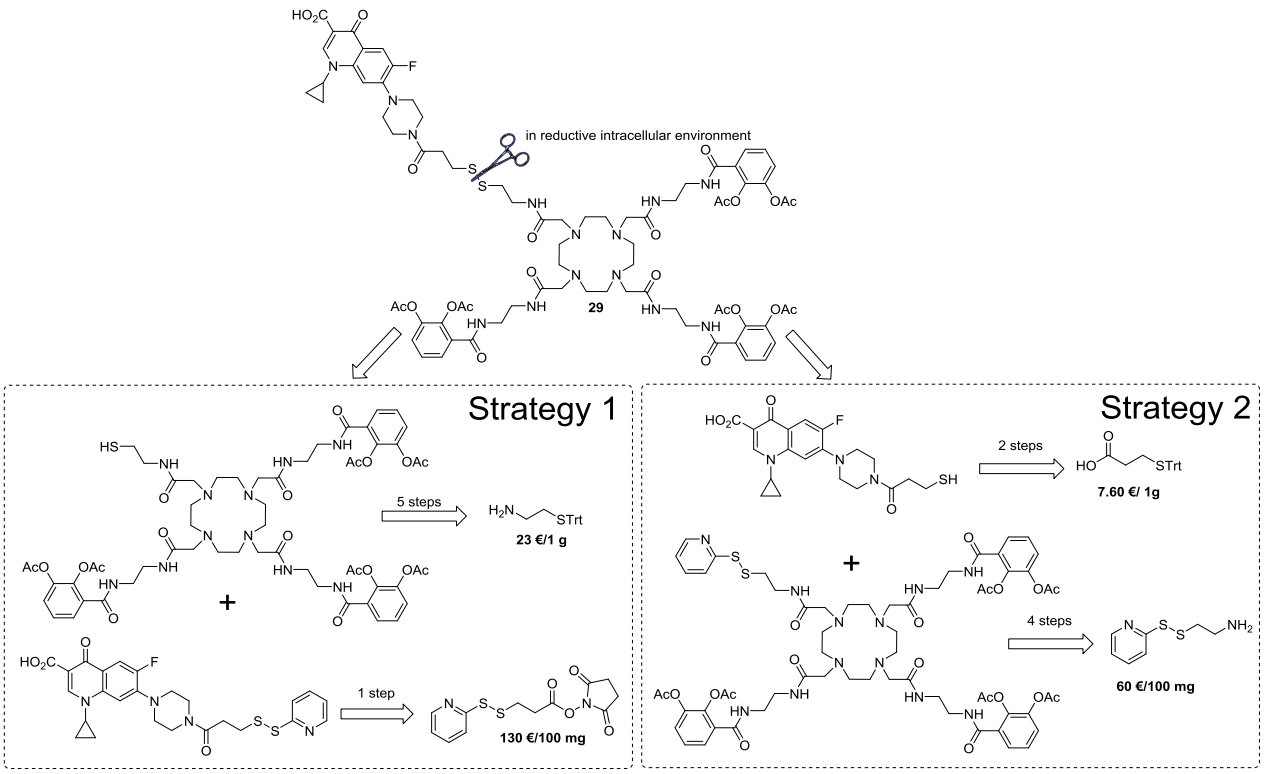

Figure 53 Retrosynthetic analysis of the cleavable ciprofloxacin conjugate.

The second strategy involves more parallel steps, which would lead to a more efficient synthetic route. However, the prices of the available starting materials for each strategy differ, and the first one is more economical in that respect. As a matter of fact, for the strategy 1, the most expensive starting material succinimidyl 3-(2-pyridyldithio)propionate (SPDP) costs 130 €/100 mg and is two steps away from the end product. In comparison, the (S)-2-pyridylthio cysteamine hydrochloride which costs 60 €/100 mg but which is 5 steps away from the expected probe. Moreover, due to up to 5 times lower experimental yields to obtain the free thiol-containing ciprofloxacin version and the difficulty to isolate the complementary siderophore, the first strategy was preferred. The direct coupling between ciprofloxacin and the SPDP led to almost quantitative yields (Figure 54).

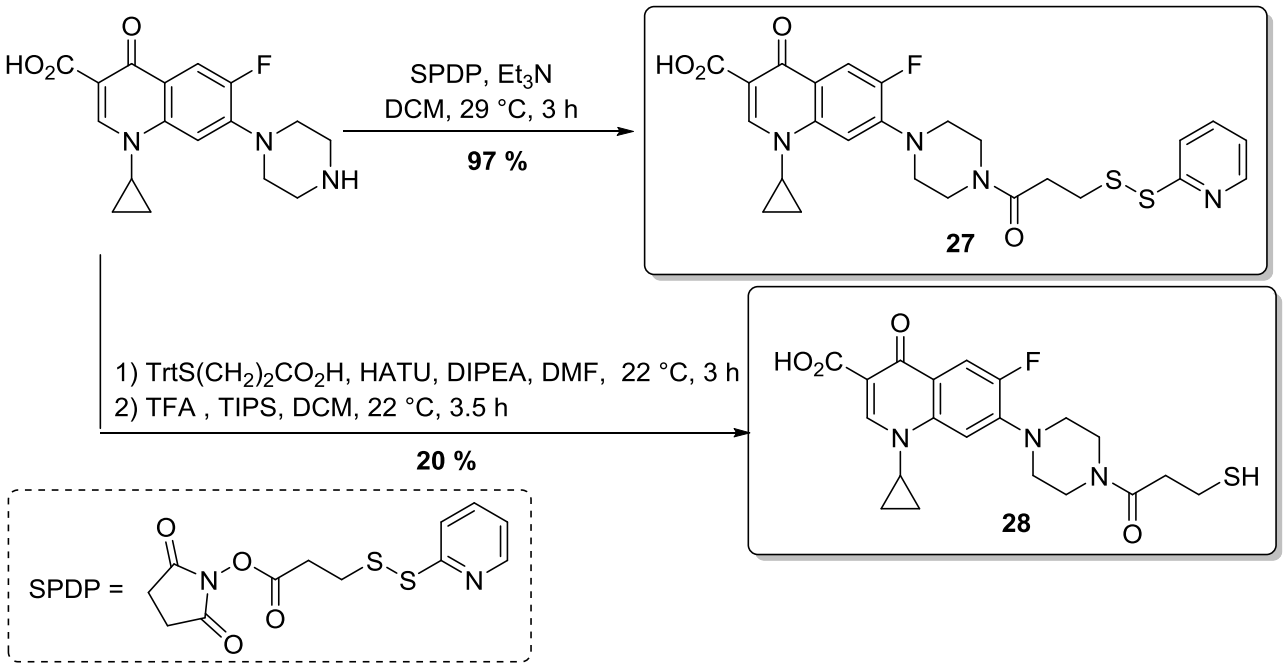

Figure 54 Synthesis of ciprofloxacin derivative **27** and **28**.

On the other end, the free thiol-containing ciprofloxacin was also synthesized over two steps starting from the HATU-activated 3-(tritylthio)propanoic acid and followed by the acidic trityl deprotection in presence of TIPS. The resulting ciprofloxacin derivative **28** is an important control molecule since it represents the theoretical delivered antibiotic after disulfide cleavage.

The alkylations using the prepared linkers **39** and **65** followed by the Boc deprotection led to the isolation of **66**. The Schotten-Baumann strategy was chosen between the catechol **40** and the S-trityl protected **66**. The trityl deprotection was obtained in acidic conditions and TIPS as a carbocation scavenger to yield **67** (Figure 55).

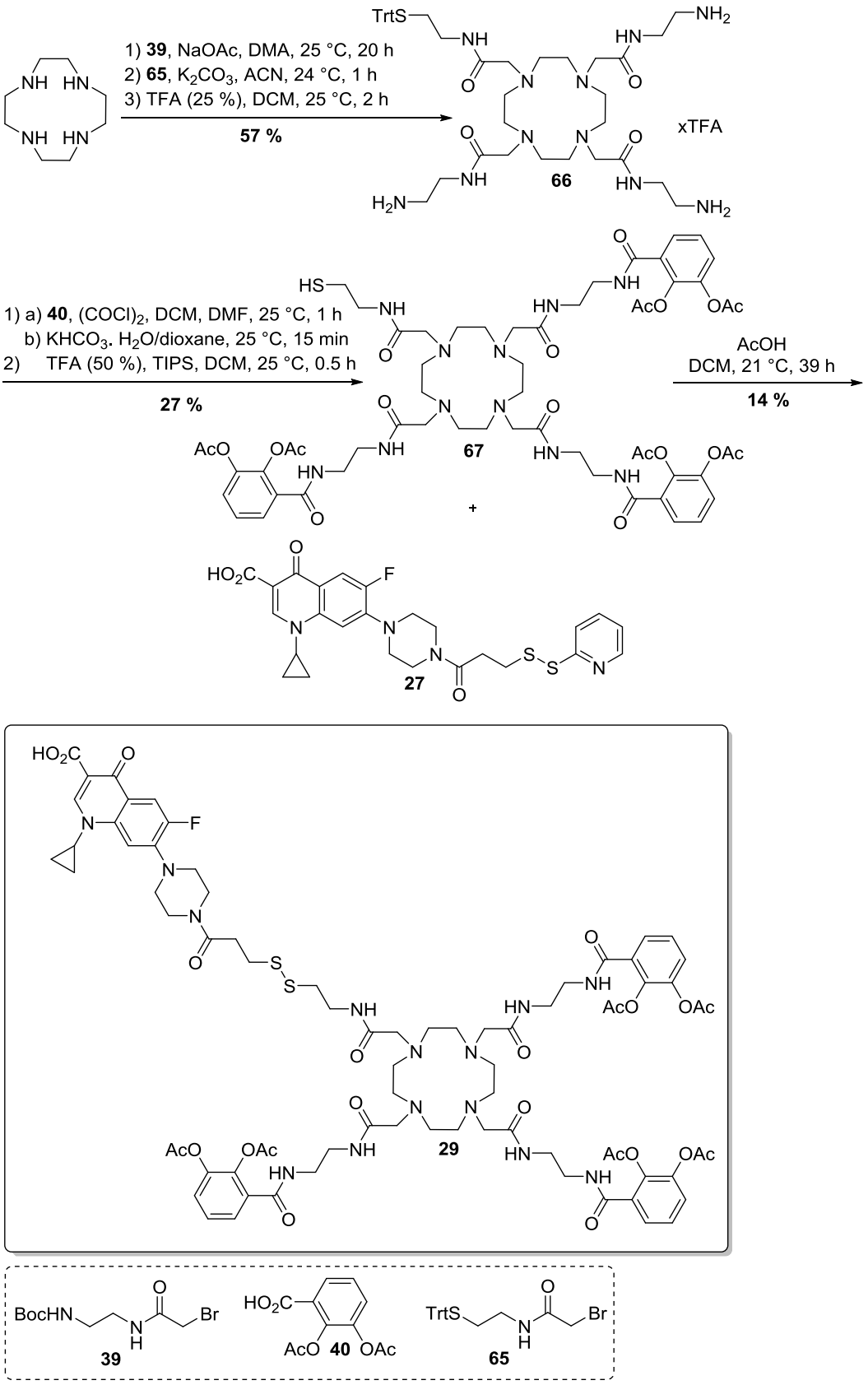

Figure 55 Synthesis of the ciprofloxacin/catechol DOTAM conjugate **29**.

After optimization of the reaction, the 2-day-long disulfide coupling between the nucleophile **67** and the electrophile **27** was achieved to afford **29** with a low overall yield of 2 % over 6 steps. The yield losses could be trackd back to partial deacetylation all along the synthetic process.

3.4.2.2. The growth inhibition assay on ciprofloxacin conjugates

The main purpose of this case study was to verify whether the use of disulfide bonds could improve the activity of the released antibiotics against *E. coli* and *P. aeruginosa* (Table 7).

Table 7 IC_{50} values of antibiotics and synthetic derivates against *E. coli* and *P. aeruginosa* in µM.

Compounds	Core	Linker	Siderophore	Payload	*E. coli*	*P. aeruginosa*
				Ciprofloxacin	0.01	0.27
26	DOTAM	PEG_3/suc	HydrH	Ciprofloxacin	100	>100
28				Ciprofloxacin-SH	6	64
29	DOTAM	EthylS	catAc	Ciprofloxacin-S	15	15

The results reveal a clear loss of activity when ciprofloxacin is derivatized. More precisely, the compound **26** showed no growth inhibition, although the ciprofloxacin is still present in the conjugated structure. In the same direction, the ciprofloxacin conjugate **29** did not show as effective growth inhibition as its parent drug. However, when compared to its released drug form **28**, the cleavable conjugate showed a slight improvement in antibacterial activity against *P. aeruginosa*. These results support the conclusion that either a cleavable linker and/or the use of acetylated catechols improve the activity of a drug. This report is one of the few of an active ciprofloxacin conjugate showing successful delivery to the cytosol. Moreover, the antimicrobial properties of the conjugate **29** shows the possibility to use cleavable linkers such as disulfide bonds in order to form active conjugates for antibiotics which have specific cytoplasmic targets. However, the drop of activity while modifying ciprofloxacin with a short thiolated linker raises the question of the usefulness of such as derivatization for other antibiotics. Indeed, the addition of a free thiol function triggers more reactivity towards Michael acceptors and undesired reactions may occur, leading to a loss in antibacterial activity.

3.4.3. The sorangicin A conjugate

In a third step, the cleavable linker has been applied to antibiotics whose antibacterial potency needs to be improved. As mentioned earlier, it can be antibiotics presenting a lower activity against Gram-negative bacteria compared to Gram-positive ones. For this purpose, this study focused on the development of novel sorangicin A conjugates. Sorangicins are RNA

polymerase inhibitors.[135] However, their binding pockets are located deeply in the RNA polymerase from *Thermus aquaticus* (Figure 56).

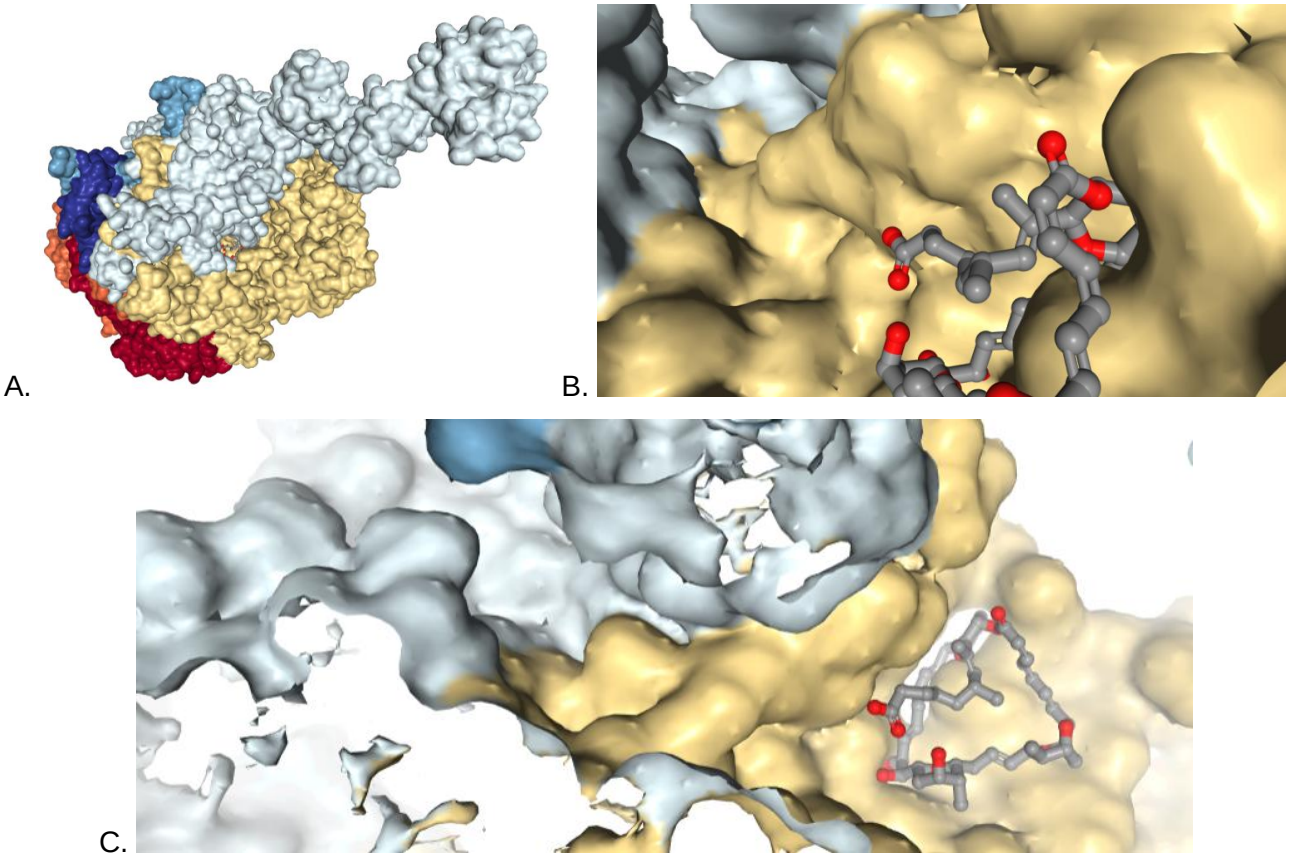

Figure 56 Co-crystal structure of *Thermus aquaticus* taq RNA polymerase-sorangicin complex.[136] A. Global view B. zoom of global view C. Side zoom with ampicillin in balls and sticks and protein in chain surface representation.

Therefore, the design of a cleavable linker for sorangicin conjugates is adapted. Moreover, the co-crystal structure shows free space in the direction of the side chain carboxylic acid (Figure 57).

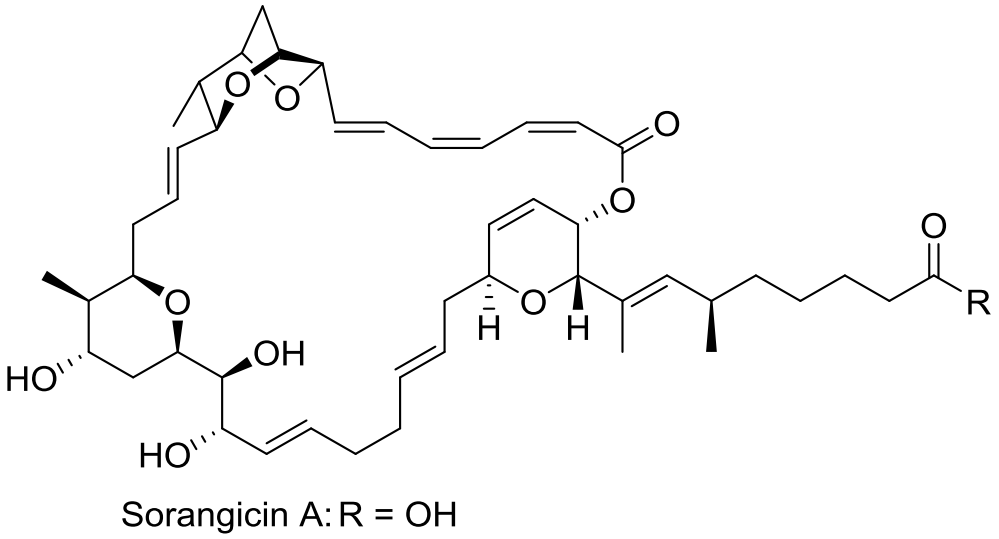

Figure 57 General structure of sorangicin A and points of derivatization (adapted from [137]).

As a first observation, sorangicin A presents high activity towards the Gram-positive bacterium *S. aureus*. However, the activity against the Gram-negative bacterium *E. coli* is 1000 fold worse (Table 8). Although the cause for such a difference is still unknown, it was hypothesized that it is partly due to the difficulty to translocate sorangicin A through the Gram-negative bacterial cell membrane. Consequently, derivatives via simple amide couplings were designed with expectations not to worsen interactions with the target protein.

The derivatization of sorangicin A was already widely investigated, especially on the side carboxylic acid function via amide coupling reactions.[137] Although the activity was slightly modulated by the modifications, the differences between Gram-negative and Gram-positive bacteria were still reaching 1000 fold in several cases of alkylamide derivatives. Indeed, even higher ratios were obtained when sorangicin A was transformed into a *N*-methoxy-*N*-methylamide derivative.

Table 8 Biological activity of sorangicin A amide derivatives (adapted from [137]).

Abbreviated name	R	MIC against *S. aureus* (µg/mL)	MIC against *E. coli* (µg/mL)
sorangicin A	**OH**	0.016-0.031	6-12
amide	**NH_2**	0.125	-
***N*-methylamide**	**NHMe**	0.062	-
***N*-dimethylamide**	**$N(Me)_2$**	0.016	25
***N*-isopropylamide**	**$N(iPr)_2$**	0.060	50
***N*-hexylamide**	**$NH(CH_2)_5CH_3$**	1	1000
***N*-benzylamide**	**NHBn**	0.065-0.125	-
***N*-methoxyamide**	**NHOMe**	0.008-0.016	25
***N*-methoxy-*N*-methylamide**	**NMe(OMe)**	0.000125	>200

These results suggest the possibility to use cleavable conjugates, whose released drug could be slightly modified on the carboxylic side chain without lowering its activity. Since the disulfide chemistry tool was established in the ciprofloxacin project, it was decided to work on similar cleavable linkers for the design of sorangicin conjugates (Figure 58).

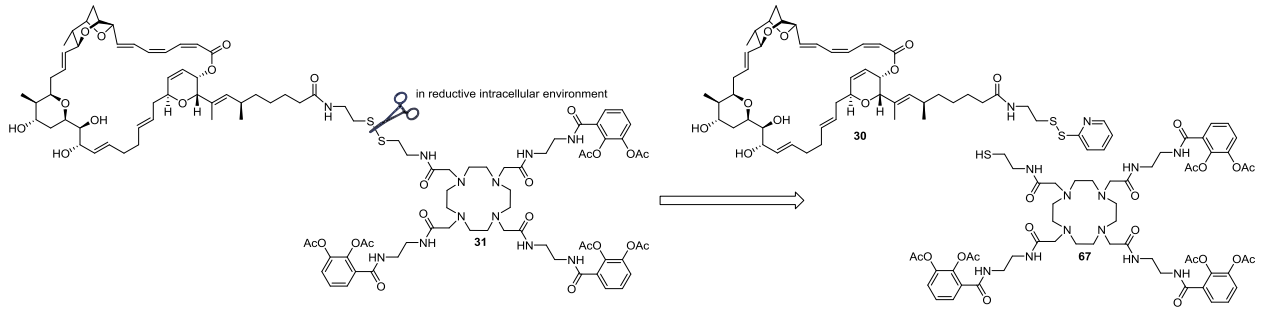

Figure 58 Design and retrosynthetic pathway of the cleavable sorangicin conjugate **31**, and structure of control compounds **30** and **67**.

This strategy offers two advantages. First of all, it enables the use of a common intermediate already synthesized for the ciprofloxacin conjugate, **67**. Moreover, it allows the use of optimized and robust conditions for the disulfide coupling as last step of the synthesis. Additionally, the intermediate **30** can be obtained from sorangicin A in a straightforward manner. The natural product was formerly isolated from the bacteria Sorangium cellulosum [135, 138] and was supplied from the MWIS department of the Helmholtz Centre for Infection Research.

3.4.3.1. Synthesis of the sorangicin A conjugate for inhibitory concentration (IC_{50}) assay

After optimization, **30** was obtained with a HATU coupling with a good yield of 75 % (Figure 59).

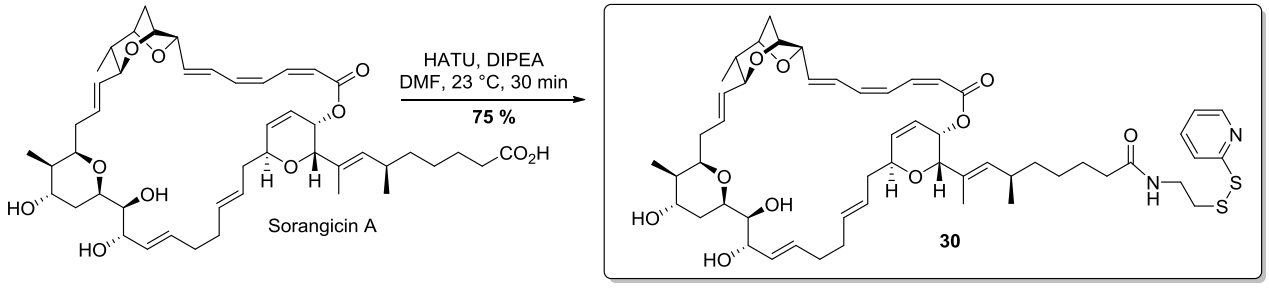

Figure 59 Synthesis of the sorangicin A derivative **30**.

The synthesis of the deprotected form of **30** was attempted as a control compound to be directly compared to the antibiotic conjugate, since it corresponds to the released drug after

cleavage. However, the derivate could not be isolated due to stability issues. It was hypothesized that a possible Michael addition occurs during the deprotection of the thiol, although no side-product of cyclization or dimerization was observed by LCMS.

After the successful preparation of the sorangicin derivative **30**, the sorangicin conjugate **31** was synthesized by using the intermediate **30** and the thiolated carrier **67** which was previously described. Using the optimized mild conditions of the ciprofloxacin conjugate procedure, the cleavable sorangicin conjugate was obtained with a yield of 25 % (Figure 60).

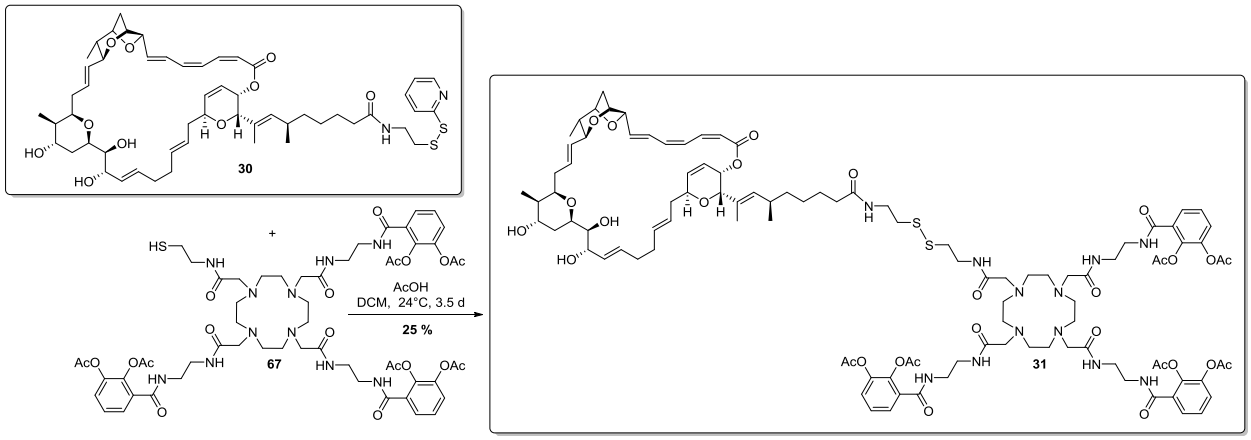

Figure 60 Synthesis of the sorangicin A/catechol DOTAM conjugate **31**.

It is noteworthy that in several cases, the protection of alcohols in sorangicin and other activating agents are described as beneficial in the literature.[137] Nevertheless, HATU coupling showed better yields on an unprotected sorangicin A. Moreover, the unprotected route was preferred due to its more straightforward, two step synthesis to the desired product with a two step synthesis starting from sorangicin A.

3.4.3.2. The inhibitory concentration (IC_{50}) assay on sorangicin A conjugates

After the successful synthesis of the sorangicin conjugate, the product was tested on a panel of Gram-negative bacteria included in the ESKAPE panel. As a control, the Gram-positive *S. aureus* was also added. In addition to the non pathogenic *E. coli* K12, three clinically relevant uropathogenic *E. coli* (UPEC) strains and one clinically relevant enteropathogenic *E. coli* (EPEC) strains were tested.

The sorangicin conjugate was tested as well as three control compounds. First of all, the sorangicin A and the released siderophore **67** were added to the experiment. However, the exact

released thiolated sorangicin could not be synthesized, and therefore its thiopyridyl-protected version **30** was tested instead (Table 9).

Table 9 IC_{50} values of sorangicin derivatives and siderophores against Gram-negative bacteria of the ESKAPE panel and MRSA in µM.

Compounds	Core	Linker	Siderophore	Payload	*E. coli* K12 MG 1655	*E. coli* E2348 /69	*E. coli* UPEC 700928	*E. coli* UPEC J96	*E. coli UPEC 536*	*P. aeruginosa*	*A. baumanii*	*K. pneumoniae*	MRSA RKI
				sorangicin A	<13	22	58	2	<4	6	6	6	<0.2
30				sorangicinS-Spyridyl	61	>100	>100	87	>100	>100	>100	>100	<0.2
67	DOTAM	EthylSH	catAc		59	>100	>100	60	>100	75	>100	>100	>100
31	DOTAM	EthylS	catAc	sorangicinS	>100	>100	>100	>100	>100	>100	>100	>100	0.7

Results were obtained with an experimental duplicate

As mentioned earlier, the activity of sorangicin A is much higher against multi-drug-resistant *S. aureus* (MRSA) RKI compared to the tested Gram-negative bacteria. However, the thiolated version **30** shows a much weaker activity towards Gram-negative bacteria. Nevertheless, the IC_{50} against MRSA is below 0.2 µM and therefore, it is suggested that the derivatives can still strongly bind to its target in order to perform an antibacterial effect. The activity of the theoretically released carrier is relatively weak against the whole panel of bacteria which is expected since the carrier is not supposed to show any antimicrobial effect. Surprinsingly, the pattern shown by the conjugate is similar to that of the sorangicin derivate. These results open several questions regarding the design of the conjugate and the hypotheses which were taken into account. The first possibility is that the initial difference of activity between Gram-positive and Gram-negative bacteria is not due to a translocation issue. On the other hand, if the translocation of sorangicin A is the fundamental issue inducing moderate-low activities towards Gram-negative bacteria, a few explanations are possible. The sorangicin conjugate could be too large to be taken up by Gram-negative bacteria but this scenario would not explain the low efficacy of the conjugate against MRSA. The second possibility is that an early extracellular cleavage could happen and no active transport via Fe(III) uptake systems would be possible. This case would also explain why the conjugate similar activities showed to the thiolated sorangicin **30**. In any case, the design of disulfide sorangicin siderophore conjugate is inappropriate for the improvement of activity against Gram-negative bacteria.

3.4.4. Toxicity studies

Considerable amount of work was invested on the studies of siderophore uptake and on the efficacy of siderophore conjugates for the detection and the treatment of bacterial infections. However, although a few probes were shown to translocate into bacteria and contain a labelling

agent, selectivity towards bacteria compared to eukaryotic cells must be achieved. Several compounds were tested to verify their toxicity towards eukaryotic cells, so that the designed molecules would be applicable for pre-clinical and clinical studies with limited undesired side effects. The cytotoxicities of the compounds were determined via the WST-1 assay.

For this purpose, it was decided to test a selected panel of compounds on 4 different eukaryotic cells: the mouse fibroblast L929, the epidermoid carcinoma line KB-31, the breast cancer MCF-7 and the conditional immortalization human fibroblast FS4-LTM. After a 5-day-long incubation of the cells in presence of the synthetic compounds at concentrations ranging from 0.2 to 100 µM, the IC_{50} value of each compound in each condition was assessed (Table 10).

Table 10 IC_{50} value of compounds for the eukaryotic cells L929, KB-31, MCF-7 and FS4-LTM in µM.

Compounds	Core	Linker	Siderophore	Payload	IC_{50} with L929 (µM)	IC_{50} with KB-31 (µM)	IC_{50} with MCF-7 (µM)	IC_{50} with FS4-LTM (µM)
				Staurosporine	<0.2	<0.2	0,3	<0.2
				Auranofin	2,6	1,9	2,2	12,5
				Ciprofloxacin	>100	>100	>100	>100
				Ampicillin	>100	>100	>100	>100
15	DOTAM	PEG_3/suc	HydrH		>100	>100	>100	>100
26	DOTAM	PEG_3/suc	HydrH	Ciprofloxacin	>100	>100	>100	>100
5	DOTAM	GABA	catAc		>100	>100	94	>100
24	DOTAM	GABA	catAc	Ampicillin	>100	79	>100	>100
25	CuDOTAM	GABA	catAc	Ampicillin	>100	>87	88	>100
9	CuDOTAM	GABA	catAc		>100	>100	43	>100
7	DOTAM	OH	catAc		>100	71	45	73

Staurosporine, auranofin, ciprofloxacin and ampicillin were used as standard compounds for toxicity studies. The two first compounds are toxic antibiotics against the 4 cell lines of interest, whereas the two last ones are non-toxic ones. A set of compounds was chosen according to their specific properties. As an example the ciprofloxacin and ampicillin conjugates **26** and **24** showed no significant toxicity as well as their corresponding carrier moieties **15** and **5**. However, the modification of the 4th arm from a GABA to a short carboxylic acid or the addition of Cu(II) into the DOTAM center slightly worsened the toxicity properties of the molecule, especially against MCF-7. To conclude, the selected set of compounds showed relatively low toxicity towards the cells L929, KB-31, MCF-7 and FS4-LTM. These results were expected by the fact that marketed antibiotics such as ciprofloxacin and ampicillin should show low toxicity properties and that the DOTA core

was already proven to be nontoxic, as it is part of several marketed products such as gadoteric acid, an approved drug for the detection of disruption areas of abnormal vascularity.[139]

4.Summary

The goal of the thesis was to study the Fe(III) affinity of designed synthetic siderophores. Besides, it was important to assess the internalization of compounds into bacterial cells. One addtitional objective was to improve the antibacterial activity of antibiotics selectively towards bacteria of the ESKAPE panel by conjugation to siderophores.

In a first step, the study of Fe(III) affinity towards the synthetic siderophores was investigated. Similar Fe(III) affinity as the natural siderophore enterobactin was observed in the Fe(CAS) assay due to the free tris catechol form. Moreover, a complexed metal into a DOTAM center such as Eu^{3+} did not show any disturbance on the Fe(III) complexation capacity of the molecule. The deacetylation process of catechols was observed as well as the Fe(III) complexation in medium and in presence of bacteria.

Secondly, the uptake of the synthetic siderophores was assessed. Growth recovery assays enabled the comparison of the siderophoric properties of the molecules compared to enterobactin and ferrichrome. A series of parameters were modified in order to optimize and understand the siderophoric effect of molecules (Figure 61). As a highlight, DOTAM-cored molecules presenting acetylated catechols showed similar growth recovery as natural siderophores in *E. coli* and *P. aeruginosa*. BODIPY siderophore conjugates labelled all the tested Gram-negative bacteria of the ESKAPE panel and the FAP system proved the internalization of the fluorogen conjugate into *E. coli*.

Eventually, ampicillin siderophore conjugates showed activities in the same range as the parent drug against *E. coli*. Moreover, the synthesis of ciprofloxacin conjugates illustrated the compatibility of using cleavable disulfide linkers. However, the translation of the similar design to a sorangicin conjugate showed a significant loss in activity in all of the tested Gram-negative bacteria. In parallel, the selected siderophores and siderophore conjugates showed low or no toxicity properties.

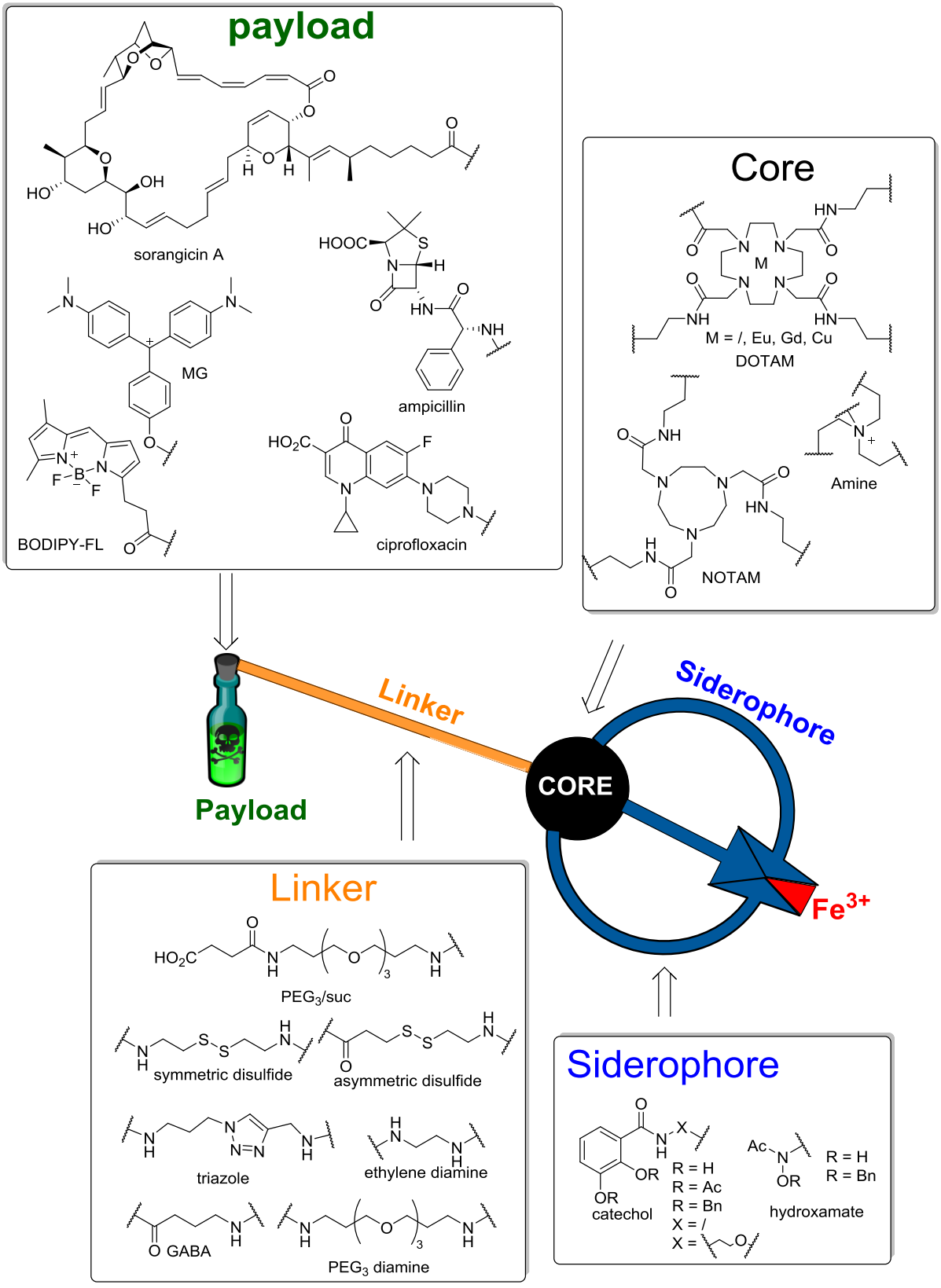

Figure 61 General structure of hexavalent siderophore conjugates of interest.

5. Outlook

The general structure of siderophore conjugates offers various possibilities for the improvement of labelling or antibacterial properties (Figure 62).

First of all, the modification of the core although not essential can show significant alterations in the siderophoric properties of the molecule. Since MECAM siderophores showed high affinitiy towards Fe(III), working on phenylic cores is an alternative to investigate.[65] Using more natural cores like trilactones from enterobactin or corynebactin is another option to capture ferric iron from the medium and be translocated into bacteria.[71] Finally, the use of metals into the DOTAM molecule must be further investigated to explore the potential of this design towards theranostic applications.

A considerable amount of research was investigated in the development of catechols as siderophore moieties. However, other siderophore functionalities such as α-hydroxycarboxylic acids and hydroxamates are present in natural siderophores and are actively transported through the bacterial membrane. More recently, hydroxypyridinone functionalities were used in advanced ß-lactam conjugates to extend the antimicrobial properties of the drug. The possibility to attach different Fe(III) chelators could be investigated. Besides, mixed siderophores could be designed from natural siderophores, synthesized and tested in order to study the effect of different Fe(III) chelators.

Disulfide linkers were essential tools for the design of selective cleavable conjugates. However, due to little information in the literature about selective bacterial intracellular cleavable linkers, self immolative linkers are to be designed in order to have access to the selective cleavable properties of the disulfide bonds and liberate the original parent drug instead of a thiolated derivate.[140]

Finally, the antibiotic is a critical element for the efficacy of antibiotic transport into the bacteria. Rifampicin might be a well-suited candidate, since its activity against *E. coli* is in some cases more than 10^5 times worse than in Gram-positive bacteria such as *S. pneumoniae*.[141] If the size of the conjugate is too large to expect any improvement of antibiotic uptake, smaller molecules such as fosfomycin could be chosen which also presents translocation issues.

More and more research is invested in the field of bioconjugation and the design of siderophore conjugates. Several ß-lactam-siderophore conjugates are currently in late stage of clinical trials. In parallel, the DOTA-type molecules already proved benefic effects for imaging applications. In a nutshell, together with the data described in this thesis, the use of DOTA-based

siderophore conjugates is a promising research towards the diagnosis and the treatment of bacterial infections.

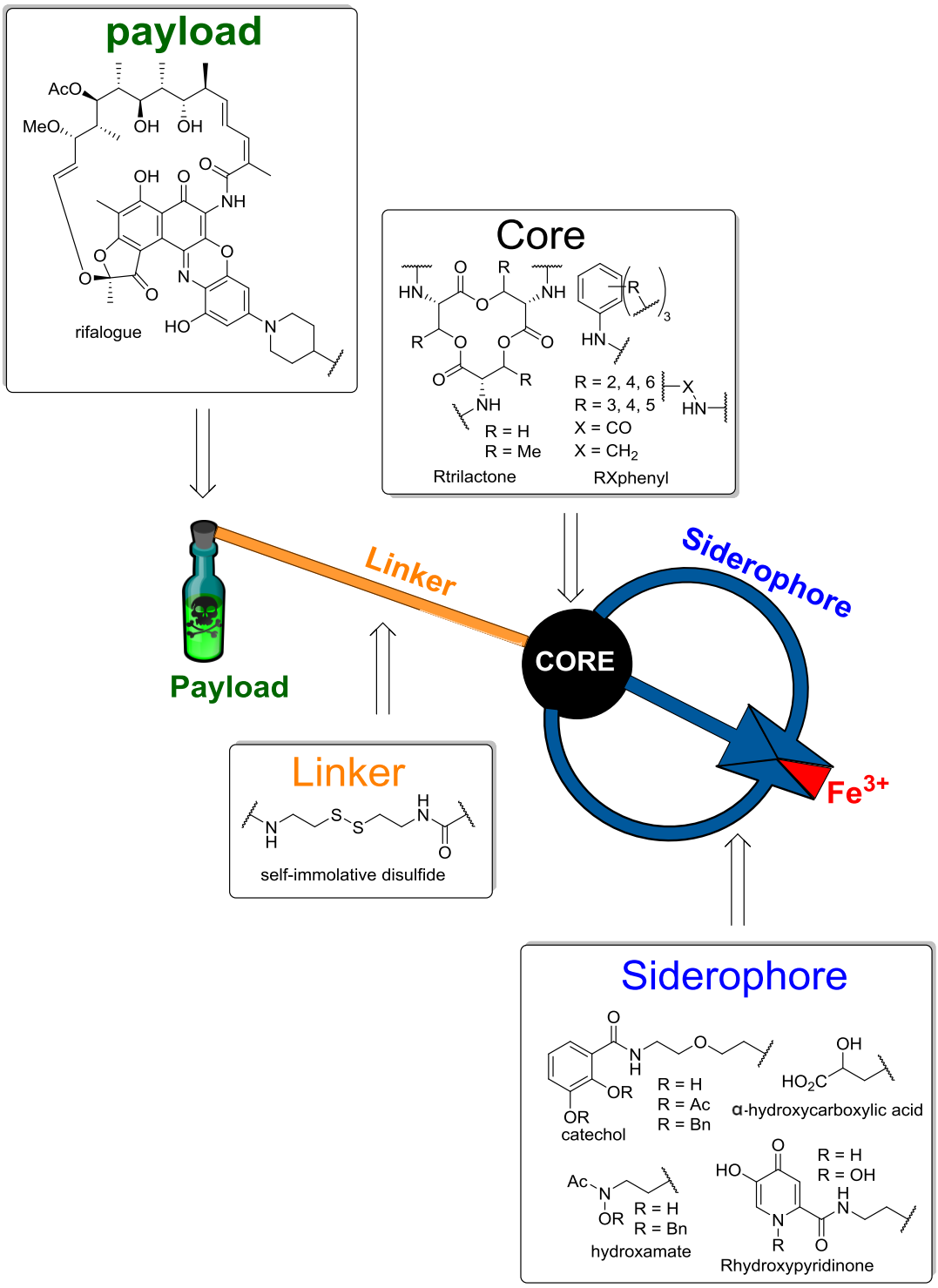

Figure 62 General outlook of the derivatization of siderophores and siderophore conjugates.

6. Materials and methods

6.1. Chemical synthesis

6.1.1. Chemical synthesis

Unless otherwise noted, all reagents were purchased from commercial suppliers and used without further purification. All solvents used for workup and purification were of HPLC grade. Moisture sensitive reactions were performed under argon atmosphere in dried glassware. Reactions were monitored by TLC, LCMS or NMR.

6.1.1.1. Flash chromatography

Flash chromatography was done either manually using appropriate glass columns filled with silicagel (Merck, Silicagel 60, 1.15111.1000, 15-40 µm) or using the Reveleris® X2 flash chromatography system and prepacked cartridges (Reveleris® Flash Cartridges Silica 40µm) from the company Büchi.

6.1.1.2. Preparative HPLC

Preparative RP high pressure liquid chromatography (HPLC) was performed on a Phenomenex Gemini C18 RP-column 00G-4436-NO, 10 µm, 110 A, 250×10.00 mm (5 mL/min) or on a Phenomenex Gemini C18 RP-column 00G-4435-PO-AX, 5 µm, 110 A, 250×21.20 mm (10 mL/min) or on a Thermo Fisher Scientific BDS Hypersil C18 RP-column 28105-259370, 5 µm, 250x30 mm, (25 mL/min) or a Macherey-Nagel Nucleosil 100-7 VP C18 RP column715691-1116949, 250×40 mm (from 25 to 50 mL/min) using a Thermo Fisher Scientific Dionex Ultimate 3000 HPLC system. Eluents, gradients and additives are given in parentheses. Product containing fractions were combined, diluted with milliQ H_2O (min. 1:1/solvent:H_2O), frozen and lyophilized.

6.1.1.3. Thin layer chromatography

Thin layer chromatography was performed on TLC Silica gel 60 F_{254} and stained according to the different staining solutions reported in Table 11.

Table 11 Description for the preparation of the TLC staining solutions.

Staining solution	formulation
$KMnO_4$	1.5 g $KMnO_4$, 10 g K_2CO_3, and 1.25 mL 10 % NaOH in 200 mL H_2O.
PMA	10 g phosphomolybdic acid in 100 mL abs. EtOH.
CAM	1 g $Ce(IV)(SO_4)_2$, 2.5 g $(NH_4)_6Mo_4O_7$ in 100 mL 10 % H_2SO_4
Anisaldehyde	135 mL abs. EtOH, 5 mL conc. H_2SO_4, 1.5 mL HOAc and 3.7 mL *p*-anisaldehyde.
Ninhydrin	1.5 g ninhydrin in 100 mL *abs.* EtOH and 3.0 mL HOAc.
Vanillin	15 g vanillin in 250 mL *abs.* EtOH and 2.5 mL conc. H_2SO_4.

6.1.1.4. Preparative thin layer chromatography

Preparative thin layer chromatography was performed on pre-coated glass plates (Merck TLC Silicagel 60 F_{254}, 1.05715.0001, 20x20 cm, max. 10-15 mg/plate and Analtech Uniplate Silica gel GF Z51305-9, 20x20 cm x 2 mm, max 100-150 mg/plate). Eluent or eluent-mixtures used and number of developments are reported in parentheses. Compounds were visualized by observation under UV light (λ = 254 or 366 nm). Compound containing silica gel fractions were scratched from the plate with a scapell, crushed to small pieces and compounds were dissolved by appropriate solvent mixtures.

6.1.1.5. Nuclear Magnetic Resonance

Nuclear Magnetic Resonance (NMR) spectra were recorded on a Bruker Avance III or a Bruker Avance III HD with cryoprobe system. ^{1}H NMR spectra were recorded at 500 MHz and 700 MHz. ^{13}C NMR spectra were recorded at 126 MHz and 176 MHz. Chemical shifts are reported in ppm relative to solvent signal. Multiplicity is indicated as follows: s (singlet); bs (broad singlet); d (doublet); t (triplet); q (quartet); m (multiplet); dd (doublet of doublets), etc.

6.1.1.6. Low resolution mass spectrometry

Low resolution mass spectrometry (LRMS) data were recorded using an Agilent 1100 HPLC system equipped with DAD detector and an API 150 EX quadrupole mass detector with electrospray ionization (ESI) (ACN-H_2O + 0.05 % TFA) or a Dionex Ultimate 3000 HPLC system equipped with a DAD detector and a Bruker amazon ion trap mass detector with electrospray ionization (ESI).

6.1.1.7. High resolution mass spectrometry

High resolution mass spectrometry (HRMS) data were recorded using a Dionex Ultimate 3000 HPLC system equipped with a DAD detector and a Bruker maXis HD QTOF mass detector with electrospray ionization (ESI).

6.1.2. Synthesis of compounds

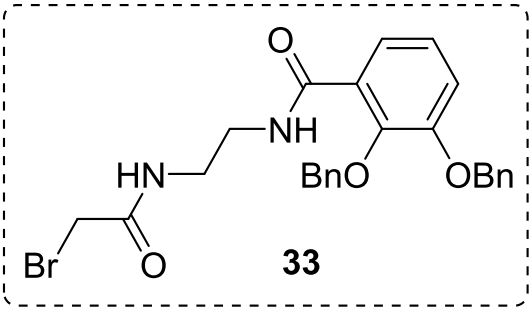

33

32 was prepared according to the procedure reported by Leydier *et al*.[142] To a solution of **32** (100 mg, 266 µmol) in DCM (250 µL) cooled to 0°C were added a solution of K_2CO_3 (44 mg, 319 µmol) in water (250 µL), and a solution of bromoacetyl bromide (28 µL, 319 µmol) in DCM (500 µL). The reaction mixture was stirred at 26 °C for 1 h. The phases were separated, and the AL was washed with DCM (2×10 mL). The OL was dried over magnesium sulfate, filtered and concentrated to yield **33** as a white solid (120 mg, 91 %). **^{1}H NMR** (500 MHz, $CDCl_3$). δ 8.19 (bt, 1H, J = 5.7 Hz, N*H*), 7.72 (dd, J = 2.8, 6.7 Hz, 1H), 7.47 (m, 2H, Ar-*H*), 7.44-7.31 (m, 9H, Ar-*H*), 7.19-7.14 (m, 2H, Ar-*H*), 5.17 (bs, 2H, ArOC*H*$_2$C$_6$H$_5$), 5.11 (bs, 2H, ArOC*H*$_2$C$_6$H$_5$), 3.76 (s, 2H, BrC*H*$_2$), 3.38 (m, 2H), 3.29 ppm (m, 2H). **^{13}C NMR** (125 MHz, $CDCl_3$). δ 166.6, 166.1, 151.7, 146.9, 136.3, 136.2, 128.9, 128.8, 128.7, 128.3, 127.6, 126.6, 124.5, 123.2, 117.4, 76.6, 71.3, 41.6, 38.7, 28.8 ppm. **ESI-HRMS**: $C_{25}H_{26}N_2O_4Br^+$ m/z = 497.1076 (calculated: 497.1070) $[M+H]^+$, error = 1.2 ppm.

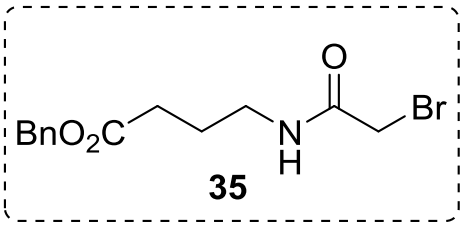

35

34 was prepared according to the procedure reported by Petrosyan *et al*.[143]. To a solution of **34** (6.00 g, 16 mmol) in DCM (50 mL) cooled to 0°C were added over 1 h a solution of K_2CO_3 (4.99 g, 36 mmol) in water (50 mL) and a solution of bromoacetyl bromide (1.72 mL, 20 mmol) in DCM (50 mL). The reaction mixture was stirred at 21 °C for 1.5 h. The phases were separated and the OL was washed with water (2×100 mL), brine (2×100 mL), dried over $MgSO_4$, filtered and concentrated to yield **19** as colorless oil (4.66 g, 90 %). **^{1}H NMR** (500 MHz, CD_3CN). δ 7.42-7.31

(m, 5H, C_6H_5), 6.95-6.74 (bs, 1H, N*H*), 5.09 (s, 2H, $CO_2CH_2C_6H_5$), 3.77 (s, 2H, CH_2Br), 3.20 (m, 2H, J = 6.9, 6.0 Hz, CH_2), 2.37 (t, 2H, *J* = 7.4 Hz, CH_2), 1.72 ppm (m, 2H, CH_2). **^{13}C NMR** (125 MHz, CD_3CN). δ 173.7, 167.1, 137.5, 129.5, 129.0, 128.9, 66.7, 39.7, 31.9, 30.0, 25.3 ppm. **ESI-HRMS**: $C_{13}H_{16}NO_3Na^+$ m/z = 336.0208 (calculated: 336.0206) $[M+Na]^+$, error = 0.6 ppm.

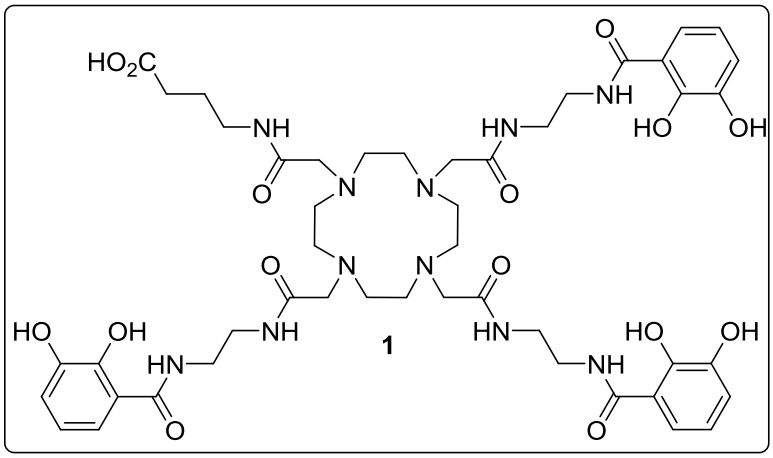

To a stirred suspension of cyclen (1.0 mg, 6 µmol) and sodium acetate (1.6 mg, 19 µmol) in DMA (100 µL) at 26°C under Ar conditions was added dropwise a yellow solution of **33** in DMA (150 µL). The reaction was stopped after 19 h stirring at 26 °C. The yellow solution was diluted in DCM (10 mL) and washed with $KHCO_3$ (10 mL) and water (10 mL), dried over Na_2SO_4, filtered and concentrated to yield yellow oil (10 mg). The crude material and K_2CO_3 (3.2 mg, 23 µmol) were suspended in ACN (250 µL), and a solution of **35** (2.4 mg, 8 µmol) in ACN (250 µL) was added dropwise for 5 min under Ar conditions at 0 °C. The suspension was stirred for 4 h at 31 °C. The yellow suspension was filtered and concentrated to yield yellow oil (15 mg). The crude material was set to a hydrogen atmosphere over 10 % Pd/C (2 mg, 2 µmol) in MeOH (500 µL) at 26-32 °C for 15 h. The black suspension was filtered through celite, washed with MeOH and concentrated to yield yellow oil, which was partially dissolved in ACN/H_2O (1000 µL), filtered and purified by RP column chromatography (250×10 mm, 40-min-long gradient from 10 to 25 % ACN in H_2O) to yield pure **1** (3.0 mg, 51 %). **^{1}H NMR** (500 MHz, CD_3CN). δ 12.48 (bs, 3H), 9.19 (bs, 2H), 8.77 (m, 3H), 8.42 (bs, 2H), 8.27 (bs, 1H), 7.90 (bs, 1H), 7.23 (m, 3H, Ar-*H*), 6.91 (m, 3H, Ar-*H*), 6.67 (m, 3H, Ar-*H*), 3.63 (bs, 7H), 3.40 (bs, 7H), 3.28 (m, 13H), 3.13 (m, 9H), 2.23 (t, 2H, J = 7.5 Hz, CH_2CO_2H), 1.65 ppm (m, 2H, $CH_2CH_2CO_2H$). **^{13}C NMR** (125 MHz, CD_3CN). δ 174.2, 169.9, 149.4, 146.2, 118.8, 118.0, 117.3, 115.1, 54.7, 54.5, 49.4, 38.4, 38.4, 38.2, 31.0, 24.2 ppm. **ESI-HRMS**: $C_{47}H_{67}N_{11}O_{15}^{2+}$ m/z = 512.7403 (calculated: 512.7404) $[M+2H]^{2+}$, error = 0.2 ppm.

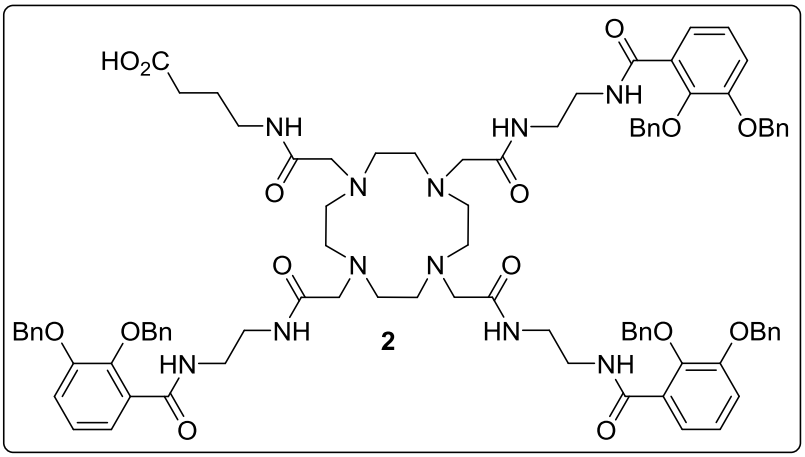

To a stirred suspension of cyclen (1.4 mg, 8.1 µmol) and sodium acetate (2.5 mg, 30.5 µmol) in DMA (100 µL) at 22 °C under Ar conditions was added dropwise a colorless solution of **33** (13.8 mg, 27.7 µmol) in DMA (150 µL). The reaction was stopped after stirring for 26 h at 23 °C. The yellow solution was diluted in DCM (10 mL), washed with $KHCO_3$ (0.5 M in water, 10 mL) and water (10 mL), dried over Na_2SO_4, filtered and concentrated to yield yellow oil. The yellow oil was diluted in DCM (5 mL), washed with $KHCO_3$ (0.5 M in water, 6 mL) and water (10 mL), dried over Na_2SO_4, filtered and concentrated to yield yellow oil (12.4 mg). The crude material, **35** (3.4 mg, 10.8 µmol) and K_2CO_3 (5.8 mg, 42.0 µmol) were suspended in ACN (0.5 mL) for 5 min under Ar conditions at 0 °C, and the colorless suspension was stirred for 4.5 h at 22 °C. The precipitate was filtered and the filtrate was concentrated. More 4KF09CR (3.3 mg, 10.5 µmol) and K_2CO_3 (5.9 mg, 42.7 µmol) were added, suspended in ACN (250 µL) for 3 min under Ar conditions at 0 °C and the pale yellow suspension was stirred for 18.5 h at 22 °C. The precipitate was filtered, and the filtrate was concentrated. The resulting yellow oil was dissolved in DCM (10 mL), washed with K_2CO_3 (3×10mL), dried over Na_2SO_4, filtered and concentrated to yield colorless oil (12 mg). The crude material was dissolved in THF (375 µL), NaOH solution (1 M in water, 125 µL) was added and RM was stirred for 4 h at 22 °C. The RM was concentrated to yield a yellow solid, then diluted in ACN (1 mL) and filtered to yield a colorless solution. A few drops of DMSO were added. The solution was purified by RP column chromatography (column: Gemini, C18, 250×10.0 mm, eluent: ACN/H_2O/0.1 % TFA, 40-min-long gradient from 20 % to 80 % ACN). The fraction of the main peak was concentrated to yield colorless oil. The resulting colorless oil was dissolved in ACN/H_2O (1/1, 0.1 % TFA, 700 µL) and filtered to yield a colorless solution. The solution was purified by RP column chromatography (column: Gemini, C18, 250×10 mm, eluent: ACN/H_2O/0.1 % TFA, 40-min-long gradient from 40 % to 70 % ACN). Fractions containing the expected product were lyophilized overnight to yield **2** as colorless oil (1.17 mg, 10 %). **^{1}H NMR** (500 MHz, CD_3CN). δ 8.01-7.90 (m, 4H), 7.54-7.46 (m, 6H), 7.46-7.34 (m, 10H), 7.34-7.26 (m, 15H), 7.25-7.16 (m, 5H), 7.16-7.02 (m,

4H), 5.19-5.01 (m, 11H), 3.94-3.38 (m, 10H), 3.35 (q, 4H), 3.30 (q, 2H), 3.27-3.22 (m, 1H), 3.22-3.16 (m, 4H), 3.16-3.10 (m, 6H), 3.10-2.82 (bs, 11H), 2.30-2.22 (m, 2H), 1.73-1.63 ppm (m, 2H). **^{13}C NMR** (125 MHz, CD_3CN). δ 175.0, 167.0, 166.9, 152.9, 146.9, 137.8, 137.7, 129.9, 129.9, 129.8, 129.6, 129.4, 129.2, 129.2, 129.0, 125.3, 125.3, 122.8, 76.6, 76.6, 71.7, 56.1, 56.0, 50.9, 40.5, 39.5, 39.4, 31.8, 25.2 ppm. **ESI-HRMS**: $C_{89}H_{103}N_{11}O_{15}^{2+}$ m/z = 782.8838 (calculated: 782.8812) $[M+2H]^{2+}$, error = 3.3 ppm.

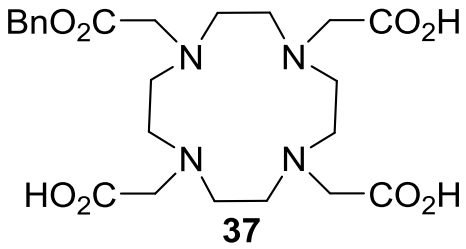

37

36 was prepared according to the procedure reported by N. Raghunand et al.[144] To a stirred solution of **36** (2.00 g, 3.9 mmol, dissolved for 10 min) and K_2CO_3 (2.15 g, 15.6 mmol) in ACN (40 mL), benzyl-2-bromoacetate (0.80 mL, 5.1 mmol) was added dropwise in the suspension under Ar conditions at 0 °C.The reaction mixture was stirred for 3 h at 25 °C. The reaction was monitored by TLC (CH_2Cl_2:MeOH/4:1) and LC-MS. The suspension was filtered, and the filtrate was concentrated to yield a white foaming solid (2.58 g). ESI-MS: $C_{35}H_{59}N_4O_8^+$ m/z = 663.5 $[M+H]^+$. The crude material (2.58 g, 3.9 mmol) was dissolved in TFA (10 mL) at 0 °C under Ar atmosphere and stirred at 25 °C for 26 h. The reaction mixture was co-evaporated with toluene (3×10 mL) to yield a green sticky solid (4.19 g). The crude material was dissolved in an HCl solution (0.1 M in H_2O, 75 mL) and lyophilized to yield a yellow solid (3.11 g). A part of the crude material (1.00 g) was diluted in ACN/H_2O (1/1), filtered and purified by RP column chromatography (column: Macherey-Nagel, C18, 250×40 mm, eluent: ACN/H_2O/0.1 % HCOOH) to yield **37** as a white solid (250 mg, 40 %). **^{1}H NMR** (500 MHz, D_6-DMSO). δ 7.38-7.30 (m, 5H, Ar-*H*), 5.11 (s, 2H, OC*H*$_2$), 3.65 (bs, 2H, C*H*$_2$COOBn), 3.49 (2×bs, 6H, C*H*$_2$COOH), 2.96 (bs, 8H), 2.82 ppm (bs, 4H). **^{13}C NMR** (125 MHz, D_6-DMSO). δ 170.9, 170.3, 163.3, 136.0, 128.5, 128.1, 128.0, 65.4, 55.3, 55.0, 54.0, 51.4, 50.4, 49.8, 49.3 ppm. **ESI-HRMS**: $C_{23}H_{35}N_4O_8^+$ m/z = 495.2449 (calculated: 495.2449) $[M+H]^+$, error = 0.2 ppm.

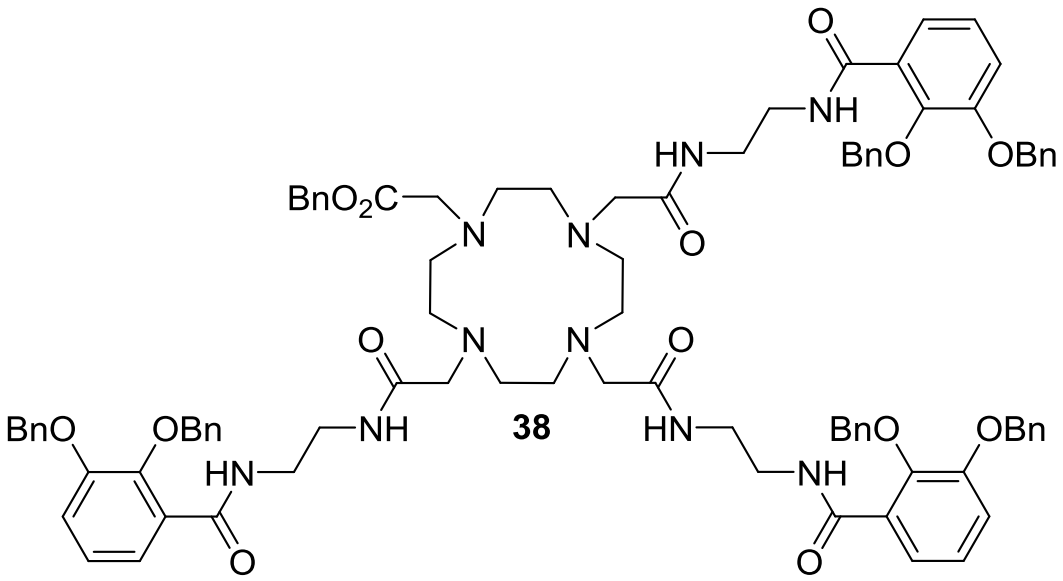

To a solution of **37** (5 mg, 10 µmol) in DMF (200 µL) were added DIPEA (6.2 µL, 36 µmol) and HATU (13 mg, 34 µmol). The reaction mixture was stirred for 15 min. **32** (16 mg, 43 µmol) was added, and the pale yellow solution was stirred at 25 °C for 1 h. The reaction mixture was directly filtered and purified by RP column chromatography (column: Phenomenex, C18, 250×21 mm, eluent: ACN/H_2O/0.1 % TFA) to yield **38** as a crystalline solid (14.5 mg, 91 %). A bigger scale of this reaction (0.25 g of **37**) led to a diminished yield (0.47 g, 59 %). **^{1}H NMR** (500 MHz, D_6-DMSO). δ 8.65 (bs, 2H, CON*H*), 8.26 (t, J = 5.7 Hz, 3H), 8.22 (t, J = 5.8 Hz, 1H), 8.10 (bs, 1H, CON*H*), 7.74 (bs, 2H, CON*H*), 7.50-7.45 (m, 6H, Ar-*H*), 7.43-7.22 (m, 32H, Ar-*H*), 7.15-7.05 (m, 6H, Ar-*H*), 5.20-5.15 (2×bs, 6H, ArOC$H_2C_6H_5$), 5.13-5.05 (2×bs, 2H, $CH_2COOCH_2C_6H_5$), 5.02-4.96 (2×bs, 6H, ArOC$H_2C_6H_5$), 3.93 (m, 4H), 3.73 (s, 2H), 3.68-2.91 ppm (m, 32H). **^{13}C NMR** (126 MHz, D6-DMSO) δ 171.4, 170.4, 166.1, 166.0, 165.1, 151.6, 145.2, 145.1, 137.1, 137.0, 136.8, 135.6, 130.8, 130.7, 128.5, 128.4, 128.3, 128.3, 128.2, 128.1, 128.1, 128.0, 127.8, 124.2, 120.9, 120.8, 119.5, 116.0, 75.2, 75.1, 70.2, 65.9, 54.6, 50.9, 50.7, 48.1, 47.7, 38.5, 38.4, 38.1 ppm. **ESI-HRMS**: $C_{92}H_{101}N_{10}O_{14}^+$ m/z = 1569.7502 (calculated: 1569.7493) $[M+H]^+$, error = 0.5 ppm.

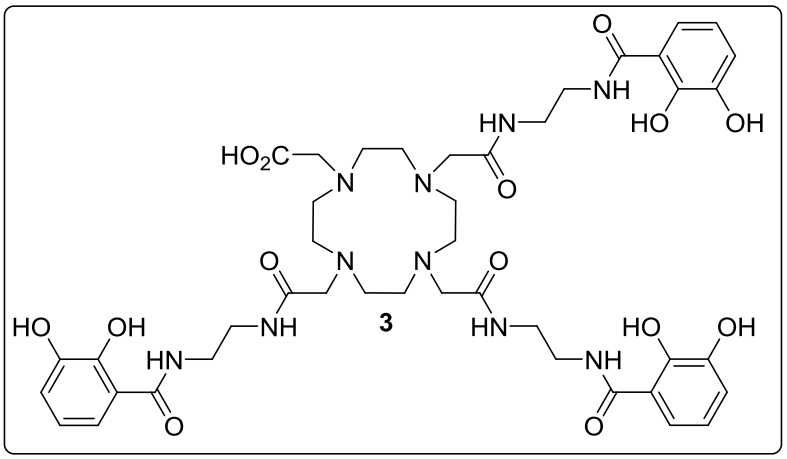

38 (100 mg, 64 µmol) was hydrogenolyzed (1 atm) over 10 % Pd/C (1 mg, 0.9 µmol) in MeOH (5 mL) for 14 h. The black suspension was filtered through celite, washed and concentrated to yield purple solid which was purifiedin by RP column chromatography (ACN/H_2O/0.1 % TFA, linear gradient 10 %-30 % ACN) to yield **3** as a pale yellow solid (54 mg, 90 %). **^{1}H NMR** (500 MHz, D_6-DMSO). δ 12.51 (bd, 3H), 9.21 (bs, 2H), 8.80 (m, 3H) 8.16 (bs, 2H), 8.26 (bs, 1H), 7.24 (t, J = 7.9 Hz, 3H, Ar-*H*), 6.91 (t, J = 6.7 Hz, 3H, Ar-*H*), 6.67 (m, 3H, Ar-*H*), 4.00-3.76 (bs, 4H), 3.65 (bs, 2H), 3.57-2.91 ppm (m, 29H). **^{13}C NMR** (125 MHz, D_6-DMSO). δ 170.1, 149.9, 146.2, 118.9, 117.9, 117.4, 115.0, 54.7, 50.5, 50.4, 48.6, 48.5, 38.6, 38.5, 38.3 ppm. **ESI-HRMS**: $C_{43}H_{59}N_{10}O_{14}^+$ m/z = 939.4207 (calculated: 939.4207) $[M+H]^+$, error < 0.1 ppm.

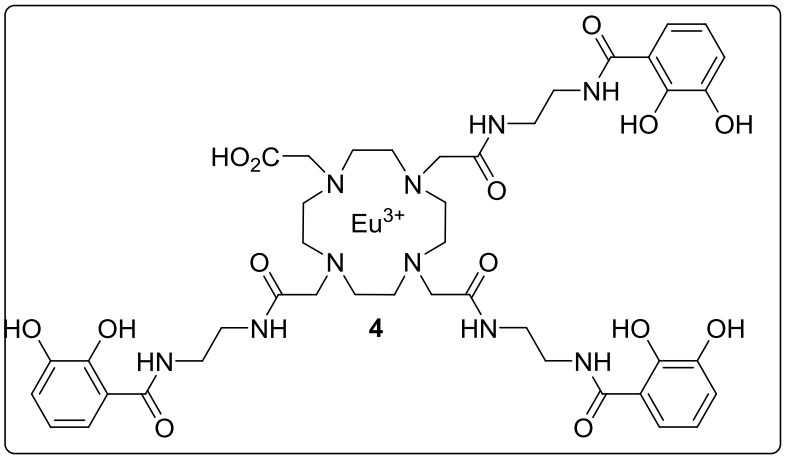

A solution of $Eu(SO_3CF_3)_3$ (19 mg, 32 µmol) in MeOH (250 µL) was added to **38** (25 mg, 16 µmol), and the resulting mixture was stirred for 48 h at 29 °C. The reaction mixture was concentrated and hydrogenolyzed (1 atm) over 10 % Pd/C (1.0 mg, 0.9 µmol) in MeOH (200 µL) for 41 h at 22 °C. The black suspension was filtered through celite, washed and concentrated to yield yellow solid, which was purified in by RP column chromatography (ACN/H_2O/ 0.1 %TFA) to

yield **4** as a white solid (12.0 mg, 69 %). **ESI-HRMS**: $C_{43}H_{57}N_{10}O_{14}Eu^{2+}$ m/z = 544.1618 (calculated: 544.1622) $[M-H]^{2+}$, error = 1.3 ppm.

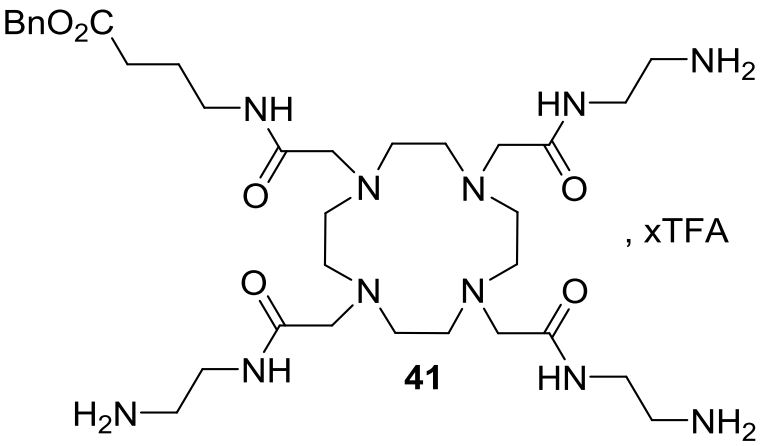

39 was prepared according to the procedure reported by Wickramaratne *et al*.[145] To a stirred white suspension of cyclen (371 mg, 2.2 mmol) and sodium acetate (584 mg, 7.1 mmol) in DMA (3 mL) at 21 °C under Ar conditions was added a solution of **39** (2.00 g, 7.1 mmol) in DMA (7 mL, 1.2 mL/h). The reaction was stopped after stirring for 20 h at 21 °C. Potassium bicarbonate solution (350 mL, 0.2 M in H_2O) was then added to the yellow solution, which was extracted with DCM (3×100 mL). The combined OLs were washed with brine (150 mL), dried over $MgSO_4$, filtered, concentrated and co-evaporated with ACN (20 mL) to yield a pale yellow solid. **35** (264 mg, 0.8 mmol) and K_2CO_3 (358 mg, 2.6 mmol) were added and suspended in ACN (5.0 mL) for 5 min under Ar conditions at 0 °C, and the yellow suspension was stirred for 3 h at 21 °C. The precipitate was filtered and the filtrate was concentrated. The resulting yellow oil was dissolved in DCM (50 mL) and washed with H_2O (3×50 mL), dried over $MgSO_4$, filtered and concentrated to yield pale yellow oil. The crude material was dissolved in DCM (4.0 mL), TFA (1.3 mL, 11.6 mmol) was added at 0 °C under Ar conditions and the yellow solution was stirred at 21 °C for 2 h and concentrated to yield yellow oil. The crude material was dissolved in ACN/H_2O (1/1, 0.1 % TFA, 1250 µL) purified by RP column chromatography (column: Phenomenex, C18, 250×40 mm, eluent: ACN/H_2O/0.1 % TFA, 40-min-long gradient from 10 % to 20 % ACN). Fractions containing the expected product were lyophilized overnight to yield **41** as pale yellow oil (403 mg, 75 %). **^{1}H NMR** (500 MHz, CD_3CN). δ 7.87 (bs, 2H), 7.52 (m, 5H), 7.44-7.23 (m, 11H), 5.11 (s, 2H, CH_2C$_6$H$_5$), 3.94 (bs, 2H), 3.83 (bs, 2H), 3.54 (q, J = 5.5 Hz, 2H), 3.52-3.38 (m, 8H), 3.39-3.19 (m, 10H), 3.19-3.06 (m, 8H), 3.06-2.93 (m, 6H), 2.41 (t, J = 7.3 Hz, 2H, $CH_2CH_2CO_2$Bn), 1.80 ppm (m, 2H, C$H_2CH_2CO_2$Bn). **^{13}C NMR** (125 MHz, CD_3CN). δ 174.0, 137.3, 129.4, 129.0, 128.9, 66.9, 56.0,

55.9, 54.9, 52.1, 49.6, 41.5, 39.7, 38.1, 37.8, 31.7, 24.9 ppm. **ESI-HRMS**: $C_{33}H_{60}N_{11}O_6^+$ m/z = 706.4723 (calculated: 706.4723) $[M+H]^+$, error < 0.1 ppm.

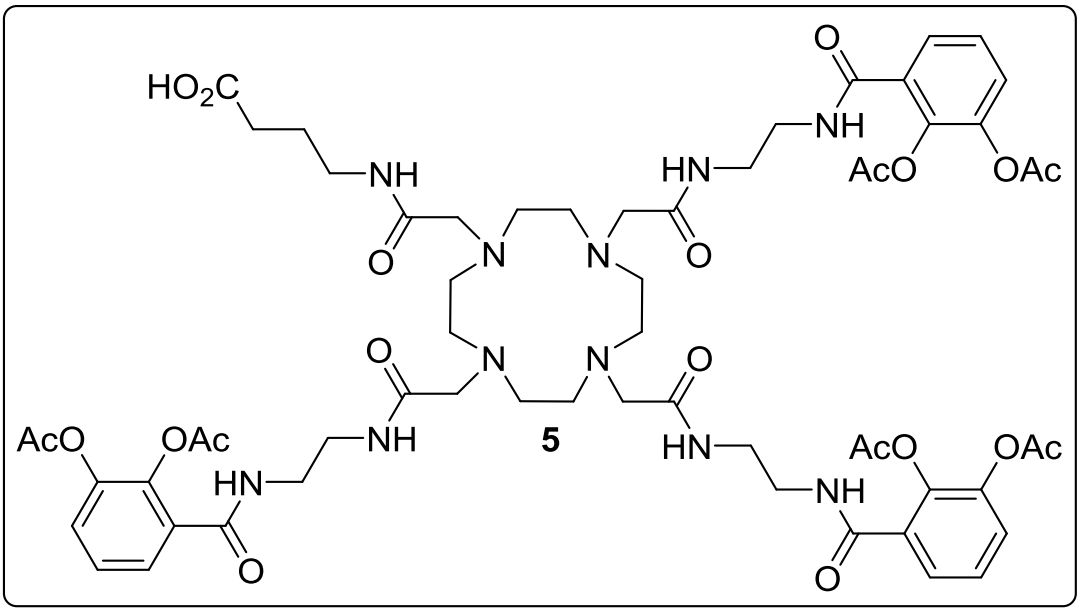

To a yellow solution of **40** (249 mg, 1.0 mmol) in DCM (2.5 mL) and DMF (0.25 mL) was added oxalyl chloride (177 µL, 2.1 mmol), and the orange solution was stirred at 20 °C for 1 h. The reaction mixture was concentrated and dried under the vacuum line for 1 h to yield brown oil. To a solution of **41** (300 mg, 0.3 mmol) in $KHCO_3$ (7.8 mL, 0.5 M in H_2O) was added dropwise an orange suspension of the acyl chloride in dioxane (7.8 mL) for 1 min in a 0 °C bath. After addition, the mixture was stirred at 20 °C for 0.5 h. After concentration the orange solid was suspended in ACN, filtered and concentrated in the vacuum line for 30 min to yield an orange solid. The crude material was set to a hydrogen atmosphere over 10 % Pd/C (32 mg, 0.03 mmol) in MeOH (5.0 mL) at 21 °C for 2 h. The black suspension was filtered through celite, washed and concentrated to yield colorless oil, which was purified by RP column chromatography (column: Phenomenex, C18, 250×40 mm, eluent: ACN/H_2O/0.1 % HCOOH, 40-min-long gradient from 20 to 50 % ACN) to yield **5** as a white solid (135 mg, 35 %). **^{1}H NMR** (500 MHz, D_6-DMSO). δ 8.39 (m, 3H), 8.19 (m, 2H), 8.13 (m, 1H), 7.47 (dd, J = 5.3, 1.3 Hz, 3H, Ar-*H*), 7.39-7.33 (m, 6H, Ar-*H*), 3.40-3.35 (m, 8H), 3.29-3.21 (m, 14H), 3.12-3.09 (m, 2H), 2.92-2.83 (m, 14H), 2.28 (s, 9H, C*H*$_3$CO$_2$), 2.22 ppm (s, 9H, C*H*$_3$CO$_2$). **^{13}C NMR** (125 MHz, D_6-DMSO). δ 174.2, 172.0, 168.4, 168.3, 167.8, 164.8, 142.8, 140.1, 130.7, 126.2, 126.1, 125.5, 124.5, 56.2, 51.0, 38.3, 38.0, 31.1, 24.5, 21.0, 20.4, 20.3, 20.2 ppm. **ESI-HRMS**: $C_{59}H_{78}N_{11}O_{21}^+$ m/z = 1276.5382 (calculated: 1276.6368) $[M+H]^+$, error = 1.1 ppm.

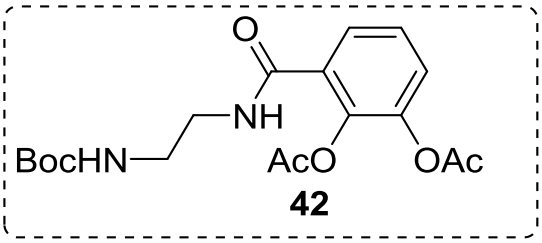

42

40 was prepared according to the procedure reported by Albrecht *et al*.[110] **40** (1190 mg, 5 mmol), HATU (2090 mg, 5.5 mmol) and DIPEA (1.7 mL, 10 mmol) were dissolved in DMF (25 mL). After 10 min, *N*-Boc-ethylenediamine (790 µL, 5 mmol) was added to the reaction mixture and stirred for 30 min under argon at room temperature. Ethyl acetate (50 mL) was added into the reaction mixture followed by aqueous work up. The OL was washed 3 times with 1N HCl and brine then dried over anhydrous sodium sulfate. After filtration and removal of the solvent, the crude compound was purified by flash silica gel column chromatography (eluent: PE : EtOAc = 1:1-1:3) to yield **42** as a white powder (580 mg, 31 %). **^{1}H NMR** (500 MHz, D_6-DMSO) δ 8.34 (t, *J* = 5.5 Hz, 1H, N*H*), 7.48 (dd, *J* = 6.6, 2.7 Hz, 1H, Ar-*H*), 7.39-7.33 (m, 2H, Ar-*H*), 6.84 (t, *J* = 5.7 Hz, 1H), 3.21 (dd, *J* = 12.4, 6.3 Hz, 2H, CH_2), 3.06 (dd, *J* = 12.4, 6.3 Hz, 2H, CH_2), 2.28 (s, 3H, CH_3), 2.22 (s, 3H, CH_3), 1.38 ppm (s, 9H, C(CH_3)$_3$). **^{13}C NMR** (126 MHz, D_6-DMSO) δ **^{13}C NMR** (126 MHz, DMSO) δ 168.3, 167.8, 164.7, 155.7, 142.8, 140.0, 130.9, 126.1, 125.4, 77.7, 28.2, 20.3, 20.3 ppm. **ESI-HRMS**: $C_{18}H_{24}N_2O_7Na^+$ m/z = 403.1476 (calculated: 403.1476) $[M+Na]^+$, error < 0.1 ppm.

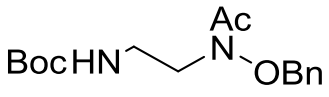

43

Tert-butyl(2-hydroxyethyl)carbamate (21.7 mmol, 3.50 g) was dissolved in dry EtOAc (175 mL). IBX (43.4 mmol, 12.2 g) was added and the reaction stirred to reflux at 60 °C for 2 h 15 min. The reaction was monitored via TLC (PE/EtOAc 1:1, R_f(Prod) = 0.51). Then, the mixture was cooled to 33 °C and the precipitate filtered. The filter cake was washed with EtOAc and the filtrate was concentrated to yield slightly yellow oil. The crude was immediately used to synthesize the oxime with optimized conditions. Tert-butyl-*N*-(2-oxoethyl)carbamate (21.7 mmol) and *O*-benzylhydroxylamine (28.2 mmol, 3.47 g) were dissolved in dry pyridine (15 mL) at 10 °C. The mixture was stirred for 2.5 h warming up to 31 °C and the reaction was monitored by TLC. The solvent was removed by co-evaporation with toluene (2x30 mL), and the crude oil was further concentrated under reduced pressure. The crude was used without further purification to synthesize the reduced intermediate with optimized conditions. To a solution of crude oxime

(21.7 mmol) in glacial acetic acid (28 mL) $NaBH_3CN$ (36.9 mmol, 3.32 g) was added at 10 °C. A pale orange suspension formed, which cleared after 30 min. The reaction was stirred for 3 h warming up to 26 °C and monitored by TLC (Hexanes/Et_2O 3:2, R_f(Prod) = 0.39, R_f(SM) = 0.65) and LC-MS analysis. Water (100 mL) was rinsed into the mixture to quench the reducing agent, and the product was extracted with Et_2O (3x100 mL). The combined OLs were washed with brine (2x50 mL), dried over $MgSO_4$, filtered and concentrated to yield the crude product as yellow oil. To a solution of the crude product (21.7 mmol) in pyridine (20 mL, 11.4 eq) under argon-atmosphere, acetic anhydride (20 mL, 9.8 eq) was added and the mixture stirred for 15 h at 26 °C. The reaction was monitored by LC-MS analysis. The solution was neutralized with saturated $NaHCO_3$ -solution, and the product was extracted with Et_2O (3x50 mL). The OLs were combined and washed with sat. $CuSO_4$-solution (40 mL) and then dried with $MgSO_4$ and filtered. The solvent was removed under reduced pressure for 24 h to yield yellow oil (7.89 g). The oil was purified by flash chromatography (m_{SiO2} = 120 g, 45-min-long gradient from EtOAc/PE:1/4 to EtOAc/PE:1/3) to yield clear viscous oil **43** (4.27 g, 64 % over 4 steps). **^{1}H NMR** (400 MHz, $CDCl_3$) δ 7.57-7.32 (m, 5H, Ar-*H*), 4.90 (bs, 1H, N*H*), 4.84 (s, 2H, C*H*$_2$C$_6$H$_5$), 3.76 (bs, 2H, CH_2CH_2), 3.37 (s, 2H, C*H*$_2$CH$_2$), 2.10 (s, 3H, C*H*$_3$CO), 1.43 ppm (s, 9H, C(C*H*$_3$)$_3$). **^{13}C NMR** (176 MHz, $CDCl_3$) δ 173.4, 171.3, 156.1, 134.4, 129.5, 129.2, 128.9, 79.6, 76.8, 46.1, 39.1, 28.5, 20.7. ppm. **ESI-HRMS**: $C_{16}H_{25}N_2O_4^+$ m/z = 309.1814 (calculated: 309.1809) $[M+H]^+$, error = 1.6 ppm.

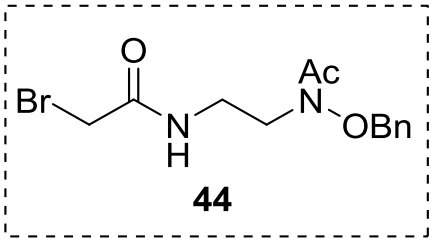

44

43 (635 mg, 2.06 mmol) was dissolved in DCM (36 mL, 312 mmol) and TFA (24 mL) was added at 0 °C under argon atmosphere. The mixture was stirred for 0.5 h warming up to 23 °C. The reaction was monitored by LC-MS analysis. Excess TFA was removed by co-evaporation with toluene (2x100 mL) to yield a white solid (780 mg). To a solution of crude salt **5** in DCM (13 mL) at 0 °C, a solution of K_2CO_3 (640 mg, 4.63 mmol) in water (6.5 mL) was added dropwise, followed by a solution of bromoacetyl bromide (499 mg, 2.47 mmol) in DCM (6.5 mL). The reaction mixture was stirred for 1.5 h warming to 22 °C. The reaction was monitored by TLC (pure EtOAc, R_f(Prod) = 0.35). The phases were separated and the OL was washed with brine (3×20 mL), dried over $MgSO_4$, filtered and concentrated to yield a pale yellow solid (730 mg). The crude material was purified by flash chromatography (m_{SiO2} = 24 g, 15-min-long gradient from pure DCM to

DCM/EtOAc:1/1) to yield **44** as a white solid (530 mg, 78 % over two steps). **^{1}H NMR** (500 MHz, CD_3OD) δ 7.53–7.34 (m, 5H, Ar-*H*), 4.91 (s, 2H, C*H*$_2$C$_6$H$_5$), 3.82 (bt, 2H, NHC*H*$_2$CH$_2$), 3.77 (s, 2H, C*H*$_2$Br), 3.45 (t, *J* = 5.9 Hz, 2H, NHCH$_2$C*H*$_2$), 2.07 ppm (s, 3H, C*H*$_3$CO). **^{13}C NMR** (126 MHz, CD_3OD) δ 175.1, 169.7, 136.0, 130.8, 130.0, 129.7, 77.3, 45.4, 38.3, 28.7, 20.5 ppm. **ESI-HRMS**: $C_{13}H_{18}BrN_2O_3^+$ m/z = 329.0500 (calculated: 329.0495) $[M+H]^+$, error = 1.5 ppm

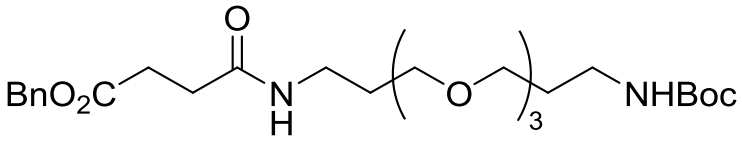

47

Succinic acid monobenzyl ester **45** and the mono *N*-Boc PEG_3 diamine linker **46** were prepared according to the procedure reported by S. Isomura et al.[146] and Iwaso *et al*[147] respectively. To a colorless solution of succinic acid monobenzyl ester **45** (0.50 g, 2.4 mmol) in DMF (10 mL) were added Et_3N (1.07 mL), **46** (0.90 g, 2.8 mmol) and pentafluorophenyl trifluoroacetate (578 µL). The pink solution was stirred for 6 h at 22 °C. The volatiles were co-evaporated with toluene (3 × 15 mL) and lyophilized overnight to yield orange oil. The compound was adsorbed on SiO_2 (5 g) and purified by NP column chromatography (m_{SiO2} = 40 g, 30-min-long gradient from neat DCM to 2.5 % MeOH in DCM to yield yellow oil **47** (1.20 g, 98 %). **^{1}H NMR** (500 MHz, $CDCl_3$) δ 7.38-7.28 (m, 5H, $CH_2C_6H_5$), 5.12 (s, 2H, C*H*$_2$C$_6$H$_5$), 3.66-3.61 (m, 4H), 3.61-3.54 (m, 6H), 3.51 (t, *J* = 6.0 Hz, 2H), 3.36 (bs, 2H), 3.20 (t, J = 6.5 Hz, 2H), 2.73 (t, J = 7.0 Hz, 2H), 2.49 (t, J = 7.0 Hz, 2H), 1.79-1.70 (m, 4H),1.43 ppm (s, 9H, C*H*$_3$C). **^{13}C NMR** (126 MHz, $CDCl_3$) δ 172.9, 171.8, 156.3, 136.0, 128.7, 128.4, 128.3, 79.3, 70.6, 70.3, 70.2, 70.1, 69.6, 66.6, 38.8, 38.4, 30.9, 29.8, 28.8, 28.6 ppm. **ESI-HRMS**: $C_{26}H_{43}N_2O_8^+$ m/z = 511.3018 (calculated: 511.3014) $[M+H]^+$, error = 0.8 ppm

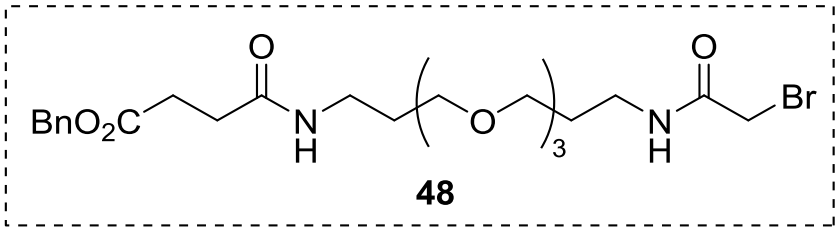

48

TFA (1.5 mL, 21.6 mmol) was added to a pale yellow solution of **47** (1.10 g, 2.2 mmol) in DCM (4.5 mL) at 0 °C and the pale yellow solution was stirred for 1 h at 28 °C. The pale yellow solution was co-evaporated with toluene (3×15 mL) to yield pale yellow oil (1.80 g). A solution of the crude material in DCM (10 mL) was cooled to 0°C. A solution of K_2CO_3 (1.82 g) in water (2.5 mL) then bromoacetyl bromide (958 µL, 11 mmol) were slowly added. The pale yellow biphasic

solution was stirred for 0.5 h at 28 °C. The solution was diluted in DCM (50 mL) and water (10 mL). The OL was separated, dried over $MgSO_4$, filtered and concentrated overnight to yield pale yellow oil (1.80 g), which was adsorbed on SiO2 (5 g) and purified by NP flash column chromatography (m_{SiO2} = 40 g, 30-min-long gradient from neat DCM to 95:2.5/DCM:MeOH) to yield the expected product **48** (930 mg, 82 %). **^{1}H NMR** (500 MHz, CD_3CN) δ 7.45-7.28 (m, 5H, Ar-*H*), 7.13-6.91 (bs, 1H, N*H*), 6.61-6.40 (bs, 1H, N*H*), 5.09 (s, 2H, C*H*$_2$C$_6$H$_5$), 3.78 (s, 2H, C*H*$_2$Br), 3.58-3.55 (m, 4H, C*H*$_2$CH$_2$), 3.54-3.50 (m, 4H), 3.48 (t, J = 6.0 Hz, 2H), 3.45 (t, J = 6.5 Hz, 2H), 3.24 (dd, J = 12.4, 6.7 Hz, 2H), 3.19 (dd, J = 12.5, 6.7 Hz, 2H), 2.59 (t, J = 6.8 Hz, 2H), 2.40 (t, J = 6.8 Hz, 2H), 1.73-1.68 (m, 2H), 1.68-1.63 ppm (m, 2H). **^{13}C NMR** (126 MHz, CD_3CN) δ 173.5, 172.0, 166.9, 137.5, 129.4, 128.9, 128.9, 71.1, 71.0, 70.8, 70.8, 69.7, 69.6, 66.7, 49.8, 38.5, 37.6, 31.1, 30.2, 30.1, 29.8 ppm. **ESI-HRMS**: $C_{23}H_{36}BrN_2O_7^+$ m/z = 531.1705 (calculated: 531.1700) $[M+2H]^{2+}$, error = 0.9 ppm

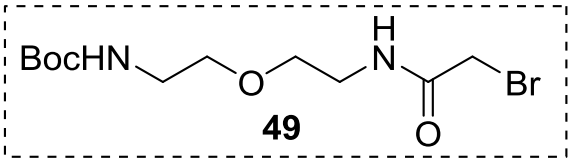

49

To a solution of *t*-Boc-*N*-amido-PEG$_1$-amine (496 mg, 2.4 mmol) in DCM (1.0 mL) cooled to 0°C were added a solution of K_2CO_3 (497 mg, 3.6 mmol) in water (1.0 mL) and a solution of bromoacetyl bromide (277 µL, 3.2 mmol) in DCM (2.5 mL). The reaction mixture was stirred at 22 °C for 3.5 h. DCM (60 mL) and H_2O (100 mL) were added to the reaction mixture. The layers were separated and the AL was washed with DCM (2×50 mL). The combined OLs were dried over sodium sulfate, filtered and concentrated to yield yellow oil **49** (760 mg, 95 %). **^{1}H NMR** (500 MHz, $CDCl_3$). δ 7.11-6.85 (bs, 1H), 5.42-5.29 (bs, 1H), 3.82 (s, 2H, C*H*$_2$Br), 3.54-3.40 (m, 4H), 3.33 (q, J = 5.5 Hz, 2H), 3.18 (q, J= 5.6 Hz, 2H), 1.41 ppm (s, 9H, C(C*H*$_3$)$_3$). **^{13}C NMR** (125 MHz, $CDCl_3$) δ 167.1, 157.0, 79.2, 70.5, 69.6, 40.9, 40.4, 30.0, 28.6 ppm. **ESI-HRMS**: $C_{11}H_{21}BrN_2O_4Na^+$ m/z = 347.0581 (calculated: 347.0577) $[M+Na]^+$, error = 1.2 ppm.

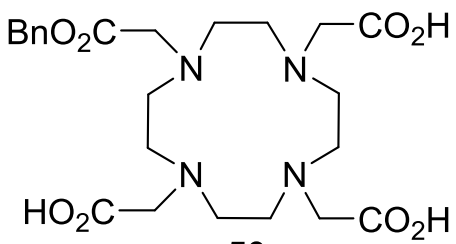

50

To a stirred suspension of **36** (2.00 g, 3.9 mmol, dissolved for 10 min) and K_2CO_3 (2.15 g, 16 mmol) in ACN (40 mL). Benzyl-2-bromoacetate (0.80 mL, 5.1 mmol) was added dropwise in the suspension under Ar conditions at 0 °C and the RM was stirred for 3 h at 25 °C. Reaction was monitored by TLC (DCM/MeOH 4/1) and LCMS. Precipitate was filtered and the filtrate was concentrated to yield a white foaming solid (2.58g). The tris *tert*-butylated intermediate was dissolved in TFA (10 mL) at 0°C under Ar conditions and stirred (500RPM) at 25 °C for 26 h. Toluene (3x10 mL) was added to the RM which was concentrated to yield a green solid (4.19 g). CR was dissolved in HCl solution in water (0.1 M, 3 x 25 mL), and lyophilized to yield yellow solid (3.11 g). Part of the crude material (1.00 g of it) was diluted in ACN/H_2O (1/1), filtered and purified by RP column chromatography (column: 250x40 mm, eluent: ACN/H_2O/0.1 % HCOOH) to yield a white solid (250 mg, 40 %). **^{1}H NMR** (500 MHz, D_6-DMSO). δ 8.20 (s, 1H), 7.39-7.31 (m, 5H, $CH_2C_6H_5$), 5.11 (s, 2H, $CH_2C_6H_5$), 3.65 (bs, 2H), 3.50 (m, 6H), 3.11-2.89 (m, 12H), 2.82 ppm (bs, 4H). **^{13}C NMR** (126 MHz, D_6-DMSO). δ 170.9, 170.3, 163.3, 136.0, 128.5, 128.1, 128.0, 65.4, 55.3, 55.0, 54.0, 51.4, 50.4, 49.8, 49.3 ppm. **ESI-HRMS**: $C_{23}H_{36}N_4O_8^+$ m/z = 495.2449 (calculated: 495.2449) $[M+H]^+$, error = 0.2 ppm.

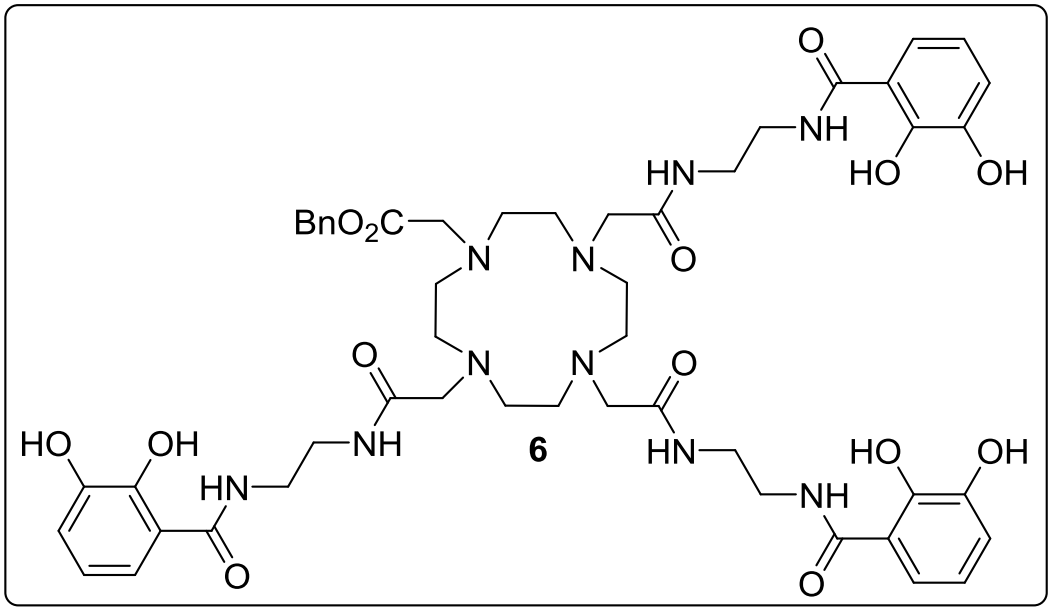

To a **42** (30 mg, 79 µmol) solution in DCM (750 µL) was added TFA (250 µL) at 0°C under Ar conditions and stirred (500RPM) at 25 °C for 0.5 h. RM was co-evaporated with Toluene (3x20 mL) to yield colorless viscous oil (39 mg). The triscarboxylic acid **50** (12 mg, 24 µmol), DIPEA (28 µL) and HATU (54 mg) were added in DMF (1.0 mL) and stirred (500RPM) for 10 min. The crude amine was added and the RM was stirred at 25 °C for 1.5 h. The suspension was filtered and

purified by RP column chromatography (ACN/H2O/0.1 % HCOOH) to yield white hygroscopic solid (9 mg, 29 %). Fractions of mainly monohydrolyzed byproduct were collected and lyophilized to yield white hygroscopic solid (13 mg). The purified material (12 mg, 9.4 µmol) was dissolved in MeOH (400 µL). DIPEA (100 µL, 574 µmol) was added to the RM which was stirred for 30 min at 25 °C. The RM was filtered and purified by RP column chromatography (ACN/H_2O/0.1 % TFA) to yield a white hygroscopic solid (7.4 mg). **^{1}H NMR** (500 MHz, D_6-DMSO). δ 12.54 (bs, 1H), 12.46 (bs, 1H), 9.20 (bs, 2H), 8.78 (m, 5H), 8.16 (bs, 1H), 7.75 (bs, 1H), 7.38-7.26 (m, 5H, $CH_2C_6H_5$), 7.26-7.20 (m, 3H, Ar-*H*), 6.91 (m, 3H, Ar-*H*), 6.66 (m, 3H, Ar-*H*), 5.09 (s, 2H, $CH_2C_6H_5$), 4.05-3.88 (m, 6H), 3.79-3.70 (bs, 2H), 3.57-3.21 (m, 22H), 3.15-2.96 ppm (m, 6H). **^{13}C NMR** (126 MHz, D_6-DMSO) δ 170.0, 169.9, 165.2, 149.5, 146.2, 146.2, 135.6, 128.4, 128.1, 128.1, 118.8, 117.9, 117.2, 115.1, 65.8, 55.0, 54.7, 54.0, 52.3, 50.9, 48.6, 48.1, 47.5, 38.7, 38.5, 38.1 ppm. **ESI-HRMS**: $C_{50}H_{66}N_{10}O_{14}^{2+}$ m/z = 515.2374 (calculated: 515.2374) $[M+2H]^{2+}$, error < 0.1 ppm.

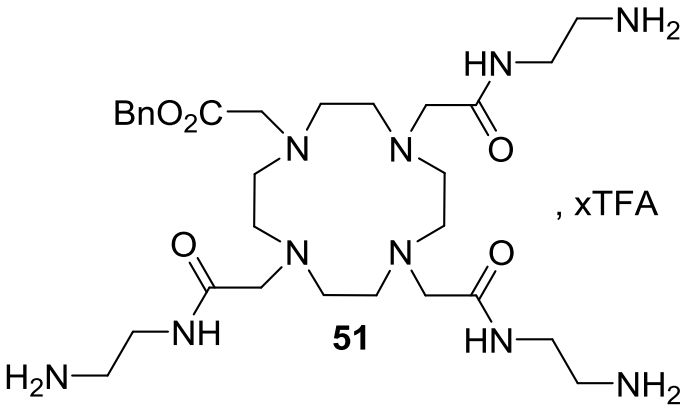

39 was prepared according to the procedure reported by Wickramaratne *et al*.[145] To a stirred white suspension of cyclen (371 mg, 2.2 mmol) and sodium acetate in DMA (3 mL) at 21 °C under Ar conditions was added a solution of **39** (2.00 g, 7.1 mmol) in DMA (7 mL, 1.2 mL/h). The reaction was stopped after 20 h stirring at 21 °C. Potassium bicarbonate solution (350 mL, 0.2 M in H_2O) was then added to the yellow solution which was extracted with DCM (3×100 mL). The combined OL were washed with brine (150 mL), dried over MgSO4, filtered, concentrated (2.50 g). The crude material was co-evaporated with ACN (20 mL) to yield a pale yellow solid (2.02 g). To a stirred suspension of the crude material (612 mg) and K_2CO_3 (359 mg, 2.6 mmol) in ACN (5.0 mL) was added benzylbromoacetate (268 µL, 1.9 mmol) dropwise for 1 min under Ar conditions at 0 °C and the suspension was stirred for 3 h at 21 °C. The precipitate was filtered and the filtrate was concentrated. The resulting yellow oil was dissolved in DCM (50 mL) and washed with H_2O (3×50 mL), dried over $MgSO_4$, filtered and concentrated to yield pale yellow oil (803 mg). To a stirred yellow solution of the crude material (740 mg) in DCM (4.0 mL) was added TFA (1.3 mL) at

0 °C under Ar conditions and the yellow solution was stirred at 21 °C for 2 h. The yellow solution was concentrated to yield yellow oil, which was dissolved in ACN/H_2O (1/1, 0.1 % TFA, 1300 µL) purified by RP column chromatography (column: Phenomenex, C18, 250×40 mm, eluent: ACN/H_2O/0.1 % TFA, 40-min-long gradient from 5 % to 20 % ACN) to yield pale yellow oil (510 mg, 82 %). **^{1}H NMR** (500 MHz, CD_3CN). δ 7.83 (bs, 2H), 7.47(bs, 2H), 7.44-7.31 (m, 9H), 5.19 (s, 2H, $CH_2C_6H_5$), 4.30-2.67 ppm (m, 36H). **^{13}C NMR** (126 MHz, CD_3CN) δ 136.3, 129.6, 129.5, 129.2, 68.2, 55.5, 54.5, 51.1, 41.1, 38.2, 38.0 ppm. **ESI-HRMS**: $C_{29}H_{55}N_{10}O_5^{2+}$ m/z = 621.4195 (calculated: 621.4195) $[M+2H]^{2+}$, error < 0.1 ppm.

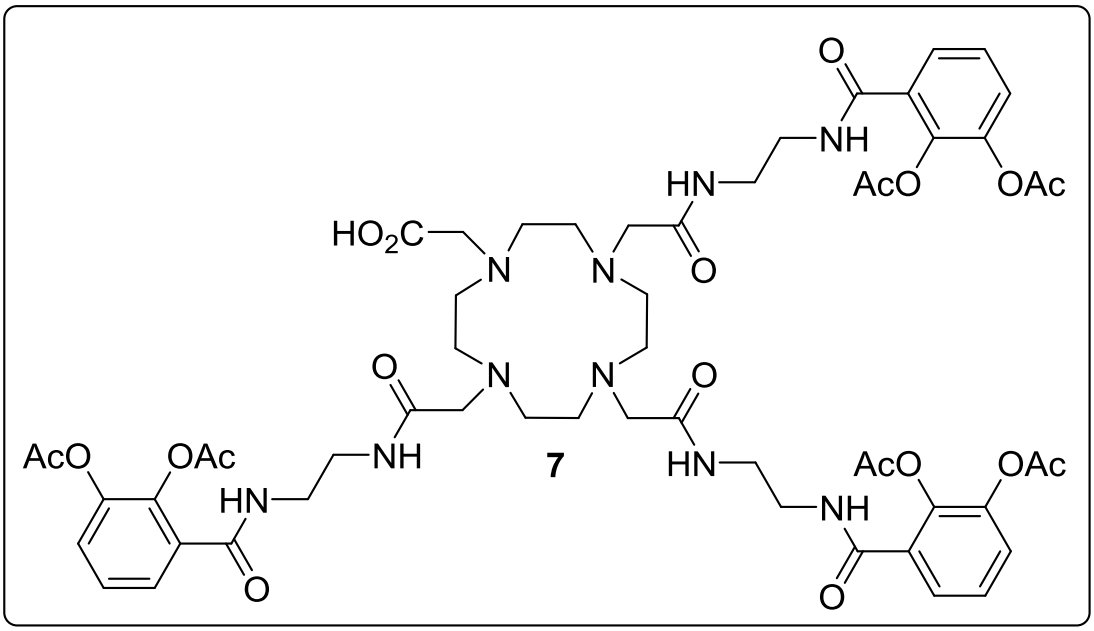

To a yellow solution of **40** (104 mg, 436 µmol) in DCM (400 µL) and DMF (100 µL) was added oxalyl chloride (74 µL, 872 µmol) and the orange solution was stirred at 20 °C for 1 h. The reaction mixture was concentrated and dried under the vacuum line for 30 min to yield brown oil. To a solution of **51** (100 mg, 104 µmol) in $KHCO_3$ (3.0 mL, 0.5 M in H_2O) was added dropwise a solution of the acyl chloride in dioxane (3.0 mL) at 21 ºC for 1 min. After addition, the mixture was stirred at 20 °C for 0.5 h. After concentration the orange solid was suspended in ACN, filtered and concentrated in the vacuum line for 30 min to yield an orange solid (220 mg). The benzylated ester (210 mg) was set to a hydrogen atmosphere over 10 % Pd/C in MeOH (1.0 mL) at 21 °C for 1 h. The black suspension was filtered through celite, washed and concentrated to yield colorless oil. The crude material was purified by RP column chromatography (column: Phenomenex, C18, 250×10 mm, eluent: ACN/H_2O/0.1 % HCOOH, 40-min-long gradient from 15 to 25 % ACN) to yield a white solid (45 mg, 36 %). **^{1}H NMR** (500 MHz, CD_3CN). δ 8.08 (s, 2H), 7.84-7.77 (bs, 2H), 7.77-7.73 (bs, 1H), 7.67-7.59 (bs, 3H), 7.54 (m, 3H, Ar-*H*), 7.30 (m, 6H, Ar-*H*), 3.51-3.46 (bs, 2H), 3.45-

3.33 (m, 10H), 3.26-3.03 (m, 12H), 2.90-2.77 (bs, 3H), 2.67-2.57 (bs, 8H), 2.26 (s, 9H, C*H*$_3$CO$_2$), 2.24 (s, 3H, C*H*$_3$CO$_2$), 2.23 ppm (s, 6H, C*H*$_3$CO$_2$). **^{13}C NMR** (176 MHz, CD_3CN) δ 171.8, 169.8, 169.7, 169.5, 169.4, 166.3, 166.3, 163.0, 144.4, 141.6, 141.6, 140.8, 131.9, 131.7, 127.6, 127.5, 127.4, 127.3, 126.8, 126.6, 62.4, 62.2, 59.2, 57.9, 54.5, 52.8, 51.7, 49.5, 41.3, 40.6, 39.9, 39.7, 21.0, 20.9, 20.9, 20.8 ppm. **ESI-HRMS**: $C_{55}H_{72}N_{10}O_{20}^{2+}$ m/z = 596.2458 (calculated: 596.2457) $[M+2H]^{2+}$, error = 0.2 ppm.

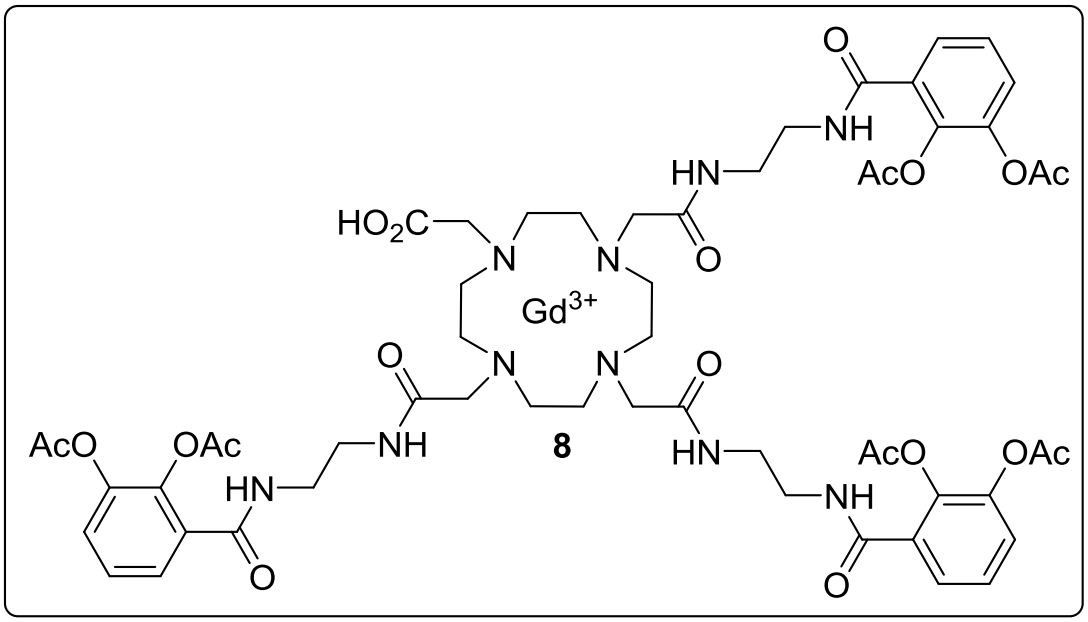

To a solution of **7** (10 mg, 8.4 µmol) in MeOH (2.0 mL) was added $GdCl_3$, $6H_2O$ (4.1 mg, 10.9 µmol). The colorless solution was stirred for 5 h at 20 °C. The RM was concentrated and diluted in ACN/H_2O (1/1, 700 µL), purified by RP column chromatography (ACN/H_2O without any acid, linear gradient 5 %-20 % ACN for 40 min) to yield a white solid (2.8 mg, 25 %). **ESI-HRMS**: $GdC_{55}H_{69}N_{10}O_{20}^{2+}$ m/z = 673.6975 (calculated: 673.6967) $[M-H]^{2+}$, error = 1.2 ppm.

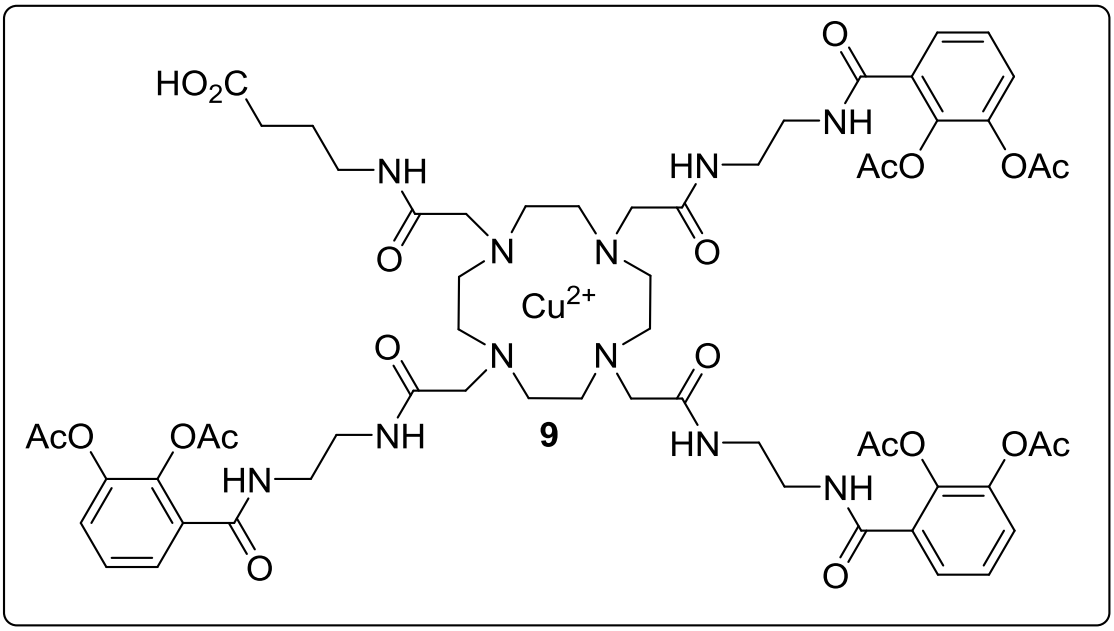

To a solution of **6** (5.0 mg, 3.9 µmol) in dried MeOH (200 µL) was added anhydrous $CuSO_4$ (1.0 mg, 6.3 µmol) under Ar and the blue solution was stirred for 15 min at 26 °C. The blue solution was concentrated, rediluted in ACN/H_2O (500 µL), filtered and purified by RP column chromatography (column: Phenomenex, C18, 250×10 mm, eluent: ACN/H_2O, 40-min-long gradient from 0 to 40 % ACN in water) to yield a blue solid (1.2 mg, 23 %). **ESI-HRMS**: $CuC_{59}H_{77}N_{11}O_{21}^{2+}$ m/z = 669.2291 (calculated: 669.2290) $[M]^{2+}$, error = 0.1 ppm.

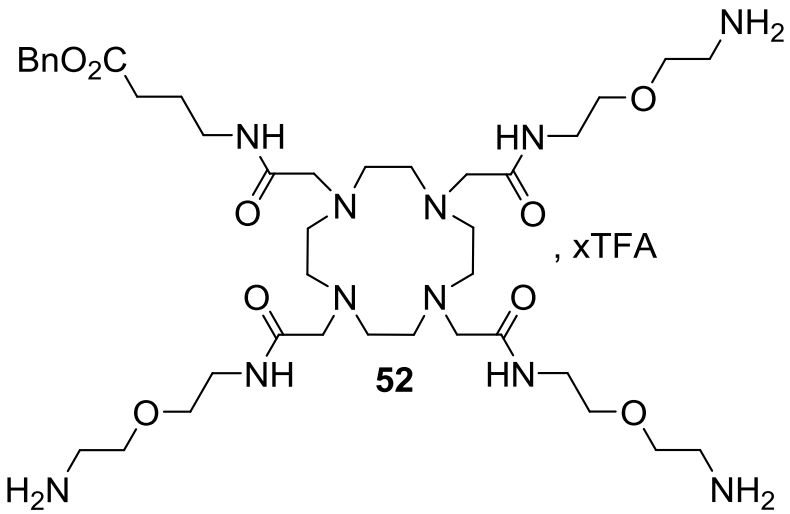

To a stirred suspension of cyclen (12 mg, 70 µmol) and sodium acetate (19 mg, 232 µmol) in DMA (500 µL) at 22 °C under Ar conditions was added dropwise a colorless solution of **49** (68 mg, 209 µmol) in DMA (1.5 mL). The reaction was stopped after stirring for 24 h at 22 °C. The pale

yellow solution was diluted in DCM (50 mL), washed with a $KHCO_3$ solution in water (0.5 M, 50 mL), dried over Na_2SO_4, filtered and concentrated to yield yellow oil (72 mg). The crude material, **35** (32 mg, 53 µmol) and K_2CO_3 (56 mg, 203 µmol) were suspended in ACN (1.0 mL) for 5 min under Ar conditions at 0 °C and the colorless suspension was stirred for 6.5 h at 22 °C. The precipitate was filtered and the filtrate was concentrated. The resulting yellow oil was dissolved in DCM (10 mL), washed with H_2O (3×5 mL), washed with $KHCO_3$ (1 M, 3×10 mL), dried over Na_2SO_4, filtered and concentrated to yield yellow oil (81 mg). The crude material was dissolved in DCM (150 µL), TFA (50 µL, 439 µmol) was added at 0 °C under Ar conditions and the yellow solution was stirred at 22 °C for 6.5 h. More TFA (100 µL) and DCM (300 µL) were added and the yellow solution was stirred at 22 °C for 17 h. The yellow solution was co-evaporated with toluene (2 mL) to yield yellow oil. The yellow oil was dissolved in ACN/H_2O (1/1, 0.1 % TFA, 800 µL) purified by RP column chromatography (column: Gemini, C18, 250×21.20 mm, eluent: ACN/H_2O/0.1 % TFA, 40-min-long gradient from 10 % to 90 % ACN). Fractions containing the expected product were lyophilized overnight to yield colorless oil (22 mg, 27 %). **^{1}H NMR** (500 MHz, CD_3CN). δ 10.04-9.14 (bs, 4H), 8.07-7.72 (m, 2H), 7.67-7.16 (m, 17H), 5.10 (s, 2H, $CO_2CH_2C_6H_5$), 3.89-3.60 (m, 12H), 3.59-3.41 (m, 8H), 3.41-3.30 (m, 6H), 3.30-2.87 (m, 24H), 2.40 (t, J= 7.4 Hz, 2H, CH_2CO_2Bn), 1.83-1.75 ppm (m, J = 7.2 Hz, 2H, $CH_2CH_2CO_2Bn$)**. ^{13}C NMR** (125 MHz, CD_3CN). δ 173.9, 137.4, 129.5, 129.1, 129.0, 70.5, 70.2, 66.9, 66.6, 66.4, 55.9, 40.6, 39.8, 39.4, 32.0, 25.1 ppm. **ESI-HRMS**: $C_{39}H_{71}N_{11}O_9Na^+$ m/z = 860.5341 (calculated: 860.5328) $[M+Na]^+$, error = 1.5 ppm.

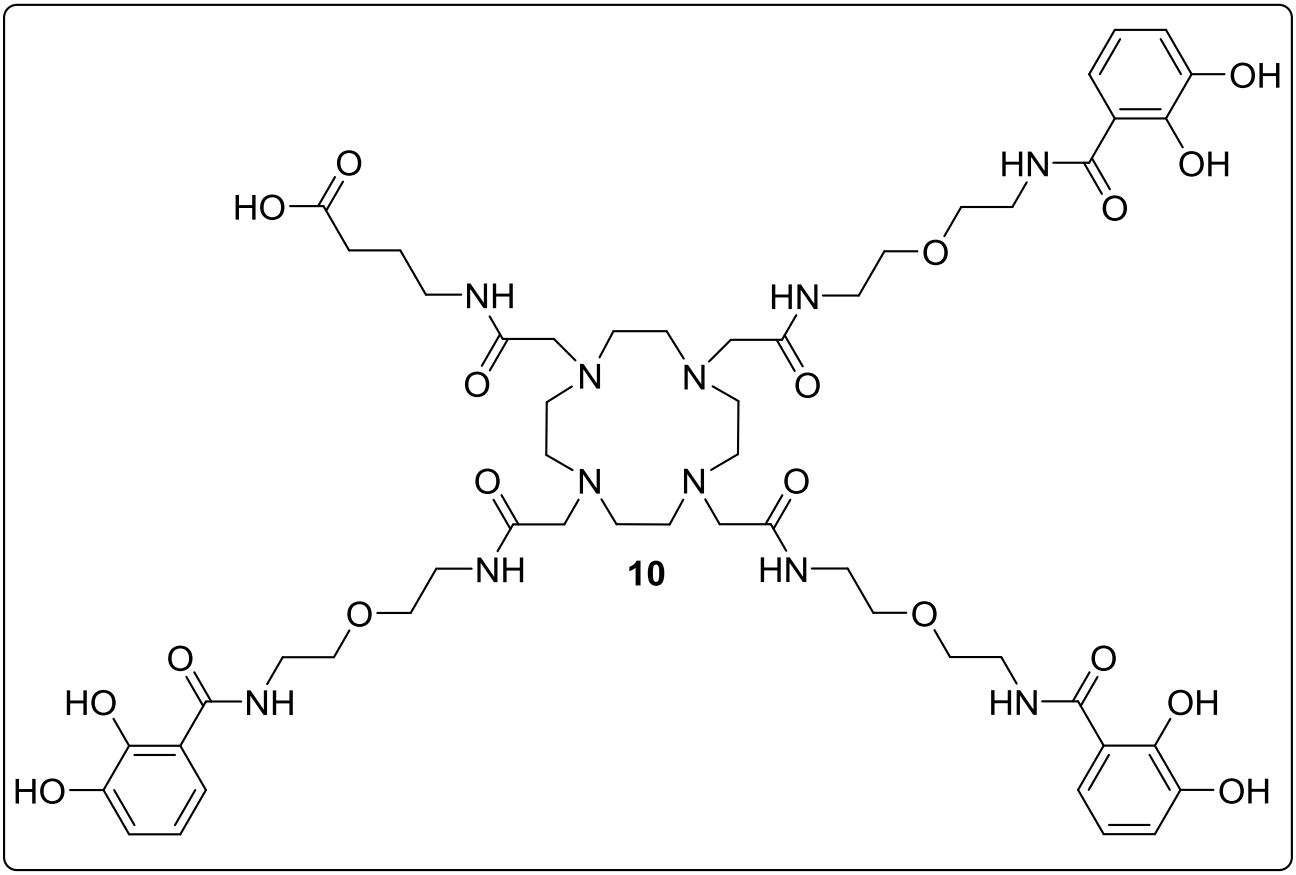

To a colorless solution of **40** (14 mg, 59 µmol) in DCM and DMF (minimum required to dissolve **40**) was added oxalyl chloride (10 µL, 118 µmol) and the colorless solution was stirred at 20 °C for 20 min. The reaction mixture was concentrated and dried under the vacuum line for 2 h to yield yellow oil, the acyl chloride. To a solution of **52** (20 mg, 17µmol) in $KHCO_3$ (500 µL, 0.5 M in H_2O) was added dropwise a light yellow solution of the acyl chloride in dioxane (500 µL) at 20 ºC. After addition, the mixture was stirred at 20 °C for 40 min. A precipitate was observed. After concentration the solid was suspended in ACN (250 µL), filtered and concentrated in the vacuum line for 1.5 h to yield a light brown solid (35.5 mg). The crude material was set to a hydrogen atmosphere over 10 % Pd/C (1.8mg, 1.7 µmol) in MeOH (1mL) at 20 °C for 17 h. Some 10 % Pd/C (1.8 mg, 1.7µmol) was added and the black suspension was stirred for 3 h. The black suspension was filtered through celite, washed and concentrated to yield a purple oil. The purple oil was purified by RP column chromatography (column: Gemini, C18, 250×21.20 mm, eluent: ACN/H_2O/0.1 % HCOOH, 40-min-long gradient from 20 % to 70 % ACN) Fractions containing the expected product were lyophilized overnight to yield a white solid. The white solid was dissolved in ACN/H_2O (3:7, 0.1 % HCOOH, 1200 µL) and was purified by RP column chromatography (column: Gemini, C18, 250×21.20 mm, eluent: ACN/H_2O/0.1 % HCOOH, 40-min-long gradient from 0 % to

40 % ACN). Fractions containing the expected product were lyophilized overnight to yield a white solid (7.4 mg, 37 %).**^{1}H NMR** (500 MHz, D_2O). δ 8.44 (s, 1H), 7.24-7.11 (m, 3H), 7.06-6.95 (m, 3H), 6.85-6.72 (m, 3H), 3.78-3.60 (m, 8H), 3.60-3.48 (m, 14H), 3.47-3.24 (m, 12H), 3.24-2.78 (m, 16H), 2.19 (t, J = 5.4 Hz, 2H), 1.74-1.65 ppm (m, 2H). **^{13}C NMR** (125 MHz, D_2O). δ 180.6, 170.5, 167.0, 147.2, 144.6, 144.6, 119.6, 119.5, 119.3, 119.3, 118.8, 118.7, 116.3, 116.2, 68.7, 68.4, 68.3, 54.9, 49.5, 38.9, 38.9, 33.5, 24.8 ppm. **ESI-HRMS**: $C_{53}H_{79}N_{11}O_{18}^{2+}$ m/z = 578.7801 (calculated: 578.7797) $[M+2H]^{2+}$, error = 0.7 ppm.

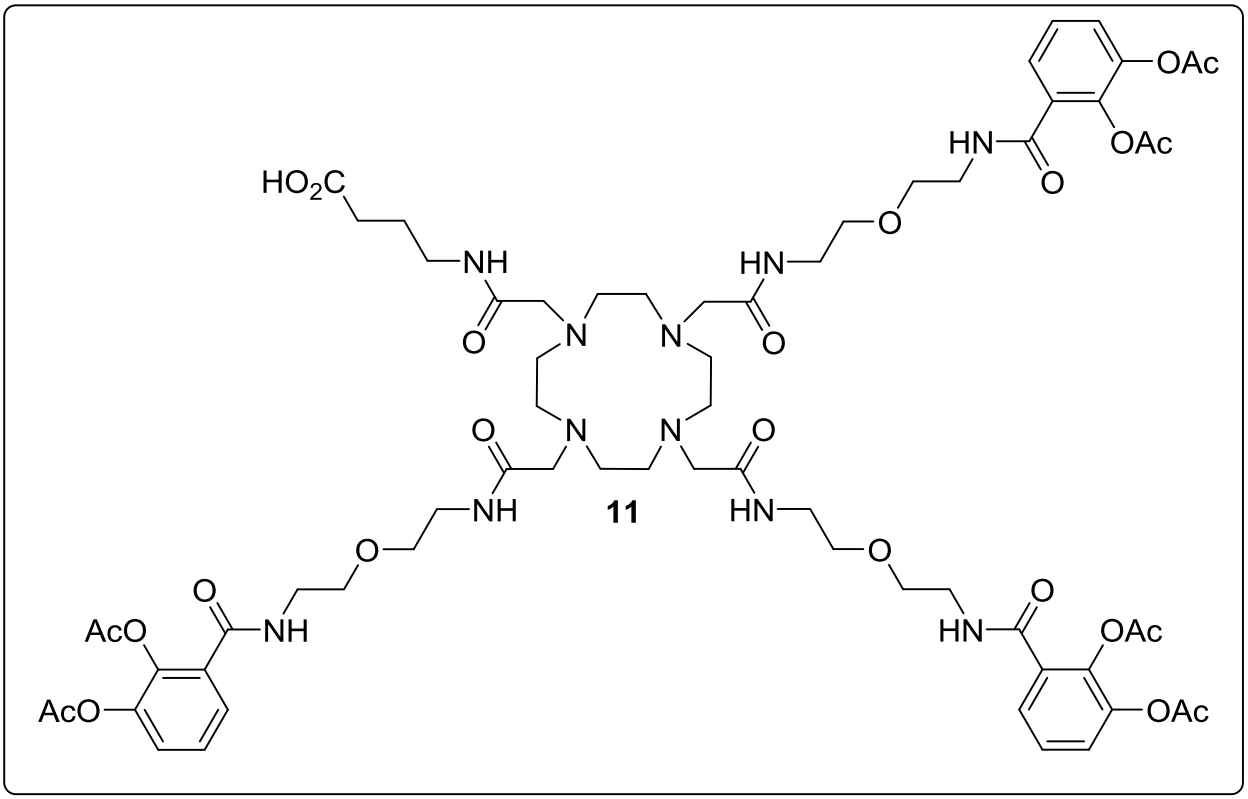

To a colorless solution of **40** (3.5 mg, 15 µmol) in CH_2Cl_2 (100 µL) and DMF (25 µL) was added oxalyl chloride (2.37 µL, 28 µmol) at 0°C under Ar condition and the colorless solution was stirred at 20 °C for 1 h. The reaction mixture was concentrated and dried under the vacuum line for 2 h to yield yellow oil, which was directly used in the next step. To a solution of **52** (5 mg, 4 µmol) in $KHCO_3$ (0.5 M in 120 µL H_2O) was added dropwise a light yellow solution of the acyl chloride in dioxane (120 µL) at 20 ºC. After addition, the mixture was stirred at 20 °C for 40 min. A precipitate was observed. After concentration the solid was suspended in ACN, filtered and concentrated in the vacuum line for 1 h to yield a light brown solid. The crude material was set to a hydrogen atmosphere of 58 % Pd/C (2.4 mg, 2.3 µmol) in MeOH (1 mL) at 20 °C for 1.5 h. The black suspension was filtered through celite, washed and concentrated to yield purple oil. The crude

material was dissolved in ACN/H_2O (1:1) and was purified by RP column chromatography (column: Gemini, C18, 250x10 mm, eluent: ACN/H2O/, 40-min-long gradient from 20 % to 70 % ACN). Fractions containing the expected product were lyophilized overnight to yield a white solid (1.7 mg, 28 %). **^{1}H NMR** (700 MHz, CD_3CN). δ 7.87 (s, 2H), 7.53-7.51 (m, 3H), 7.41-7.22 (m, 12H), 3.57-3.54 (m, 6H), 3.52-3.49 (m, 6H), 3.49-3.44 (m, 8H), 3.41-3.27 (m, 8H), 3.25-3.13 (m, 4H), 3.13-2.82 (m, 18H), 2.32-2.30 (t, 3H), 2.27-2.26 (m, 18H), 1.75-1.71 ppm (m, 2H). **^{13}C NMR** (175 MHz, CD_3CN). δ 175.1, 169.7, 169.6, 166.4, 144.2, 141.2, 132.0, 127.6, 127.3, 126.8, 70.0, 69.3, 55.7, 50.8, 40.2, 40.0, 39.4, 31.9, 25.3, 20.8 ppm. **ESI-HRMS**: $C_{65}H_{89}N_{11}O_{24}^{2+}$ m/z = 704.8117 (calculated: 704.8114) $[M+2H]^{2+}$, error = 0.4 ppm.

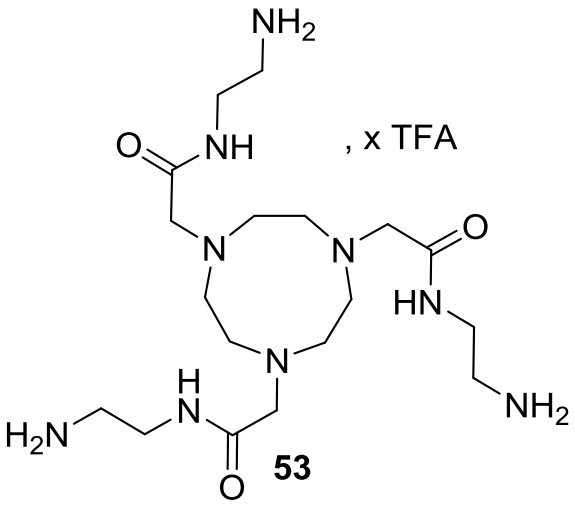

53

39 was prepared according to the procedure reported by Wickramaratne *et al*.[145] To a stirred pale yellow solution of 1,4,7-triazacyclononane, 3HCl (5 mg, 21 µmol) and **39** (18 mg, 65 µmol) in DMA (200 µL) was added a KOH (8 mg, 147 µmol) solution in H_2O (200 µL) and the resulting pale yellow solution was stirred for 1 h at 22 °C. The resulting solution was diluted in DCM (5 mL) and a $KHCO_3$ (1 M in H_2O, 20 mL). The layers were separated and the AL was washed with DCM (2×5 mL). The combined OLs were dried over Na_2SO_4, filtered and concentrated to yield pale yellow viscous oil (21 mg). To a stirred pale yellow solution of crude material (21 mg) in DCM (150 µL) was added TFA (50 µL) at 0 °C under Ar conditions and the yellow solution was stirred at 22 °C for 4 h. The yellow RM was co-evaporated with toluene (2 mL) to yield yellow oil. The resulting yellow oil was dissolved in ACN/H_2O (1/1, 0.1 % TFA, 800 µL) purified by RP column chromatography (column: Phenomenex, C18, 250×10 mm, eluent: ACN/H_2O/0.1 % TFA, 40-min-long gradient from 10 % to 70 % ACN) to yield pale yellow oil (24 mg). The resulting yellow oil was dissolved in ACN/H_2O (1/1, 0.1 % TFA, 800 µL) purified by RP column chromatography (column: Phenomenex, C18, 250×10 mm, eluent: ACN/H_2O/0.1 % TFA, 40-min-long gradient from 0 % to 20 % ACN) to

yield pale yellow oil (15 mg, 94 %). **^{1}H NMR** (500 MHz, CD_3CN) δ 8.10-8.06 (bt, 3H, N*H*CO), 7.83-7.65 (m, 9H, $CH_2NH_3^+$), 3.62 (s, 5H), 3.55–3.43 (m, 8H), 3.15-3.07 (bs, 7H), 2.96-2.90 ppm (s, 10H). **^{13}C NMR** (126 MHz, CD_3CN) δ 171.3, 58.6, 50.5, 40.6, 38.0, 29.6 ppm. **ESI-HRMS**: $C_{18}H_{39}N_9O_3Na^+$ m/z = 452.3061 (calculated: 452.3068) $[M+Na]^+$, error = 1.5 ppm.

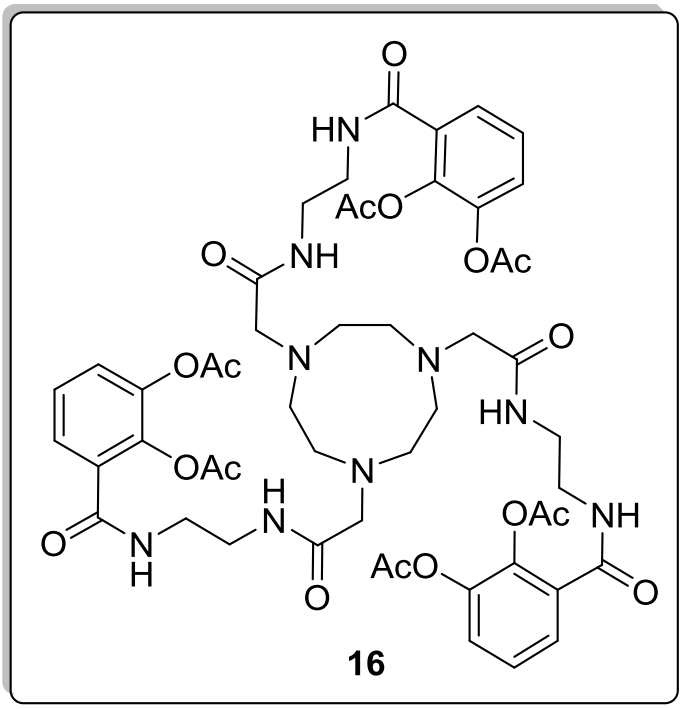

16

To a colorless solution of **40** (19 mg, 78 µmol) in DCM (200 µL) and DMF (20 µL) was added oxalyl chloride (13 µL, 156 µmol) and the colorless solution was stirred at 21 °C for 1 h. The colorless solution was concentrated and dried under the vacuum line for 2 h to yield orange oil. To a solution of **53** (15 mg, 19 µmol) in $KHCO_3$ (500 µL, 0.5 M in H_2O) was added dropwise a solution of the crude acyl chloride in dioxane (500 µL) at 21 ºC for 1 min. Exothermicity was observed. After addition, the mixture was stirred at 21 °C for 0.5 h. After concentration the orange solid was suspended in ACN/H_2O, filtered and purified by RP column chromatography (C18, 250×21.2mm, 40-min-long gradient from 20 % to 70 % ACN in H_2O) to yield a white solid (4.7 mg, 22 %). **^{1}H NMR** (700 MHz, CD_3CN) δ 7.77-7.73 (bt, J = 5.6 Hz, 3H, N*H*CO), 7.55-7.51 (dd, J = 6.3, 3.1 Hz, 3H, Ar-*H*), 7.49-7.45 (bt, J = 5.6 Hz, 3H, N*H*CO), 7.32-7.28 (m, 6H, Ar-*H*), 3.55 (s, 6H, CH_2CONH), 3.43–3.39 (m, 6H, CH_2NH), 3.34–3.28 (m, 6H, CH_2NH), 2.26 (s, 9H, CH_3CO_2), 2.23 ppm (s, 9H, CH_3CO_2). **^{13}C NMR** (176 MHz, CD_3CN) δ 170.3, 169.9, 169.3, 166.2, 144.3, 141.5, 131.6, 127.4, 127.1, 126.7, 58.7, 50.5, 40.1, 39.8, 20.8, 20.8 ppm. **ESI-HRMS**: $C_{51}H_{65}N_9O_{18}^{2+}$ m/z = 545.7229 (calculated: 545.7218) $[M+2H]^{2+}$, error = 2.0 ppm.

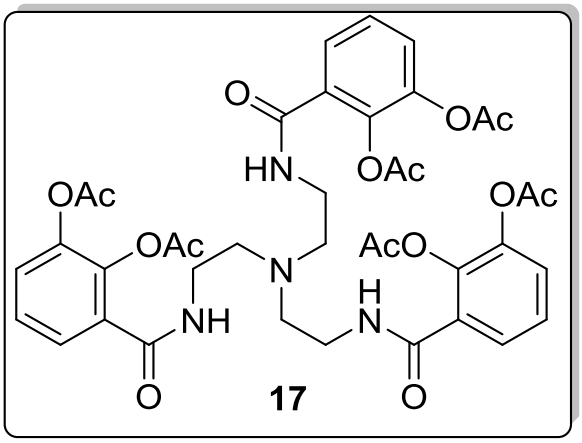

40 (27 mg, 113 µmol), DIPEA (42 µL, 241 µmol) and HATU (52 mg, 137 µmol) were added in DMF (500 µL) and stirred for 5 min. Tris(2-aminoethyl)amine (5.1 µL, 34 µmol) was added and the yellow solution was stirred at 25 °C for 15 min. The yellow solution was diluted in EtOAc (10 mL) and washed with a LiCl solution (5 %, 3×10 mL), brine (3×10 mL), dried over $MgSO_4$ and concentrated to yield pale yellow oil (22 mg). The crude material was diluted in ACN/H_2O (1/1, 0.1 % HCOOH) purified by RP column chromatography (ACN/H_2O without any acid, linear gradient 20 %-70 % ACN for 40 min) to yield a white solid (2.6 mg, 10 %). **^{1}H NMR** (500 MHz, MeOD) δ 7.44 (dd, J = 7.7, 1.5 Hz, 3H, Ar-H), 7.33 (dd, J = 8.1, 1.6 Hz, 3H, Ar-*H*), 7.24 (t, J = 8.0 Hz, 3H, Ar-*H*), 3.70 (m, 6H, C*H*$_2$), 3.45 (m, 6H, C*H*$_2$), 2.29 (s, 9H, C*H*$_3$CO$_2$), 2.23 ppm (s, 9H, C*H*$_3$CO$_2$). **^{13}C NMR** (126 MHz, MeOD) δ 169.9, 144.5, 141.7, 127.7, 127.4, 127.4, 55.4, 37.0, 20.6, 20.4 ppm. **ESI-HRMS**: $C_{39}H_{43}N_4O_{15}^+$ m/z = 807.2718 (calculated: 807.2719) $[M+H]^+$, error = 0.1 ppm.

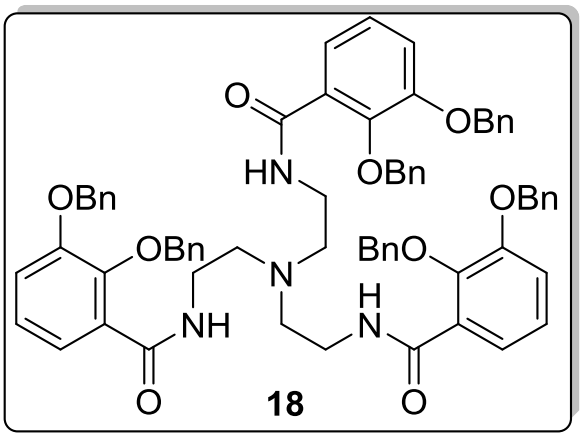

2,3-bis(benzyloxy)benzoic acid **54** (104 mg, 310 µmol), DIPEA (122 µL, 701 µmol) and HATU (126 mg, 331 µmol) were added in DMF (1.0 mL) and stirred for 5 min. Tris(2-aminoethyl)amine (15 µL, 100 µmol) was added and the yellow solution was stirred at 25 °C for 10 min. The yellow solution was diluted in EtOAc (25 mL), brine (3×50 mL), dried over $MgSO_4$ and concentrated to yield pale yellow oil (162 mg). The crude material was dissolved in DCM (0.5 mL)

and purified by NP flash column chromatography (m_{SiO2} = 4 g, 20-min-long gradient from neat DCM to DCM:EtOAc/1:1) to yield viscous oil (75 mg, 68 %). **^{1}H NMR** (500 MHz, MeOD) δ 7.47-7.40 (m, 6H, Ar-H), 7.38-7.29 (m, 9H, Ar-H), 7.28-7.22 (m, 9H, Ar-H), 7.22-7.15 (m, 12H, Ar-H), 7.07-7.02 (t, J = 8.0 Hz, 3H, Ar-H), 5.09 (s, 6H, C*H*$_2$C$_6$H$_5$), 4.98 (s, 6H, C*H*$_2$C$_6$H$_5$), 3.14 (t, J = 6.2 Hz, 6H, CH$_2$C*H*$_2$), 2.39 ppm (m, 6H, C*H*$_2$CH$_2$). **^{13}C NMR** (126 MHz, MeOD) δ 168.3, 153.3, 147.6, 138.3, 138.1, 129.7, 129.6, 129.5, 129.4, 129.2, 129.0, 125.5, 122.8, 118.0, 77.1, 72.1, 53.3, 38.9, 38.4 ppm. **ESI-HRMS**: $C_{69}H_{67}N_4O_9^+$ m/z = 1095.4894 (calculated: 1095.4903) $[M+H]^+$, error = 0.8 ppm.

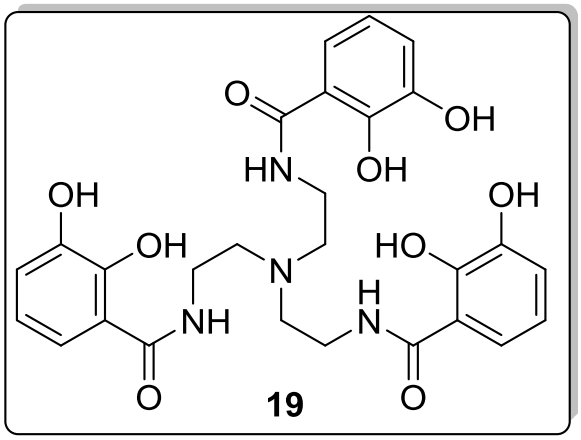

19

2,3-bis(benzyloxy)benzoic acid **54** (38 mg, 113 µmol), DIPEA (42 µL, 239 µmol) and HATU (52 mg, 137 µmol) were added in DMF (500 µL) and stirred for 5 min. Tris(2-aminoethyl)amine (5.1 µL, 34 µmol) was added and the yellow solution was stirred at 25 °C for 10 min. The yellow solution was diluted in EtOAc (10 mL), washed with a LiCl solution (5 %, 3×10 mL), a HCl solution (1 M, 3×10 mL), a Na_2CO_3 solution (0.1 M, 3×10 mL), brine (3×10 mL), dried over $MgSO_4$ and concentrated to yield pale yellow oil (45 mg). The crude material was set to a hydrogen atmosphere over 10 % Pd/C (4 mg, 3.4 µmol) in MeOH at 21 °C for 23 h. The black suspension was filtered through celite, washed and concentrated to yield colorless oil (19 mg). The crude material was diluted in ACN/H_2O (1000 µL, 1/1) and purified by RP column chromatography (column: Phenomenex, C18, 250×21 mm, eluent: ACN/H_2O/0.1 % TFA, 40-min-long gradient from 10 to 70 % ACN) to yield brown oil (18 mg, 90 %). **^{1}H NMR** (500 MHz, MeOD) δ 7.10 (dd, J = 8.1, 1.5 Hz, 3H, Ar-H), 6.90 (dd, J = 7.8, 1.5 Hz, 3H, Ar-H), 6.64 (t, J = 8.0 Hz, 3H, Ar-H), 3.85 (t, J = 5.7 Hz, 6H, CH$_2$C*H*$_2$), 3.66 ppm (t, J = 5.7 Hz, 6H, C*H*$_2$CH$_2$). **^{13}C NMR** (126 MHz, MeOD) δ 172.8, 149.8, 147.3, 120.2, 120.1, 119.8, 116.7, 55.7, 36.2 ppm. **ESI-HRMS**: $C_{27}H_{31}N_4O_9^+$ m/z = 555.2077 (calculated: 555.2086) $[M+H]^+$, error = 1.6 ppm

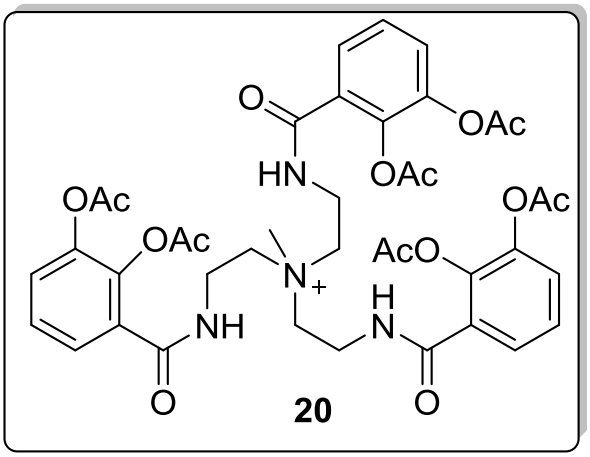

20

Tris(2-aminoethyl)amine (1.00 g, 6.83 mmol) was dissolved in a mixture of water and dioxane (10 mL/ 20 mL). The colorless solution was cooled to 0 °C and NaOH (2.5 g, 62 mmol) and Boc_2O (10.9 g, 50 mmol) were added and the colorless solution was stirred for 62 h at 22 °C. The resulting white suspension was diluted in water (50 mL) and extracted with EtOAc (3×50 mL), dried over $MgSO_4$, filtered and concentrated to yield a white solid (3.50 g). The crude material (51 mg, 100 µmol) was dissolved in dried acetonitrile and MeI (84 µL, 1344 µmol) and K_2CO_3 (31 mg, 224 µmol) were added to the colorless solution. The RM was stirred for 49 h. The solution was diluted in ether (10 mL). The OL was extracted with water (3 x 10 mL). The aqueous phase was concentrated to yield an orange solid (m_{CR} = 28.0 mg).To a stirred crude (28 mg) light yellow solution in DCM (400 µL) was added TFA (100 µL) at 0 °C under Ar conditions and the yellow solution was stirred at 24 °C for 3 h. The RM was concentrated to yield a light white solid (m = 27 mg). To a colorless solution of **40** (46 mg, 195 µmol) in DCM (200 µL) and DMF (100 µL) was added oxalyl chloride (32 µL, 383 µmol) and the colorless solution was stirred at 25 °C for 1 h. The colorless solution was concentrated and dried under the vacuum line to yield yellow oil. To a solution of the crude quarternary amine (28 mg, 48 µmol) in $KHCO_3$ (1340 µL, 0.5 M in H_2O) was added dropwise a yellow solution of the acyl chloride in dioxane (770 µL). After addition, the orange mixture was stirred at 25 °C for 30 min and then lyophilized to yield a brown solid. The brown solid was suspended in ACN, filtered and concentrated for 1 h to yield brown oil (110 mg) which was purified by RP column chromatography (column: Phenomenex, C18, 250×40 mm, eluent: ACN/H_2O, 40-min-long gradient from 20 % to 45 % ACN) to yield a white solid (2.5 mg, 6 %). The yield was calculated based on I^- as a counterion, although it was not determined. **^{1}H NMR** (500 MHz, CD_3CN). δ 8.71 (t, J = 5.5 Hz, 3H, N*H*), 7.49 (dd, J = 7.2, 1.8 Hz, 9H, Ar-*H*), 7.47-7.37 (m, 6H, Ar-*H*), 3.75-3.68 (m, 6H, CH_2), 3.62-3.55 (m, 6H, CH_2), 2.29 (s, 9H, CH_3CO), 2.26 ppm (s, 9H, CH_3CO). **^{13}C NMR** (125 MHz, CD_3CN). δ 168.3, 167.9, 165.2, 142.9, 140.1,

130.0, 126.4, 126.0, 59.5, 32.9, 20.3, 20.3 ppm. **ESI-HRMS**: $C_{40}H_{45}N_4O_{15}^+$ m/z = 821.2890 (calculated: 821.2876) $[M]^+$, error = 1.7 ppm.

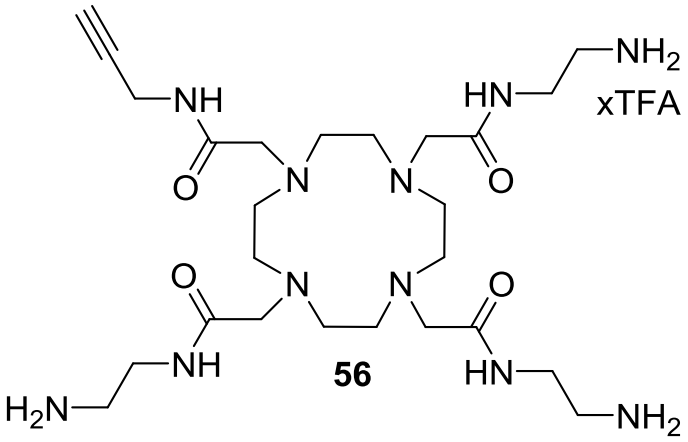

56

39 was prepared according to the procedure reported by Wickramaratne *et al*.[145] To a stirred white suspension of cyclen (61 mg, 0.4 mmol) and sodium acetate (96 mg, 1.2 mmol) in DMA (0.5 mL) at 23 °C under Ar conditions was added a solution of **39** (330 mg, 1.2 mmol) in DMA (1.0 mL, 250 µL/h). The reaction mixture was stirredfor 20 h at 23 °C. A $KHCO_3$ solution (100 mL, 0.5 M in H_2O) was then added to the yellow solution, which was extracted with DCM (3×50 mL). The combined OLs were washed with brine (100 mL), dried over Na_2SO_4, filtered and concentrated to yield yellow oil. The crude material was suspended with K_2CO_3 (196 mg, 1.4 mmol) in ACN (0.5 mL). **55** was prepared according to the procedure reported by Abedin *et al*.[148]. A solution of **55** (81 mg, 0.5 mmol) in ACN (1.0 mL) was added for 1 min under Ar conditions at 0 °C, and the suspension was stirred for 2 h at 23 °C. The precipitate was filtered and the filtrate was concentrated. The resulting yellow oil was dissolved in DCM (50 mL) and washed with H_2O (3×25 mL), dried over $MgSO_4$, filtered and concentrated to yield a pale yellow solid (524 mg). The crude material was dissolved in DCM, TFA (1.5 mL, 19.6 mmol) was added at 0 °C under Ar conditions, and the yellow solution was stirred at 22 °C for 4 h. The yellow solution was concentrated to yield brown oil, which was dissolved in ACN/H_2O (1/1, 0.1 % TFA, 1300 µL), purified by RP column chromatography (column: C18, 250×30 mm, eluent: ACN/H_2O/0.1 % TFA, 40-min-long gradient from 0 % to 25 % ACN) to yield **56** as yellow oil (193 mg, 60 %). **^{1}H NMR** (500 MHz, CD_3CN). δ 10.05 (bs, 7H, N*H*), 8.28-7.14 (m, 9H), 4.05-3.81 (m, 3H), 3.58-3.38 (m, 6H), 3.38 (bs, 4H), 3.21-3.09 (m, 5H), 3.01 (bs, 12H), 2.91 ppm (bs, 9H). **^{13}C NMR** (125 MHz, CD_3CN). δ 173.3, 72.8, 55.9, 55.1, 51.9, 50.1, 41.5, 40.7, 38.6, 38.2, 38.0, 35.8, 29.7, 20.7 ppm. **ESI-HRMS**: $C_{25}H_{50}N_{11}O_4^+$ m/z = 568.4042 (calculated: 568.4042) $[M+H]^+$, error < 0.1 ppm.

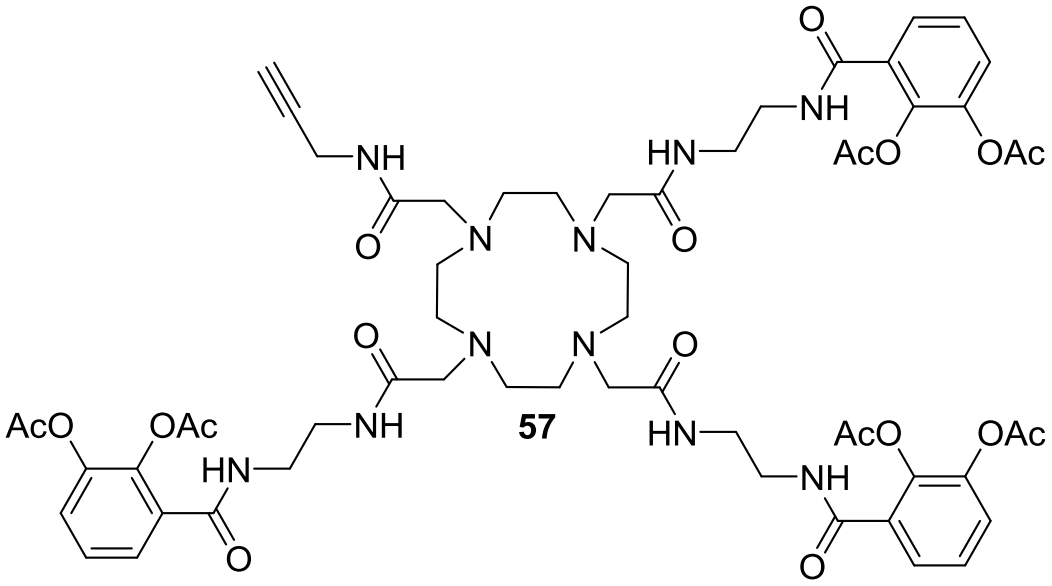

To a colorless solution of **40** (46 mg, 192 µmol) in DCM (200 µL) and DMF (25 µL) was added oxalyl chloride (33 µL, 390 µmol), and the pale yellow solution was stirred at 21 °C for 0.5 h. The reaction mixture was concentrated and dried under vacuum for 0.5 h to yield a yellow solid. To a solution of **56** (50 mg, 55 µmol) in $KHCO_3$ (1.5 mL, of a 0.5 M solution in H_2O) was added dropwise a pale yellow suspension of the acyl chloride in dioxane (1.5 mL) for 1 min at 0 °C. The pale yellow solution was stirred at 22 °C for 30 min. The pale yellow solution was concentrated, diluted in ACN (2 mL), filtered and concentrated to yield pale yellow oil (110 mg). The yellow oil was diluted in ACN/H_2O (600 µL) and purified by RP column chromatography (Phenomenex C18, 250×21.2 mm, 40-min-long gradient from 10 to 40 % ACN in H_2O) to yield **57** as a white solid (19 mg, 29 %). **^{1}H NMR** (500 MHz, CD_3CN). δ 8.02 (bs, 1H), 7.68 (bs, 1H), 7.54 (m, 4H), 7.45 (bs, 1H), 7.33 (m, 9H), 3.92 (m, 2H), 3.79-3.49 (m, 7H), 3.49-3.38 (m, 7H), 3.38-3.27 (m, 7H), 3.27-3.00 (m, 15H), 2.49 (t, J = 1.8 Hz, 1H), 2.25 ppm (m, 18H). **^{13}C NMR** (125 MHz, CD_3CN). δ 169.6, 169.4, 166.5, 166.5, 144.3, 141.4, 131.4, 127.5, 127.3, 126.8, 126.8, 80.8, 72.5, 56.0, 51.2, 50.8, 47.2, 40.3, 40.2, 29.4, 20.9, 20.8 ppm. **ESI-HRMS**: $C_{58}H_{75}N_{11}O_{19}^{2+}$ m/z = 614.7617 (calculated: 614.7615) $[M+2H]^{2+}$, error = 0.3 ppm.

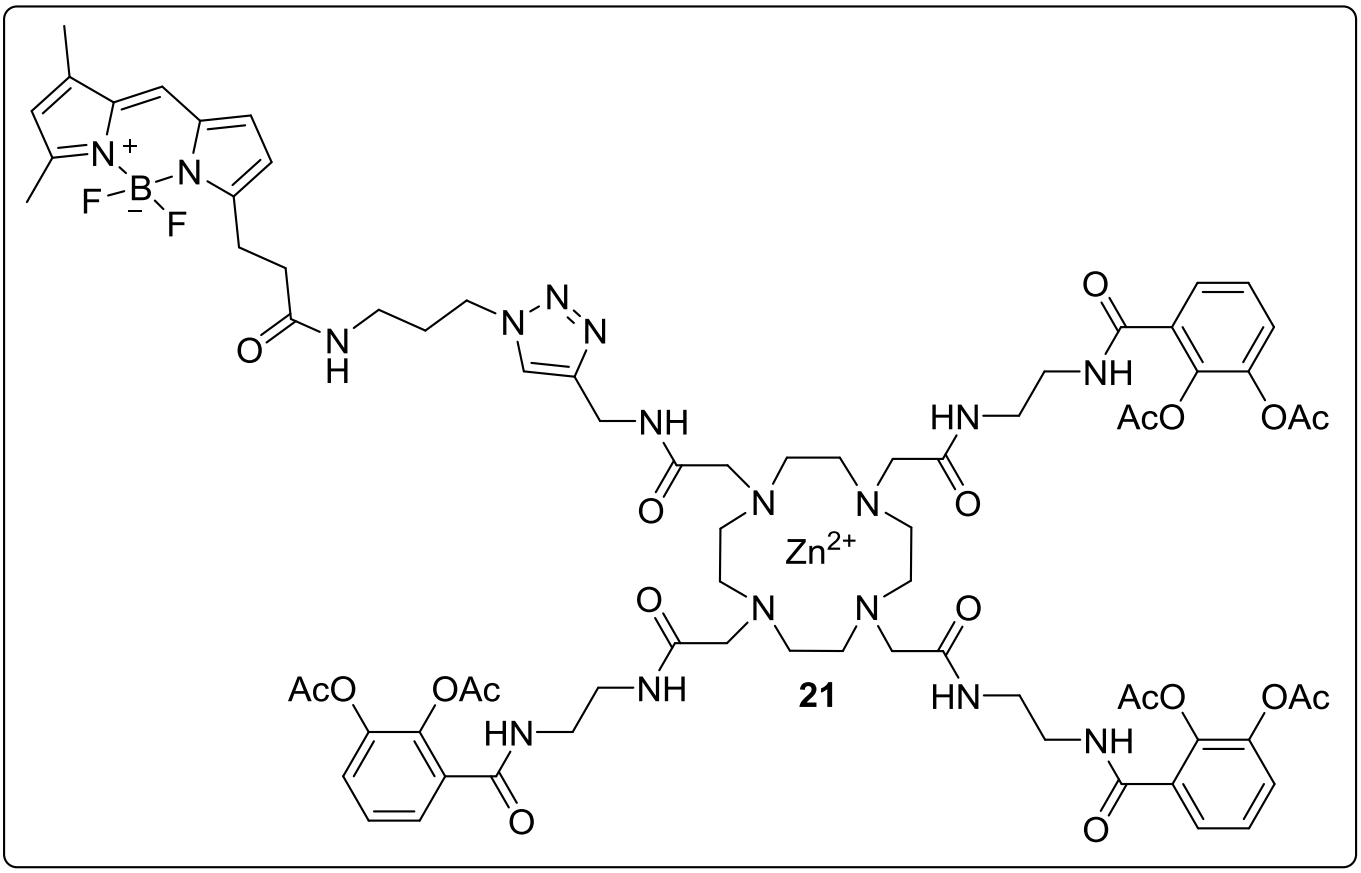

To a solution of **57** (2.5 mg, 2.0 µmol) and BODIPY FL-azide (0.8 mg, 2.2 µmol) in DMSO (40 µL) and *t*BuOH (25 µL) was added a solution of TBTA (0.4 mg, 8.1 µmol) in DMSO (10 µL). $Zn(OAc)_2$ (1.1 mg, 6.1 µmol) was added to the solution, which was stirred for 30 min. A premixed yellow solution of $CuSO_4$ (0.36 mg, 2.2 µmol) and Na ascorbate (0.44 mg, 2.2 µmol) in water (25 µL) was added to the orange solution, which was stirred for 15 min. The resulting orange solution was diluted in ACN/H_2O (700 µL) and purified by RP column chromatography (Phenomenex C18, 250×10 mm, 2 runs of 40-min-long gradient from 10 to 40 % ACN in H_2O) to yield **21** as an orange solid (0.7 mg, 21 %). **^{1}H NMR** (500 MHz, CD_3CN). δ 7.66 (m, 3H), 7.55 (m, 4H), 7.32 (m, 9H), 6.99 (s, 1H), 6.75 (m, 1H), 6.47-6.21 (m, 3H), 4.40 (s, 1H), 4.27 (s, 2H), 3.68-3.20 (m, 20H), 3.14 (bt, 2H), 3.08 (bs, 3H), 3.00-2.80 (bs, 6H), 2.80-2.60 (bs, 6H), 2.53 (m, 3H), 2.49 (s, 3H), 2.26 (s, 12H, CH_3CO_2), 2.23 (s, 6H, CH_3CO_2), 1.00 (s, 4H), 0.21 ppm (m, 3H). **^{13}C NMR** (176 MHz, CD_3CN). δ 173.1, 172.8, 172.4, 172.0, 169.8, 169.7, 169.5, 169.3, 166.6, 161.3, 158.4, 146.0, 144.7, 144.3, 144.2, 141.4, 141.3, 136.0, 134.2, 131.4, 131.3, 131.2, 129.5, 127.6, 127.5, 127.4, 127.0, 126.9, 125.8, 124.3, 121.5, 57.2, 56.8, 51.8, 51.4, 48.4, 40.8, 40.7, 39.5, 39.5, 36.9, 35.7, 35.0, 30.7, 25.1, 21.1, 20.9, 20.8, 15.1, 11.4, 11.4 ppm. **^{19}F NMR** (CD_3CN, 471 MHz). δ

-146.3 ppm (q, ^{1}J = 33 Hz, 2F). **ESI-HRMS**: $C_{75}H_{94}N_{17}O_{20}BF_2Zn^{2+}$ m/z = 832.8127 (calculated: 832.8107) $[M]^{2+}$, error = 2.4 ppm.

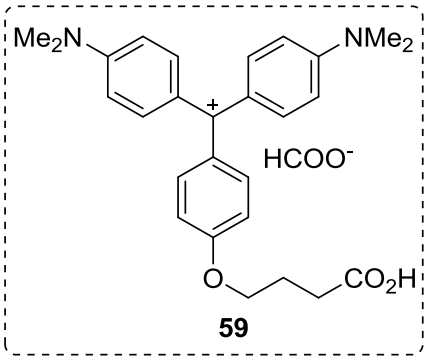

59

58 was prepared according to the procedure reported by Szent-Gyorgyi *et al*.[122] To a light blue solution of **58** (200 mg, 462 µmol) in DCM (5 mL) was added *p*-chloranil (170 mg, 691 µmol). The reaction mixture was stirred at 25 °C for 2 h and diluted in DCM (50 mL) and water (100 mL). The AL was extracted with DCM (5×100 mL), and the combined OLs were washed with brine (100 mL), dried over $MgSO_4$, filtered and concentrated to yield a dark blue solid. The crude material was dissolved in ACN:H_2O (1:1) and purified by RP column chromatography (column: Phenomenex, C18, 250×21 mm, eluent: ACN/H_2O/0.1 % HCOOH). The fractions were lyophilized to yield **59** as a dark blue solid (25 mg, 11 %). **^{1}H NMR** (500 MHz, CD_3OD). δ 7.47 (d, J = 9.3 Hz, 4H, Ar-*H*), 7.41 (d, J = 8.9 Hz, 2H, Ar-*H*), 7.22 (d, J = 8.9 Hz, 2H, Ar-*H*), 7.08 (d, J = 9.4 Hz, 2H, Ar-*H*), 4.26 (t, J = 6.3 Hz, 2H, OCH_2), 3.36 (s, 12H, CH_3), 3.13 (s, 1H), 2.58 (t, J = 7.2 Hz, 2H, CH_2CO_2H), 2.19 ppm (m, 2H, $CH_2CH_2CH_2$). **^{13}C NMR** (125 MHz, CD_3OD). δ 179.8, 176.8, 165.7, 158.4, 141.9, 138.9, 133.3, 128.3, 116.0, 114.4, 68.8, 40.8, 31.2, 25.6 ppm. **ESI-HRMS:** $C_{27}H_{31}N_2O_3^{+}$ m/z = 431.2335 (calculated: 431.2329) $[M]^{+}$, error = 1.4 ppm.

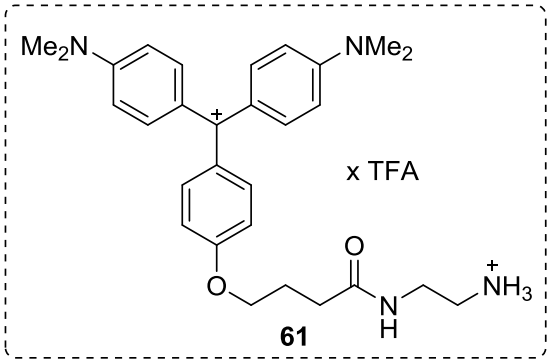

61

60 was prepared according to the procedure reported by Szent-Gyorgyi *et al*.[149]. To a light blue solution of **60** (10.6 mg, 17 µmol) in EtOAc (1.0 mL) was added *p*-chloranil (9.4 mg, 38 µmol).

The reaction mixture was refluxed for 1 h, filtered and concentrated to yield dark blue oil. The crude material was dissolved in EtOH:HCl (37 %) (1:1 mL) and stirred for 2 h at 25 °C. The reaction was monitored by LC-MS. The dark solution was diluted in water (30 mL) and washed with EtOAc (3×20 mL). The AL was lyophilized to yield a blue solid (8.0 mg). The crude material was purified by RP column chromatography (column: Phenomenex, C18, 250×10 mm, eluent: ACN/H_2O/0.1 % TFA). The fractions were lyophilized to yield **61** as a dark blue solid (6.0 mg, 52 %). **^{1}H NMR** (500 MHz, D_6-DMSO). δ 8.12 (br s, 1H, CON*H*), 7.83 (br s, 3H, NH_3), 7.33 (dd, J = 9.2, 8.8 Hz, 6H, Ar-*H*), 7.20 (d, J = 8.8 Hz, 2H, Ar-*H*), 7.07 (d, J = 9.4 Hz, 4H, Ar-*H*), 4.17 (t, J = 6.4 Hz, 2H, OCH_2), 3.33-3.24 (m, 2H, CONHCH_2), 3.28 (s, 12H), 2.87 (m, 2H, C$H_2$$NH_3$), 2.32 (t, J = 7.4 Hz, 2H, CH_2CONH), 2.02 ppm (m, 2H, CH_2C$H_2$$CH_2$). **^{13}C NMR** (125 MHz, D_6-DMSO). δ 176.0, 172.4, 163.5, 156.3, 140.1, 137.4, 131.3, 126.3, 115.0, 113.6, 67.8, 38.7, 36.5, 31.5, 24.5 ppm. **ESI-HRMS**: $C_{29}H_{37}N_4O_2^+$ m/z = 473.2960 (calculated: 473.2911) $[M-H]^+$, error = 10.4 ppm The analyzed data showed accordance to previously published ones.[149]

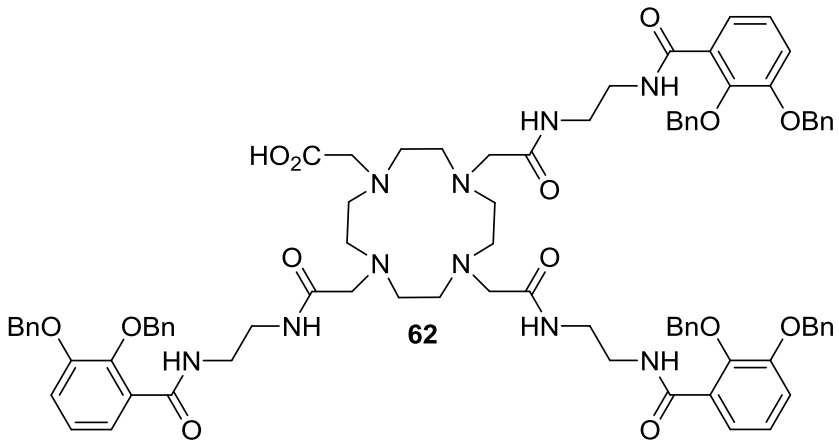

To a solution of **38** (50 mg, 32 µmol) in THF (300 µL) was added a LiOH solution (1 M in H_2O, 100 µL). The reaction was monitored by TLC (CH_2Cl_2:MeOH/8:2, UV), and the solution was stirred for 4 h at 25 °C. The reaction mixture was concentrated, rediluted in ACN (1.3 mL), filtered and purified by RP column chromatography (column: Phenomenex, C18, 250×21 mm, eluent: ACN/H_2O/0.1 % TFA) to yield **62** as colorless oil (40.7 mg, 87 %). **^{1}H NMR** (500 MHz, D_6-DMSO). δ 8.52 (bs, 2H, CON*H*), 8.27 (t, J = 5.9 Hz, 2H, CON*H*), 8.23 (t, J = 5.9 Hz, 1H, CON*H*), 8.18 (bs, 1H, CON*H*), 7.80 (bs, 1H), 7.51-7.45 (m, 6H, Ar-*H*), 7.43-37 (m, 6H, Ar-*H*), 7.37-7.31 (m, 9H, Ar-*H*), 7.31-7.24 (m, 12H, Ar-*H*),7.15-7.06 (m, 6H, Ar-*H*), 5.21-5.16 (2×bs, 6H, ArOC$H_2$$C_6H_5$), 5.02-4.97 (2×bs, 6H, ArOC$H_2$$C_6H_5$), 4.07-2.94 ppm (m, 36H, DOTAM + NHCH_2CH_2NH). **^{13}C NMR** (125 MHz, D_6-DMSO). δ 166.1, 166.0, 151.6, 145.2, 145.2, 137.0, 136.8, 130.8, 128.5, 128.4,

128.2, 128.0, 127.7, 124.2, 120.9, 116.0, 75.2, 75.1, 70.2, 38.8, 38.1 ppm. **ESI-HRMS**: $C_{85}H_{95}N_{10}O_{14}^{+}$ m/z = 1479.7032 (calculated: 1479.7024) $[M+H]^{+}$, error = 0.5 ppm.

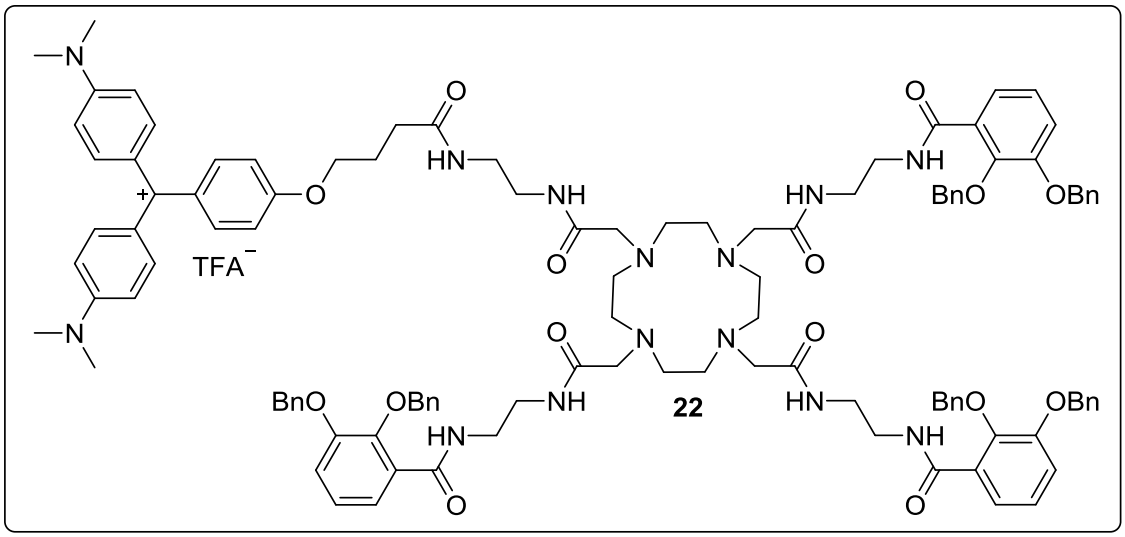

To a solution of **62** (10.0 mg, 6.8 µmol) in DMF (200 µL) were successively added HATU (4.4 mg, 11.6 µmol) and DIPEA (4.7 µL, 27.0 µmol). The reaction mixture was stirred at 25 °C for 10 min. A solution of **61** (11.1 mg, 20.3 µmol) in DMF (50 µL) was added to the reaction mixture and stirred for 1 h at 25 °C. More DIPEA (4.7 µL, 27.0 µmol) and HATU (4.4 mg, 11.6 µmol) were added to the reaction mixture, which was stirred for 3 further hours. The reaction mixture was filtered and purified by RP column chromatography (column: Phenomenex, C18, 250×10 mm, eluent: ACN/H_2O/0.1 % TFA, linear gradient from 30 % to 80 % ACN)**.** The fractions were gathered and lyophilized to yield **22** as a dark blue solid (8.5 mg, 13.8±0.6 % of water content assessed by ^{1}H NMR, 56 %). **^{1}H NMR** (700 MHz, D_6-DMSO). δ 8.38 (bs, 3H, CON*H*), 8.26 (m, 3H, CON*H*), 8.00-7.81 (m, 2H, CON*H*), 7.46 (d, J = 7.3 Hz, 6H, Ar-*H*), 7.38 (t, J = 7.5 Hz, 6H, Ar-*H*), 7.36-7.31 (m, 9H, Ar-*H*), 7.31-7.24 (m, 18H, Ar-*H*), 7.15-7.07 (m, 8H, Ar-*H*), 7.03 (d, J = 9.3 Hz, 4H, Ar_{MG}-*H*), 5.21-5.14 (2×bs, 6H, ArOC$H_2C_6H_5$), 5.01-4.96 (2×bs, 6H, ArOC$H_2C_6H_5$), 4.07 (t, J = 6.3 Hz, 2H, MG CH_2NHCO), 3.77-3.53 (bs, 9H), 3.39-3.28 (m, 10H), 3.26 (s, 13H), 3.22-3.10 (m, 15H), 2.23 (t, J = 7.5 Hz t, 2H, CH_2CONH), 2.02 ppm (m, J = 7.0, 6.0 Hz, 2H, $CH_2CH_2CH_2$). **^{13}C NMR** (176 MHz, D_6-DMSO). δ 176.0, 171.9, 166.1, 163.4, 156.3, 151.6, 145.1, 140.1, 137.3, 137.0, 136.7, 131.3, 130.8, 128.5, 128.3, 128.2, 128.0, 127.7, 126.2, 124.2, 120.9, 116.0, 114.9, 113.6, 75.1, 70.2, 67.8, 54.5, 49.6, 40.4, 40.0, 38.6, 38.4, 31.6, 24.6 ppm. **ESI-HRMS**: $C_{114}H_{131}N_{14}O_{15}^{3+}$ m/z = 645.3300 (calculated: 645.3301) $[M+2H]^{3+}$, error = 0.2 ppm.

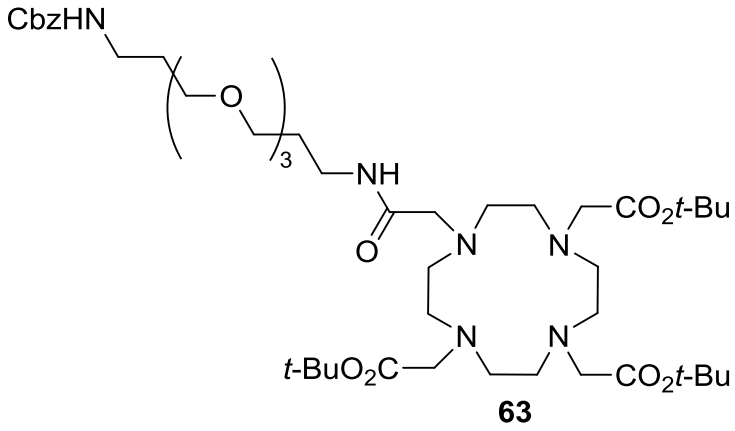

63

Into a flask were added THF (200 mL, 0.1 M), 4,7,10-trioxa-1,13-tridecanediamine (22.0 mL, 100 mmol), triethylamine (2.77 mL, 20.0 mmol), and MeOH (70 mL, 0.3 M). The flask was fitted with a dropping funnel, maintained under a nitrogen atmosphere, and cooled in an ice bath (0 ºC). Benzyl chloroformate (2.84 mL, 20.0 mmol) was dissolved in THF (100 mL, 0.2 M) and added dropwise (over 45 min) to the reaction mixture, which was allowed to warm to room temperature and stirred (30 min). Volatiles were removed under reduced pressure. The crude mixture was diluted with brine (200 mL) and sodium carbonate (10 % aqueous, 40 mL), extracted with ether (150 + 2×100 mL), washed with brine (100 mL), and dried with sodium sulfate. Volatiles were removed under reduced pressure, to yield a mixture (approximately 4:1) of monocarbamate and dicarbonate, which was used directly for the next step. Crude monocarbamate: ^{1}H NMR ($CDCl_3$, 500 MHz) δ 7.36–7.28 (m 5H, Bn), 5.58–5.52 (brs, 1H, NHZ), 5.09 (s, 2H, Bn), 3.65–3.45 (m, 12H, 6×CH_2–O), 3.33–3.27 (m, 2H, CH_2–NHZ), 2.77 (t, J = 6.8 Hz, 2H, CH_2–NH_2), 1.80–1.66 (m, 4H, 2×C–CH_2–C).[150]Bromoacetyl bromide (287 µl, 3.3 mmol) was added dropwise to the crude material (1062 mg, 3 mmol) and TEA (837 µl, 6 mmol) in 12 ml dichloromethane at 0°C. The reaction mixture was allowed to stir for 2 h, and the temperature gradually rose to room temperature. The solvents were evaporated followed by aqueous work up and extraction with ethyl acetate. The OL was washed with 10 % citric acid, water and saturated sodium bicarbonate and brine and dried over anhydrous sodium sulfate, filtered and concentrated. ESI-MS: $C_{20}H_{31}BrN_2O_6$ *m*/*z* = 475.2 [M+H$^+$].To a stirred solution of **36** (925 mg, 1.8 mmol) and K_2CO_3 (994 mg, 7.2 mmol) in ACN (50 mL) was added the crude material (1067 mg, 2.25 mmol) in ACN (20 mL) within 10 min. Stirring was continued overnight under argon at room temperature. The precipitate was filtered and the filtrate concentrated. The resulting oil was purified by RP-HPLC (10 % to 90 % ACN) or Flash silica gel column chromatography (eluent: DCM:MeOH = 9:1-4:1) yielding **63** (0.644 g, 39 %) as a white solid. **^{1}H NMR** (500 MHz, Chloroform-*d*) δ 8.30 (s, 1H, N*H*), 7.34 (bs, 2H, Ar), 7.33 (bs, 2H, Ar), 7.32–7.26 (m, 1H), 5.42 (s, 1H, N*H*), 5.07 (s, 2H, C*H*$_2$Ar), 4.10

(bs, 2H, CH_2), 3.88 (bs, 2H, CH_2), 3.65-3.44 (m, 22H, CH_2), 3.30-3.27 (m, 6H, CH_2), 3.03 (bs, 8H, CH_2), 1.77-1.75 (m, 4H, $CH_2CH_2CH_2$-), 1.48 (s, 9H, *t*Bu), 1.41 ppm (s, 18H, *t*Bu). **^{13}C NMR** (125 MHz, $CDCl_3$) δ 169.9, 156.7, 137.0, 128.6, 128.2, 82.6, 70.6, 70.5, 70.2, 70.2, 69.6, 69.0, 66.6, 55.4, 55.3, 54.9, 52.0, 49.0, 39.3, 37.4, 29.6, 29.0, 28.2, 28.1 ppm. **ESI-HRMS**: $C_{46}H_{81}N_6O_{12}^+$ m/z = 909.5905 (calculated: 909.5907) $[M+H]^+$, error = 0.2 ppm.

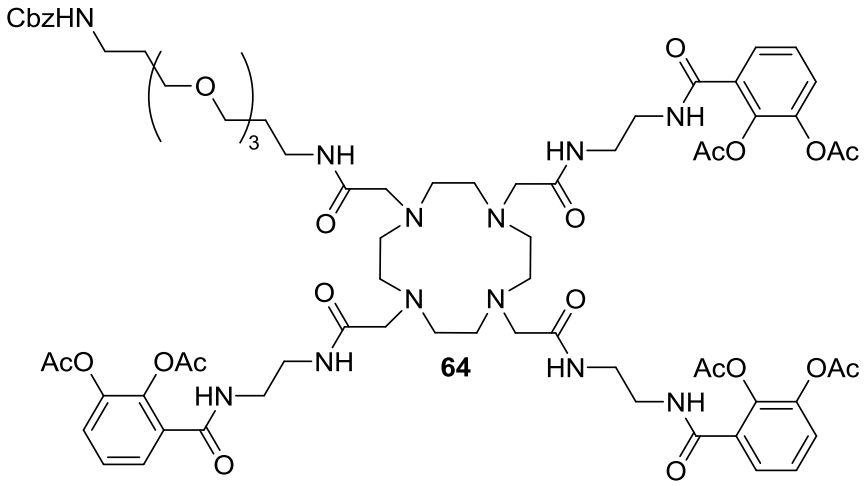

63 (91 mg, 0.1 mmol) was dissolved in 3 mL 95 % TFA/H_2O, and the reaction mixture was stirred for 2 h under argon at room temperature. The reaction was monitored by LC-MS. After the reaction was complete, the solvent was 3 times co-evaporated with toluene. The crude product was used without further purification in the next step. ESI-MS found: $[M+H]^+$ = 741.8. ^{1}H NMR (500 MHz, Methanol-d_4) δ 7.42-7.30 (m, 5H, Ar), 5.11 (s, 2H, -CH_2-Ar), 3.87-3.24 (m, 40H, -CH_2), 1.80 (m, 4H, $-CH_2CH_2CH_2-$). ^{13}C NMR (125 MHz, MeOD) δ 162.95, 162.68, 158.85, 138.50, 129.50, 128.99, 128.75, 119.35, 117.03, 71.50, 71.44, 71.15, 71.08, 69.98, 69.77, 67.32, 55.81, 54.68, 51.13, 39.24, 38.07, 30.85, 30.21. For removal of the Boc protection group, **42** (80 mg, 0.21 mmol) was dissolved in 3 mL 50 % TFA/DCM, and the reaction mixture was stirred for 10 min under argon at room temperature. The reaction was monitored by LC-MS. After the reaction was complete, the solvent was 3 times co-evaporated with toluene. The crude product was used without further purification in the next step. ESI-MS found: $[M+H]^+$ = 281.2. The crude arboxylic acid (52 mg, 0.07 mmol), HATU (80 mg, 0.21 mmol) and DIPEA (40 µL, 0.23 mmol) were dissolved in 3 mL DMF/CH_2Cl_2 (1:1). After 10 min, the reaction mixture was added into the unprotected form of **42** (66 mg, 0.21 mmol) and stirred 30 min under argon at room temperature. The solution was concentrated in vacuum to remove the DCM, then directly and immediately purified by HPLC to give **64** (40 mg, 37 %) as a white powder. **^{1}H NMR** (500 MHz, CD_3OD) δ 7.58-7.50 (m, 3H), 7.41-7.31 (m, 10H), 5.09 (s, 2H, C$H_2C_6H_5$), 3.71-3.45 (m, 27H), 3.38 (q, *J* = 10.0, 8.0

Hz, 10H), 3.30 (t, *J* = 6.9 Hz, 6H), 3.26-3.19 (m, 6H), 2.35-2.28 (m, 18H, CO_2CH_3), 1.78 ppm (dp, *J* = 12.9, 6.4 Hz, 5H). **^{13}C NMR** (125 MHz, CD_3OD). δ 170.0, 169.9, 168.3, 158.8, 144.7, 141.8, 138.5, 131.8, 129.5, 129.0, 128.7, 127.7, 127.2, 127.2, 125.6, 116.5, 71.5, 71.4, 71.2, 70.0, 69.7, 67.3, 56.2, 40.6, 40.0, 39.3, 38.3, 30.9, 30.3, 20.7, 20.4 ppm. **ESI-HRMS**: $C_{73}H_{100}N_{12}O_{24}^{2+}$ m/z = 764.3469 (calculated: 764.3481) $[M+2H]^{2+}$, error = 1.7 ppm.

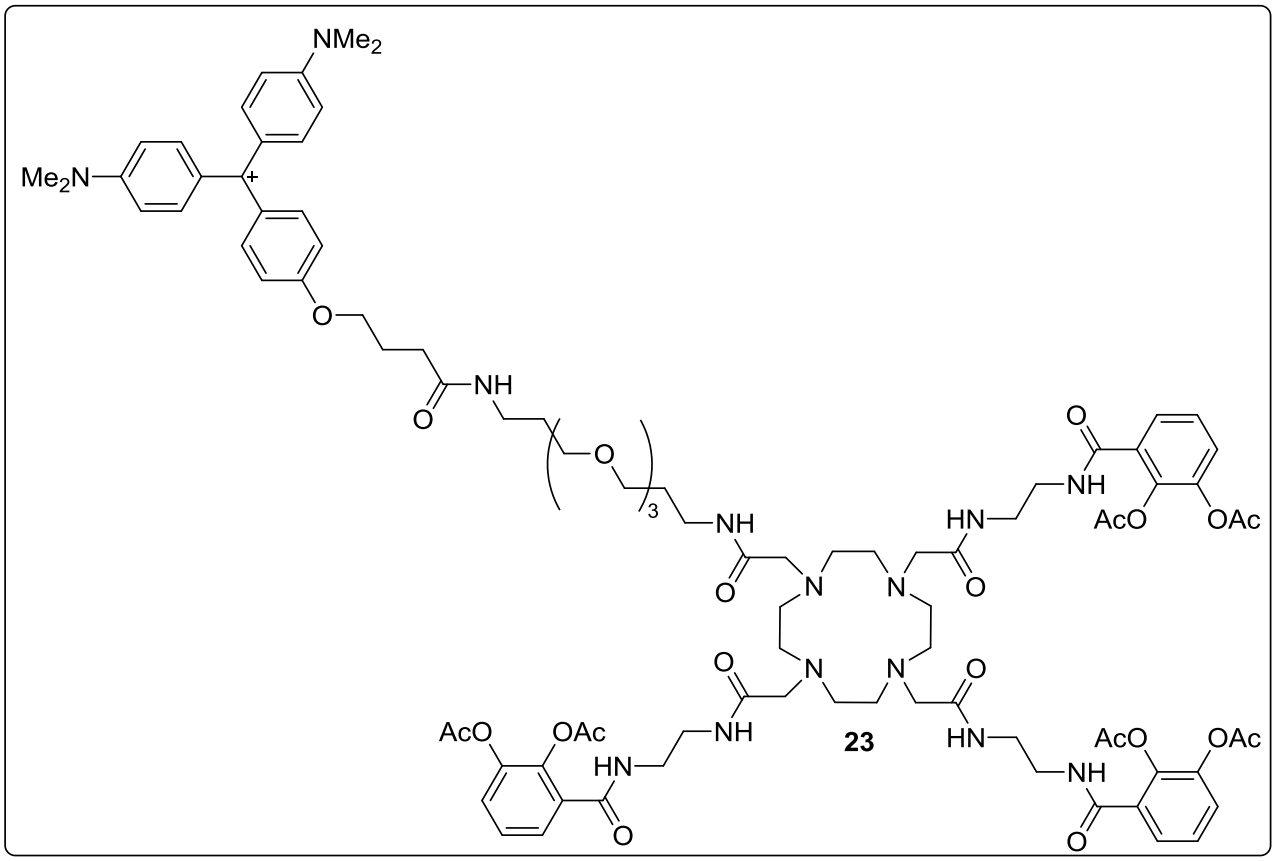

64 (31 mg, 20 µmol) was hydrogenolyzed (1 atm) over 10 % Pd on carbon (4 mg) in MeOH (5 mL) for 12 h. The Pd/C was removed by filtration, and the MeOH was removed by evaporation. Compounds were analyzed by LC/MS. ESI-MS found: $[M+2H]^{2+}$ = 698.0. This procedure was repeated. To a solution of **59** (25 mg, 54 µmol) in DMF (2 mL) were successively added HATU (21 mg, 55 µmol) and DIPEA (16 µL, 92 µmol). A solution of the crude amine (44 mg, 32 µmol) in DMF (3 mL) was added to the reaction mixture and stirred for 1 h at 25 °C. The reaction mixture was filtered and purified by RP column chromatography (column: Phenomenex, C18, 250×21 mm, eluent: ACN/H_2O/0.1 % HCOOH, linear gradient from 10 % to 70 % ACN)**.** The fractions were gathered and lyophilized to yield **23** as a dark blue solid (0.4 mg, 1 %). **^{1}H NMR** (700 MHz, D_6-DMSO). δ 8.42 (m, 4H, CON*H*), 7.88 (m, 1H, CON*H*), 7.49 (d, J = 7.4 Hz, 2H), 7.41-7.28 (m, 11H, Ar-*H*), 7.19 (d, J = 8.9 Hz, 2H, Ar-*H*), 7.07 (d, J = 9.4 Hz, 4H, Ar-*H*), 4.14 (t, 2H), 3.76 (m, 2H),

3.52-3.46 (m, 8H), 3.46-3.41 (m, 7H), 3.40-3.35 (m, 7H), 3.34-3.26 (m, 23H), 3.25-3.20 (m, 7H), 3.19-3.05 (m, 12H), 2.30-2.20 (2×s, 18H, C*H*$_3$COO), 1.99 (m, 2H), 1.68-1.59 (m, 4H), 1.31-1.20 ppm (m, 4H). **^{13}C NMR** (175 MHz, *D*$_6$-DMSO). δ 176.1, 171.3, 168.3, 167.8, 164.9, 163.5, 156.3, 142.9, 140.1, 137.4, 131.3, 130.6, 126.3, 126.2, 126.1, 125.6, 115.0, 113.6, 69.7, 69.5, 68.1, 68.0, 67.8, 63.3, 54.6, 53.6, 49.6, 42.9, 40.4, 40.0, 38.6, 38.4, 35.8, 31.5, 29.4, 29.0, 24.7, 20.3, 20.3 ppm. **ESI-HRMS**: $C_{92}H_{123}N_{14}O_{24}^{3+}$ m/z = 602.6272 (calculated: 602.6273) $[M+2H]^{3+}$, error = 0.2 ppm.

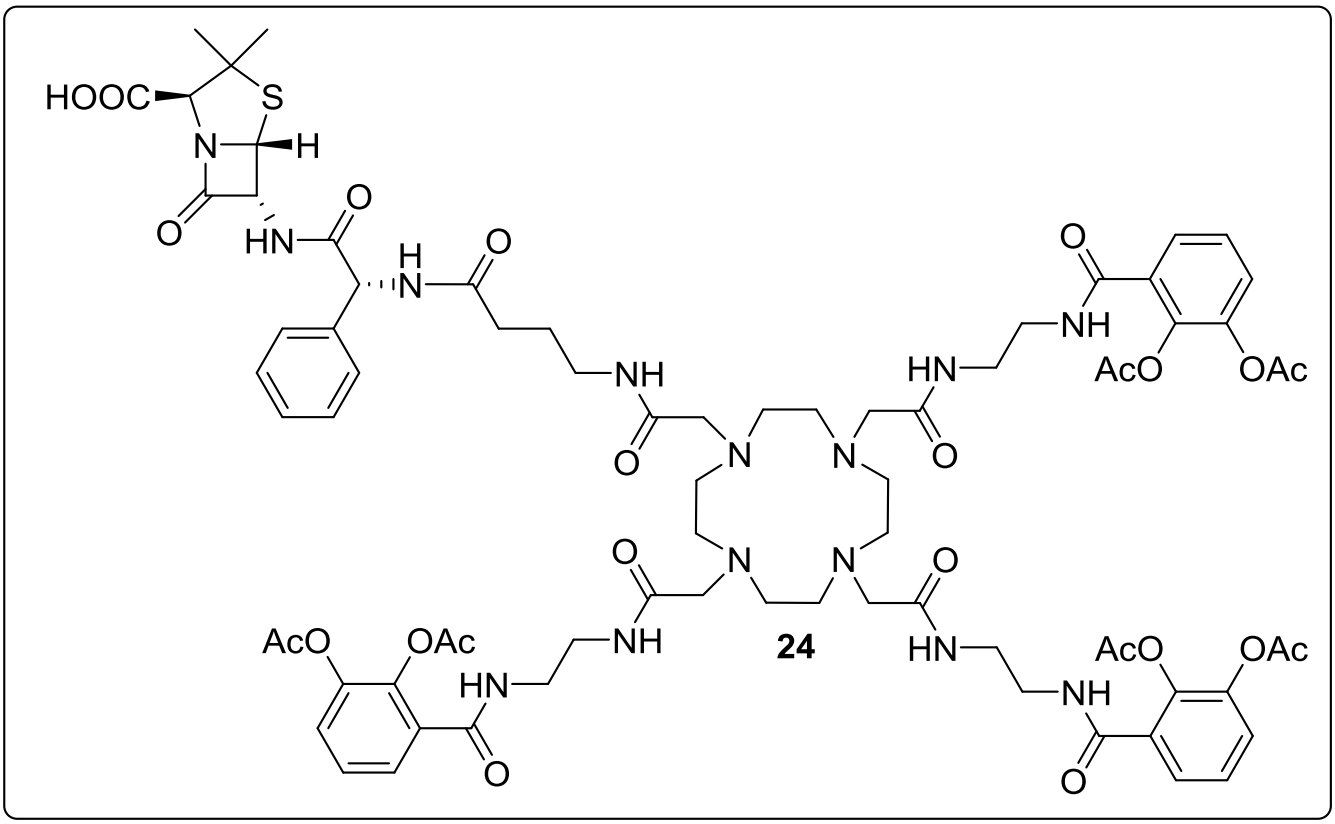

To a solution of **6** (10.0 mg, 7.8 µmol) and *N*-methylmorpholine (4.3 µL, 39 µmol) in anhydrous DMF (100 µL) was added ethyl chloroformate (3.7 µL, 39 µmol) at 21 ºC, and the reaction mixture was stirred for 10 min. A solution of ampicillin (13.7 mg, 39 µmol) and Et_3N (16.4 µL, 118 µmol) in DMF (50 µL) was added, and the mixture was stirred for 15 min at 21 ºC. The colorless solution was purified by preparative HPLC (column: Phenomenex, C18, 250×10 mm, eluent: ACN/H_2O/0.1 % HCOOH, 40-min-long gradient from 20 to 30 % ACN). The fractions were lyophilized to yield **24** as a white solid (7.1 mg, 56 %). **^{1}H NMR** (500 MHz, *D*$_6$-DMSO). δ 9.08 (d, 1H), 8.51 (d, 1H), 8.41 (m, 3H), 8.21 (bs, 2H), 8.11 (m, 1H), 7.47 (dd, J = 5.4, 1.2 Hz, 3H, Ar-*H*), 7.41 (d, J = 5.2 Hz, 3H, Ar-*H*), 7.38-7.30 (m, 8H, Ar-*H*), 5.71 (d, J = 5.9 Hz, 1H), 5.49 (m, 1H), 5.37

(d, J = 2.9 Hz, 1H), 4.16 (d, J = 9.6 Hz, 1H), 3.42-3.13 (m, 24H), 3.13-3.00 (m, 3H), 2.95-2.79 (m, 11H), 2.25 (s, 18H, CH_3CO_2), 1.53 (s, 3H, CCH_3), 1.40 ppm (s, 3H, CCH_3). **^{13}C NMR** (125 MHz, D_6-DMSO). δ 173.3, 173.2, 171.6, 170.2, 169.7, 168.9, 168.3, 167.8, 164.7, 160.5, 142.8, 140.1, 138.3, 138.1, 138.0, 130.7, 128.2, 128.2, 127.6, 127.5, 127.2, 127.1, 126.9, 126.1, 126.1, 125.5, 70.8, 70.6, 67.2, 67.1, 63.8, 58.0, 58.0, 56.2, 55.4, 53.8, 51.1, 38.8, 38.2, 30.4, 26.7, 26.7, 25.4, 20.3, 20.2 ppm. **ESI-HRMS**: $C_{75}H_{96}N_{14}O_{24}S^{2+}$ m/z = 804.3216 (calculated: 804.3216) $[M+2H]^+$, error < 0.1 ppm.

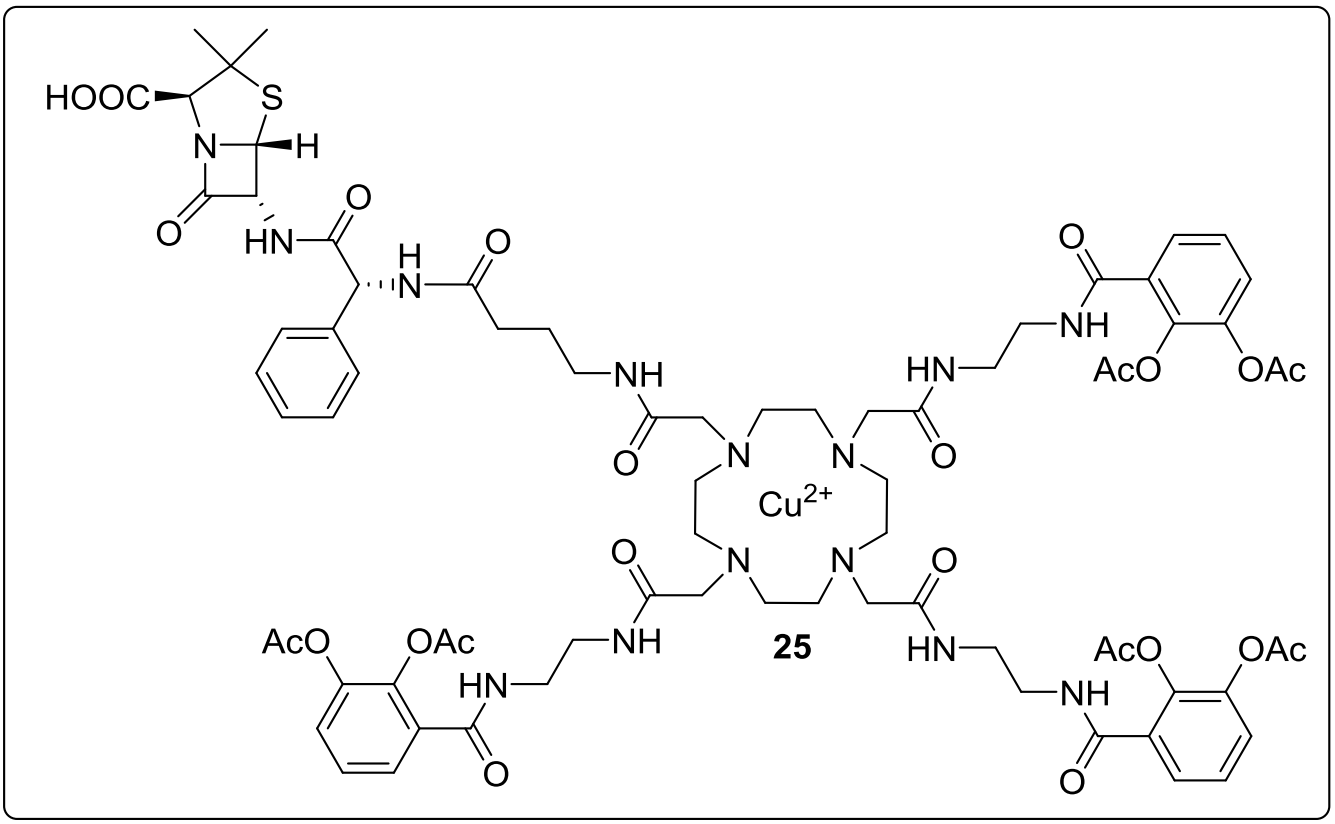

To a solution of **24** (4.0 mg, 2.5 µmol) in dried MeOH (200 µL) was added anhydrous $CuSO_4$ (1.1 mg, 6.9 µmol) under Ar, and the blue solution was stirred for 15 min at 26 °C. The blue solution was concentrated, rediluted in ACN/H_2O (600 µL), filtered and purified by RP column chromatography (column: Phenomenex, C18, 250×10 mm, eluent: ACN/H_2O, 40-min-long gradient from 10 to 40 % ACN in water) to yield **25** as a blue solid (3.5 mg, 85 %). **ESI-HRMS**: $C_{75}H_{94}N_{14}O_{24}SCu^{2+}$ m/z = 834.7787 (calculated: 834.7786) $[M]^{2+}$, error = 0.2 ppm.

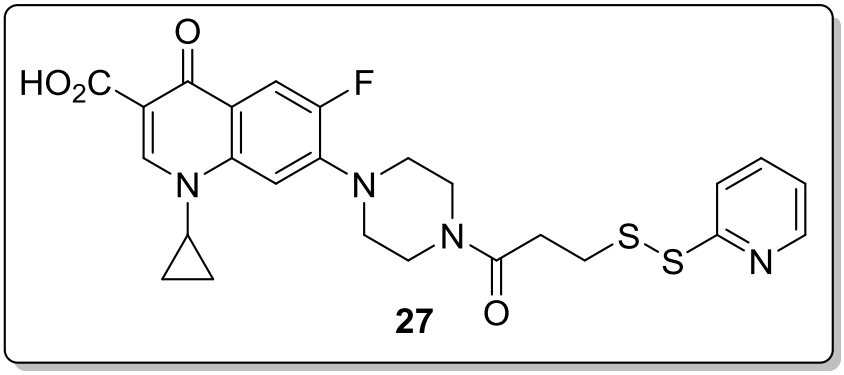

27

A white suspension of ciprofloxacin (21 mg, 64 µmol) DCM (2.0 mL) and Et_3N (9 µL, 64 µmol) was added to *N*-Succinimidyl 3-(2-pyridyldithio) propionate (SPDP, 20 mg, 64 µmol) and the resulting yellow solution was stirred for 3 h at 29 °C. The yellow solution was concentrated to 300 µL and purified by NP flash column chromatography (m_{SiO2} = 4 g, 30-min-long gradient from neat DCM to 5 % MeOH in DCM). The pure fractions were concentrated to yield **27** (33 mg, 97 %). **^{1}H NMR** (500 MHz, $CDCl_3$) δ 8.78 (s, 1H), 8.70 (d, J = 5.5 Hz, 1H), 8.16 (m, 2H), 8.04 (d, J = 12.8 Hz, 1H), 7.55 (m, 1H), 7.47 (d, J = 7.1 Hz, 1H), 3.87-3.82 (m, 2H), 3.80-3.75 (m, 2H), 3.65-3.60 (m, 1H), 3.43-3.40 (m, 2H), 3.35-3.32 (m, 2H), 3.21 (t, J = 6.7 Hz, 2H), 2.98 (t, J = 6.7 Hz, 2H), 2.70 (s, 1H), 1.49-1.43 (m, 2H), 1.21-1.17 ppm (m, 2H). **^{13}C NMR** (126 MHz, $CDCl_3$) δ 177.3, 168.7, 167.1, 158.3, 147.7, 144.0, 142.9, 139.2, 124.6, 122.9, 120.7, 112.8, 112.6, 108.4, 106.0, 50.1, 45.3, 41.8, 35.7, 34.1, 32.4, 29.8, 25.6, 8.5 ppm. **^{19}F NMR** (471 MHz, $CDCl_3$) δ -121.3 ppm (dd, 12.7, 7.0 Hz, 1F). **ESI-HRMS**: $C_{25}H_{25}FN_4O_4S_2^+$ m/z = 529.1376 (calculated: 529.1374) $[M+H]^+$, error = 0.4 ppm.

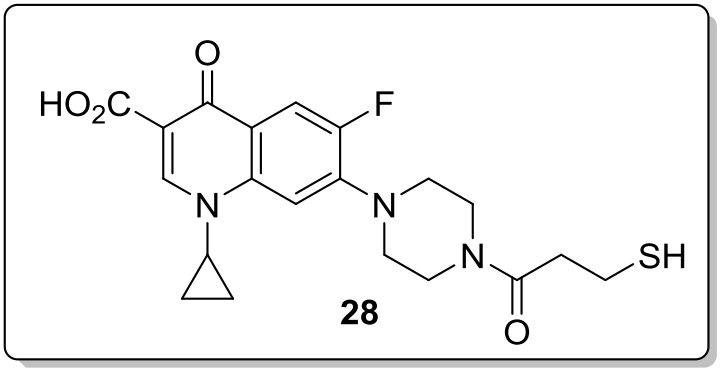

28

DMF (250 µL) was added to 3-(tritylthio) propanoic acid (23 mg, 66 µmol), under Ar conditions. Under Ar conditions at 0 °C, DIPEA (32 µL), HATU (34 mg, 89 µmol) and ciprofloxacin (20 mg, 60 µmol) were added. The yellow RM was stirred for 3 h at 22 °C. The yellow RM was concentrated to yield a yellow solid. The solid was dissolved in ACN (2 mL) and filtered. The yellow

solution was again concentrated to yield yellow oil (52 mg). To a stirred yellow solution of the crude material (52 mg) in DCM (150 µL) was added TFA (150 µL) and TIPS (18 µL) at 0 °C under Ar conditions and the resulting orange solution was stirred at 22 °C for 3.5 h. The orange solution was co-evaporated with toluene (1 mL) to yield a yellow solid. (52 mg) The resulting yellow solid was dissolved in ACN/H_2O (1/1, 0.1 % TFA, 1 mL).The yellow suspension was filtered to yield a yellow solution, which was purified by RP column chromatography (column: Gemini, C18, 250×21.2 mm, eluent: ACN/H_2O/0.1 % TFA, 40-min-long gradient from 20 to 70 % ACN) to yield a white solid (4.95 mg). **^{1}H NMR** (500 MHz, D_6-DMSO). δ 15.18 (s, 1H), 8.67 (s, 1H), 7.93 (d, J = 13.2 Hz, 1H), 7.58 (d, J = 7.5 Hz, 1H), 3.86-3.78 (m, 1H), 3.75-3.64 (m, 4H), 3.41-3.26 (m, 8H), 2.75-2.65 (m, 4H), 2.40 (t, J = 7.9 Hz, 1H), 1.36-1.29 (m, 2H), 1.22-1.15 ppm (m, 2H). **^{13}C NMR** (126 MHz, D_6-DMSO) δ 176.4, 169.2, 165.9, 153.9-152.0 (d, 249 Hz), 148.1, 145.0-144.9 (d, 10Hz), 139.1, 118.9-118.8 (d, 8 Hz), 111.1-110.9 (23 Hz), 106.8, 106.7-106.6 (d, 3Hz), 49.6, 49.2, 44.4, 40.7, 36.4, 35.9, 19.6, 7.6 ppm. **^{19}F NMR** (471 MHz, D_6-DMSO) δ -121.8 ppm (dd, J = 13.1, 7.5 Hz, 1F). **ESI-HRMS**: $C_{20}H_{23}FN_3O_4S^+$ m/z = 420.1380 (calculated: 420.1388) $[M+H]^+$, error = 1.9 ppm.

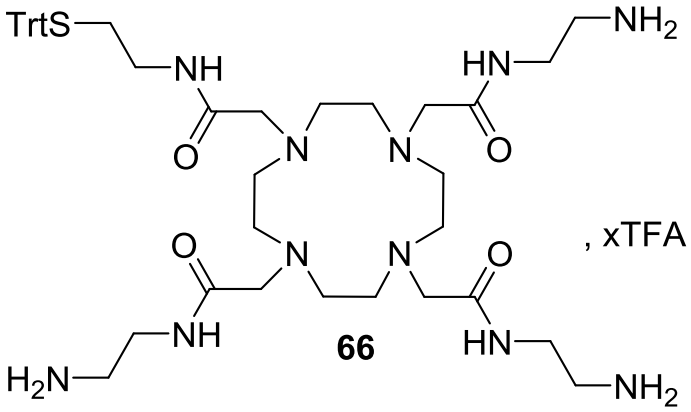

66

39 was prepared according to the procedure reported by Wickramaratne *et al*.[145]To a stirred suspension of cyclen (20 mg, 116 µmol) and sodium acetate (32 mg, 384 µmol) in DMA (200 µL) at 0°C under Ar conditions was added for 3 h a solution of **39** (108 mg, 384 µmol) in DMA (200 µL). The reaction was stirred for 20 h at 25 °C. The yellow suspension was diluted in DCM (20 mL) and $KHCO_3$ (20 mL, 1 M in H_2O). The OL was separated, dried over $MgSO_4$, filtered through paper and concentrated to yield pale yellow oil (159 mg). To a stirred suspension of crude material (65 mg) and K_2CO_3 (26 mg, 186 µmol) in ACN (250 µL) was added a **65** (25 mg, 57 µmol) solution in DMA (250 µL, the compound was insoluble in ACN) dropwise for 5 min under Ar conditions at 0 °C and the suspension was stirred for 1 h at 24 °C. The precipitate was filtered and the filtrate was concentrated. The resulting yellow oil was dissolved in DCM (20 mL) and washed with H_2O (3×30 mL), dried over $MgSO_4$, filtered and concentrated to yield a pale yellow solid (83 mg). To a

stirred pale yellow solution of crude material in DCM (400 µL) was added TFA (100 µL) at 0 °C under Ar conditions and the resulting bright yellow solution was stirred at 25 °C for 2 h. The yellow solution was concentrated to yield yellow oil which was dissolved in ACN/H_2O (1/1, 0.1 % TFA) and purified by RP column chromatography (Gemini, 250×20.2mm, 40-min-long gradient from 10 to 40 % ACN in H_2O + 0.1 % TFA) to yield colorless oil (32 mg, 57 %). **^{1}H NMR** (500 MHz, D_6-DMSO). δ 8.65 (bs, 1H, N*H*), 8.55 (bs, 2H, N*H*), 8.43 (bs, 1H, N*H*), 7.98 (bs, 9H, NH_3^+), 7.42-7.29 (m, 12H, Ar-*H*), 7.29-7.22 (m, 3H, Ar-*H*), 3.86-2.76 (m, 38H, NCH_2), 2.26 ppm (t, J = 7.2 Hz, 2H, SCH_2). **^{13}C NMR** (126 MHz, D_6-DMSO) δ 168.5, 144.4, 129.1, 128.1, 126.9, 118.1, 66.2, 54.3, 49.4, 38.4, 37.8, 36.6, 31.0, 1.2 ppm. **ESI-HRMS**: $C_{43}H_{66}N_{11}O_4S^+$ m/z = 832.5013 (calculated: 832.5014) $[M+H]^+$, error = 0.1 ppm.

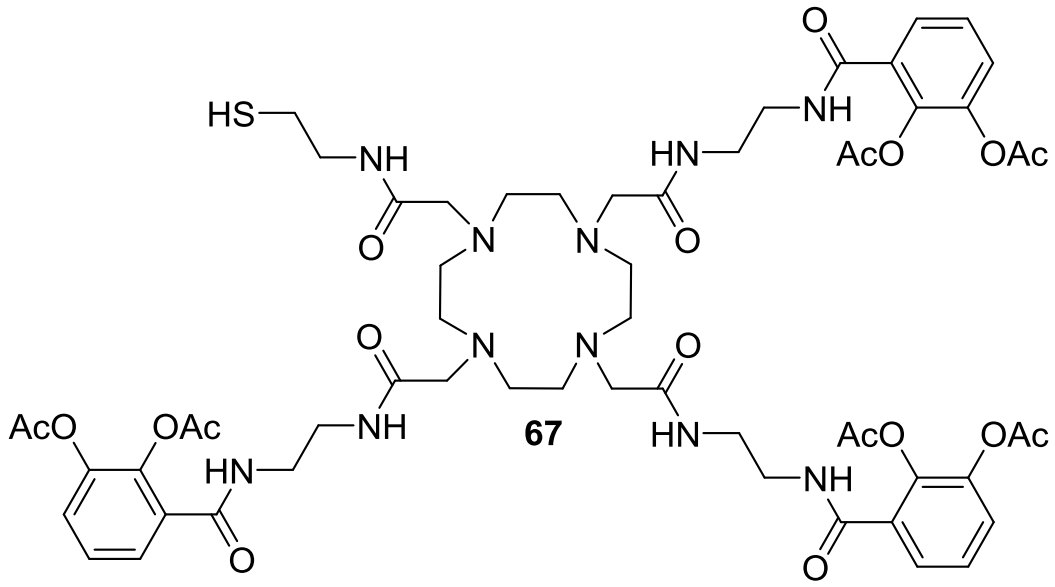

To a yellow solution of **40** (22 mg, 92 µmol) in DCM (200 µL) and DMF (30 µL) was added oxalyl chloride (16 µL, 185 µmol) and the colorless solution was stirred at 25 °C for 15 min. The reaction mixture was concentrated and dried under the vacuum line for 1 h to yield pale yellow viscous oil. To a solution of **66** (31 mg, 26 µmol) in $KHCO_3$ (700 µL, 0.5 M in H_2O) was added dropwise a colorless solution of the crude acyl chloride in dioxane (700 µL) at 25ºC for 1 min in a 0 °C bath. After addition, the yellow solution was stirred at 25 °C for 15 min. After concentration, the yellow solid (78 mg) was suspended in ACN, filtered and concentrated in the vacuum line for 30 min to yield yellow oil (48 mg). To a stirred yellow solution of crude material in DCM (400 µL) was added TIPS (8 µL) and TFA (400 µL) at 0 °C under Ar conditions and the resulting yellow solution was stirred at 25 °C for 1.5 h. The yellow solution was co-evaporated with toluene (1 mL) to yield pale yellow oil. The pale yellow oil was dissolved in ACN/H_2O (1/1, 1.0 mL) and purified by RP column chromatography (Gemini, 250×20.2mm, 40-min-long gradient from 10 to 60 % ACN in

H_2O + 0.1 % HCOOH) to yield a white solid (9 mg, 27 %). **^{1}H NMR** (700 MHz, CD_3CN). δ 7.83-7.65 (m, 3H, N*H*), 7.61-7.41 (m, 7H), 7.35-7.27 (m, 6H), 3.52-3.25 (m, 22H), 3.02-2.65 (m, 16H), 2.58-2.54 (m, 2H), 2.27-2.22 ppm (m, 18H, C*H*$_3$CO$_2$). **^{13}C NMR** (176 MHz, CD_3CN) δ 170.8, 169.6, 169.3, 166.4, 160.9, 160.7, 144.2, 141.4, 131.6, 127.4, 127.2, 126.7, 57.7, 52.8, 43.2, 40.4, 39.9, 24.5, 20.8, 20.8 ppm. **ESI-HRMS**: $C_{57}H_{75}N_{11}O_{19}S^{2+}$ m/z = 625.7556 (calculated: 625.7553) $[M+2H]^{2+}$, error = 0.5 ppm.

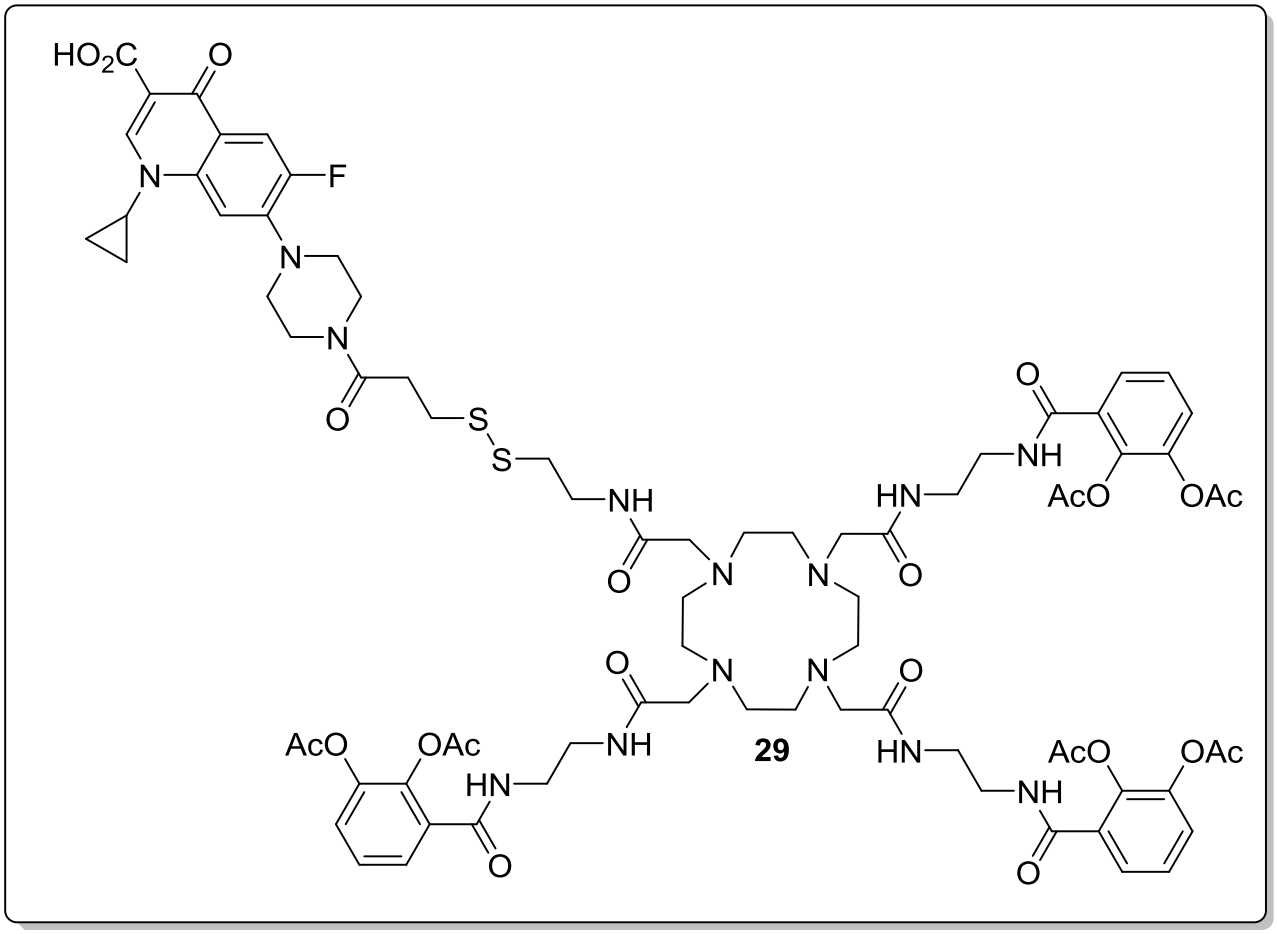

29

67 (8.0 mg, 6.4 µmol) was dissolved in DCM (1.0 mL) followed by addition of acetic acid (1.0 mL) to adjust the pH to 2.0 and was added to **27** (4.7 mg, 8.9 µmol). The reaction was stirred for 39 h. The solution was concentrated, dissolved in ACN/H_2O (600 µL), filtered and purified by 2 successive RP column chromatography (C18, 10 mm, 40-min-long gradient from 20 to 35 % of ACN in H_2O + 1 % AcOH) to yield **29** as a white solid (1.5 mg, 14 %). **^{1}H NMR** (700 MHz, CD_3CN). δ 8.71 (s, 1H, NC*H*), 7.96 (d, J = 13.2 Hz, 1H, CFC*H*), 7.66-7.59 (bs, 2H, N*H*), 7.59-7.45 (m, 5H, N*H*+Ar-*H*), 7.44-7.37 (bs, 2H, N*H*), 7.37-3.22 (m, 6H, Ar-*H*), 3.80-3.60 (m, 6H), 3.52-3.22 (m, 16H), 3.06-2.90 (m, 8H), 2.82 (t, J = 6.7 Hz, 2H), 2.78 (t, J = 6.9 Hz, 2H), 2.72-2.49 (bs, 12H), 2.30-2.10 (m, 31H), 1.37-1.30 (m, 2H, C*H*$_2$CH), 1.16-1.10 ppm (m, 2H, C*H*$_2$CH). **^{13}C NMR** (176 MHz, CD_3CN)

δ 178.2, 173.0, 172.6, 170.4, 169.6, 169.5, 169.3, 167.5, 166.1, 155.3, 153.8, 149.2, 146.4, 146.3, 144.2, 141.4, 140.5, 131.7, 127.4, 127.1, 126.7, 120.7, 120.6, 112.4, 112.3, 108.4, 107.5, 59.5, 54.3, 50.8, 50.4, 45.8, 42.0, 41.0, 39.5, 39.0, 38.5, 36.7, 35.3, 33.5, 20.8, 20.8, 8.6 ppm. **ESI-HRMS**: $C_{77}H_{97}FN_{14}O_{23}S_2^{2+}$ m/z = 834.3129 (calculated: 834.3133) $[M+2H]^{2+}$, error = 0.5 ppm.

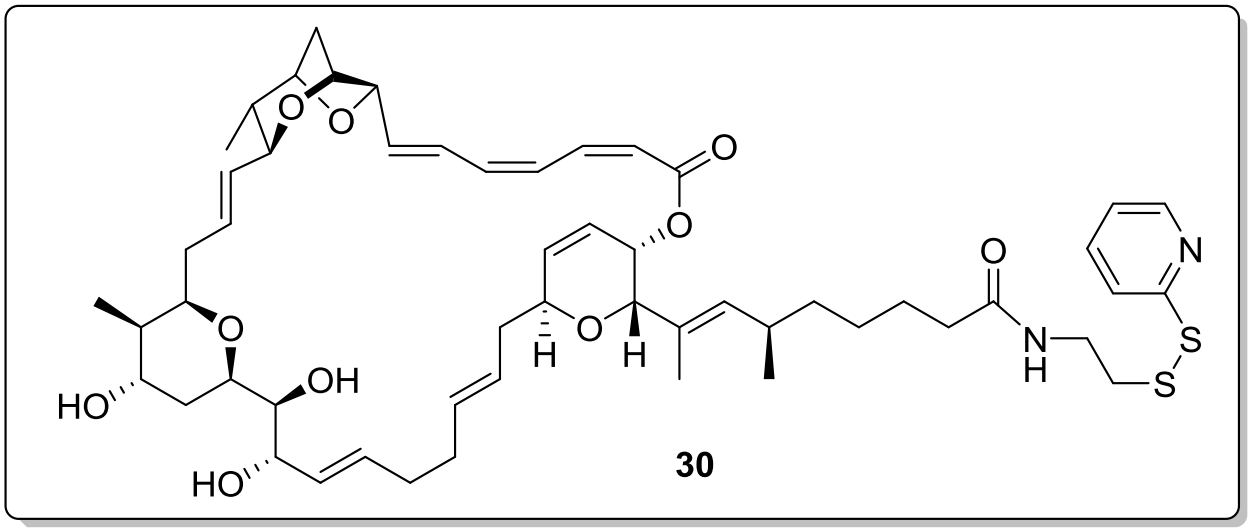

30

HATU (26 mg, 68 µmol) was added to a stirring solution of sorangicin A (50 mg, 62 µmol) in DMF (2 mL) at 23 °C under argon conditions and DIPEA (25 µL, 142 µmol) was added. The reaction mixture was stirred for 15 min and (S)-(2)-pyridylthiocysteamine, HCl (25 mg, 112 µmol) was added to the pale yellow solution which was stirred for 30 min at 23 °C. The compound was concentrated and suspended in ACN, filtered and purified by RP column chromatography (column: Gemini C18 250x21.20mm, 40-min-long gradient from 50 to 80 % ACN in H_2O + 0.1 % CH_3COOH) to yield a white solid (45 mg, 75 %). **^{1}H NMR** (700 MHz, CD_3CN). δ 8.47 (m, 1H), 7.77-7.70 (m, 2H), 7.19 (ddd, J = 6.6, 4.8, 1.9 Hz, 3H), 7.14-7.06 (m, 2H), 6.99-6.93 (m, 1H), 6.88 (m, 1H), 6.44-6.39 (m, 1H), 6.23 (dd, J = 15.3, 4.2 Hz, 1H), 6.10 (dd, J = 10.0, 3.1 Hz, 1H), 5.99 (ddd, 10.0, 5.9, 2.2 Hz, 1H), 5.66 (dt, J = 14.6, 6.1 Hz, 1H), 5.59 (d, J = 10.4 Hz, 1H), 5.53-5.48 (m, 2H), 5.45 (s, 1H), 5.37-5.34 (m, 1H), 5.31 (dd, J = 5.9, 1.8 Hz, 1H), 5.24 (d, J = 9.8 Hz, 1H), 4.49 (m, 1H), 4.34 (m, 2H), 4.21 (d, J = 6.4 Hz, 1H), 4.17 (s, 1H), 4.09-4.04 (m, 1H), 3.79 (m, 2H), 3.72 (dd, J = 9.5, 7.5 Hz, 1H), 3.61-3.55 (m, 1H), 3.41 (m, 2H), 3.36 (dd, *J* = 7.7, 4.4 Hz, 1H), 3.23 (bs, 1H), 2.90 (t, *J* = 6.5 Hz, 1H), 2.37-2.30 (m, 1H), 2.23-2.18 (m, 1H), 2.12-2.00 (m, 5H), 1.98-1.96 (m, 1H), 1.83 (dd, *J* = 11.5, 1.4 Hz, 1H), 1.64 (d, *J* = 13.8 Hz, 1H), 1.57 (s, 2H), 1.55-1.45 (m, 2H), 1.39-1.29 (m, 2H), 1.29-1.21 (m, 1H), 1.21-1.15 (m, 1H), 1.15-1.08 (m, 1H), 0.81 (dd, *J* = 6.9, 4.9 Hz, 4H), 0.74 ppm (d, *J* = 6.7 Hz, 2H). **^{13}C NMR** (176 MHz, CD_3CN) δ 174.4, 166.6, 160.5, 150.6, 138.5, 138.3, 137.4, 136.7, 135.9, 133.6, 133.4, 133.4, 133.1, 131.5, 130.7, 129.9, 128.1, 126.8, 126.2, 123.7, 122.1, 120.7, 119.6, 81.3, 80.3, 80.2, 77.1, 76.7, 74.7, 74.3, 73.9, 73.5, 70.3, 65.7, 41.5, 39.6,

39.0, 38.7, 38.2, 38.0, 37.0, 36.6, 34.8, 33.8, 33.3, 32.5, 31.2, 27.9, 26.4, 21.6, 15.3, 14.5, 10.7 ppm. **ESI-HRMS**: $C_{54}H_{75}N_2O_{10}S_2^+$ m/z = 975.4852 (calculated: 975.4858) $[M+H]^+$, error = 0.6 ppm.

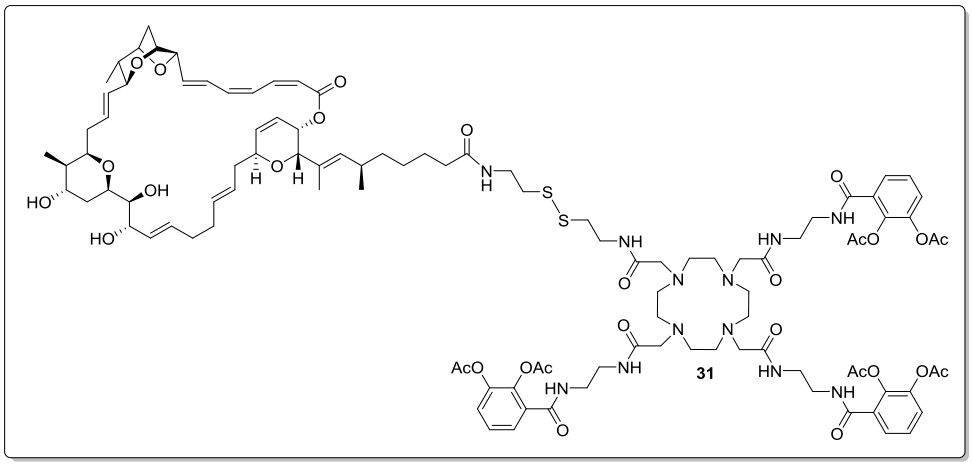

67 (9.9 mg, 7.9 µmol) was dissolved in DCM (500 µL) followed by addition of acetic acid (500 µL) to adjust the pH to 2.0 and was added to **30** (10 mg, 10.4 µmol). The reaction was stirred at 24°C 3.5 days. The solution was lyophilized (29 mg), dissolved in ACN/H_2O (900 µL), filtered and purified by RP column chromatography (C18, 22mm, 40-min-long gradient from 10 to 50 % of ACN in H_2O+1 % AcOH) to yield a white solid (4.2 mg, 25 %). **^{1}H NMR** (700 MHz, CD_3CN). δ 7.62 (bt, 2H), 7.57 (bt, 1H), 7.50 (m, 3H, Ar-*H*), 7.40 (m, 2H), 7.36-7.28 (m, 6H, Ar-*H*), 7.13-7.06 (m, 2H), 6.96-6.92 (m, 2H), 6.41 (m, 1H), 6.23 (dd, J = 15.3, 4.1 Hz, 1H), 6.10 (dd, J = 10.0, 3.0 Hz, 1H), 6.00 (ddd, 9.9, 5.9, 2.2 Hz, 1H), 5.67 (m, 2H), 5.58 (d, J = 10.2 Hz, 1H), 5.50 (m, 4H), 5.38-5.33 (m, 2H), 5.33-5.30 (dd, J = 5.8, 1.7 Hz, 1H), 5.24 (d, J = 9.8 Hz, 1H), 4.49 (m, 1H), 4.34 (m, 2H), 4.21 (d, J = 6.5 Hz, 1H), 4.16 (s, 1H), 3.81-3.76 (m, 2H), 3.72 (dd, J = 9.4, 7.5 Hz, 1H), 3.60-3.56 (m, 1H), 3.48-3.30 (m, 18H), 2.81-2.74 (m, 8H). 2.36-2.29 (m, 4H), 2.26 (s, 9H, C*H*$_3$CO$_2$Ar), 2.24 (2×s, 9H, C*H*$_3$CO$_2$Ar), 2.22-2.05 (m, 22H), 1.86-1.80 (m, 2H), 1.57 (bd, J = 0.7 Hz, 3H), 1.55 (m, 1H), 1.53-1.44 (m, 4H), 1.40-1.30 (m, 3H), 1.29-1.21 (m, 2H), 1.17 (m, 2H), 1.11 (m, 2H), 1.19 (m, 1H), 0.81 (dd, J = 8.9, 6.9 Hz, 6H), 0.74 ppm (d, J = 6.7 Hz, 3H). **^{13}C NMR** (176 MHz, CD_3CN). δ 207.5, 174.7, 172.5, 169.6, 169.3, 166.6, 166.4, 144.2, 141.4, 138.3, 137.4, 136.7, 135.9, 133.6, 133.4, 133.3, 133.1, 131.6, 131.5, 130.6, 129.9, 128.1, 127.5, 127.2, 126.8, 126.8, 126.2, 123.7, 119.7, 81.3, 80.3, 80.2, 79.1, 78.9, 78.7, 77.3, 76.7, 74.8, 74.7, 74.3, 73.9, 73.4, 70.3, 65.6, 41.5, 39.6, 39.2, 38.7, 38.5, 38.3, 37.9, 36.9, 36.6, 34.8, 33.9, 33.3, 32.5, 31.4, 30.9, 28.0, 26.5, 21.7, 20.9, 20.8 (*C*H$_3$CO$_2$Ar), 20.7, 15.3, 14.6, 10.8 ppm. **ESI-HRMS:** $C_{106}H_{146}N_{12}O_{29}S_2^{2+}$ m/z = 1057.4870 (calculated: 1057.4875) $[M+2H]^{2+}$, error = 0.5 ppm

6.2. Biological assays

6.2.1. Fe(CAS) assay

The chrome azurol S (CAS) assay was performed for assessing iron complexation.[112] The solutions were prepared in a 96 well plate (Corning CELLBIND Surface, black, transparent flat bottom) and the absorbance of each solution was measured by spectrophotometry with a Tecan Infinite 200 pro reader (Tecan, Switzerland).

All used glassware was previously cleaned with 12 M HCl and milliQ water. The stock solutions of hexadecyltrimethylammonium bromide (HDTMA, 10 mM in water), $FeCl_3$ (1 mM in a 10 mM HCl solution) and CAS (2 mM in water) were respectively obtained by adding 3.64 mg in 1 mL H_2O, 16.22 mg in 100 mL HCl (10 mM) and 12.11 mg in 10 mL water.

A solution of HDTMA (10 mM, 600 µL) was placed in a 10 mL volumetric flask and diluted with water. A mixture of a $FeCl_3$ solution (1 mM in 10 mM HCl, 150 µL) and an aqueous CAS solution (2 mM, 750 µL) was slowly added under stirring. Anhydrous piperazine (431 mg) was dissolved in water (about 5 mL) and HCl (12 M, 625 µL) was carefully added. The buffer solution (pH = 5.56) was rinsed into the volumetric flask which was filled with water to afford a 10 mL of CAS assay solution. 5-sulfosalicylic acid (10.2 mg) was dissolved in the solution to form the Fe(CAS) solution.

15 µM stock solutions of enterobactin and **1-4** were prepared and added at different concentrations into a 96 well plate in triplicate (Table 12).

Table 12 CAS assay concentrations.

Volume of **1-4** or enterobactin (µL)	0	10	20	30	40	60	120
Volume of Fe(CAS) (µL)	40	40	40	40	40	40	40
Total volume (µL)	200	200	200	200	200	200	200
Concentration of **1-4** or enterobactin (µM)	0	0.75	1.5	2.25	3.0	4.5	9.0
Concentration of Fe(CAS) (µM)	3.0	3.0	3.0	3.0	3.0	3.0	3.0
Equivalent of **1-4** or enterobactin (eq)	0	0.25	0.5	0.75	1.0	1.5	3.0

The mixed solutions were analyzed after 17 h to assure that the equilibrium was reached. The absorbance of each solution was measured. The full spectra of 3 representative experiments were first analyzed between 300 and 800 nm.

6.2.2. The MS-MS assay

The measurements of exact mass in tandem with MS-spectra were performed with a UPLC-ESI-Q-TOF-MS instrument that consisted of an UltiMate 3000 (Thermo Fisher Scientific, Waltham, USA) UPLC coupled to a maxisIITM HD mass spectrometer (Bruker Daltonic, Billerica, USA). The MRM method was established with an AB SciexQTrap 6500 (AB Sciex Germany GmbH, Darmstadt, Germany) coupled to Agilent 1290 UHPLC (Agilent Technologies, Santa Clara, CA, USA). A tabletop incubator was used. The OD_{600} was measured using Sigma Plot, 4-parameter logistics function. The data were analyzed with the MultiQuant software (AB Sciex Germany GmbH, Darmstadt, Germany).

A culture of *E. coli*ΔentB grown in LB was washed twice with LMR medium and adjusted to OD_{600} = 1. Compounds were added to the culture or to blank LMR medium for 0, 4 or 24 h at RT. The bacteria were removed by centrifugation and ice cold acetonitrile (4 vol) was added to the bacterial supernatant or the blank LMR. After 15 min vortexing and centrifugation (13000 RPM, 10min, 4°C), the respective supernatant was used for measuring the ion transitions in the MRM-mode. Data were analyzed using the MultiQuant software.

6.2.3. Growth recovery assay

All *E. coli* strains were obtained from Coli Genetic Stock Center (Yale, USA) and have the following characteristics:

- Strain BW25113 (CSGC# 7636) ➔parental strain, (wt)
- Strain JW0588-1 (CGSC# 11768) ➔entA mutant, Kanamycin resistant

The *P. aeruginosa* strains have the following characteristics:

- *P. aeruginosa* strain PAO1 (wildtype), obtained from Susanne Häußler (HZI, Braunschweig)
- *P. aeruginosa* strain PAS283 (ΔpvdF ΔpchA), obtained from Isabell Schalk (IREBS, Strasbourg)

The LB-medium was acquired from Luria/Miller, Roth. Enterobactin and Ferrichrome (Sigma, F8014-1MG) were purchased from Sigma Aldrich. The compounds of interest were prepared as a 10 mM DMSO stock solution. Kanamycin was used from a 50 mg/mL stock solution in H_2O. Sterile 96 well plates with lid were used for the growth recovery assay. The LMR medium composition and preparation is described in Table 13.

Table 13 Composition and preparation of LMR medium for bacterial culture in iron-limited conditions.

Compound	Concentration	Remarks

KH_2PO_4	176 mM	Prepare as 10x stock
NaOH	100 mM	
$(NH_4)_2SO_4$	12,6 mM	
$MgSO_4$	2 mM	Prepare as 500x stock
Glycerol	0.2 % (w/w)	
$FeCl_3$, 6 H_2O	100 µM	Prepare as 500x trace metal solution (TMS).
$CaCl_2$	40 µM	
$MnCl_2$, 4 H_2O	20 µM	
$ZnSO_4$, 7 H_2O	20 µM	
$CoCl_2$, 6 H_2O	4 µM	
$CuCl_2$	4 µM	
$NiCl_2$, 6 H_2O	4 µM	
Na_2MoO_4, 2 H_2O	4 µM	
Na_2SeO_3	4 µM	
H_3BO_4	4 µM	

Bacterial strains used for the assay were *E. coli* BW25113 (wildtype), *E. coli* JW0588-1 (ΔentA), *P. aeruginosa* PAO1 (wildtype) and *P. aeruginosa* PAS283 (ΔpvdFΔpchA). The latter was obtained from Isabell Schalk (IREBS, Strasbourg). *E. coli*ΔentA mutant was always cultured in presence of 50 µg/mL kanamycin.

For *E. coli* strains, overnight cultures were grown to full confluency in 20 mL of LB medium in baffled flask. Starter cultures were prepared by diluting the overnight culture to OD_{600nm} = 0.2 in 25 mL LB, baffled flask and growing them until OD_{600nm} = 0.5 for approximately 1 h. For pellet starter cultures: 5 mL, 4500 ×g, 5 min, resuspend in 5 mL LMR was performed and the process was repeated. The OD_{600nm} was measured and the assay culture was prepared from the dilution of LMR-suspended starter culture to OD_{600nm}=0.01 in 10 mL LMR.

To prepare the test compounds and assay plates, 1 mM stocks of test compounds in DMSO in 0.2 mL tubes were prepared. For a single sample, 1.5 µL of test compound was required. Each compound was tested on 3 strains: wildtype, ΔentA, ΔentB, and LMR medium was used for blank control. Test compounds were transferred to an empty 96 well plate with a multichannel pipette. Each sample was measured as double replicate (except for blank control). 148.5 µL of bacterial assay culture or LMR medium was transferred to respective wells with multichannel pipette, mixed by pipetting up/down. Empty wells were filled with LMR medium. The plate was sealed with parafilm and incubated for 48 h at 37°C. The OD_{600nm} was measured and blank correction was performed by subtracting blank control values from respective sample reads.

For *P. aeruginosa* studies, the overnight cultures were prepared from 20 mL of MHB, baffled flask. The starter cultures were obtained from the dilution of the overnight culture to OD_{600nm}=0.2 in 25 mL MHB, baffled flask and the growth until OD_{600nm} = 0.5 for approximately 1 h. The assay

culture was obtained by dilution from the starter culture to OD_{600nm}=0.01 in 10 mL of MHB/H_2O (50/50) supplemented with 600 µM bipyridyl.

Procedure to prepare the test compounds and the assay plates is the same as for *E. coli*, except for the following modifications. The MHB/H_2O (50/50) medium containing 600 µM bipyridyl was used instead of LMR medium. The sealed plate was incubated only for 24 h at 37°C before OD_{600nm} was determined. The standard deviations were below 7 % for ($OD_{probemutant}$-$OD_{DMSOmutant}$)/(OD_{DMSOwt}-$OD_{DMSOmutant}$)

6.2.4. Flow cytometry

The flow cytometry experiments were performed using a LSRFortessa™ with FACSDiva™ software (BD Biosciences, Heidelberg, Germany) and evaluated using the FlowJo software (FLOWJThe flow cytomO LLC, Oregon, US).

Flow cytometric analysis and confocal microscopy of ESKAPE pathogens was performed after 4 h incubation with **21** or BODIPY-FL. Cells were washed twice with PBS and the OD_{600} was adjusted to 0.025 with sterile-filtered PBS. 100000 cells per sample were analyzed using a LSRFortessa™ with FACSDiva™ software. Detection of BODIPY was performed with the 488 nm laser in combination with 525/50 nm band pass filter. Data was evaluated using FlowJo software.

6.2.5. Confocal microscopy

The confocal microscope was an ECLIPSE Ti (Nikon) equipped with UltraVIEWVoX spinning disc (Perkin Elmer, Waltham, US), ORCA-R2 camera (Hamamatsu Photonics, Japan) and Volocity software 6.1.1 (Perkin Elmer, Waltham, US).

For confocal microscopy cells treated as described above were placed into chamber slides (Ibidi GmbH, Martinsried, Germany) and covered with a pad consisting of 1 % agarose. Imaging was performed using the confocal microscope ECLIPSE Ti.

6.2.6. The FAP assay

The sequence of FAP6.2[122] was synthesized by GenScript (NJ, USA) and cloned into a pET23-expression vector (Novagen/Merck, Darmstadt, Germany). Chemically competent *E. coli* Origami™ B (DE3) pLysS (Novagen/Merck, Darmstadt, Germany) were transformed with pET23_FAP6.2_His and selected for ampicillin resistance yielding *E. coli*_FAP6.2. The expression of FAP6.2 under different concentrations of IPTG was monitored by Western Blot using His-tag

specific antibody (Relia Tech, Wolfenbüttel, Germany). Purification of HIS-tagged FAP6.2 was performed using Ni-NTA-agarose (Qiagen, Hilden, Germany). 500 mL LB-Medium containing selection antibiotics tetracycline, kanamycin and ampicillin were inoculated from a 5 mL overnight culture of *E. coli*_FAP6.2. At OD600 of 0.8 the expression of FAP6.2 was induced by the addition of 1 mM IPTG and the culture was kept under continuous agitation overnight. For protein purification the cells were centrifuged (5000x g, 10 min, 4 °C) and resuspended in 20 mM Tris, 500 mM NaCl pH 7.9. After driving of the bacteria through a french press (1500 psi, Thermo Scientific, Waltham, US) and centrifugation (20000x g, 30 min, 4 °C) imidazole was added to the supernatant to a final concentration of 30 mM. The supernatant was then incubated with 1 mL prewashed Ni-NTA-agarose (washed with 1 mL H_2O followed by 5x1 mL 20 mM Tris, 500 mM NaCl, pH 7.9) for 2 h at 4 °C. Using a poly-prep chromatopgraphy column (BioRad, Hercules, US) the Ni-NTA-agarose was washed with 20 mL of 20 mM Tris, 500 mM NaCl, 30 mM imidazole, pH 7.9. FAP6.2-His was eluted with 2 mL 50 mM Tris, 150 mM NaCl, 5 mM $CaCl_2$, 300 mM imidazole, pH 7.5 and dialyzed for 2 h against 50 mM Tris, 150 mM NaCl, 5 mM $CaCl_2$, pH 7.5. Glycerol was added to a final concentration of 10 % for storage of FAP6.2 at -20 °C. Protein concentration was determined using a NanoDrop™ 2000 (Thermo Scientific, Waltham, US).

6.2.6.1. Fluorospectrometry

An overnight culture of *E. coli_FAP6.2* was diluted 1:100 in MH2 medium and grown until an OD_{600} of 0.8 was reached. IPTG was added at 1µM final concentration and after 4 h the OD_{600} was adjusted to 2. For assessing uptake of MG-conjugates black 96 well plates with clear bottom with 100 µL of bacterial culture each well were used. Compounds were added at 10 µM final concentration. Fluorescence was monitored over 16 h post compound additions using a Tecan Infinite 200 pro reader (Tecan, Switzerland) in bottom read mode. Each test was measured in triplicate. Szent-Gyorgyi et al. already described that chemical derivatization of MG led to compounds with different binding affinities, fluorescence intensities and excitation/emission spectra[151]. Likewise conjugation of different DOTA-cores to MG yielded conjugates possessing different fluorescence intensities upon binding to FAP6.2. To enable comparison with regard to bacterial uptake, recombinantly expressed FAP6.2 (S3,B) was incubated with the different MG-conjugates in a molar ratio of 4:1 and the fluorescence emission at 665nm with excitation at 610 nm were recorded (S3, C). The fluorescence values obtained for FAP + MG-conjugates were corrected by the values obtained from a non-FAP-protein + MG-conjugates (S3, D). The different values for MG-conjugates were used for calculating the ratio between free MG and the respective

MG-conjugate. All fluorescence values measured during live kinetics were corrected by this factor afterwards.

6.2.6.2. Flow cytometry and confocal microscopy for MG-conjugates

Flow cytometric analysis and confocal microscopy of *E. coli_FAP6.2* was performed upon 16 h incubation with MG-conjugates. For flow cytometry cells were washed oncewith PBS and the OD_{600} was adjusted to 0.025 with sterile-filtered PBS. At least 10000 cells per sample were analyzed using aLSRFortessa™ with FACSDiva™ software (BD Biosciences, Heidelberg, Germany). For detection of MG-derived fluorescence the 640 nm laser was used in combination with 670/14 nm band pass filter. Data was evaluated using FlowJo software (FLOWJO LLC, Oregon, US). For confocal microscopy cells were placed into chamber slides (Ibidi GmbH, Martinsried, Germany) and covered with a pad consisting of 1 % agarose. Imaging was performed using the confocal microscope ECLIPSE Ti (Nikon) equipped with UltraVIEWVoX spinning disc (Perkin Elmer, Waltham, US), ORCA-R2 camera (Hamamatsu Photonics, Japan) and Volocity software 6.1.1 (Perkin Elmer, Waltham, US). Propidium iodide was added at final concentration of 50 µg/mL for 20 min and cells were washed once with PBS before confocal analysis.

6.2.7. Inhibitory concentration assay

All *E. coli* strains were obtained from Coli Genetic Stock Center (Yale, USA) and have the following characteristics:

- Strain BW25113 (CSGC# 7636) ➔ parental strain, wt
- Strain JW5086-3 (CGSC#: 11165) ➔ fepA mutant, Kanamycin resistant
- Strain JW0587-1 (CGSC#: 8704) ➔ entB mutant, Kanamycin resistant
- Strain JW0588-1 (CGSC# 11768) ➔ entA mutant, Kanamycin resistant

The LB-medium was acquired from Luria/Miller, Roth. Ciprofloxacin and kanamycin were purchased from Sigma Aldrich. Sterile 96 well plates with lid were used for the minimum inhibitory concentration assay. A stock solution of bipyridyl (BP) in H_2O (1 mg/mL) was used. The OD_{600} measurement was obtained using the microplate spectrophotometer power wave XS2 (Bio Tek, Winooski, US), and IC_{50} values were calculated using Sigma Plot (Systat Software GmbH, Erkrath, Germany) and four parameter logistics curve regression.

To evaluate the potential of DOTAM as carrier, antimicrobial activity assays were performed. Bacterial strains used were *E. coli* BW25113 (as wildtype), JW0587-1 (*ΔentB*), JW0588-1 (*ΔentA*), JW5086-3 (*ΔfepA*). Bacteria were cultured at 37°C in a shaker at 150 RPM. Overnight cultures contained 5 mL of LB medium and 30 µg/mL Kanamycin for *ΔentA/ΔentB/ΔfepA*-mutants. Overnight cultures were diluted 1:100 with 5 mL LB-medium and grown to an OD_{600} of 0.5-0.8. Cultures were then diluted with MH medium to a final OD_{600} of 0.01 and transferred to 96 well half area plates. Test compounds dissolved in DMSO were added to a maximum final concentration of 1 % of DMSO and serially diluted. The plate was wrapped with parafilm and incubated in a shaker at 150 RPM and 37 °C for 24 h. Bacterial growth was determined by measuring OD_{600}. Mean values of IC_{50} obtained from at least an experimental triplicate are reported.

6.2.8. Toxicity assay

The mouse fibroblast L929, human cervix carcinoma KB-3-1 and human breast cancer MCF-7 cell lines used for the toxicity assays correspond to the references DSM ACC 2, DSM ACC and DSM ACC 115 respectively. FS4-LTM is human fibroblast from InScreenex.[152] A stock solution of 10 mM for each compound in DMSO was used. 158 WST-1 was a ready-to-use solution by Roche. The reading was performed with the infinite 200 PRO plate reader, Tecan, Männedrof, Switzerland.

The effect of compounds on cell viability was probed with a WST-1 test using the procedure of Ishiyama *et al*.[153] as modified by Sasse *et al.*[154]. The following immortalized cell lines were used: mouse fibroblast cell line L929, human cervix carcinoma cell line KB-3-1 and human breast cancer cell line MCF-7. Briefly, the subconfluent cells were washed with Earle's Balanced Salt Solution, Gibco, without Ca and Mg, trypsinized and re-suspended in Dulbecco's modified eagle's medium that contained 5 % fetal bovine serum (FBS) or Roswell Park Memorial Institute medium that contained 5 % FBS, 0.5 % Minimum Essential Medium Non-Essential Amino Acids, Gibco (MEM NEAA), 0.5 % GlutaMAX (Gibco) and insulin at 5 µg/mL (MCF-7). 25µl µL of serial dilutions of the test compounds (100 up to 0.2 µM) were added to 25µl µL aliquots of a cell suspension (1500 cells for KB3-1 and L929, 3000 cells for MCF-7) in 384 well microtiter plates. Blank and solvent controls were incubated under identical conditions. The compounds were incubated for 5 days with cell lines L929, KB-3-1, and MCF-7. After the incubation period 3 µL WST-1 was added. The incubation time of the plates at 37 °C varied between the cell lines from 20 min for KB-3-1 to 2 h for MCF-7 before measuring at 450 nm (reference 600 nm) at the Infinite 200 PRO plate reader. The percentage of viable cells was calculated as the mean with respect to the controls set

to 100 %. The EC_{50} values were determined with Sigma Plot. Mean values of IC_{50} obtained from two biological replicates are reported.

[1] J. Ho, P. A. Tambyah, D. L. Paterson, *Multiresistant Gram-negative infections: a global perspective, Current Opinion in Infectious Diseases* **2010**, *23*, 546-553.

[2] X. Ning, S. Lee, Z. Wang, D. Kim, B. Stubblefield, E. Gilbert, N. Murthy, *Maltodextrin-based imaging probes detect bacteria in vivo with high sensitivity and specificity, Nature Materials* **2011**, *10*, 602-607.

[3] K. Ferreira, H. Y. Hu, V. Fetz, H. Prochnow, B. Rais, P. P. Muller, M. Bronstrup, *Multivalent Siderophore-DOTAM Conjugates as Theranostics for Imaging and Treatment of Bacterial Infections, Angewandte Chemie, International Edition in English* **2017**, *56*, 8272-8276.

[4] K. Lewis, *Platforms for antibiotic discovery, Nature Reviews Drug Discovery* **2013**, *12*, 371-387.

[5] A. Schatz, E. Bugle, S. A. Waksman, *Streptomycin, a Substance Exhibiting Antibiotic Activity Against Gram-Positive and Gram-Negative Bacteria.∗†, Proceedings of the Society for Experimental Biology and Medicine* **1944**, *55*, 66-69.

[6] D. H. Williams, *The glycopeptide story - how to kill the deadly 'superbugs', Natural Product Reports* **1996**, *13*, 469-477.

[7] K. M. G. O'Connell, J. T. Hodgkinson, H. F. Sore, M. Welch, G. P. C. Salmond, D. R. Spring, *Combating Multidrug-Resistant Bacteria: Current Strategies for the Discovery of Novel Antibacterials, Angewandte Chemie International Edition* **2013**, *52*, 10706-10733.

[8] V. M. D'Costa, C. E. King, L. Kalan, M. Morar, W. W. L. Sung, C. Schwarz, D. Froese, G. Zazula, F. Calmels, R. Debruyne, G. B. Golding, H. N. Poinar, G. D. Wright, *Antibiotic resistance is ancient, Nature* **2011**, *477*, 457.

[9] O'Neill J (chair) - *Antimicrobial Resistance:Tackling a crisis for the health and wealth of nations*, http://amr-review.org/

[10] European Centre for Disease Prevention and Control - *The bacterial challenge: time to react*, http://www.ema.europa.eu/docs/en_GB/document_library/Report/2009/11/WC500008770.pdf

[11] U.S. Department of Health and Human Services, Centers for Disease Control and Prevention - *Antibiotic resistance threats in the United States, 2013*, https://www.cdc.gov/drugresistance/threat-report-2013/pdf/ar-threats-2013-508.pdf

[12] H. W. Boucher, G. H. Talbot, J. S. Bradley, J. E. Edwards, D. Gilbert, L. B. Rice, M. Scheld, B. Spellberg, J. Bartlett, *Bad Bugs, No Drugs: No ESKAPE! An Update from the Infectious Diseases Society of America, Clinical Infectious Diseases* **2009**, *48*, 1-12.

[13] aL. B. Rice, *Federal Funding for the Study of Antimicrobial Resistance in Nosocomial Pathogens: No ESKAPE, The Journal of Infectious Diseases* **2008**, *197*, 1079-1081; bC. A. Arias , B. E. Murray *Antibiotic-Resistant Bugs in the 21st Century — A Clinical Super-Challenge, New England Journal of Medicine* **2009**, *360*, 439-443.

[14] G. Tillotson, *A crucial list of pathogens, The Lancet Infectious Diseases* **2017**.

[15] aM. Giannouli, S. Cuccurullo, V. Crivaro, A. Di Popolo, M. Bernardo, F. Tomasone, G. Amato, S. Brisse, M. Triassi, R. Utili, R. Zarrilli, *Molecular Epidemiology of Multidrug-Resistant Acinetobacter baumannii in a Tertiary Care Hospital in Naples, Italy, Shows the Emergence of a Novel Epidemic Clone, Journal of Clinical*

Microbiology **2010**, *48*, 1223-1230; bJ. Li, C. R. Rayner, R. L. Nation, R. J. Owen, D. Spelman, K. E. Tan, L. Liolios, *Heteroresistance to Colistin in Multidrug-Resistant Acinetobacter baumannii, Antimicrobial Agents and Chemotherapy* **2006**, *50*, 2946-2950.

[16] National Institutes of Health - *Announcement of Requirements and Registration for "Antimicrobial Resistance Rapid, Point-of-Need Diagnostic Test" Challenge*, **2017**, https://www.federalregister.gov/documents/2016/09/08/2016-21328/announcement-of-requirements-and-registration-for-antimicrobial-resistance-rapid-point-of-need

[17] aW. Wohlleben, Y. Mast, E. Stegmann, N. Ziemert, *Antibiotic drug discovery, Microbial Biotechnology* **2016**, *9*, 541-548; bA. Davin-Regli, J. M. Bolla, C. E. James, J. P. Lavigne, J. Chevalier, E. Garnotel, A. Molitor, J. M. Pages, *Membrane permeability and regulation of drug "influx and efflux" in enterobacterial pathogens, Current Drug Targets* **2008**, *9*, 750-759.

[18] P. Panizzi, M. Nahrendorf, J. L. Figueiredo, J. Panizzi, B. Marinelli, Y. Iwamoto, E. Keliher, A. A. Maddur, P. Waterman, H. K. Kroh, F. Leuschner, E. Aikawa, F. K. Swirski, M. J. Pittet, T. M. Hackeng, P. Fuentes-Prior, O. Schneewind, P. E. Bock, R. Weissleder, *In vivo detection of Staphylococcus aureus endocarditis by targeting pathogen-specific prothrombin activation, Nature Medicine* **2011**, *17*, 1142-1146.

[19] X. Ning, W. Seo, S. Lee, K. Takemiya, M. Rafi, X. Feng, D. Weiss, X. Wang, L. Williams, V. M. Camp, M. Eugene, W. R. Taylor, M. Goodman, N. Murthy, *PET Imaging of Bacterial Infections with Fluorine-18-Labeled Maltohexaose, Angewandte Chemie International Edition* **2014**, *53*, 14096-14101.

[20] E. A. Weinstein, A. A. Ordonez, V. P. DeMarco, A. M. Murawski, S. Pokkali, E. M. MacDonald, M. Klunk, R. C. Mease, M. G. Pomper, S. K. Jain, *Imaging Enterobacteriaceae infection in vivo with ¹⁸F-fluorodeoxysorbitol positron emission tomography, Science Translational Medicine* **2014**, *6*, 259ra146-259ra146.

[21] G. J. Stasiuk, N. J. Long, *The ubiquitous DOTA and its derivatives: the impact of 1,4,7,10-tetraazacyclododecane-1,4,7,10-tetraacetic acid on biomedical imaging, Chemical Communications* **2013**, *49*, 2732-2746.

[22] aH. Y. Hu, N. H. Lim, D. Ding-Pfennigdorff, J. Saas, K. U. Wendt, O. Ritzeler, H. Nagase, O. Plettenburg, C. Schultz, M. Nazare, *DOTAM derivatives as active cartilage-targeting drug carriers for the treatment of osteoarthritis, Bioconjugate Chemistry* **2015**, *26*, 383-388; bF. Wojciechowski, M. Suchy, A. X. Li, H. A. Azab, R. Bartha, R. H. E. Hudson, *A Robust and Convergent Synthesis of Dipeptide−DOTAM Conjugates as Chelators for Lanthanide Ions: New PARACEST MRI Agents, Bioconjugate Chemistry* **2007**, *18*, 1625-1636; cL. M. De León-Rodríguez, Z. Kovacs, *The Synthesis and Chelation Chemistry of DOTA−Peptide Conjugates, Bioconjugate Chemistry* **2008**, *19*, 391-402.

[23] J. M. M. Michael T. Madigan, David A. Stahl, David P. Clark, *Brock Biology of Microorganisms*, 13th ed., **2012**.

[24] L. Brown, J. M. Wolf, R. Prados-Rosales, A. Casadevall, *Through the wall: extracellular vesicles in Gram-positive bacteria, mycobacteria and fungi, Nature Reviews Microbiology* **2015**, *13*, 620-630.

[25] C. Leoff, E. Saile, D. Sue, P. Wilkins, C. P. Quinn, R. W. Carlson, E. L. Kannenberg, *Cell Wall Carbohydrate Compositions of Strains from the Bacillus*

cereus Group of Species Correlate with Phylogenetic Relatedness, Journal of Bacteriology **2008**, *190*, 112-121.

[26] B. Halliwell, J. M. Gutteridge, *Oxygen toxicity, oxygen radicals, transition metals and disease, Biochemical Journal* **1984**, *219*, 1-14.

[27] D. R. Peralta, C. Adler, N. S. Corbalán, E. C. Paz García, M. F. Pomares, P. A. Vincent, *Enterobactin as Part of the Oxidative Stress Response Repertoire, PLOS ONE* **2016**, *11*, e0157799.

[28] J. D. Faraldo-Gomez, M. S. P. Sansom, *Acquisition of siderophores in Gram-negative bacteria, Nature Reviews Molecular Cell Biology* **2003**, *4*, 105-116.

[29] U. E. Schaible, S. H. E. Kaufmann, *Iron and microbial infection, Nature Reviews Microbiology* **2004**, *2*, 946.

[30] N. C. Andrews, *Disorders of iron metabolism, New England Journal of Medicine* **1999**, *341*, 1986-1995.

[31] J. J. Bullen, Griffiths, E, *Iron and infection : molecular, physiological and clinical aspects*, 2nd ed., **1999**.

[32] A. R. Bogdan, M. Miyazawa, K. Hashimoto, Y. Tsuji, *Regulators of Iron Homeostasis: New Players in Metabolism, Cell Death, and Disease, Trends in Biochemical Sciences*, *41*, 274-286.

[33] M. Miethke, M. A. Marahiel, *Siderophore-Based Iron Acquisition and Pathogen Control, Microbiology and Molecular Biology Reviews : MMBR* **2007**, *71*, 413-451.

[34] D. H. Goetz, M. A. Holmes, N. Borregaard, M. E. Bluhm, K. N. Raymond, R. K. Strong, *The Neutrophil Lipocalin NGAL Is a Bacteriostatic Agent that Interferes with Siderophore-Mediated Iron Acquisition, Molecular Cell* **2002**, *10*, 1033-1043.

[35] T. H. Flo, K. D. Smith, S. Sato, D. J. Rodriguez, M. A. Holmes, R. K. Strong, S. Akira, A. Aderem, *Lipocalin 2 mediates an innate immune response to bacterial infection by sequestrating iron, Nature* **2004**, *432*, 917-921.

[36] aM. A. Fischbach, H. Lin, L. Zhou, Y. Yu, R. J. Abergel, D. R. Liu, K. N. Raymond, B. L. Wanner, R. K. Strong, C. T. Walsh, A. Aderem, K. D. Smith, *The pathogen-associated iroA gene cluster mediates bacterial evasion of lipocalin 2, Proceedings of the National Academy of Sciences* **2006**, *103*, 16502-16507; bR. J. Abergel, M. C. Clifton, J. C. Pizarro, J. A. Warner, D. K. Shuh, R. K. Strong, K. N. Raymond, *The Siderocalin/Enterobactin Interaction: A Link between Mammalian Immunity and Bacterial Iron Transport1, Journal of the American Chemical Society* **2008**, *130*, 11524-11534.

[37] K. M. Schmidt-Ott, K. Mori, J. Y. Li, A. Kalandadze, D. J. Cohen, P. Devarajan, J. Barasch, *Dual Action of Neutrophil Gelatinase–Associated Lipocalin, Journal of the American Society of Nephrology* **2007**, *18*, 407-413.

[38] M. A. Fischbach, H. Lin, D. R. Liu, C. T. Walsh, *How pathogenic bacteria evade mammalian sabotage in the battle for iron, Nature Chemical Biology* **2006**, *2*, 132-138.

[39] aM. A. Bachman, V. L. Miller, J. N. Weiser, *Mucosal Lipocalin 2 Has Pro-Inflammatory and Iron-Sequestering Effects in Response to Bacterial Enterobactin, PLOS Pathogens* **2009**, *5*, e1000622; bM. Raffatellu, M. D. George, Y. Akiyama, M. J. Hornsby, S.-P. Nuccio, T. A. Paixao, B. P. Butler, H. Chu, R. L. Santos, T. Berger, T. W. Mak, R. M. Tsolis, C. L. Bevins, J. V. Solnick, S. Dandekar, A. J. Bäumler, *Lipocalin-2 Resistance Confers an Advantage to Salmonella enterica*

Serotype Typhimurium for Growth and Survival in the Inflamed Intestine, Cell Host & Microbe **2009**, *5*, 476-486.

[40] B. R. Wilson, A. R. Bogdan, M. Miyazawa, K. Hashimoto, Y. Tsuji, *Siderophores in Iron Metabolism: From Mechanism to Therapy Potential, Trends in Molecular Medicine* **2016**, *22*, 1077-1090.

[41] H. E. Kubitschek, *Cell volume increase in Escherichia coli after shifts to richer media, Journal of Bacteriology* **1990**, *172*, 94-101.

[42] aV. Braun, H. Killmann, *Bacterial solutions to the iron-supply problem, Trends in Biochemical Sciences* **1999**, *24*, 104-109; bV. Braun, C. Bös, M. Braun, H. Killmann, *Outer Membrane Channels and Active Transporters for the Uptake of Antibiotics, The Journal of Infectious Diseases* **2001**, *183*, S12-S16.

[43] R. C. Hider, X. Kong, *Chemistry and biology of siderophores, Natural Product Reports* **2010**, *27*, 637-657.

[44] O. Cunrath, V. A. Geoffroy, I. J. Schalk, *Metallome of Pseudomonas aeruginosa: a role for siderophores, Environmental Microbiology* **2016**, *18*, 3258-3267.

[45] aL. Escolar, J. Perez-Martin, V. de Lorenzo, *Opening the iron box: transcriptional metalloregulation by the Fur protein, J Bacteriol* **1999**, *181*, 6223-6229; bV. Braun, *Avoidance of iron toxicity through regulation of bacterial iron transport, Biological Chemistry* **1997**, *378*, 779-786.

[46] D. Ferreira, A. M. L. Seca, D. C.G.A, A. M. S. Silva, *Targeting human pathogenic bacteria by siderophores: A proteomics review, Journal of Proteomics* **2016**, *145*, 153-166.

[47] aS. C. Andrews, A. K. Robinson, F. Rodríguez-Quiñones, *Bacterial iron homeostasis, FEMS Microbiology Reviews* **2003**, *27*, 215-237; bK. D. Krewulak, H. J. Vogel, *Structural biology of bacterial iron uptake, Biochimica et Biophysica Acta* **2008**, *1778*, 1781-1804; cK. Schauer, D. A. Rodionov, H. de Reuse, *New substrates for TonB-dependent transport: do we only see the 'tip of the iceberg'?, Trends in Biochemical Sciences* **2008**, *33*, 330-338.

[48] aM. Miethke, M. A. Marahiel, *Siderophore-based iron acquisition and pathogen control, Microbiology and Molecular Biology Reviews : MMBR* **2007**, *71*, 413-451; bM. Ballouche, P. Cornelis, C. Baysse, *Iron metabolism: a promising target for antibacterial strategies, Recent patents on anti-infective drug discovery* **2009**, *4*, 190-205; cA. D. Ferguson, V. Braun, H. P. Fiedler, J. W. Coulton, K. Diederichs, W. Welte, *Crystal structure of the antibiotic albomycin in complex with the outer membrane transporter FhuA, Protein Science* **2000**, *9*, 956-963; dV. Braun, A. Pramanik, T. Gwinner, M. Koberle, E. Bohn, *Sideromycins: tools and antibiotics, BioMetals* **2009**, *22*, 3-13.

[49] aT. J. Brickman, M. A. McIntosh, *Overexpression and purification of ferric enterobactin esterase from Escherichia coli. Demonstration of enzymatic hydrolysis of enterobactin and its iron complex, Journal of Biological Chemistry* **1992**, *267*, 12350-12355; bM. Caza, A. Garenaux, F. Lepine, C. M. Dozois, *Catecholate siderophore esterases Fes, IroD and IroE are required for salmochelins secretion following utilization, but only IroD contributes to virulence of extra-intestinal pathogenic Escherichia coli, Molecular Microbiology* **2015**, *97*, 717-732.

[50] aR. C. Hider, X. Kong, *Chemistry and biology of siderophores,* **2010**, *27*, 637-657; bJ. M. Harrington, T. Gootz, M. Flanagan, M. Lall, J. O'Donnell, J. Winton, J.

Mueller, A. L. Crumbliss, *Characterization of the aqueous iron(III) chelation chemistry of a potential Trojan Horse antimicrobial agent: chelate structure, stability and pH dependent speciation, BioMetals* **2012**, *25*, 1023-1036; cM. G. P. Page, *Siderophore conjugates, Annals of the New York Academy of Sciences* **2013**, *1277*, 115-126; dU. Mollmann, L. Heinisch, A. Bauernfeind, T. Kohler, D. Ankel-Fuchs, *Siderophores as drug delivery agents: application of the "Trojan Horse" strategy, BioMetals* **2009**, *22*, 615-624.

[51] E. J. Stewart, F. Aslund, J. Beckwith, *Disulfide bond formation in the Escherichia coli cytoplasm: an in vivo role reversal for the thioredoxins, The EMBO Journal* **1998**, *17*, 5543-5550.

[52] T. Horiyama, K. Nishino, *AcrB, AcrD, and MdtABC multidrug efflux systems are involved in enterobactin export in Escherichia coli, PLOS ONE* **2014**, *9*, e108642.

[53] aH. Killmann, C. Herrmann, A. Torun, G. Jung, V. Braun, *TonB of Escherichia coli activates FhuA through interaction with the β-barrela, Microbiology* **2002**, *148*, 3497-3509; bV. Braun, K. Hantke, *Recent insights into iron import by bacteria, Current Opinion in Chemical Biology* **2011**, *15*, 328-334.

[54] aK. Poole, L. Young, S. Neshat, *Enterobactin-mediated iron transport in Pseudomonas aeruginosa, Journal of Bacteriology* **1990**, *172*, 6991-6996; bC. R. Dean, S. Neshat, K. Poole, *PfeR, an enterobactin-responsive activator of ferric enterobactin receptor gene expression in Pseudomonas aeruginosa, Journal of Bacteriology* **1996**, *178*, 5361-5369.

[55] aB. Ghysels, U. Ochsner, U. Möllman, L. Heinisch, M. Vasil, P. Cornelis, S. Matthijs, *The Pseudomonas aeruginosa pirA gene encodes a second receptor for ferrienterobactin and synthetic catecholate analogues, FEMS Microbiology Letters* **2005**, *246*, 167-174; bD. Mossialos, G. D. Amoutzias, *Siderophores in fluorescent pseudomonads: new tricks from an old dog, Future Microbiol* **2007**, *2*, 387-395; cP. Cornelis, *Iron uptake and metabolism in pseudomonads, Applied Microbiology and Biotechnology* **2010**, *86*, 1637-1645.

[56] E. E. Wyckoff, B. E. Allred, K. N. Raymond, S. M. Payne, *Catechol Siderophore Transport by Vibrio cholerae, Journal of Bacteriology* **2015**, *197*, 2840-2849.

[57] F. W. Twort, G. L. Y. Ingram, *A Method for Isolating and Cultivating the Mycobacterium enteritidis chronicae pseudotuberculosae bovis, Johne, and some Experiments on the Preparation of a Diagnostic Vaccine for Pseudo-tuberculous Enteritis of Bovines, Proceedings of the Royal Society of London. Series B, Containing Papers of a Biological Character* **1912**, *84*, 517-542.

[58] T. Ito, J. B. Neilands, *Products of "Low-iron Fermentation" with Bacillus subilis: Isolation, Characterization and Synthesis of 2,3-Dihydroxybenzoylglycine1,2, Journal of the American Chemical Society* **1958**, *80*, 4645-4647.

[59] I. G. O'Brien, G. B. Cox, F. Gibson, *Biologically active compounds containing 2,3-duhydroxybenzoic acid and serine formed by Escherichia coli, Biochimica et Biophysica Acta (BBA) - General Subjects* **1970**, *201*, 453-460.

[60] W. F. Penwell, N. DeGrace, S. Tentarelli, L. Gauthier, C. M. Gilbert, B. A. Arivett, A. A. Miller, T. F. Durand-Reville, C. Joubran, L. A. Actis, *Discovery and Characterization of New Hydroxamate Siderophores, Baumannoferrin A and B, produced by Acinetobacter baumannii, ChemBioChem* **2015**, *16*, 1896-1904.

[61] A. Yekkour, A. Meklat, C. Bijani, O. Toumatia, R. Errakhi, A. Lebrihi, F. Mathieu, A. Zitouni, N. Sabaou, *A novel hydroxamic acid-containing antibiotic produced by a Saharan soil-living Streptomyces strain, Letters in Applied Microbiology* **2015**, *60*, 589-596.

[62] M. Petrik, C. Zhai, H. Haas, C. Decristoforo, *Siderophores for molecular imaging applications, Clinical and translational imaging* **2017**, *5*, 15-27.

[63] aG. Xiao, D. van der Helm, R. C. Hider, P. S. Dobbin, *Structure-stability relationships of 3-hydroxypyridin-4-one complexes, Journal of the Chemical Society, Dalton Transactions* **1992**, 3265-3271; bU. Möllmann, L. Heinisch, A. Bauernfeind, T. Köhler, D. Ankel-Fuchs, *Siderophores as drug delivery agents: application of the "Trojan Horse" strategy, BioMetals* **2009**, *22*, 615-624; cK. D. Krewulak, H. J. Vogel, *Structural biology of bacterial iron uptake, Biochimica et Biophysica Acta (BBA) - Biomembranes* **2008**, *1778*, 1781-1804; dM. Miethke, M. A. Marahiel, *Siderophore-Based Iron Acquisition and Pathogen Control, Microbiology and Molecular Biology Reviews* **2007**, *71*, 413-451.

[64] K. P. Guerra, R. Delgado, *Homo-and heterodinuclear complexes of the tris(catecholamide) derivative of a tetraazamacrocycle with Fe3+, Cu2+ and Zn2+ metal ions, Dalton Transactions* **2008**, 539-550.

[65] W. R. Harris, K. N. Raymond, F. L. Weitl, *Ferric ion sequestering agents. 6. The spectrophotometric and potentiometric evaluation of sulfonated tricatecholate ligands, Journal of the American Chemical Society* **1981**, *103*, 2667-2675.

[66] J. M. Meyer, M. A. Abdallah, *The Fluorescent Pigment of Pseudomonas fluorescens: Biosynthesis, Purification and Physicochemical Properties, Microbiology* **1978**, *107*, 319-328.

[67] R. T. Reid, D. H. Livet, D. J. Faulkner, A. Butler, *A siderophore from a marine bacterium with an exceptional ferric ion affinity constant, Nature* **1993**, *366*, 455-458.

[68] Z. Jiang, M. Chen, X. Yu, Z. Xie, *7-Hydroxytropolone produced and utilized as an iron-scavenger by Pseudomonas donghuensis, BioMetals* **2016**, *29*, 817-826.

[69] Maud E. S. Achard, Kaiwen W. Chen, Matthew J. Sweet, Rebecca E. Watts, K. Schroder, Mark A. Schembri, Alastair G. McEwan, *An antioxidant role for catecholate siderophores in Salmonella, Biochemical Journal* **2013**, *454*, 543-549.

[70] C. T. Walsh, J. Liu, F. Rusnak, M. Sakaitani, *Molecular studies on enzymes in chorismate metabolism and the enterobactin biosynthetic pathway, Chemical Reviews* **1990**, *90*, 1105-1129.

[71] K. N. Raymond, E. A. Dertz, S. S. Kim, *Enterobactin: an archetype for microbial iron transport, Proceedings of the National Academy of Sciences of the United States of America* **2003**, *100*, 3584-3588.

[72] E. D. Weinberg, *The Lactobacillus anomaly: total iron abstinence, Perspectives in Biology and Medicine* **1997**, *40*, 578-583.

[73] T. A. Wencewicz, T. E. Long, U. Möllmann, M. J. Miller, *Trihydroxamate Siderophore–Fluoroquinolone Conjugates Are Selective Sideromycin Antibiotics that Target Staphylococcus aureus, Bioconjugate Chemistry* **2013**, *24*, 473-486.

[74] aM. A. Fischbach, C. T. Walsh, *Antibiotics for Emerging Pathogens, Science* **2009**, *325*, 1089-1093; bD. J. Payne, M. N. Gwynn, D. J. Holmes, D. L. Pompliano, *Drugs*

for bad bugs: confronting the challenges of antibacterial discovery, Nature Reviews Drug Discovery **2007**, *6*, 29-40.

[75] P. Klahn, M. Bronstrup, *Bifunctional antimicrobial conjugates and hybrid antimicrobials, Natural Products Reports* **2017**, *34*, 832-885.

[76] aK. Katsu, K. Kitoh, M. Inoue, S. Mitsuhashi, *In vitro antibacterial activity of E-0702, a new semisynthetic cephalosporin, Antimicrobial Agents and Chemotherapy* **1982**, *22*, 181-185; bN. A. Watanabe, T. Nagasu, K. Katsu, K. Kitoh, *E-0702, a new cephalosporin, is incorporated into Escherichia coli cells via the tonB-dependent iron transport system, Antimicrobial Agents and Chemotherapy* **1987**, *31*, 497-504; cS. Nakagawa, M. Sanada, K. Matsuda, N. Hazumi, N. Tanaka, *Biological activity of BO-1236, a new antipseudomonal cephalosporin, Antimicrobial Agents and Chemotherapy* **1987**, *31*, 1100-1105; dT. Hashizume, M. Sanada, S. Nakagawa, N. Tanaka, *Comparison of transport pathways of catechol-substituted cephalosporins, BO-1236 and BO-1341, through the outer membrane of Escherichia coli, Journal of Antibiotics* **1990**, *43*, 1617-1620; eJ. M. Roosenberg, 2nd, Y. M. Lin, Y. Lu, M. J. Miller, *Studies and syntheses of siderophores, microbial iron chelators, and analogs as potential drug delivery agents, Current Medicinal Chemistry* **2000**, *7*, 159-197.

[77] L. Vértesy, W. Aretz, H.-W. Fehlhaber, H. Kogler, *Salmycin A–D, Antibiotika aus Streptomyces violaceus, DSM 8286, mit Siderophor-Aminoglycosid-Struktur, Helvetica Chimica Acta* **1995**, *78*, 46-60.

[78] J. M. Roosenberg, 2nd, M. J. Miller, *Total synthesis of the siderophore danoxamine, Journal of Organic Chemistry* **2000**, *65*, 4833-4838.

[79] G. Benz, T. Schröder, J. Kurz, C. Wünsche, W. Karl, G. Steffens, J. Pfitzner, D. Schmidt, *Konstitution der Desferriform der Albomycine δ1, δ2, ε, Angewandte Chemie International Edition in English* **1982**, *21*, 1322-1335.

[80] aA. Hartmann, H. P. Fiedler, V. Braun, *Uptake and conversion of the antibiotic albomycin by Escherichia coli K-12, European Journal of Biochemistry* **1979**, *99*, 517-524; bV. Braun, K. Gunthner, K. Hantke, L. Zimmermann, *Intracellular activation of albomycin in Escherichia coli and Salmonella typhimurium, Journal of Bacteriology* **1983**, *156*, 308-315.

[81] T. A. Wencewicz, U. Mollmann, T. E. Long, M. J. Miller, *Is drug release necessary for antimicrobial activity of siderophore-drug conjugates? Syntheses and biological studies of the naturally occurring salmycin "Trojan Horse" antibiotics and synthetic desferridanoxamine-antibiotic conjugates, BioMetals* **2009**, *22*, 633-648.

[82] T. C. Johnstone, E. M. Nolan, *Beyond Iron: Non-Classical Biological Functions of Bacterial Siderophores, Dalton Transactions* **2015**, *44*, 6320-6339.

[83] S. Bieler, F. Silva, C. Soto, D. Belin, *Bactericidal Activity of both Secreted and Nonsecreted Microcin E492 Requires the Mannose Permease, Journal of Bacteriology* **2006**, *188*, 7049-7061.

[84] aE. M. Nolan, C. T. Walsh, *Investigations of the MceIJ-catalyzed posttranslational modification of the microcin E492 C-terminus: linkage of ribosomal and nonribosomal peptides to form "trojan horse" antibiotics, Biochemistry* **2008**, *47*, 9289-9299; bS. Duquesne, D. Destoumieux-Garzon, J. Peduzzi, S. Rebuffat, *Microcins, gene-encoded antibacterial peptides from enterobacteria, Natural Products Reports* **2007**, *24*, 708-734.

[85] aJ. M. Pages, C. E. James, M. Winterhalter, *The porin and the permeating antibiotic: a selective diffusion barrier in Gram-negative bacteria, Nature Reviews: Microbiology* **2008**, *6*, 893-903; bA. H. Delcour, *Outer membrane permeability and antibiotic resistance, Biochimica et Biophysica Acta* **2009**, *1794*, 808-816; cR. E. Hancock, *The bacterial outer membrane as a drug barrier, Trends in Microbiology* **1997**, *5*, 37-42.

[86] C. Ji, P. A. Miller, M. J. Miller, *Iron Transport-Mediated Drug Delivery: Practical Syntheses and In Vitro Antibacterial Studies of Tris-catecholate Sidero-phore-Aminopenicillin Conjugates Reveals Selectively Potent Anti-Pseudomonal Activity, Journal of the American Chemical Society* **2012**, *134*, 9898-9901.

[87] aS. Harada, S. Tsubotani, T. Hida, H. Ono, H. Okazaki, *Structure of lactivicin, an antibiotic having a new nucleus and similar biological activities to β-lactam antibiotics, Tetrahedron Letters* **1986**, *27*, 6229-6232; bY. Nozaki, N. Katayama, H. Ono, S. Tsubotani, S. Harada, H. Okazaki, Y. Nakao, *Binding of a non-beta-lactam antibiotic to penicillin-binding proteins, Nature* **1987**, *325*, 179-180; cY. Nozaki, N. Katayama, S. Harada, H. Ono, H. Okazaki, *Lactivicin, a naturally occurring non-beta-lactam antibiotic having beta-lactam-like action: biological activities and mode of action, Journal of Antibiotics* **1989**, *42*, 84-93.

[88] J. Starr, M. F. Brown, L. Aschenbrenner, N. Caspers, Y. Che, B. S. Gerstenberger, M. Huband, J. D. Knafels, M. M. Lemmon, C. Li, S. P. McCurdy, E. McElroy, M. R. Rauckhorst, A. P. Tomaras, J. A. Young, R. P. Zaniewski, V. Shanmugasundaram, S. Han, *Siderophore Receptor-Mediated Uptake of Lactivicin Analogues in Gram-Negative Bacteria, Journal of Medicinal Chemistry* **2014**, *57*, 3845-3855.

[89] K. Calvopiña, K.-D. Umland, A. M. Rydzik, P. Hinchliffe, J. Brem, J. Spencer, C. J. Schofield, M. B. Avison, *Sideromimic Modification of Lactivicin Dramatically Increases Potency against Extensively Drug-Resistant Stenotrophomonas maltophilia Clinical Isolates, Antimicrobial Agents and Chemotherapy* **2016**, *60*, 4170-4175.

[90] S. Mushtaq, M. Warner, D. Livermore, *Activity of the siderophore monobactam BAL30072 against multiresistant non-fermenters, Journal of Antimicrobial Chemotherapy* **2010**, *65*, 266-270.

[91] M. G. P. Page, C. Dantier, E. Desarbre, *In Vitro Properties of BAL30072, a Novel Siderophore Sulfactam with Activity against Multiresistant Gram-Negative Bacilli, Antimicrobial Agents and Chemotherapy* **2010**, *54*, 2291-2302.

[92] P. G. Higgins, D. Stefanik, M. G. Page, M. Hackel, H. Seifert, *In vitro activity of the siderophore monosulfactam BAL30072 against meropenem-non-susceptible Acinetobacter baumannii, Journal of Antimicrobial Chemotherapy* **2012**, *67*, 1167-1169.

[93] T. Mima, B. H. Kvitko, D. A. Rholl, M. G. P. Page, E. Desarbre, H. P. Schweizer, *In vitro activity of BAL30072 against Burkholderia pseudomallei, International Journal of Antimicrobial Agents* **2011**, *38*, 157-159.

[94] aB. Hofer, C. Dantier, K. Gebhardt, E. Desarbre, A. Schmitt-Hoffmann, M. G. Page, *Combined effects of the siderophore monosulfactam BAL30072 and carbapenems on multidrug-resistant Gram-negative bacilli, Journal of Antimicrobial Chemotherapy* **2013**, *68*, 1120-1129; bT. A. Russo, M. G. Page, J. M. Beanan, R. Olson, A. M. Hujer, K. M. Hujer, M. Jacobs, S. Bajaksouzian, A. Endimiani, R. A. Bonomo, *In*

vivo and in vitro activity of the siderophore monosulfactam BAL30072 against Acinetobacter baumannii, Journal of Antimicrobial Chemotherapy **2011**, *66*, 867-873.

[95] aA. Ito, N. Kohira, S. K. Bouchillon, J. West, S. Rittenhouse, H. S. Sader, P. R. Rhomberg, R. N. Jones, H. Yoshizawa, R. Nakamura, M. Tsuji, Y. Yamano, *In vitro antimicrobial activity of S-649266, a catechol-substituted siderophore cephalosporin, when tested against non-fermenting Gram-negative bacteria, Journal of Antimicrobial Chemotherapy* **2016**, *71*, 670-677; bT. Ito-Horiyama, Y. Ishii, A. Ito, T. Sato, R. Nakamura, N. Fukuhara, M. Tsuji, Y. Yamano, K. Yamaguchi, K. Tateda, *Stability of Novel Siderophore Cephalosporin S-649266 against Clinically Relevant Carbapenemases, Antimicrobial Agents and Chemotherapy* **2016**, *60*, 4384-4386.

[96] G. S. Tillotson, *Trojan Horse Antibiotics—A Novel Way to Circumvent Gram-Negative Bacterial Resistance?, Infectious Diseases* **2016**, *9*, 45-52.

[97] N. Ohi, B. Aoki, T. Kuroki, M. Matsumoto, K. Kojima, T. Nehashi, *Semisynthetic beta-lactam antibiotics. III. Effect on antibacterial activity and comt-susceptibility of chlorine-introduction into the catechol nucleus of 6-[(R)-2-[3-(3,4-dihydroxybenzoyl)-3-(3-hydroxypropyl)-1-ureido]-2- phenylacetamido]penicillanic acid, Journal of Antibiotics* **1987**, *40*, 22-28.

[98] aT. Katsube, R. Echols, J. C. Arjona Ferreira, H. K. Krenz, J. K. Berg, C. Galloway, *Cefiderocol, a Siderophore Cephalosporin for Gram-Negative Bacterial Infections: Pharmacokinetics and Safety in Subjects With Renal Impairment, Journal of Clinical Pharmacology* **2017**, *57*, 584-591; bN. Kohira, J. West, A. Ito, T. Ito-Horiyama, R. Nakamura, T. Sato, S. Rittenhouse, M. Tsuji, Y. Yamano, *In Vitro Antimicrobial Activity of a Siderophore Cephalosporin, S-649266, against Enterobacteriaceae Clinical Isolates, Including Carbapenem-Resistant Strains, Antimicrobial Agents and Chemotherapy* **2016**, *60*, 729-734.

[99] T. J. Wadas, E. H. Wong, G. R. Weisman, C. J. Anderson, *Coordinating Radiometals of Copper, Gallium, Indium, Yttrium and Zirconium for PET and SPECT Imaging of Disease, Chemical Reviews* **2010**, *110*, 2858-2902.

[100] T. Zheng, J. L. Bullock, E. M. Nolan, *Siderophore-mediated cargo delivery to the cytoplasm of Escherichia coli and Pseudomonas aeruginosa: syntheses of monofunctionalized enterobactin scaffolds and evaluation of enterobactin-cargo conjugate uptake, Journal of the American Chemical Society* **2012**, *134*, 18388-18400.

[101] L. Heinisch, S. Wittmann, T. Stoiber, A. Berg, D. Ankel-Fuchs, U. Möllmann, *Highly Antibacterial Active Aminoacyl Penicillin Conjugates with Acylated Bis-Catecholate Siderophores Based on Secondary Diamino Acids and Related Compounds, Journal of Medicinal Chemistry* **2002**, *45*, 3032-3040.

[102] T. M. Bateman, *Advantages and disadvantages of PET and SPECT in a busy clinical practice, Journal of Nuclear Cardiology* **2012**, *19*, 3-11.

[103] aJ. J. Harrison, R. J. Turner, D. A. Joo, M. A. Stan, C. S. Chan, N. D. Allan, H. A. Vrionis, M. E. Olson, H. Ceri, *Copper and Quaternary Ammonium Cations Exert Synergistic Bactericidal and Antibiofilm Activity against Pseudomonas aeruginosa, Antimicrobial Agents and Chemotherapy* **2008**, *52*, 2870-2881; bR. E. Juárez-Hernández, P. A. Miller, M. J. Miller, *Syntheses of Siderophore–Drug Conjugates*

Using a Convergent Thiol–Maleimide System, ACS Medicinal Chemistry Letters **2012**, *3*, 799-803.

[104] S. C. Ghosh, K. L. Pinkston, H. Robinson, B. R. Harvey, N. Wilganowski, K. Gore, E. M. Sevick-Muraca, A. Azhdarinia, *Comparison of DOTA and NODAGA as chelators for (64)Cu-labeled immunoconjugates, Nuclear Medicine and Biology* **2015**, *42*, 177-183.

[105] aE. T. Clarke, A. E. Martell, *Stabilities of the Fe(III), Ga(III) and In(III) chelates of N,N',N''-triazacyclononanetriacetic acid, Inorganica Chimica Acta* **1991**, *181*, 273-280; bV. Kubíček, J. Havlíčková, J. Kotek, G. Tircsó, P. Hermann, É. Tóth, I. Lukeš, *Gallium(III) Complexes of DOTA and DOTA−Monoamide: Kinetic and Thermodynamic Studies, Inorganic Chemistry* **2010**, *49*, 10960-10969; cS. C. Ghosh, K. L. Pinkston, H. Robinson, B. R. Harvey, N. Wilganowski, K. Gore, E. M. Sevick-Muraca, A. Azhdarinia, *Comparison of DOTA and NODAGA as chelators for 64Cu-labeled immunoconjugates, Nuclear Medicine and Biology* **2015**, *42*, 177-183.

[106] L. Heinisch, P. Gebhardt, R. Heidersbach, R. Reissbrodt, U. Möllmann, *New synthetic catecholate-type siderophores with triamine backbone, BioMetals* **2002**, *15*, 133-144.

[107] A. X. Li, F. Wojciechowski, M. Suchy, C. K. Jones, R. H. Hudson, R. S. Menon, R. Bartha, *A sensitive PARACEST contrast agent for temperature MRI: Eu3+-DOTAM-glycine (Gly)-phenylalanine (Phe), Magnetic Resonance in Medicine* **2008**, *59*, 374-381.

[108] S. Lei, B. Jin, Q. Zhang, Z. Zhang, X. Wang, R. Peng, S. Chu, *Synthesis of bifunctional biscatecholamine chelators for uranium decorporation, Polyhedron* **2016**, *119*, 387-395.

[109] B. Jagadish, G. L. Brickert-Albrecht, G. S. Nichol, E. A. Mash, N. Raghunand, *On the Synthesis of 1,4,7-Tris(tert-butoxycarbonylmethyl)-1,4,7,10-tetraazacyclododecane, Tetrahedron Letters* **2011**, *52*, 2058-2061.

[110] M. Albrecht, M. Baumert, H. D. F. Winkler, C. A. Schalley, R. Frohlich, *Hierarchical self-assembly of metallo-dendrimers, Dalton Transactions* **2010**, *39*, 7220-7222.

[111] H. S. Rho, H. S. Baek, S. M. Ahn, J. W. Yoo, D. H. Kim, H. G. Kim, *Studies on depigmenting activities of dihydroxyl benzamide derivatives containing adamantane moiety, Bioorganic & Medicinal Chemistry Letters* **2009**, *19*, 1532-1533.

[112] B. Schwyn, J. B. Neilands, *Universal chemical assay for the detection and determination of siderophores, Analytical Biochemistry* **1987**, *160*, 47-56.

[113] K. Knop, R. Hoogenboom, D. Fischer, U. S. Schubert, *Poly(ethylene glycol) in Drug Delivery: Pros and Cons as Well as Potential Alternatives, Angewandte Chemie International Edition* **2010**, *49*, 6288-6308.

[114] R. Wayne, K. Frick, J. B. Neilands, *Siderophore protection against colicins M, B, V, and Ia in Escherichia coli, Journal of Bacteriology* **1976**, *126*, 7-12.

[115] R. Ankenbauer, S. Sriyosachati, C. D. Cox, *Effects of siderophores on the growth of Pseudomonas aeruginosa in human serum and transferrin, Infection and Immunity* **1985**, *49*, 132-140.

[116] D. Van der Helm, J. R. Baker, D. L. Eng-Wilmot, M. B. Hossain, R. A. Loghry, *Crystal structure of ferrichrome and a comparison with the structure of ferrichrome A, Journal of the American Chemical Society* **1980**, *102*, 4224-4231.

[117] S. Ray Banerjee, Z. Chen, M. Pullambhatla, A. Lisok, J. Chen, R. C. Mease, M. G. Pomper, *Preclinical Comparative Study of (68)Ga-Labeled DOTA, NOTA, and HBED-CC Chelated Radiotracers for Targeting PSMA, Bioconjugate Chemistry* **2016**, *27*, 1447-1455.

[118] N. Ohi, B. Aoki, T. Shinozaki, K. Moro, T. Noto, T. Nehashi, H. Okazaki, I. Matsunaga, *Semisynthetic beta-lactam antibiotics. I. Synthesis and antibacterial activity of new ureidopenicillin derivatives having catechol moieties, Journal of Antibiotics* **1986**, *39*, 230-241.

[119] S. G. Agalave, S. R. Maujan, V. S. Pore, *Click Chemistry: 1,2,3-Triazoles as Pharmacophores, Chemistry – An Asian Journal* **2011**, *6*, 2696-2718.

[120] aD. K. Dalvie, A. S. Kalgutkar, S. C. Khojasteh-Bakht, R. S. Obach, J. P. O'Donnell, *Biotransformation Reactions of Five-Membered Aromatic Heterocyclic Rings, Chemical Research in Toxicology* **2002**, *15*, 269-299; bW. S. Horne, M. K. Yadav, C. D. Stout, M. R. Ghadiri, *Heterocyclic Peptide Backbone Modifications in an α-Helical Coiled Coil, Journal of the American Chemical Society* **2004**, *126*, 15366-15367.

[121] K. Lang, J. W. Chin, *Cellular Incorporation of Unnatural Amino Acids and Bioorthogonal Labeling of Proteins, Chemical Reviews* **2014**, *114*, 4764-4806.

[122] C. Szent-Gyorgyi, B. F. Schmidt, Y. Creeger, G. W. Fisher, K. L. Zakel, S. Adler, J. A. J. Fitzpatrick, C. A. Woolford, Q. Yan, K. V. Vasilev, P. B. Berget, M. P. Bruchez, J. W. Jarvik, A. Waggoner, *Fluorogen-activating single-chain antibodies for imaging cell surface proteins, Nature Biotechnology* **2008**, *26*, 235-240.

[123] S. Saurabh, A. M. Perez, C. J. Comerci, L. Shapiro, W. E. Moerner, *Super-resolution Imaging of Live Bacteria Cells Using a Genetically Directed, Highly Photostable Fluoromodule, Journal of the American Chemical Society* **2016**, *138*, 10398-10401.

[124] Q. Yan, S. L. Schwartz, S. Maji, F. Huang, C. Szent-Gyorgyi, D. S. Lidke, K. A. Lidke, M. P. Bruchez, *Localization microscopy using noncovalent fluorogen activation by genetically encoded fluorogen-activating proteins, Chemphyschem* **2014**, *15*, 687-695.

[125] J. F. Fisher, S. O. Meroueh, S. Mobashery, *Bacterial resistance to beta-lactam antibiotics: compelling opportunism, compelling opportunity, Chemical Reviews* **2005**, *105*, 395-424.

[126] M. F. Chellat, L. Raguž, R. Riedl, *Targeting Antibiotic Resistance, Angewandte Chemie International Edition* **2016**, *55*, 6600-6626.

[127] P. Lagace-Wiens, E. Rubinstein, *Adverse reactions to beta-lactam antimicrobials, Expert Opinion on Drug Safety* **2012**, *11*, 381-399.

[128] E. Sugawara, K. Nagano, H. Nikaido, *Alternative folding pathways of the major porin OprF of Pseudomonas aeruginosa, FEBS Journal* **2012**, *279*, 910-918.

[129] T. Kline, M. Fromhold, T. E. McKennon, S. Cai, J. Treiberg, N. Ihle, D. Sherman, W. Schwan, M. J. Hickey, P. Warrener, P. R. Witte, L. L. Brody, L. Goltry, L. M. Barker, S. U. Anderson, S. K. Tanaka, R. M. Shawar, L. Y. Nguyen, M. Langhorne, A. Bigelow, L. Embuscado, E. Naeemi, *Antimicrobial effects of novel siderophores linked to beta-lactam antibiotics, Bioorganic and Medicinal Chemistry* **2000**, *8*, 73-93.

[130] H. Kishida, S. Unzai, D. I. Roper, A. Lloyd, S.-Y. Park, J. R. H. Tame, *Crystal Structure of Penicillin Binding Protein 4 (dacB) from Escherichia coli, both in the Native Form and Covalently Linked to Various Antibiotics, Biochemistry* **2006**, *45*, 783-792.

[131] S. J. Milner, A. Seve, A. M. Snelling, G. H. Thomas, K. G. Kerr, A. Routledge, A. K. Duhme-Klair, *Staphyloferrin A as siderophore-component in fluoroquinolone-based Trojan horse antibiotics, Organic & Biomolecular Chemistry* **2013**, *11*, 3461-3468.

[132] aB. D. Bax, P. F. Chan, D. S. Eggleston, A. Fosberry, D. R. Gentry, F. Gorrec, I. Giordano, M. M. Hann, A. Hennessy, M. Hibbs, J. Huang, E. Jones, J. Jones, K. K. Brown, C. J. Lewis, E. W. May, M. R. Saunders, O. Singh, C. E. Spitzfaden, C. Shen, A. Shillings, A. J. Theobald, A. Wohlkonig, N. D. Pearson, M. N. Gwynn, *Type IIA topoisomerase inhibition by a new class of antibacterial agents, Nature* **2010**, *466*, 935-940; bD. T. King, G. A. Wasney, M. Nosella, A. Fong, N. C. Strynadka, *Structural Insights into Inhibition of Escherichia coli Penicillin-binding Protein 1B, Journal of Biological Chemistry* **2017**, *292*, 979-993.

[133] aS. R. Md-Saleh, E. C. Chilvers, K. G. Kerr, S. J. Milner, A. M. Snelling, J. P. Weber, G. H. Thomas, A.-K. Duhme-Klair, A. Routledge, *Synthesis of citrate–ciprofloxacin conjugates, Bioorganic & Medicinal Chemistry Letters* **2009**, *19*, 1496-1498; bR. Cormier, W. N. Burda, L. Harrington, J. Edlinger, K. M. Kodigepalli, J. Thomas, R. Kapolka, G. Roma, B. E. Anderson, E. Turos, L. N. Shaw, *Studies on the antimicrobial properties of N-acylated ciprofloxacins, Bioorganic & Medicinal Chemistry Letters* **2012**, *22*, 6513-6520; cP.-T. Chen, W.-P. Lin, A.-R. Lee, M.-K. Hu, *New 7-[4-(4-(un)Substituted)piperazine-1-carbonyl]- piperazin-1-yl] Derivatives of Fluoroquinolone: Synthesis and Antimicrobial Evaluation, Molecules* **2013**, *18*, 7557; dM. A. Ibrahim, S. S. Panda, A. S. Birs, J. C. Serrano, C. F. Gonzalez, K. A. Alamry, A. R. Katritzky, *Synthesis and antibacterial evaluation of amino acid–antibiotic conjugates, Bioorganic & Medicinal Chemistry Letters* **2014**, *24*, 1856-1861.

[134] C. Lin, J. F. Engbersen, *The role of the disulfide group in disulfide-based polymeric gene carriers, Expert opinion on drug delivery* **2009**, *6*, 421-439.

[135] H. Irschik, R. Jansen, K. Gerth, G. Hofle, H. Reichenbach, *The sorangicins, novel and powerful inhibitors of eubacterial RNA polymerase isolated from myxobacteria, Journal of Antibiotics* **1987**, *40*, 7-13.

[136] E. A. Campbell, O. Pavlova, N. Zenkin, F. Leon, H. Irschik, R. Jansen, K. Severinov, S. A. Darst, *Structural, functional, and genetic analysis of sorangicin inhibition of bacterial RNA polymerase, EMBO Journal* **2005**, *24*, 674-682.

[137] R. Jansen, D. Schummer, H. Irschik, G. Höfle, *Antibiotics from gliding bacteria, XLII. Chemical modification of sorangicin A and structure — Activity relationship I: Carboxyl and hydroxyl group derivatives, Liebigs Annalen der Chemie* **1990**, *1990*, 975-988.

[138] R. Jansen, V. Wray, H. Irschik, H. Reichenbach, G. Höfle, *Isolation and spectroscopic structure elucidation of sorangicin a, a new type of macrolide-polyether antibiotic from gliding bacteria - XXX, Tetrahedron Letters* **1985**, *26*, 6031-6034.

[139] T. Seithe, J. Braun, M. Wolf, J. Vahldiek, D. Wolny, J. Auer, J. Pociej, O. Heine, B. Hamm, M. de Bucourt, *Diagnostic efficacy and safety of gadoteric acid MR*

mammography in 1537 patients, European Journal of Radiology **2016**, *85*, 2281-2287.

[140] A. Alouane, R. Labruère, T. Le Saux, F. Schmidt, L. Jullien, *Self-Immolative Spacers: Kinetic Aspects, Structure–Property Relationships, and Applications, Angewandte Chemie International Edition* **2015**, *54*, 7492-7509.

[141] *Rifamycin analogs and uses thereof*, **2008**, US7342011 (B2).

[142] A. Leydier, Y. Lin, G. Arrachart, R. Turgis, D. Lecerclé, A. Favre-Reguillon, F. Taran, M. Lemaire, S. Pellet-Rostaing, *EDTA and DTPA modified ligands as sequestering agents for uranyl decorporation, Tetrahedron* **2012**, *68*, 1163-1170.

[143] A. Petrosyan, P. Ehlers, S. Reimann, T. V. Ghochikyan, A. S. Saghyan, A. Spannenberg, S. Lochbrunner, P. Langer, *Synthesis of tetraaryl- and tetraalkenylpyrazines by Suzuki–Miyaura reactions of tetrachloropyrazine, Tetrahedron* **2015**, *71*, 6803-6812.

[144] N. Raghunand, G. P. Guntle, V. Gokhale, G. S. Nichol, E. A. Mash, B. Jagadish, *Design, Synthesis, and Evaluation of 1,4,7,10-Tetraazacyclododecane-1,4,7-triacetic Acid Derived, Redox-Sensitive Contrast Agents for Magnetic Resonance Imaging, Journal of Medicinal Chemistry* **2010**, *53*, 6747-6757.

[145] T. M. Wickramaratne, V. C. Pierre, *Turning an Aptamer into a Light-Switch Probe with a Single Bioconjugation, Bioconjugate Chemistry* **2015**, *26*, 63-70.

[146] S. Isomura, P. Wirsching, K. D. Janda, *An Immunotherapeutic Program for the Treatment of Nicotine Addiction: Hapten Design and Synthesis, The Journal of Organic Chemistry* **2001**, *66*, 4115-4121.

[147] K. Iwaso, Y. Takashima, A. Harada, *Fast response dry-type artificial molecular muscles with [c2]daisy chains, Nature Chemistry* **2016**, *8*, 625-632.

[148] M. J. Abedin, L. Liepold, P. Suci, M. Young, T. Douglas, *Synthesis of a Cross-Linked Branched Polymer Network in the Interior of a Protein Cage, J. Am. Chem. Soc.* **2009**, *131*, 4346-4354.

[149] C. Szent-Gyorgyi, B. F. Schmidt, Y. Creeger, G. W. Fisher, K. L. Zakel, S. Adler, J. A. J. Fitzpatrick, C. A. Woolford, Q. Yan, K. V. Vasilev, P. B. Berget, M. P. Bruchez, J. W. Jarvik, A. Waggoner, *Fluorogen-activating single-chain antibodies for imaging cell surface proteins, Nat Biotechnol.* **2008**, *26*, 235-240.

[150] C. E. Jakobsche, P. J. McEnaney, A. X. Zhang, D. A. Spiegel, *Reprogramming Urokinase into an Antibody-Recruiting Anticancer Agent, ACS Chem. Biol.* **2011**, *7*, 316-321.

[151] C. Szent-Gyorgyi, B. F. Schmidt, Y. Creeger, G. W. Fisher, K. L. Zakel, S. Adler, J. A. Fitzpatrick, C. A. Woolford, Q. Yan, K. V. Vasilev, P. B. Berget, M. P. Bruchez, J. W. Jarvik, A. Waggoner, *Fluorogen-activating single-chain antibodies for imaging cell surface proteins, Nat Biotechnol* **2008**, *26*, 235-240.

[152] M. Krasavin, V. Parchinsky, G. Kantin, O. Manicheva, M. Dogonadze, T. Vinogradova, B. Karge, M. Brönstrup, *New nitrofurans amenable by isocyanide multicomponent chemistry are active against multidrug-resistant and poly-resistant Mycobacterium tuberculosis, Bioorganic & Medicinal Chemistry* **2017**, *25*, 1867-1874.

[153] M. Ishiyama, H. Tominaga, M. Shiga, K. Sasamoto, Y. Ohkura, K. Ueno, *A combined assay of cell viability and in vitro cytotoxicity with a highly water-soluble*

tetrazolium salt, neutral red and crystal violet, Biological & Pharmaceutical Bulletin **1996**, *19*, 1518-1520.

[154] F. Sasse, H. Steinmetz, T. Schupp, F. Petersen, K. Memmert, H. Hofmann, C. Heusser, V. Brinkmann, P. von Matt, G. Hofle, H. Reichenbach, *Argyrins, immunosuppressive cyclic peptides from myxobacteria. I. Production, isolation, physico-chemical and biological properties, Journal of Antibiotics* **2002**, *55*, 543-551.

7. Contributions

I hereby declare that I wrote this PhD thesis with the topic ‘Synthesis of siderophore-based conjugate to detect and treat bacterial infections’ independently and without additional auxiliary material or support than indicated herein. Published information, which has been cited, is listed as references. I furthermore declare that this thesis has not been submitted as a PhD thesis elsewhere. I am aware to keep all materials that confirm that this thesis is my own work available until the thesis evaluation is completed.

I also declare that synthesis of **12-15** and **26** was performed by the supervised MSc student Isabell Schneider and that the MS-MS, growth recovery, fluorescence microscopy, FAP, MIC and toxicity assays were conducted by Dr Verena Fetz, Dr Hans Prochnow, Volker Berndt and Bianka Karge.

Kevin Ferreira

Braunschweig,

KEVIN FERREIRA

27 years old, French & Portuguese,
Schöppenstedter Str. 37, 38100, Braunschweig, Germany
+49 (0)176 4567-9559/knfr64@gmail.com/www.linkedin.com/in/kevfer

WORK EXPERIENCE

2014-pres (3y) Project at HZI GmbH, **Germany** in organic synthesis of *siderophore-based bioconjugates for the diagnosis and treatment of bacterial infections* and *uridine derivatives*
➔Collaboration with different groups (HZI, ETH, TU Braunschweig) and people from different backgrounds (pharmacology, spectroscopy, microbiology, immunology).
➔Supervision of interns/trainees/technicians on different projects in English/German
➔Familiar with low scale reaction (50 µg), MIC assays, fluorescence microscopy, preclinical, growth recovery and toxicity experiments, PET and fluorescence imaging.
➔In charge of 2 preparative HPLC Dionex Ultimate 3000, 1 Agilent LCMS, inventory organization.
➔Pharmaceutical and quality management, GMP, isolation, elucidation of bioactive compounds, medicinal chemistry (Davidson college and Novartis), translational research (C-COMEND) courses.

2014 (6m) Project at Merck KGaA, **Germany** in organic synthesis of *HTM for OLED applications*
➔Purification by recrystallizations and sublimations to reach purity >99.9%. Extensive use of standard organic chemistry techniques, air and water-sensitive reactions etc.
➔Familiar with cyclic voltammetry, atomic analysis, reporting skills in formal documentation, GMP**.**

2013 (6m) Project at Hexion Inc., **Belgium** with Dr. F. Simal in emulsion polymerization
➔Characterization and formulation of latex (pressure sensitive adhesive applications)
➔Synthesis of latex materials at 2-3 kg scale and grit content, opacity, solid content, shear, peel 180, loop tack, DSC, GC, QC experiments.

2012-13(6m) Project at Chem0vation Ltd, **United Kingdom** with Dr. I. Matthews in organic synthesis *for pharmaceutical and biotech companies* (Novartis, Astrazeneca etc.)
➔Worked on 4 different projects with the synthesis of standard/innovative building block molecules and modification of natural product.
➔Familiar with HPLC-MS, 1/2D NMR etc.

2012 (7m) Project at UFRGS, **Brazil** with Dr. S. Guterres in *nanocapsule synthesis by polymer precipitation* for cosmetic application (sunscreens)
➔Familiar with HPLC, mastersizer, mini-spray dryer, zetasizer, turbiscan, nanosight, SEM, Franz cell equipments, cosmetic formulation and FDA regulations.

2011 (2m) Project at Chimie ParisTech university, **France** with Dr V. Vidal & V. Michelet in organic synthesis on addition of *alpha-disubstituted aldehydes onto unactivated alkynes by metallo organocatalysis*.
➔ Familiar with 1 mg scale stereoselective reaction, methodology, GC, ^{1}H NMR, ^{13}C NMR etc.

EDUCATION

2014-2018 **Ph.D.** at LUH, Germany in Chemical Biology.
2014 **M.Sc.** and **engineer** at ENSCM, **France** in fine organic & healthcare biomolecule chemistry.
2012-2013 Sandwich year (industrial experience) in organic and polymer chemistry
BRAFITEC student exchange at UFRGS, **Brazil** in optimisation of chemical industry projects, cosmetology classes**.**
2011 B.Sc. at ENSCM, **France** in organic synthesis, computational chemistry, analytical chemistry, material, polymer science, computer control, environment, management, quality, H&S.

SCIENTIFIC ACHIEVEMENTS

Patents Prof. M. Brönstrup, Prof. H. Hu, K. Ferreira, Dr. V. Fetz, Dr. G. Sergeev, Dr. B. Rais, **WO2016026841**.
Papers • K. Ferreira *et al. Angew. Chem. Int. Ed.* **2017**, *56*, 8272/*Angew. Chem.* ***2017****, 129, 8384.*

Molecular “Trojan horses” render infections visible, HZI press release, July 2017.
HZI interview of “Science in 60s”, July 2017.

- S. Doberenz, K. Ferreira, S. Häußler, about uridine derivatives (in preparation)

Prize

- 1st Prize for oral presentation for 8th International PhD and ESR Symposium at HZI, Germany.
- 1st Prize for oral presentation for 10th International PhD Symposium at HZI, Germany.
- Selected for the best poster competition at the 2nd training of the COST Action 2017, Portugal.
- Audience Prize for oral presentation for Famelab Braunschweig 2016, Germany.
- 2nd Prize for oral presentation for 9th International PhD Symposium at HZI, Germany.
- 2nd Prize for oral cross topic presentation for 7th annual retreat at HZI, Germany.
- 3rd Prize for oral presentation for 8th annual retreat at HZI, Germany.

ADDITIONAL SKILLS

Languages

French	Portuguese (Portugal/Brazil)	English	German	Spanish
Mother tongue	Mothertongue/fluent	Fluent (TOEIC: 910)	B2	Fluent

Computer skills

- Chemistry: Chemdraw, SciFinder, Belstein, Spresi, SeeSAR, PyMol, Chimera, Molinspiration, PDB, Drug Database
- Others: Word, Excel, Power Point, MS project, Front Page, Maple, Visual Basic.

EXTRA-CURRICULAR ACTIVITIES

Responsabilities

- Scientific advisor for a Nutraceutical Startup company

➔ Provide latest scientific information on extracted natural products.

- Partner with LR Health & Beauty systems GmbH in network marketing

➔ Familiar with direct selling, networking and product commercialisation.
➔Enhanced presentation skills.

- Member of the Erasmus club and student government of the Graduate School. In charge of organizations of events, trips, management of groups and waiter(5 h/week)

➔Communication and management abilities, working within deadline
➔In charge of stock management
➔Team and competitive spirit

Private lessons

Mathematics, physics & chemistry given to high school and university students.
➔Strengthened my organization abilities to lead the different courses
➔Needed to adapt strategies to suit student’s varied profiles.

Sport

Soccer, running (Berlin Marathon 2016) and volleyball (Captain and coach for 6 years), 4 years of refereeing competitions
➔ Improved my concentration
➔ Taught me team and competitive spirit
➔ Capacity of improving strategies and leadership

Interests

Photography, american & brazilian cinema and movies about memory and cultural differences.
British/American news and conferences such as BBC website or TED conferences.

REFERENCES

Prof. Dr. Mark Brönstrup: mark.broenstrup@helmholtz-hzi.de
Dr. Ian Matthews: imatthews@chemovation.com
Dr. François Simal: Francois.simal@momentive.com